Nitrate aerosol: implications for global air quality, human health and climate

Hana Carol Pearce

Submitted in accordance with the requirements for the degree of
Doctor of Philosophy

University of Leeds

School of Earth and Environment

October 2019

Declaration of authorship

The candidate confirms that the work submitted is her own and that appropriate credit has been given where reference has been made to the work of others.

Acknowledgements

I would like to thank my supervisors, Graham Mann, Steve Arnold and Fiona O'Connor for their guidance throughout this project. Special thanks go to my "honorary" supervisor, Steve Rumbold, for his support and encouragement. I would like to acknowledge Ed Butt for help with the $PM_{2.5}$-attributable mortality calculations in Chapter 5 and Alex Rap for calculating the aerosol radiative effects in Chapter 6.

This research was made possible by funding from the Leeds/York National Environment Research Council Doctoral Training Partnership Scheme and the UK Meteorological Office. The simulations in this thesis were run using the ARCHER high performance computing facility and data processing was carried out using the Faculty of Environment computer systems and the JASMIN data analysis environment. I am grateful for technical support provided by the National Centre for Atmospheric Science modelling helpdesk and the Centre for Environmental Modelling and Computing. Chapter 4 includes comparisons to multi-model concentrations from the nitrate AeroCom Phase III experiment.

It has been an honour to work alongside brilliant researchers within the aerosol modelling group and Biosphere-Atmosphere Group at Leeds and I am especially thankful to Ken Carslaw, Ed Butt, Kirsty Pringle, Steve Turnock, Mark Richardson, Cat Scott and Carly Reddington for both technical support and helpful discussions of this research. A special mention also for my fellow PhD students Lauren Marshall, Lucy Recchia, Mike O'Sullivan, Ol Halliday and Ilkka Matero.

I don't have the words to thank my family and friends for their unending patience and support throughout this process. I would especially like to thank my parents and also Michael and Holly for helping me to the finish line. Finally, I would like to dedicate this work to my grandparents, Jack and Jackie Pearce.

Abstract

This thesis investigates the influence of atmospheric nitrate aerosol on air quality, human health and the present day aerosol cloud-albedo radiative effect. This research represents the first application of the UM-UKCA model with the nitrate-extended version of the GLOMAP-mode aerosol microphysics module.

The UM-UKCA model generally represents the spatial distribution of annual mean nitrate, ammonium and sulphate aerosol concentrations well ($R > 0.6$) over Europe and North America but performs less well over East Asia. The model tends to underestimate concentrations relative to ground-based and aircraft observations. However, global burdens and mean surface concentrations of nitrate (NO_3^-), ammonium (NH_4^+) and sulphate (SO_4^{2-}) aerosol are within the multi-model range simulated by participating models in the AeroCom Phase III (AP3) nitrate intercomparison. The inclusion of heterogeneous N_2O_5 hydrolysis in UM-UKCA decreases regional low model bias of nitrate aerosol, particularly in wintertime. The size distribution of simulated NO_3^- is sensitive to the approach applied to treat the gas-particle partitioning of the inorganic NO_3^--NH_4^+-SO_4^{2-}-Na^+-Cl^- aerosol system. Reverting to an equilibrium approach to treat the gas-particle partitioning leads to overestimation of coarse mode nitrate aerosol, relative to applying a hybrid approach, at the expense of nitric acid uptake into the fine mode.

The contribution of nitrate aerosol to surface $PM_{2.5}$ and to the $PM_{2.5}$-attributable health burden over the EU28, USA, India and China is quantified. Of these regions, nitrate aerosol made the greatest relative contribution to present day (year 2008) annual mean AWM and PWM $PM_{2.5}$ (13.4% - 16.3%) and to $PM_{2.5}$-attributable mortality (15.6%; 31,500 [20,100 - 41,300] deaths) over the EU28. Comparison to a scenario with year 1980 emissions, demography and background disease rates showed that the relative contribution of nitrate aerosol to the total ambient $PM_{2.5}$-attributable mortality increased over the EU28 (6.2% to 15.6%), USA (3.9% to 7.8%), India (1.3% to 3.4%) and China (4.0% to 5.8%) as a result of recent decadal changes.

Finally, it is found that simulated N_3, N_{50} and CDNC undergo large relative regional increases of up to 60%, when nitrate aerosol formation is included using a hybrid gas-particle partitioning approach. A global mean PD nitrate cloud albedo radiative effect of -0.007 Wm^{-2} was calculated using the hybrid approach, though the influence of nitrate aerosol on regional radiative effects was larger (-0.5 to +1 W m^{-2}). Reverting to an equilibrium gas-particle partitioning approach resulted in a weaker response of aerosol number concentrations and CDNC to nitrate aerosol formation over much of the Northern Hemisphere and cloudy marine regions in the Southern Hemisphere, leading to a sign reversal in the PD nitrate cloud albedo radiative effect to +0.011 W m^{-2}. It is therefore concluded that models applying an equilibrium approach to treat nitrate aerosol formation may under-represent the influence of nitrate aerosol on aerosol properties and aerosol-cloud radiative effects.

Table of Contents

Abbreviations

AP3	**A**eroCom **P**hase **III**
ACCMIP	**A**tmospheric **C**hemistry and **C**limate **M**odel **I**ntercomparison **Project**
ADIENT	**A**ppraising the **D**irect **I**mpacts of **A**erosol on **C**limate
AeroCom	**Aero**sol **C**omparisons between **O**bservations and **M**odels Project
AIE	**A**erosol **I**ndirect **E**ffect
AMoN	**A**mmonia **Mon**itoring Network
AOD	**A**erosol **O**ptical **D**epth
AR5	**5**th **A**ssessment **R**eport of the IPCC
ARCTAS	**A**rctic **R**esearch of the **C**omposition of the **T**roposphere from **A**ircraft and **S**atellites Project
AWM	**A**rea **w**eighted **m**ean
CAE	**C**loud **A**lbedo **E**ffect
CASTNET	**C**lean **A**ir **S**tatus and **T**rends **Net**work
CCN	**C**loud **C**ondensation **N**uclei
CDN	**C**loud **D**roplet **N**umber
CDNC	**C**loud **D**roplet **N**umber **C**oncentration
CLASSIC	**C**oupled **L**arge-scale **S**imulator for **S**tudies in **C**limate aerosol scheme
CMIP	**C**oupled **M**odel **I**ntercomparison **P**roject
COPD	**C**hronic obstructive pulmonary disease
CTM	**Chemical transport model**
D	**D**iameter
DJF	**D**ecember, **J**anuary and **F**ebruary
EANET	Acid Deposition Monitoring **Net**work in **E**ast **A**sia
EMEP	**E**uropean **M**onitoring and **E**valuation **P**rogramme
EU and EU28	**E**uropean **U**nion (**28** member states)
EUCAARI	**Eu**ropean Integrated Project on **A**erosol **C**loud Climate and **Ai**r Quality **I**nteractions
EUSAAR	**Eu**ropean **S**upersites for **A**tmospheric **A**erosol **R**esearch
FT	**F**ree **T**roposphere
GASSP	**G**lobal **A**erosol **S**ynthesis and **S**cience **P**roject aerosol database
GBD	**G**lobal **B**urden of **D**isease

GLOMAP-mode	Modal version of the **G**lobal **M**odel of **A**erosol **P**rocesses
GUAN	**G**erman **U**ltrafine **A**erosol **N**etwork
HTAP	**H**emispheric **T**ransport of **A**ir **P**ollution
HyDiS-1.0	**Hy**brid D**i**ssolution **S**olver
ICEALOT	**I**nternational **C**hemistry **E**xperiment in the **A**rctic **LO**wer **T**roposphere
IERs	**I**ntegrated **E**xposure **R**esponse functions
IHD	**I**schemic **H**eart **D**isease
IMPROVE	**I**ntegrated **M**onitoring of **PRO**tected **V**isual **E**nvironment
IPCC	**I**ntergovernmental **P**anel on **C**limate **C**hange
ISCCP	**I**nternational **S**atellite **C**loud **C**limatology **P**roject
JJA	**J**une, **J**uly and **A**ugust
LRI	**L**ower **R**espiratory **I**nfection
MACCity	**MACC** and **City**Zen project
MAM	**M**arch, **A**pril and **M**ay
N_3	**N**umber concentration of particles with diameter greater than **3 nm**
N_{50}	**N**umber concentration of particles with diameter greater than **50 nm**
NMB	**N**ormalised **M**ean **B**ias
OP3	**O**xidant and **P**articulate **P**hotochemical **P**rocesses Above a South East Asian Rainforest project
PD	**P**resent **D**ay
PI	**P**re-**i**ndustrial
PM_{10}	**P**articulate **m**atter with aerodynamic dry diameter below **10** μm
$PM_{2.5}$	**P**articulate **m**atter with aerodynamic dry diameter below **2.5** μm
PWM	**P**opulation **w**eighted **m**ean
R	Pearson correlation coefficient
RCP	**R**epresentative **C**oncentration **P**athway
RR	**R**elative **R**isk
SOA	**S**econdary **O**rganic **A**erosol
SOCRATES	**S**uite of **C**ommunity **R**adiative **T**ransfer codes based on **E**dwards and **S**lingo
SON	**S**eptember, **O**ctober and **N**ovember
STP	**S**tandard **T**emperature and **P**ressure (298K, 1 atm)
TMREL	**T**heoretical **M**inimum **R**isk **E**xposure **L**evel
TOA	**T**op **o**f the **A**tmosphere

TOMCAT	**T**oulouse **O**ff-line **M**odel of **C**hemistry and **T**ransport
UKCA	**U**nited **K**ingdom **C**hemistry and **A**erosol Project
UM or MetUM	UK **Met**eorological Office **U**nified **M**odel
VOCALS-UK	**V**AMOS **O**cean-**C**loud-**A**tmosphere-**L**and Regional Experiment
WHO	**W**orld **H**ealth **O**rganisation
YLL	**Y**ears of **L**ife **L**ost

List of Tables

List of Figures

1. Introduction

1.1 Motivation

Nitrate aerosol constitutes a major component of atmospheric particulate matter in industrialised regions over Europe (Schaap et al., 2004; Crosier et al., 2007; Putaud et al., 2010; Morgan et al., 2010a; Squizzato et al., 2013), the USA (Malm et al., 2004; Silva et al., 2007; Hand et al., 2012; Pusede et al., 2016) and Asia (Pathak et al., 2009; Ying et al., 2014; Snider et al., 2016). Like other aerosol, the presence of atmospheric nitrate affects the Earth's climate through its direct scattering of radiation and modification of cloud properties. Furthermore, its contribution to fine particulate matter at the surface degrades air quality, adversely affects human health and influences atmospheric chemistry and ecology.

The third phase of the Aerosol Comparisons between Observations and Models (AeroCom Phase III) intercomparison exercise found that the global nitrate aerosol burden was equivalent to approximately a third of sulphate in terms of total global burden and global mean surface concentration (Bian et al., 2017). However, the inter-model diversity in simulated nitrate concentrations was large, with the global mean nitrate aerosol burden ranging by a factor of 13.4 and global mean surface nitrate concentrations varying by a factor of 9.4 between the 9 participating models.

Long-term exposure to ambient fine particulate matter ($PM_{2.5}$: mass concentration of particles with a dry diameter below 2.5 μm) has been linked to approximately 4.2 million premature deaths globally through the exacerbation of respiratory, cardiovascular and cerebrovascular disease (Cohen et al., 2017). Previous work shows that nitrate aerosol makes a large (>25%) contribution to regional population-weighted $PM_{2.5}$ over Europe and is one of four major aerosol components driving a global increase in population-weighted $PM_{2.5}$ since 1990, after organic aerosols and before sulphate and ammonium aerosol (Li et al., 2017). Studies have focussed on industrial and transport-related emissions and have increasingly focussed on the agricultural emissions sector as a means of reducing $PM_{2.5}$ concentrations and its associated health burden, through reducing precursors to ammonium nitrate aerosol formation (Megaritis et al.,

2013; Bessagnet et al., 2014; Paulot and Jacob, 2014; Lee et al., 2015; Lelieveld et al., 2015; Bauer et al., 2016; Pozzer et al., 2017). The importance of nitrate aerosol for $PM_{2.5}$-attributable mortality is implied by these studies, but its specific contribution to mortality has never been directly quantified.

Climate-related risks to livelihoods, food security and water supply are projected to increase with global warmings of 1.5 °C and 2 °C, resulting in impacts also on health, human security and economic growth (Masson-Delmotte et al., 2018). Global atmospheric models of increasing complexity have been developed to better understand atmospheric aerosol composition and aerosol-climate feedbacks. However, the radiative effect of atmospheric aerosol has remained highly uncertain through successive assessments of the Intergovernmental Panel on Climate Change (IPCC; Boucher et al., 2013). Despite its large contribution to atmospheric composition, the radiative impacts of nitrate aerosol have been understudied relative to other aerosol species, such as sulphate, mainly due to complexities in simulating its semi-volatile nature. The Fifth Assessment Report from the IPCC (AR5) yielded a global mean radiative forcing due to aerosol-radiation interactions from nitrate aerosol of -0.11 (-0.3 - -0.03) W m^{-2}, though the majority of contributing models to the 5th Coupled Model Intercomparison Project (CMIP5) did not simulate nitrate aerosol (Boucher et al., 2013; Myhre et al., 2013b). Five of the ten participating Atmospheric Chemistry and Climate Model Intercomparison Project (ACCMIP) models accounted for nitrate aerosol in their simulations (Shindell et al., 2013). The indirect (cloud albedo) aerosol effect of nitrate aerosol is particularly poorly understood having been assessed by a small number of dedicated global model studies (Bellouin et al., 2011; Xu and Penner, 2012).

The relative importance of nitrate aerosol for climate is expected to increase in the coming decades under projected emission scenarios (Adams et al., 2001; Bauer et al., 2007; Bellouin et al., 2011; Hauglustaine et al., 2014; Bauer et al., 2016; Paulot et al., 2016). Several global modelling studies have identified that nitrate aerosols could overtake sulphate by the end of the 21st century as the dominant scattering aerosol species (e.g. Bauer et al., 2007; Bellouin et al., 2011; Hauglustaine et al., 2014), which would decelerate projected decreases in global mean aerosol forcing where nitrate aerosol has not been considered.

Despite its recognised importance for air quality and climate, the treatment of nitrate aerosol in composition-climate models is often heavily simplified or omitted completely. Ammonium nitrate is semi-volatile, with two-way gas-particle partitioning occurring into and out of the particle phase. Representation of this semi-volatile inorganic aerosol system can add considerable complexity to global model simulations and, in the interest of computational efficiency, simplified partitioning schemes that assume instantaneous equilibrium have become the convention. However, this equilibrium approach can overestimate the uptake of nitric acid into coarse mode aerosol at the expense of submicron aerosol formation (Ansari and Pandis, 1999; Capaldo et al., 2000; Moya et al., 2001; Feng and Penner, 2007; Benduhn et al., 2016). To address this, some models have applied a more physically realistic hybrid approach, which calculates partitioning to the particle phase using either an equilibrium assumption or dynamic mass transfer, depending on the particle size (Capaldo et al., 2000; Feng and Penner, 2007; Trump et al., 2015; Benduhn et al., 2016). The implications for model radiative transfer of applying a simplified equilibrium approach as opposed to a more physically realistic hybrid approach for simulating nitrate aerosol have not been previously quantified.

1.2 Thesis Aims

The overall aim of the work in this thesis is to evaluate atmospheric nitrate aerosol concentrations and quantify the significance of nitrate aerosol for air pollution, human premature mortality and climate. The primary research tool used in this thesis is the Met Office's Unified Model (UM) with the United Kingdom Chemistry and Aerosol sub-model (UKCA), applying the recently developed nitrate-extended version of the modal Global Model of Aerosol Processes (GLOMAP-mode). This version of GLOMAP-mode applies a hybrid approach to treat the two way gas-particle partitioning of inorganic semi-volatile species, which has been shown to give a physically realistic representation of the size-resolved sulphate-nitrate-ammonium-sodium-chloride aerosol system whilst retaining computational efficiency (Benduhn et al., 2015). Chapter 2 provides the background and status of existing literature on nitrate aerosol and

its impacts. The research tools and methodologies employed in this thesis are described in Chapter 3. The aims and research questions to be addressed in results Chapters 4, 5 and 6 are detailed below. Finally, conclusions and avenues for future research are summarised in Chapter 7.

1. The first research aim is to comprehensively evaluate the size-resolved nitrate, ammonium and sulphate aerosol concentrations in UM-UKCA on seasonal and annual mean timescales. The following questions are to be addressed:

    (a) How well does the global model reproduce observed seasonal and annual mean secondary inorganic aerosol and precursor gas concentrations compared to surface observations over Europe, the USA and East Asia?

    (b) Does the model capture vertical variability in secondary inorganic aerosol concentrations compared to field campaign aircraft-based measurements?

    (c) Are the UM-UKCA simulated annual mean secondary inorganic aerosol concentrations within the range of those simulated by other models in the AeroCom Phase III multi-model intercomparison exercise?

    (d) How are size-resolved nitrate aerosol concentrations influenced when using a physically realistic benchmark hybrid approach for gas-particle partitioning compared to a simpler and conventionally adopted equilibrium approach?

    (e) What is the influence of activating heterogeneous N_2O_5 hydrolysis on simulated seasonal mean nitrate aerosol concentrations?

    (f) What future developments are recommended to the nitrate aerosol representation in the UM-UKCA model?

2. The second research aim is to quantify the contribution of nitrate aerosol to regional present day $PM_{2.5}$ composition and attributable mortality, and the changing influence of nitrate aerosol on mortality resulting from post-1980

emission changes over Europe, the USA, India and China. The following questions will be addressed:

(a) How does the inclusion of nitrate aerosol formation in UM-UKCA influence the simulated $PM_{2.5}$, compared to observations over Europe, the United States, India and China?

(b) What fraction of the area-weighted and population-weighted mean $PM_{2.5}$ concentrations is associated with nitrate aerosol in these regions?

(c) What is the present day impact of long-term exposure to atmospheric nitrate aerosol on regional health burdens, in terms of premature mortality and years of life lost?

(d) How has the impact of nitrate aerosol on area-weighted and population weighted mean $PM_{2.5}$ composition been altered as a result of post-1980 changes in anthropogenic emissions?

(e) How has the contribution of nitrate aerosol to premature mortality changed as a result of post-1980 changes in anthropogenic emissions, demography and background disease?

3. The third aim of this thesis is to quantify the radiative impact of present day nitrate aerosol via its influence on cloud albedo, using two gas-particle partitioning approaches. The following questions are investigated:

(a) How does nitrate aerosol formation influence present day atmospheric total particle number concentrations?

(b) What is the influence of nitrate aerosol formation on N_{50} and cloud droplet number concentrations?

(c) What is the present day cloud albedo radiative effect of nitrate aerosol formation resulting from the above changes in particle number and cloud droplet number concentrations?

d) Is a hybrid gas-particle partitioning mechanism important for all of the above, compared to a conventional equilibrium gas-particle partitioning approach?

2. Background and status of existing work

2.1 Tropospheric aerosol

Atmospheric aerosol are suspensions of solid and/or liquid particles in air, with diameters ranging over four orders of magnitude from a few nanometres to around 100 μm (Seinfeld and Pandis, 2006). Aerosol are either emitted directly into the atmosphere (i.e. primary aerosol) or are formed in the atmosphere by chemical reactions (i.e. secondary aerosol). Primary aerosol and gas-phase aerosol precursors are produced from a variety of natural and anthropogenic sources. Anthropogenic aerosol found in the troposphere consist mainly of sulphate (SO_4^{2-}), nitrate (NO_3^-), ammonium (NH_4^+), black carbon (BC) and organic carbon (OC). Natural components of the tropospheric aerosol include mineral dust, sea salt and volcanic sulphate. The size distribution is an important characteristic of an aerosol population and is usually defined in terms of four diameter (D) range classifications (Seinfeld and Pandis, 2006): nucleation (D < 10 nm), Aitken (10 nm < D < 100 nm), accumulation (100 < D < 1 μm) and coarse (D > 1 μm).

The size, composition and mass of aerosol is determined by microphysical processes, including nucleation, condensation, coagulation, hygroscopic growth, ageing and in-cloud processing. Aerosol sinks include dry deposition and wet scavenging by precipitation. Dry deposition describes the removal of particles to the Earth's surface by gravity (sedimentation), impaction and/or diffusion. Wet scavenging of aerosol is associated with precipitation and includes both nucleation and impaction scavenging. Nucleation scavenging occurs within the cloud when aerosol particles act as cloud condensation or ice nuclei and are dissolved or embedded in the resulting hydrometeors. Impaction scavenging occurs in- and below-cloud when falling hydrometeors collide with airborne particles, collect them and subsequently carry them down to the surface.

The spatial distribution of atmospheric aerosol is strongly dependent on the distribution of sources and sinks, which control the lifetime of aerosol in the atmosphere as it is transported. The lifetime of aerosol in the troposphere is typically on the order of a few days to weeks (Seinfeld and Pandis, 2006). This

relatively short atmospheric lifetime of aerosols, combined with an inhomogeneous geographical distribution of aerosol sources, leads to large variability in the spatial distribution of global aerosol.

The impacts of atmospheric aerosol on air quality, climate, atmospheric chemistry and ecology (see Section 2.2) are dependent on the aerosol size, composition, concentration and spatial distribution. Global aerosol microphysics models of increasing complexity have been developed to represent the aerosol system and incorporated into climate and Earth system models, in order to accurately characterise these impacts.

2.2 Impacts of atmospheric aerosol

2.2.1 Air quality and health impacts of aerosol

The presence of atmospheric aerosol at the surface leads to degradation of ambient air quality. Long-term exposure to atmospheric PM_{10} (i.e. the mass of particulate matter with aerodynamic dry diameters below 10 μm) and $PM_{2.5}$ (of diameter below 2.5 μm) can contribute to increases in premature mortality, morbidity and lower life expectancy (Dockery et al., 1994; Pope et al., 1995; Pope III and Dockery, 2006). Atmospheric aerosol particles therefore most adversely impact on health when present in populated regions at sizes below these thresholds. Long-term exposure to $PM_{2.5}$ is associated with approximately 4.2 million premature deaths globally per year (Cohen et al., 2017), making it a major contributing factor to regional and global burdens of disease (Forouzanfar et al., 2016; Lim et al., 2012).

The adverse health implications from long-term exposure to $PM_{2.5}$ include increased mortality from acute lower respiratory infections, cerebrovascular disease, ischaemic heart disease, chronic obstructive pulmonary disease and lung cancer (Burnett et al., 2014). Integrated exposure response functions (IERs) have been developed as a means of quantifying the relative risk to human health of exposure to $PM_{2.5}$ (Pope et al., 2009; Pope et al., 2011; Burnett et al., 2014). Table 2.1 shows the air quality guideline and interim targets for annual mean concentrations of $PM_{2.5}$ and PM_{10} set by the World Health Organisation (WHO). It is estimated that approximately 87% of the global population currently live in

areas where mean ambient $PM_{2.5}$ concentrations exceed the WHO air quality guideline of 10 μg m^{-3} (Apte et al., 2015).

Table 2.1 *WHO air quality guidelines and interim targets for particulate matter: annual mean concentrations.*

	PM_{10} (μg m^{-3})	$PM_{2.5}$ (μg m^{-3})
Interim target-1 (IT-1)	70	35
Interim target-2 (IT-2)	50	25
Interim target-3 (IT-3)	30	15
Air quality guideline	20	10

2.2.2 Aerosol radiative effects

Aerosol can modify the Earth's atmospheric radiative budget and therefore exert a radiative forcing on the climate system through direct, indirect and semi-direct interactions with radiation. The 5th Assessment report (AR5) of the Intergovernmental Panel on Climate Change (IPCC) uses the term 'effective radiative forcing' to describe the change in radiative balance from both instantaneous radiative perturbations and subsequent rapid adjustments (Boucher et al., 2013). Since the AR5, the effective radiative forcing from aerosol has been categorised into aerosol-radiation interactions (direct and semi-direct effects) and aerosol-cloud interactions (indirect cloud albedo and lifetime effects). The direct and indirect effects are described individually here.

2.2.2.1 The direct aerosol radiative effect

Particles in the atmosphere can directly scatter or absorb incoming solar radiation. The extent to which particles interact with radiation is determined by their size, composition and optical properties. Scattering aerosol increase the planetary albedo and have a cooling effect on climate, while absorbing aerosol may warm or cool the climate depending on the albedo of the underlying surface.

The scattering efficiency of particles is greatest at sizes between 380 nm and 750 nm because incoming solar radiation peaks at these wavelengths.

Table 2.2 shows the global and annual mean radiative forcing due to aerosol-radiation interactions between 1750 and the present day from the last four IPCC assessments. The direct aerosol radiative effect is thought, overall, to lead to a cooling effect on global climate, with AR5 reporting a total global mean radiative forcing of -0.35 ± 0.5 W m^{-2}. However, the magnitude of this forcing remains a major uncertainty with little reduction in the uncertainty range over successive IPCC reports, despite developments in global aerosol modelling and understanding of aerosol processes. Nitrate aerosol has been under-represented in successive IPCC reports when investigating individual aerosol contributions to the direct radiative forcing, with no evaluation of its forcing included in the second and third assessment reports and with the majority of CMIP5 models also excluding it from their simulations (Boucher et al., 2013; Myhre et al., 2013b).

Table 2.2 *Global and annual mean RF (W m^{-2}) due to aerosol-radiation interactions between 1750 and 2011 of seven aerosol components for the IPCC Fifth Assessment Report (AR5) and for the second (SAR), third (TAR) and fourth (AR4) assessment reports where available. The uncertainty range is given in brackets. The end years for the SAR, TAR and AR4 are 1993, 1998 and 2005, respectively. From Boucher et al. (2013).*

Global Mean Radiative Forcing (W m^{-2})				
	SAR	TAR	AR4	AR5
Sulphate aerosol	−0.40 (−0.80 to −0.20)	−0.40 (−0.80 to −0.20)	−0.40 (−0.60 to −0.20)	−0.40 (−0.60 to −0.20)
Black carbon aerosol from fossil fuel and biofuel	+0.10 (+0.03 to +0.30)	+0.20 (+0.10 to +0.40)	+0.20 (+0.05 to +0.35)	+0.40 (+0.05 to +0.80)
Primary organic aerosol from fossil fuel and biofuel	Not estimated	−0.10 (−0.30 to −0.03)	−0.05 (0.00 to −0.10)	−0.09 (−0.16 to −0.03)
Biomass burning	−0.20 (−0.60 to −0.07)	−0.20 (−0.60 to −0.07)	+0.03(−0.09 to +0.15)	−0.0 (−0.20 to +0.20)
Secondary organic aerosol	Not estimated	Not estimated	Not estimated	−0.03 (−0.27 to +0.20)
Nitrate	Not estimated	Not estimated	−0.10 (−0.20 to 0.00)	−0.11 (−0.30 to −0.03)
Dust	Not estimated	−0.60 to +0.40	−0.10 (−0.30 to +0.10)	−0.10 (−0.30 to +0.10)
Total	Not estimated	Not estimated	−0.50 (−0.90 to −0.10)	−0.35 (−0.85 to +0.15)

2.2.2.2 Indirect aerosol radiative effects

Aerosol particles can also modify climate indirectly via the modification of cloud properties (radiative properties and precipitation efficiency). Aerosol particles of certain size and chemical composition act as cloud condensation nuclei (CCN), thereby providing a surface on which water vapour can condense and grow to

liquid water droplets. The presence of CCN lowers the supersaturation needed for droplet growth to below that required for homogenous nucleation of water droplets. Particles can also act as ice nuclei, which enable ice formation from water vapour and reduce the energy barrier required for super-cooled liquid water droplets to freeze above approximately -40°C (Rogers and Yau, 1989).

The main mechanisms through which aerosol indirectly influence the climate are the *cloud albedo* (Twomey, 1977) and *lifetime* (Albrecht, 1989) effects. The former, also known as the *first aerosol indirect effect*, occurs when an increase in the number concentration of cloud condensation nuclei (CCN) at a constant liquid water content leads to more numerous but smaller droplets. The resulting increase in cloud reflectivity has a cooling effect on climate (Twomey, 1977). The latter, also termed the *second aerosol indirect effect*, refers to the increase in cloud lifetime arising from the slower growth of these smaller cloud droplets to form precipitable rain drops. This prolongs the radiative cooling from clouds.

2.2.3 Aerosol influence on atmospheric chemistry

As introduced in Section 2.2.2, many atmospheric aerosol components scatter incoming solar radiation. These can impact on photolysis rates and perturb photochemical oxidant production (e.g. Benas et al., 2013; Xing et al., 2017). Tropospheric aerosol also provide a surface on which heterogeneous chemical reactions can occur, with implications for gas-phase chemistry. For example, Tie et al. (2003) found that the heterogeneous hydrolysis of dinitrogen pentoxide (N_2O_5) provides an important sink pathway for NO_x, with consequences for ozone (O_3) formation, and Pope et al. (2015) found that overestimations in wintertime NO_x column concentrations over Europe were reduced when heterogeneous N_2O_5 hydrolysis was included in air quality simulations. HO_2 uptake is also enhanced by the presence of aerosol, with implications for the oxidative capacity of the atmosphere (e.g. Macintyre and Evans, 2011; Huijnen et al., 2014). For example, decreasing trends in regional $PM_{2.5}$ over the North China Plain have been found to slow down the uptake of HO_2 and enhance O_3 formation (Li et al., 2019). Heterogeneous uptake of gases, for example onto dust, has also been the focus of many studies (e.g. Karydis et al., 2016; Tang et al., 2017). The presence of aerosol in cloud can also alter rainwater pH, which in turn can

influence aerosol formation. For example, the in-cloud oxidation of SO_2 by O_3 to form sulphate aerosol is pH dependent (e.g. Turnock, 2016).

Aerosol chemistry interactions are important for nitrate aerosol, which itself is formed from heterogeneous reactions of nitrogen species (N_2O_5, NO_3 and HNO_3). Several studies have suggested that the presence of nitrate in aerosol can inhibit heterogeneous N_2O_5 hydrolysis and therefore self-limit nitrate aerosol formation (e.g. Bertram and Thornton, 2009). Nitrate can also be formed from the reactive uptake of trace gases onto dust and sea salt particles (Karydis et al., 2016; Chen et al., 2016) and provides a major sink for NO_x species. Ammonium nitrate aerosol is semi-volatile and re-releases nitric acid and ammonia gas under certain atmospheric conditions (see Section 2.3), therefore influencing the spatial distribution of these gases.

2.2.4 Ecological impacts of aerosol

Atmospheric aerosol and gases can contribute to ecological issues of acidification and eutrophication when deposited to soil, vegetation canopy and freshwaters (Bouwman et al., 2002). The scattering of radiation by aerosol also changes the amount of direct and diffuse radiation that reaches vegetation with implications for plant photosynthesis (e.g. Mercado et al., 2009; Mahowald, 2011; Rap et al., 2015). Nitrogen is also important as a nutrient and the deposition of nitrate aerosol may enhance the growth of vegetation, with potential implications also for terrestrial carbon sequestration (e.g. Mahowald, 2011; O'Sullivan et al., 2019).

Acidification is the build-up of protons in soil and freshwaters, leading to reductions in the pH and subsequent damage to these systems. The deposition of acidifying compounds, including nitrate, ammonium and sulphate aerosol and their precursor gases of nitric acid, ammonia and sulfuric acid is subject to large regional variations (Rodhe et al., 2002). Such deposition is damaging to ecology and also human infrastructure. Eutrophication is the over-enrichment of a lake or body of water with nutrients, inducing excessive plant and algal growth and resulting in oxygen depletion and loss of biodiversity. It is most often caused by run-off of nitrogen and phosphorus based fertilisers but is also influenced by aerosol deposition, where nitrogen is often a limiting nutrient in biomass

production (Bergström and Jansson, 2006; Bouwman et al., 2002). Secondary inorganic aerosols have a longer atmospheric lifetime than their precursor gases and can therefore influence spatial patterns of acid and nitrogen deposition.

Another interaction of aerosol with vegetation arises through its impact on radiation. By scattering incoming radiation, atmospheric aerosol reduces direct radiation that reaches the canopy but increases the diffuse fraction of radiation. The reduction in direct radiation inhibits photosynthesis efficiency while the increased diffusivity encourages photosynthesis by illuminating sections of the lower canopy that would have otherwise been shaded. These effects compete to determine whether atmospheric aerosol will encourage or inhibit vegetation growth (e.g. Mercado et al., 2009; Rap et al., 2015; O'Sullivan et al., 2016). Nitrogen availability can also enhance or inhibit the growth of vegetation, with potential implications for the terrestrial carbon sink (Mahowald, 2011; O'Sullivan et al., 2019). These ecological impacts and feedbacks will not be studied in this thesis but provide further motivation for studying atmospheric aerosol, and secondary inorganic aerosol in particular.

2.3 Nitrate aerosol formation

Inorganic nitrate aerosol is formed in the atmosphere from the reaction of its precursor species, mainly gaseous nitric acid and alkaline gas and aerosol species including ammonia, sea salt and dust.

Figure 2.1 shows an overview of tropospheric inorganic nitrogen chemistry. Semi-volatile ammonium nitrate is produced from the reaction of nitric acid (HNO_3) with ammonia (NH_3). Globally, ammonia emissions are dominated by agricultural practices, which can contribute 90 – 100% of NH_3 emissions in Western Europe and the United States (Bouwman et al., 1997; Sutton et al., 2000). Nitric acid is formed from reactions of emitted nitrogen oxides (NO_x). NO_x emission sources include anthropogenic fossil fuel combustion and agriculture, biomass burning soil and lightning (e.g. Olivier et al., 1998; Jaeglé et al., 2005; Tost, 2017; van der Werf et al., 2010). NO_x is inefficiently dry and wet deposited to the Earth's surface and nitric acid formation therefore represents its main

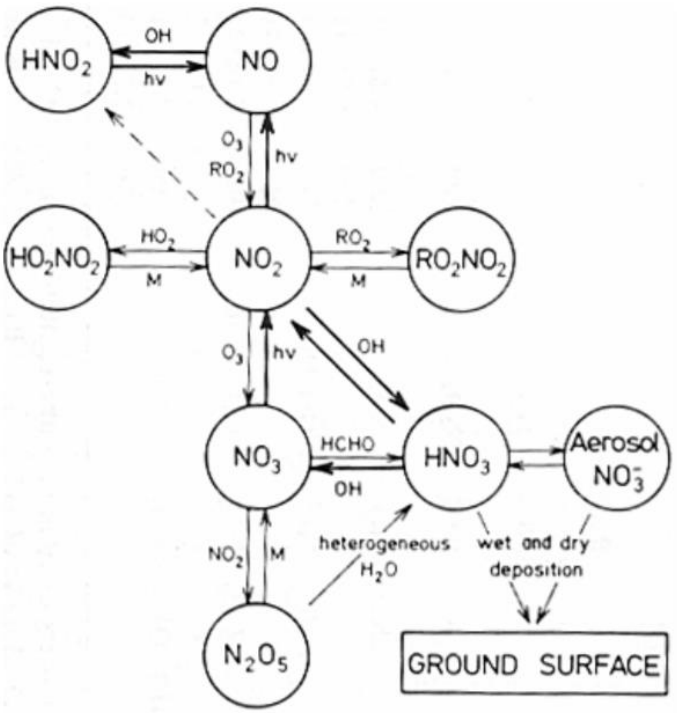

Figure 2.1 *Overview of tropospheric inorganic nitrogen chemistry. From Finlayson-Pitts and Pitts Jr (1999)*

removal sink. There are two main chemical pathways through which NO_x is converted to nitric acid. The first is the daytime reaction of nitrogen dioxide (NO_2) with the hydroxyl radical, OH (equation 2.1).

$$NO_2 + OH \rightarrow HNO_3 \qquad (2.1)$$

The second pathway for nitric acid formation involves formation of the NO_3 radical and heterogeneous N_2O_5 hydrolysis, following equations 2.2 to 2.4. These reactions form the dominant nitric acid formation pathway during darkness because the intermediary NO_3 radical and N_2O_5 are rapidly photo-dissociated in sunlight (equations 2.5 to 2.8)

$$NO_2 + O_3 \rightarrow NO_3 + O_2 \qquad (2.2)$$

$$NO_3 + NO_2 \rightarrow N_2O_5 \qquad (2.3)$$

$$N_2O_5 + H_2O \xrightarrow{aerosol} 2HNO_3 \qquad (2.4)$$

$$N_2O_5 + hv \rightarrow NO_2 + NO_3 \quad (2.5)$$

$$NO_3 + hv \rightarrow NO + O_2 \quad (2.6)$$

$$NO_3 + hv \rightarrow NO_2 + O \quad (2.7)$$

$$N_2O_5\ (+M) \rightarrow NO_2 + NO_3\ (+M) \quad (2.8)$$

Some of this nitric acid will react during the day to reproduce NO_x but this is a relatively slow reaction. Most nitric acid is removed through wet or dry deposition and through uptake into the particulate phase to form nitrate aerosol. Dry deposition of HNO_3 is approximately 10 times faster than that of particulate phase nitrate (Seinfeld and Pandis, 1998) and this gas-particle partitioning therefore influences the removal rate of atmospheric total nitrate (i.e. the sum of both gaseous nitric acid and particulate nitrate aerosol; Aw and Kleeman, 2003; Fagerli and Aas, 2008).

As mentioned, nitric acid can condense onto existing aerosol particles to form particulate nitrate aerosol. Over continental regions nitric acid is mostly neutralised in the aerosol phase by the presence of ammonia (NH_3), forming ammonium nitrate (NH_4NO_3) by equations 2.9 and 2.10. Ammonium nitrate is dissolved (internally mixed) with other components within liquid aerosol and its formation occurs via dissolution: a combination of condensation and partial dissociation (Benduhn et al., 2016).

$$NH_{3\,(g)} + HNO_{3\,(g)} \leftrightarrow NH_4NO_{3\,(s,aq)} \quad (2.9)$$

$$NH_{3\,(g)} + HNO_{3\,(g)} \leftrightarrow NH_{4\,(l)}^{+} + NO_{3\,(l)}^{-} \quad (2.10)$$

The reaction of nitric acid with ammonia to produce ammonium nitrate is a major formation pathway for nitrate aerosol, particularly in continental regions. NH_4NO_3 is semi-volatile in nature, such that it can re-evaporate from the aerosol aqueous phase depending on ambient conditions. The equilibrium between gaseous nitric acid, gaseous ammonia and particulate phase nitrate aerosol contributes to spatial and temporal variability in nitrate aerosol concentration. Nitrate concentrations have been observed to regularly peak in the upper boundary layer where colder temperatures and higher relative humidity favours

the particulate phase (e.g. Morino et al., 2006; Crosier et al., 2007; Morgan et al., 2010b). The semi-volatile nature of nitrate aerosol also contributes to large diurnal variability in its concentration as particulate is formed at night and re-volatises throughout the day (Morgan et al., 2010b; Aan de Brugh et al., 2012; Pusede et al., 2016). Seasonal variability also arises, with higher nitrate aerosol concentrations often measured in the colder winter months and in springtime episodes associated with agricultural NH_3 emissions (e.g. Hand et al., 2012; Perrino et al., 2014; Vieno et al., 2016).

The formation of ammonium nitrate is not only dependent on atmospheric nitric acid and ammonia concentrations but also on sulphate aerosol and gaseous sulphuric acid concentrations. Ammonium nitrate has a low vapour pressure so preferentially condenses onto pre-existing aerosol, namely sulphate. However, dissolution of nitric acid into the aqueous aerosol phase only proceeds once the present sulphuric acid is fully neutralised by ammonia because this determines the amount of excess ammonia available to stabilise nitric acid within the aerosol. In regimes where excess nitric acid is available, a decrease in sulphate aerosol concentration may therefore indirectly increase nitrate aerosol concentrations. The response of fine aerosol mass and aerosol radiative forcing to changes in precursor concentrations can therefore be non-linear.

Nitrate aerosol is also formed by the uptake of nitric acid onto sea salt and dust particles (e.g. Savoie and Prospero, 1982; Allen et al., 2015; Liu et al., 2015; Karydis et al., 2016; Bian et al., 2017). Nitrate aerosol formed by these pathways are non-volatile, with gaseous nitric acid partitioning irreversibly into the particulate phase and predominantly into the coarse mode. The heterogeneous reaction of nitric acid with sea salt produces sodium nitrate ($NaNO_3$) aerosol and hydrogen chloride as per equation 2.11 and is a large source of nitrate aerosol (e.g. Allen et al., 2015; Liu et al., 2015; Itahashi et al., 2016). Sea salt aerosol also provides a surface on which heterogeneous N_2O_5 hydrolysis can occur, producing nitric acid (eq. 2.4).

$$NaCl_{(s)} + HNO_{3\,(g)} \rightarrow NaNO_{3\,(s)} + HCl_{(g)} \qquad (2.11)$$

Another major pathway for nitrate aerosol formation is via the adsorption of nitric acid onto dust and reaction with other light metallic species, including calcium, magnesium and potassium, as in equations 2.12 to 2.14 (e.g. Karydis et al., 2016; Bian et al., 2017).

$$Ca^{2+}_{(s)} + 2NO^{-}_{3\,(g)} \rightarrow Ca(NO_3)_2 \quad (2.12)$$

$$Mg^{2+}_{(s)} + 2NO^{-}_{3\,(g)} \rightarrow Mg(NO_3)_2 \quad (2.13)$$

$$K^{+}_{(s)} + NO^{-}_{3(g)} \rightarrow KNO_3 \quad (2.14)$$

2.4 Existing studies on nitrate aerosol

The complex nature of nitrate aerosol formation, including its co-dependency on several precursor species and its semi-volatility (see Section 2.3), provides a challenge for global aerosol models. The remaining sections of this chapter describes the challenges associated with representing the two-way (semi-volatile) gas-particle partitioning of nitrate aerosol in global chemistry models in addition to the current scientific understanding of atmospheric nitrate aerosol concentrations and its implications for air quality, human health and climate.

2.4.1 Gas to particle partitioning of nitrate aerosol in global models

The semi-volatile partitioning of size-resolved nitrate aerosol between the gas and particle phase presents a major challenge for global aerosol models. Several approaches have been adopted within models, which may be divided into equilibrium, dynamic and hybrid approaches.

Conventionally, thermodynamic equilibrium models have been applied, in which the mass transfer between gaseous nitric acid and particle phase nitrate aerosol is instantaneous. Such models include EQUISOLV I and II (Jacobson et al., 1996; Jacobson, 1999), ISORROPIA I and II (Nenes et al., 1998; Fountoukis and Nenes, 2007), EQSAM (Metzger and Lelieveld, 2007), INCA (Hauglustaine et al., 2014) and RPMARES (Henze et al., 2007; based on MARS-A, Binkowski and Roselle, 2003), the majority of which have been included in the AeroCom Phase III nitrate aerosol intercomparison (Bian et al., 2017). The advantage of the equilibrium

approach is its speed, stability and relative simplicity. However, the equilibrium approach is thought to be invalid when considering gas-particle partitioning to the coarse mode (Wexler and Seinfeld, 1992; Meng and Seinfeld, 1996), which occurs on atmospheric timescales longer than typical model timesteps. Studies have shown that equilibrium models underestimate fine mode aerosol (Ansari and Pandis, 1999; Moya et al., 2001; Feng and Penner, 2007; Benduhn et al., 2016), as a consequence of their lack of suitability in simulating coarse mode nitrate aerosol formation.

To address this, dynamic mass transfer methods have been developed to more realistically represent the gas-particle partitioning of nitrate (e.g. MADM-A, Pilinis et al., 2000; MOSAIC, Zaveri et al., 2008). However, the need to integrate the governing equations with respect to time across multiple particle sizes (equilibration times) results in numerical "stiffness" and can be computationally prohibitive in global atmospheric models. For this reason, several models have applied a 'hybrid' approach, whereby the model makes a size-selective decision to use either an equilibrium or a dynamic treatment for gas to aerosol partitioning (e.g. HDYN, Capaldo et al., 2000; Feng and Penner, 2007; Trump et al., 2015; Hy-DiS-1.0, Benduhn et al., 2016). In practice, this means applying an equilibrium approach for partitioning to the aerosol fine mode, where the assumption of instantaneous equilibrium is valid, while a more transient (dynamic) approach is used to simulate the coarse mode partitioning. Thus, hybrid approaches provide a compromise between accuracy and computational expense.

Feng and Penner (2007) and Benduhn et al. (2016) found that equilibrium schemes overestimate mass transfer to the coarse mode and so underestimate fine mode nitrate aerosol concentrations. Trump et al. (2015), on the other hand, found that the equilibrium scheme overestimated PM_1 nitrate in regions with significant coarse mode sea salt and dust concentrations in Europe but that the hybrid approach improved the representation of nitrate concentrations (fine and coarse) in these regions. Regardless, the effect of using a more physically realistic hybrid approach to gas to particle partitioning on nitrate aerosol size and concentration is expected to influence nitrate aerosol radiative effects. However, no studies have compared the influence of the gas-particle partitioning approach

on aerosol radiative effects and the thermodynamic equilibrium method remains the standard approach when simulating nitrate aerosol formation (e.g. among the participating AeroCom Phase III models; Bian et al., 2017).

2.4.2 Observed and simulated nitrate aerosol abundance

Observation and model-based studies have found that nitrate aerosol forms an important component of regional atmospheric aerosol, particularly in urban areas, over Europe (Schaap et al., 2004; Crosier et al., 2007; Putaud et al., 2010; Morgan et al., 2010a; Squizzato et al., 2013), the USA (Malm et al., 2004; Silva et al., 2007; Hand et al., 2012; Pusede et al., 2016) and Asia (Pathak et al., 2009; Ying et al., 2014; Snider et al., 2016). For example, Hand et al. (2012), analysing 2005-2008 monthly and annual mean observations, found that ammonium nitrate contributed up to 50% of surface $PM_{2.5}$ in urban and rural regions of the Midwest and Western USA, while still contributing 10-15% of $PM_{2.5}$ far from major sources. They observed high seasonality in ammonium nitrate concentrations with peak concentrations in wintertime. Over Europe, Morgan et al. (2010a) found that ammonium nitrate and organic matter typically contributed 20 – 50% of the non-refractory particulate mass in airborne measurements, with nitrate aerosol dominating the boundary layer aerosol composition in North Western Europe. NH_4NO_3 exhibits greater spatial heterogeneity than SO_4^{2-} (e.g. Snider et al., 2016) as a result of spatial variation in NH_3 and NO_x sources.

Furthermore, observations indicate that the contribution of nitrate to airborne particulate matter is disproportionately enhanced in high pollution episodes (Yin and Harrison, 2008; Morgan et al., 2010a; Crosier et al., 2007; Vieno et al., 2016). Yin and Harrison (2008) found that nitrate accounted for a relatively higher 46% of $PM_{2.5}$ and 39% of PM_{10} on high pollution days when PM_{10} exceeded 50 μg m^{-3}. The reasons for this are not fully understood. The occurrence of high-nitrate haze episodes in China (Yang et al., 2017; Pan et al., 2016), however, indicate that the dominance of nitrate aerosol over other species in polluted conditions may be a global occurrence.

The largest multi-model assessment of nitrate aerosol abundance to date is the AeroCom Phase III intercomparison (AP3; Bian et al., 2017), following from the previous Phase II assessment (Myhre et al., 2013a). All nine AP3 models

simulated large surface and column nitrate concentrations over China, south Asia, Europe and the US, in regions coincident with high NO_x and NH_3 emissions. Several models also simulated high concentrations over the Middle East, South America, Africa and Australia associated with high dust concentrations or NH_3 and NO_x-emitting fires. The AP3 models yielded a mean global nitrate aerosol burden of 0.63 Tg, equivalent to 35% of the mean sulphate burden, but with a factor of 13.4 diversity between the maximum and minimum model global NO_3^- burden. Average global surface nitrate aerosol concentrations of 0.23 μg kg^{-1} were simulated, representing a similar 36.5% of the mean sulphate surface concentration. However, the multi-model global mean surface nitrate concentrations varied by a factor of 9.4.

Contributing to the diversity in nitrate aerosol formation, Bian et al. (2017) found a high multi-model diversity in the concentrations of precursor species. Atmospheric nitric acid burdens varied by a factor of 9, thought to reflect differences in O_3-HO_x-NO_x chemistry and mechanisms for nitrate aerosol production. Wet deposition dominated the diversity in NH_3 and NH_4^+ and NO_3^- lifetime. The study also found that inclusion of the heterogeneous formation of nitrate on dust and sea salt was a dominant determinant of nitrate aerosol formation and size distribution between the fine and coarse modes, forming over 80% of the nitrate aerosol burden in the two models that submitted full NO_3^- budgets. Notably, however the study included only models that used a thermodynamic equilibrium approach to the nitrate aerosol partitioning (see Section 2.4.1), with various assumptions applied to account for the coarse mode nitrate formation.

Relatively few studies have focussed on the implications of heterogeneous N_2O_5 hydrolysis for nitrate aerosol formation (e.g. Riemer et al., 2003; Alexander et al., 2009). Previous atmospheric modelling studies have tended to focus on the implications of heterogeneous N_2O_5 hydrolysis for NO_x, O_3 and OH concentrations from urban to global spatial scales (e.g. Riemer et al., 2003; Dentener and Crutzen, 1993; Macintyre and Evans, 2010; Pope et al., 2015; Tie et al., 2001). Alexander et al. (2009) determined that N_2O_5 hydrolysis controls 18% of the global, annual-mean tropospheric total inorganic nitrate (nitric acid + nitrate aerosol) burden in the GEOS-Chem model and that it provides the

dominant formation pathway for surface total nitrate (up to 74%) in the high Northern latitudes and Arctic. N_2O_5 hydrolysis therefore has the potential to impact regional air quality and aerosol radiative effects through its influence on nitrate aerosol abundance.

2.4.3 Historic changes in anthropogenic emissions

Anthropogenic emissions of aerosol and aerosol precursor gases have increased globally throughout the industrial era (e.g. Lamarque et al., 2010), with implications for atmospheric composition, climate and air quality. Emissions of NO_x, NH_3 and SO_2 are of particular relevance for nitrate aerosol formation. Emissions of NO_x, NH_3 and SO_2 emissions have previously been deemed to peak globally in 1990, 1990 and 1980, respectively (Lamarque et al., 2010), though subsequent estimates from the Community Emissions Data System (CEDS) have found global increases beyond these years driven largely by enhanced emissions from Asia (Hoesly et al., 2018). Post-1980 emissions trends have been subject to large regional variability, driven by changing influences from air quality legislation, technological advancements, economic development and energy consumption. Since 1980, anthropogenic emissions of most species have decreased over North America and Europe. In the same time period, emissions have increased over India and China, although recent reports suggest that emissions from China have begun to stabilise since 2010 following changes to emission standards for power plants (Liu et al., 2016). Figure 2.2 shows 1980-2010 changes in SO_2 and NO_x emissions over Europe, the USA, India and China as collated by Granier et al. (2011). Over Europe, total anthropogenic SO_2 emissions decreased by 73% between 1980 and 2004 (Vestreng et al., 2007), with similar decreases by 73% and 70 – 90% between 1980 and 2010 corroborated by Granier et al. (2011) and Tørseth et al. (2012), respectively. European NO_x emissions decreased by 30% overall between 1980 and 2010, while NH_3 emissions increased by 25% as a result of unregulated agricultural emissions (Granier et al., 2011). In the USA, SO_2 and NO_x emissions decreased by 58% and 30% respectively, while NH_3 emissions increased by 6% between 1980 and 2010 (Granier et al., 2011). Over India, total SO_2, NO_x and NH_3 emissions increased by 337%, 192% and 2% respectively between 1980 and 2008 (Granier et al., 2011). Emissions from China also increased by 96%, 170% and 63% for SO_2, NO_x and

NH_3, between 1980 and 2010 respectively (Granier et al., 2011). While SO_2 emissions were reported to have decreased by 9.2% between 2006 and 2010 (Lu et al., 2011), a mean annual growth rate in NO_x of 6.7% had been maintained between 2006 and 2009 (Lamsal et al., 2011).

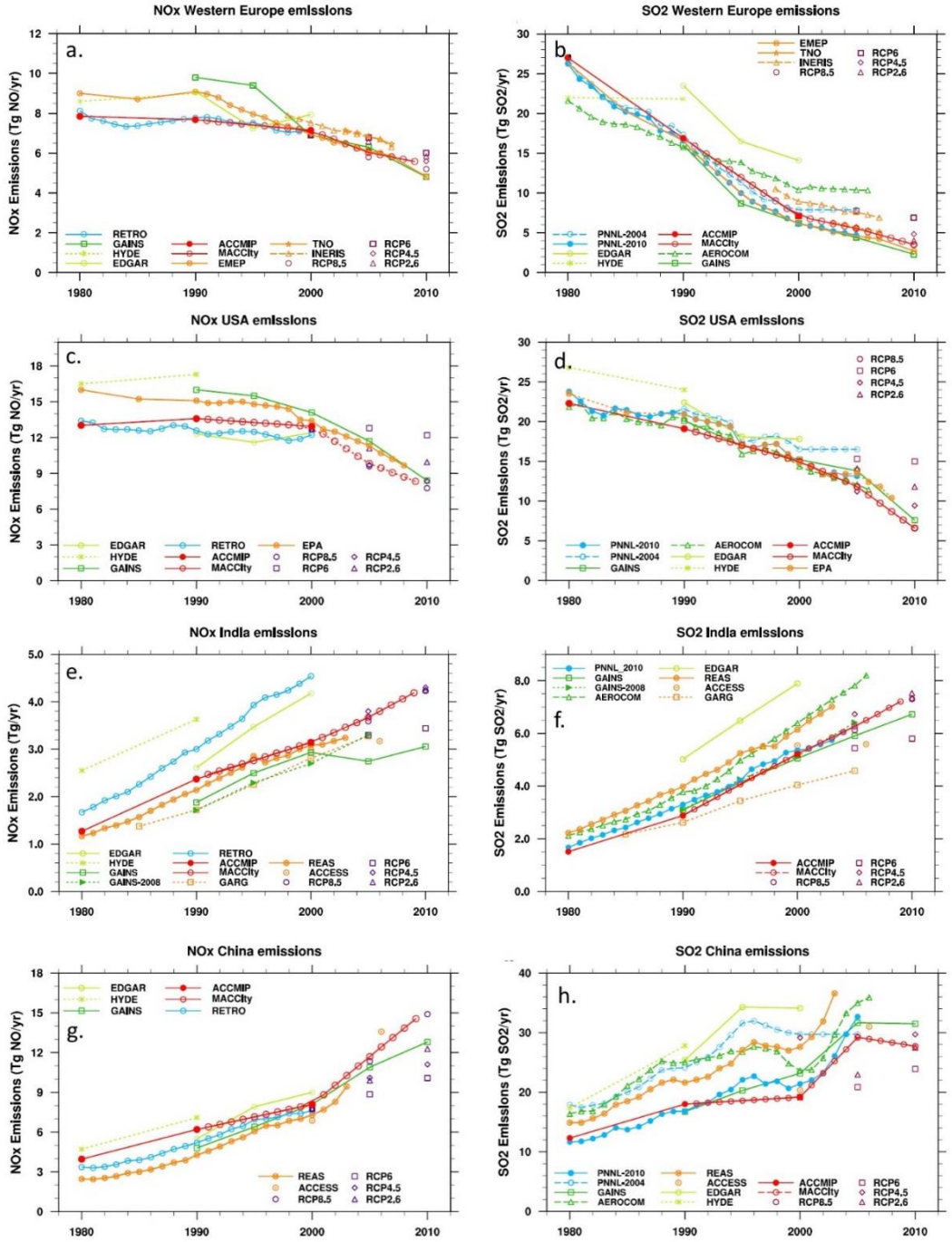

Figure 2.2 *Temporal evolution of NO_x (left column) and SO_2 (right column) emissions between 1980 and 2010 over (a-b) Western Europe, (c-d) USA, (e-f) India and (g-h) China. Adapted from Granier et al. (2011).*

2.4.4 Historic trends in $PM_{2.5}$ and associated mortality

Several studies have investigated trends in $PM_{2.5}$ concentrations on global and regional spatial scales over the past few decades (Leibensperger et al., 2012; Tørseth et al., 2012; Turnock et al., 2015; Li et al., 2017) with some also assessing historic trends in $PM_{2.5}$-attributable mortality (Wang et al., 2017; Butt et al., 2017; Cohen et al., 2017). These observation and modelling based studies conclude that, overall, $PM_{2.5}$ concentrations have decreased in Europe and North America in recent decades, while increasing over India and China, in response to regional emission changes (see Section 2.4.3). Recent observations, however, do suggest that $PM_{2.5}$ concentrations have stabilised and started to decline over China since 2015, likely as a result of recent legislated efforts to reduce pollution (Silver et al., 2018).

The numbers of deaths associated with long-term exposure to $PM_{2.5}$ ($PM_{2.5}$-attributable premature mortality) in these regions have also changed in recent decades, as a result of these changes in $PM_{2.5}$ concentrations, baseline disease rates and demography (population number and age). Based on a combination of satellite-derived $PM_{2.5}$, atmospheric modelling and ground based observations, Cohen et al. (2017) deduced that rates of mortality due to ambient $PM_{2.5}$ have decreased globally between 1990 and 2015 but that the absolute number of ambient $PM_{2.5}$-attributable deaths has increased globally from 3.5 million deaths in 1990 to 4.2 million in 2015. The rise in deaths resulted from growing and ageing populations, along with increasing $PM_{2.5}$ in low and middle income countries in east and south Asia. Wang et al. (2017) simulated regional 1990-2010 trends in $PM_{2.5}$ and ascertained that $PM_{2.5}$-attributable mortality increased in East Asia and South Asia by 21% and 85%, respectively, in this period. Decreases in $PM_{2.5}$-attributable mortality by 67% and 58% were calculated over Europe and high-income North America, respectively.

Butt et al. (2017) applied the UM-UKCA model to quantify $PM_{2.5}$-attributable mortality back to the year 1960 when long-term ground-based and satellite monitoring were yet to be established. Figure 2.3 shows trends in global and

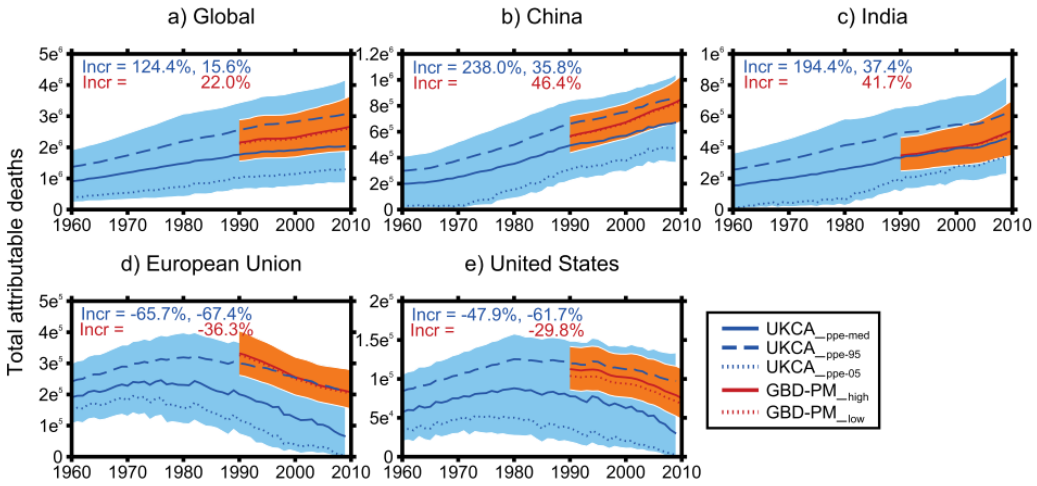

Figure 2.3 *Annual total attributable deaths for (a) global, (b) China, (c) India, (d) European Union and (e) United States with shaded regions denoting uncertainty range from UM-UKCA perturbed parameter ensemble estimates (light blue) and satellite-derived product (orange). Percentage change in deaths are given for UM-UKCA [Incr = (2009-1960)/1960, (2009 – 1990/1990 in blue] and satellite (GBD-PM$_{high}$)[(2009-1990)/1990 in red)]. From Butt et al. (2017).*

regional $PM_{2.5}$-attributable mortality from this study. Butt et al. (2017) simulated 1960-2010 increases in population-weighted mean $PM_{2.5}$ over China and India of 52.7% and 69.8%, respectively with increases in $PM_{2.5}$-attributable mortality of 238% and 194%, respectively. In contrast, population-weighted $PM_{2.5}$ were reduced over the European Union (EU) and USA by 55.3% and 38%, respectively with associated reductions in mortality by 65.7% and 47.9%, respectively, between 1960 and 2009. However, nitrate aerosol was not accounted for in these simulations and its contribution to long term trends in $PM_{2.5}$ were therefore not represented.

2.4.5 Historic trends in nitrate aerosol concentration

Understanding how emission changes have influenced the speciation of atmospheric aerosol can inform assessments of aerosol-climate impacts and policy-making to reduce $PM_{2.5}$ and its associated negative health impacts. Despite its large contribution to aerosol concentrations in the Northern

Hemisphere, relatively little research has given attention to historic changes in nitrate aerosol concentration. Long-term observations from 1990 onwards indicate that airborne nitrate aerosol concentrations have declined over the USA (Leibensperger et al., 2012; Xing et al., 2015) and Europe (Fagerli and Aas, 2008; Xing et al., 2015; Tørseth et al., 2012), though at lesser rates of decline than sulphate aerosol. Observed nitrate aerosol concentrations have also fallen at a lower rate than NO_x emissions in many locations (Fagerli and Aas, 2008; Tørseth et al., 2012). It is largely accepted that non-linearity between decreases in NO_x emission and atmospheric nitrate concentrations arise from the co-dependence of NH_4NO_3 on NH_3 availability, where reductions in SO_2 emissions are combined with level or increasing NH_3 emissions. This co-dependence has been the subject of much research (e.g. Ansari and Pandis, 1998; Erisman and Schaap, 2004; Fagerli and Aas, 2008; Pinder et al., 2008; Pye et al., 2009; Heald et al., 2012; Harrison et al., 2013; Holt et al., 2015; Wang et al., 2013) and of debate in light of recent aerosol acidity measurements (Weber et al., 2016; Murphy et al., 2017; Guo et al., 2018).

Long-term observations of atmospheric nitrate aerosol are spatially and temporally limited, with little coverage outside of Europe and the USA and no long-term monitoring of nitrate established prior to the year 1990. Furthermore, the filterpack method widely employed for measurements can be subject to bias when separating gas phase HNO_3 and particulate nitrate aerosol (Slanina et al., 2001; Vecchi et al., 2009). In combination with observations, global modelling can therefore provide insight into variability in the aerosol chemical composition over multi-decadal time periods.

Li et al. (2017) examined global trends in the chemical composition of population-weighted mean $PM_{2.5}$ using a combination of simulated and satellite-derived $PM_{2.5}$. Nitrate aerosol was one of four main components of the average population-weighted mean (PWM) $PM_{2.5}$ found to have significantly increased globally at a rate of 0.05 $\mu g\ m^{-3}\ yr^{-1}$ between 1989 and 2013, behind organic aerosol (0.10 $\mu g\ m^{-3}\ yr^{-1}$) and ahead of sulphate (0.04 $\mu g\ m^{-3}\ yr^{-1}$) and ammonium (0.03 $\mu g\ m^{-3}\ yr^{-1}$). The most pronounced increasing trends in population-weighted mean nitrate concentrations were found over China and northern India

with the greatest decreases identified over the USA and Europe (>± 0.1 μg m^{-3} yr^{-1}). Nitrate exhibited the largest of the aerosol trends analysed over East Asia driving 35% of the annual increase in PWM $PM_{2.5}$ and continuing to increase significantly after 2006 and 2013 despite insignificant decreases in PWM $PM_{2.5}$. Xing et al. (2015) also simulated decreases in nitrate aerosol over Europe (-0.03 μg m^{-3} yr^{-1}) and increases over Eastern China (+0.097 μg m^{-3} yr^{-1}) between 1990 and 2010 but, contrary to observed trends, found increases in simulated nitrate concentration over the Eastern USA (0.014 μg m^{-3} yr^{-1}) as a result of increasing NH_3 emissions. These studies found that area-weighted and population-weighted mean nitrate concentrations have undergone substantial trends in recent decades. This suggests that nitrate aerosol could be implicit in changing $PM_{2.5}$-attributable mortality rates, though its contribution to mortality has not been directly evaluated in previous studies.

2.4.6 Future nitrate aerosol projections

The relative importance of nitrate compared to other aerosol species is likely to increase under future projected emission scenarios. However, projections of atmospheric nitrate aerosol are made more uncertain by its aforementioned co-dependence on NO_x, NH_3 and SO_2 availability, with global SO_2 and NO_x emissions projected to decline and NH_3 emissions projected to increase in the next century under most Coupled Model Intercomparison Project (CMIP) Phase 5 Representative Concentration Pathways (RCPs; van Vuuren et al., 2011). Having already peaked over Europe and the USA, global SO_2 emissions over Asia are projected to peak in 2020 and decrease rapidly thereafter to the year 2100 in all RCPs. Similarly, NO_x emissions peaked over the USA and Europe in the 1980s and are projected to decrease globally to 2100. Global NH_3 emissions, however, are projected to continually increase under all RCPs except in RCP4.5 where emissions remain relatively stable until 2100 (van Vuuren et al., 2011). Furthermore, relatively few studies have predicted future nitrate concentrations and impacts compared to other aerosol species, with only 4 of the 10 Atmospheric Chemistry and Climate Model Intercomparison Project (ACCMIP) models for example including nitrate in long-term climate simulations (Shindell et al., 2013). The number of potential future anthropogenic emission scenarios has been expanded to 9 scenarios for the sixth CMIP phase, covering a range of

potential socio-economic and technological development pathways with future radiative forcing outcomes (Rao et al., 2017; Gidden et al., 2018). Like in the RCPs for CMIP6, global emissions of NO_x and SO_2 are projected to decrease between the present day and year 2100, with NH_3 emissions remaining level or increasing, in the CMIP6 scenarios that assume climate change mitigation is undertaken (Rao et al., 2017).

Of the global models that have made future predictions of nitrate aerosol, most estimate that the total burden of atmospheric nitrate aerosol will increase by 2100 under future emission scenarios (Adams et al., 2001; Bellouin et al., 2011; Hauglustaine et al., 2014; Bauer et al., 2016; Paulot et al., 2016). Pye et al. (2009) simulated a near-constant global NO_3^- burden by 2050 when changes in both climate and emissions were considered, with the impacts of higher ammonia availability on semi-volatile nitrate concentrations offset by increases in temperature. Bauer et al. (2007) found low dependence of year 2030 nitrate aerosol on climate and a stronger dependence on NH_3 emissions. There is wider variability between models in estimates of surface nitrate aerosol trends, with some projecting that concentrations will increase in the next century under increased availability of ammonia (Bellouin et al., 2011) and others predicting a stabilisation or decrease in global or regional nitrate estimates as NO_x emissions decline (Hauglustaine et al., 2014; Bauer et al., 2016; Pusede et al., 2016; Trail, 2014; Paulot et al., 2016). These studies found decreases in projected surface NO_3^- concentrations resulting from reductions in anthropogenic NO_x emissions and heterogeneous production rates of HNO_3 following reductions in total aerosol surface area. Meanwhile, increases in NH_3 emission drive increases in simulated NO_3^- formation in the free troposphere, where nitric acid is not the limiting species.

Regardless of the direction of change in nitrate aerosol concentration, its relative importance for aerosol impacts on air quality and climate is expected to increase as global sulphate concentrations decrease in response to SO_2 emission reductions (Shindell et al., 2013). Several global modelling studies have identified that nitrate aerosols could replace sulphate by the end of the 21st century as the dominant aerosol species, which would act to decelerate the projected decrease in global mean aerosol forcing (e.g. Bauer et al., 2007;

Bellouin et al., 2011; Hauglustaine et al., 2014). The likely increasing importance of nitrate aerosol for future aerosol concentrations but uncertainty between model projections further motivates the investigation of processes influencing nitrate aerosol formation and historical trends in nitrate concentration.

2.4.7 Health effects of nitrate aerosol

Short and long-term exposure to fine particulate matter ($PM_{2.5}$ and PM_{10}) are major global risk factors associated with adverse health effects (see Section 2.2.1 and references therein). Legislation and guidance remain focussed on reducing the total non-speciated airborne mass of particulate matter with dry diameters below 10μm (PM_{10}) and 2.5 μm ($PM_{2.5}$), with a few exceptions where individual components, such as lead, are targeted. There is strong evidence that exposure to this finer portion of particulate matter is associated with the greatest disease burden, with further research suggesting that no lower concentration threshold exists below which $PM_{2.5}$ exposure can be deemed safe (Beelen et al., 2014). As an important component of fine particulate matter (see Section 2.4.2), consideration of nitrate aerosol is therefore required when quantifying health impacts of $PM_{2.5}$ exposure and identifying strategies for reducing atmospheric pollution and its associated disease burden.

2.4.7.1 Nitrate aerosol toxicity

Epidemiological and toxicological evidence for the long-term effects of individual $PM_{2.5}$ components is limited (Wyzga & Rohr, 2015) and, in keeping with current legislation, components of $PM_{2.5}$ are assumed in almost all studies to be equal in toxicity. Concentration-exposure response functions have been developed to relate $PM_{2.5}$ concentrations to subsequent health effects (Pope et al., 2009; Pope et al., 2011; Burnett et al., 2014; Shin et al., 2016; Pope et al., 2018) and have been applied widely in studies to determine the health impacts, including premature mortality and years of life lost, of multi-component $PM_{2.5}$.

It has been suggested that nitrate and sulphate aerosols are less harmful to human health than other components of air pollution, for example than combustion-derived particles (Tuomisto et al., 2008; WHO, 2013). Reasons cited for the perceived lower health impact of nitrate and sulphate are their high solubility and abundance in the human body. Schlesinger and Cassee (2003) and

Reiss et al. (2007) indicated a low health impact of nitrate aerosol. However, these reviews found very few toxicological and epidemiological studies pertaining to nitrate, making it difficult to confidently determine whether the species is less harmful than the average $PM_{2.5}$ (WHO, 2013). Wyzga and Rohr (2015) later concluded that epidemiological and toxicological studies are too few and inconsistent to infer causality between long-term exposure to individual components and health effects but noted that significant associations of nitrates and sulphates with negative health outcomes have been observed in several long-term epidemiological studies (Ostro et al., 2011; Wilhelm et al., 2011; Basu et al., 2014). Notably, Ostro et al. (2011) found that long-term exposure to both nitrate and sulphate was positively associated with cardiopulmonary mortality. In terms of mechanism, it is thought that cations from secondary inorganic aerosol components may produce an interactive biological effect when present in combination with other pollutants, for example by influencing acidity or by reacting with transition metals and polycyclic aromatic hydrocarbons (Cassee et al., 2013). A larger body of short-term epidemiological and toxicological evidence exists (Rohr and Wyzga, 2012). Klemm et al. (2011) found daily mortality in Atlanta to be significantly associated only with the nitrate fraction of $PM_{2.5}$. Ostro et al. (2007) observed a significant association between mortality and nitrate concentrations, along with $PM_{2.5}$, elemental carbon and several metallic species. However, overall, short-term studies neither provide compelling evidence for a link between nitrate and mortality nor exonerate its role in negative health outcomes (Rohr and Wyzga, 2012).

2.4.7.2 Nitrate aerosol health impacts

Despite its important role in particulate composition, enhanced contribution to $PM_{2.5}$ in high pollution episodes (see Section 2.4.2) and potential toxicity, the premature mortality associated with short and long-term exposure to nitrate aerosol has not been directly quantified to date. There is gathering consensus, however, that mortality from long-term exposure to $PM_{2.5}$ is influenced by the agricultural emission sector, through the role of ammonia in sulphate and nitrate aerosol formation (Lelieveld et al., 2015; Pozzer et al., 2017). Thus, a role of nitrate aerosol in adversely impacting human health is implied but not directly quantified by these studies.

Lelieveld et al. (2015) found agricultural emissions to be the leading source category for atmospheric $PM_{2.5}$ concentrations over Europe, Russia, Turkey, Korea, Japan and the Eastern USA, given that ammonia was often the limiting species in atmospheric sulphate and nitrate formation over these regions. They also found agriculture to be the second largest contributing sector to outdoor air pollution-related mortality globally, after residential energy use, contributing one fifth (659,400 premature deaths per year) to the global total when assuming uniform toxicity of all components forming $PM_{2.5}$. Pozzer et al. (2017) simulated a substantial decrease in $PM_{2.5}$ concentrations over Europe, North America and East Asia when agricultural NH_3 emissions were abated. Based on present day population number and age structure, they estimated that a 50% reduction of NH_3 emissions would prevent 250,000 $PM_{2.5}$-attributable premature deaths per year globally. Regionally, this represented reductions of 30%, 19%, 8% and 3% over North America, Europe, East and South Asia, respectively.

The conclusions of Lelieveld et al. (2015) and Pozzer et al. (2017) are reinforced by other works which have found emissions from the agricultural sector to provide an effective control on $PM_{2.5}$ via their influence on sulphate and nitrate aerosol concentrations (Brandt et al., 2013; Megaritis et al., 2013; Bessagnet et al., 2014; Paulot and Jacob, 2014; Lee et al., 2015; Bauer et al., 2016). Tsimpidi et al. (2008) note the combined air quality benefit of reducing SO_2 and NO_X emissions through controlling both ammonium sulphate and nitrate. Li et al. (2017) noted the role of nitrate aerosol in driving 25 year trends in population weighted mean $PM_{2.5}$ (see Section 2.4.5) and its importance (25% contribution) for population-weighted mean $PM_{2.5}$, in particular, over Europe. Again, these studies imply that potential health benefits could result from reducing $PM_{2.5}$ through targeting nitrate aerosol concentrations.

2.4.8 Radiative effects of nitrate aerosol

2.4.8.1 Direct radiative effect

Several global modelling studies have estimated the influence of atmospheric nitrate aerosol on present day climate, although these are relatively few in comparison to evaluations of other aerosol species such as sulphate and black carbon. These studies reported either present day (PD) direct radiative effects

or the direct anthropogenic forcing associated with nitrate aerosol, i.e. the change in nitrate radiative effect since a pre-industrial (PI) era baseline.

Table 2.3 compares the global model assessments of nitrate direct radiative forcing to date. Uncertainty in nitrate direct radiative effects remains high, with single model studies prior to the year 2012 yielding global PI to PD nitrate direct TOA anthropogenic forcings of between -0.023 W m^{-2} (Myhre et al., 2009) and -0.19 W m^{-2} (Adams et al., 2001). The AeroCom Phase II intercomparison (Myhre et al., 2013a) included eight models that calculated the PI to PD nitrate radiative forcing, resulting in a mean estimate of -0.08 ± 0.04 W m^{-2} with a multi model range of -0.02 W m^{-2} to -0.12 W m^{-2}. The ACCMIP ensemble found a mean nitrate global direct forcing of -0.19 ± 0.18 W m^{-2} with over an order of magnitude range between models from -0.03 W m^{-2} to -0.41 W m^{-2}. More recently, Hauglustaine et al. (2014) derived a PI to PD global mean nitrate direct radiative forcing of -0.056 W m^{-2}, equivalent to approximately 18% of their calculated sulphate direct forcing, using the LMDz-INCA model. Li et al. (2015) calculated a global PI to PD nitrate direct forcing of -0.025 W m^{-2} with GEOS-Chem. Lund et al. (2018) calculated a similar nitrate direct forcing of -0.02 W m^{-2}, equivalent to 7% of the sulphate direct radiative forcing, using OsloCTM3 and applying the CEDS v16 emission inventory (Hoesly et al., 2018). The magnitude of the direct radiative forcing from nitrate aerosol was shown to increase between 1990 and 2015 among the GISS, OsloCTM2 and EMEP models by Myhre et al. (2017), with a wider model range in forcing than other aerosol components. The single model study of Xu and Penner (2012) calculated the nitrate aerosol direct radiative forcing using a hybrid approach to treat semi-volatile nitrate aerosol formation. They calculated a forcing equivalent to approximately double that of Hauglustaine et al. (2014) and at the higher magnitude end of estimates from multi-model intercomparisons, though the difference in forcing estimate cannot be attributed to the partitioning approach alone.

Table 2.3 *Summary of nitrate direct radiative effect and anthropogenic forcing assessments. All values given in W m^{-2}. Extended from Xu and Penner (2012).*

	Direct effect (PD)		Direct effect (PI)		Anthropogenic forcing	
	TOA	Surface	TOA	Surface	TOA	Surface
Lund et al. (2018)	-	-	-	-	-0.02	-
Li et al. (2015)	-	-	-	-	-0.025	-
Hauglustaine et al. (2014)	-	-	-	-	-0.056	-
Myhre et al. (2013a)*	-	-	-	-	-0.08 ± 0.04 (-0.12 to -0.02)	-
Boucher et al. (2013) and Myhre et al. (2013b)*	-	-	-	-	-0.11 (-0.30 to -0.03)	-
Shindell et al. (2013)*	-	-	-	-	-0.19 ± 0.18 (-0.41 to -0.03)	-
Xu and Penner (2012)	-0.14	-0.18	-0.02	-0.02	-0.12	-0.16
Bellouin et al. (2011)	-	-	-	-	-0.12	-
Myhre et al. (2009)	-	-	-	-	-0.023	-
Forster et al. (2007)*	-	-	-	-	-0.10 (-0.2 to 0.0)	-
Bauer et al. (2007)	-0.11		-0.05		-0.06	-
Myhre et al. (2006)	-0.02					
Liao and Seinfeld (2005)	-0.22	-0.21	-0.06	-0.06	-0.16	-0.15
Liao et al. (2004)	-0.14	-0.17	-	-	-	-
Jacobson (2001)	-0.07	-0.07	-	-	-	-
Adams et al. (2001)	-0.30	-	-0.11	-	-0.19	-

* Multi-model assessment.

2.4.8.2 Indirect cloud-albedo radiative effect

Though large uncertainty remains in quantifying the nitrate aerosol direct radiative effect, its indirect radiative forcing remains far more understudied.

The condensation of nitric acid vapour onto existing particles to form nitrate aerosol alters the composition, size and number concentration of the aerosol population. For example, increases in aerosol size have been observed during haze pollution episodes in China when the nitrate aerosol contribution to aerosol was significantly increased (Che et al., 2016). Uptake of nitric acid gas also enhances water uptake and hygroscopic growth of the aerosol (Kulmala et al., 1995; 1998b; Makkonen et al., 2012). Nitrate aerosol formation can therefore influence aerosol activation to cloud droplets and modify cloud albedo, leading to an indirect forcing on climate.

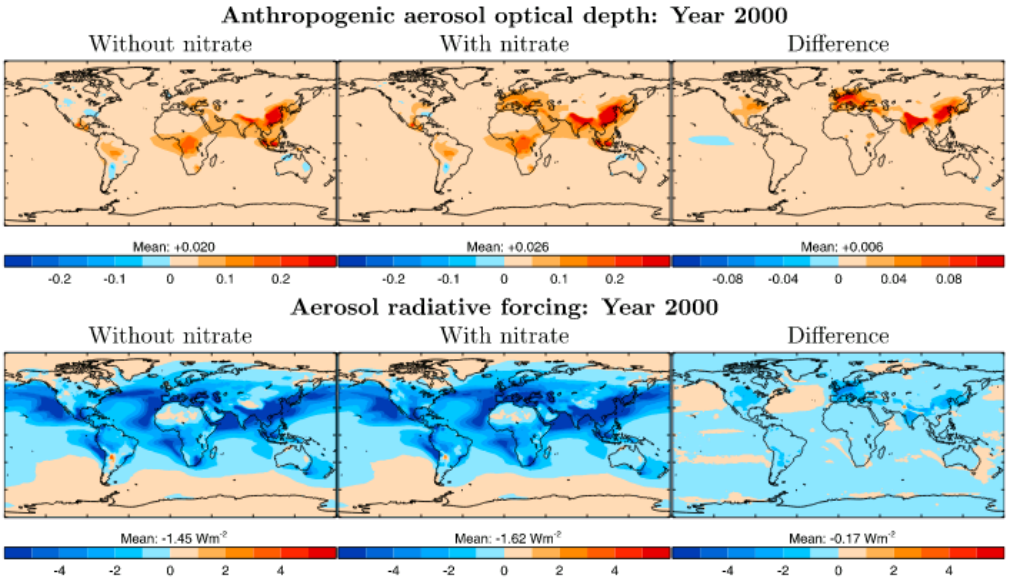

Figure 2.4 *Anthropogenic aerosol optical depth (0.55 μm) and all-sky top-of-atmosphere aerosol (direct and first indirect) radiative forcing (W m^{-2}) simulated for the year 2000 by HadGEM2-ES CMIP5 simulations. The influence of nitrate aerosol is shown as the absolute difference (right) between values with nitrate aerosol excluded (left) and included (middle). Adapted from Bellouin et al., 2011.*

Though nitrate aerosol is increasingly considered in assessments of CDNC and radiative forcing from aerosol-cloud interactions as modelling capabilities improve (e.g. Leibensperger et al., 2012; Skeie et al., 2011; Fanourgakis et al.,

2019; Myhre et al., 2017), few dedicated modelling studies have quantified a global indirect radiative forcing from nitrate aerosol (Bellouin et al., 2011; Xu and Penner, 2012) and so this effect remains in need of further research. Other studies have focussed on regional nitrate aerosol cloud albedo radiative forcing (e.g. Li et al., 2009; Wang et al., 2010; Drugé et al., 2019; Zhang et al., 2015).

Bellouin et al. (2011) simulated a pre-industrial to present day nitrate first indirect forcing (aerosol cloud albedo forcing) of -0.05 W m^{-2} using the mass based CLASSIC aerosol scheme in UM-UKCA. Regionally, the nitrate aerosol forcing (including direct forcing) was greatest over high nitrate regions of Europe, the USA, India and China (Figure 2.4). To minimise computational expense, aerosol number and mass were assumed to vary proportionally in the mass based CLASSIC scheme. However, processes affecting aerosol mass without affecting aerosol number, and vice versa, are important when simulating cloud condensation nuclei concentrations, with representation of these processes providing more realistic estimates of the aerosol indirect effects (Bellouin et al., 2013). The nitrate aerosol cloud albedo effect has not subsequently been evaluated in the UM-UKCA model using the more recently adopted GLOMAP-mode microphysical scheme (described in Section 3.2.3), which simulates aerosol number independently of aerosol mass.

Furthermore, Bellouin et al. (2011) applied a thermodynamic equilibrium assumption for the gas-particle partitioning of nitric acid and only represented accumulation mode nitrate. The size partitioning of nitrate is relevant for CCN estimation and models that assume thermodynamic equilibrium in the NO_3^--NH_4^+-SO_4^{2-}—Na^+-Cl^- may not resolve the influence on CCN accurately (e.g. Benduhn et al., 2016). The GLOMAP-mode approach applies a more physically realistic 'hybrid' approach to represent nitrate aerosol formation across the four main soluble aerosol modes but the resulting nitrate aerosol radiative effects using this approach in UM-UKCA have never been quantified.

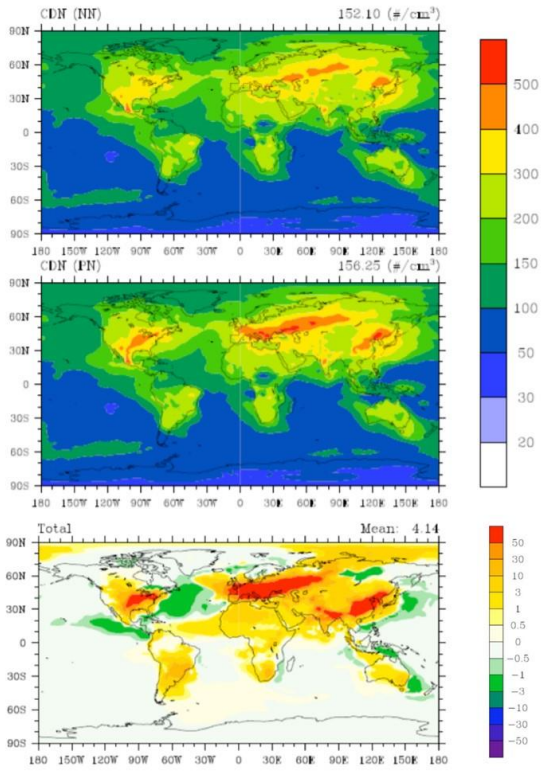

Figure 2.5 *The contribution of nitrate aerosol to cloud droplet number concentration (Δ # cm^{-3}) at 930 mb as simulated by the IMPACT model for the year 2000, given as the absolute difference (bottom) between CDNC simulated with nitrate aerosol excluded (top) and included (middle). Adapted from Xu and Penner (2012).*

Xu and Penner (2012) calculated a smaller combined nitrate and ammonium first indirect aerosol radiative forcing of -0.01 W m^{-2} with the IMPACT global aerosol and chemistry model. They applied a hybrid dynamical partitioning approach, though did not compare their results with those simulated using a conventional equilibrium approach. Figures 2.5 and 2.6 show the absolute and percentage changes in cloud droplet number (CDN) concentration (CDNC) simulated by Xu and Penner (2012). The study found that the influence of nitrate and ammonium aerosols on CDNC was greatest in the Northern Hemisphere (see Figure 2.5 and blue line in Figure 2.6) and close to the surface where simulated nitrate and ammonium concentrations were higher. Overall, they simulated increases in global mean CDNC by about 3% at 930 mb when nitrate and ammonium aerosol were added. Nitrate aerosol formation led to a peak change in zonal annual mean cloud droplet number concentration (of up to

approximately 20%) between 20° N and 60° N, corresponding spatially with regions where simulated nitrate aerosol concentrations were greatest.

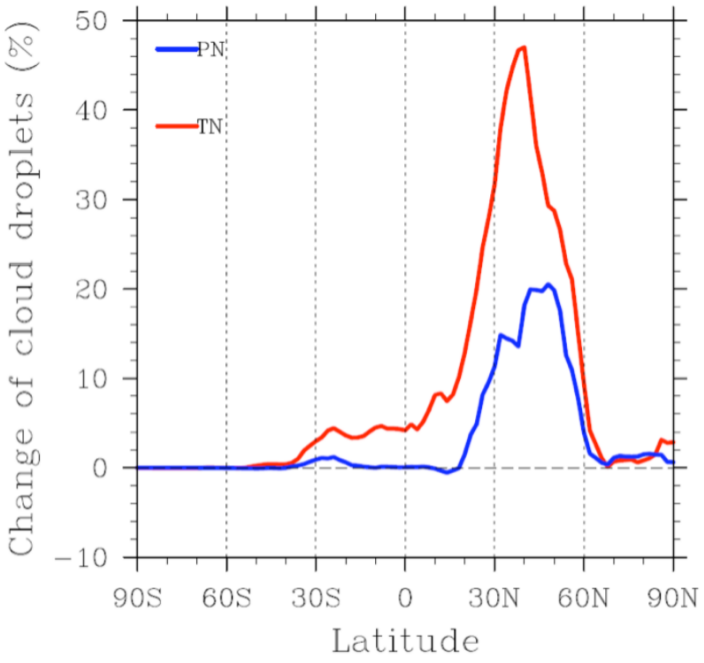

Figure 2.6 *The percentage change in zonal mean CDNC for the year 2000 when the effects of nitrate aerosol (PN) and total nitrate (TN; nitric acid plus nitrate aerosol) are accounted for in the IMPACT model. From Xu and Penner (2012).*

Xu and Penner (2012) further inferred that the presence of soluble gaseous nitric acid enhanced the activation of smaller particles by lowering the critical super-saturation and increasing aerosol hygroscopicity. The nitric acid effect on CDNC was associated with a radiative forcing of -0.08 W m^{-2}. Increases in zonal mean CDNC peaked at a higher 46% near 40 °N when the influence of soluble gaseous nitric acid was included in addition to nitrate aerosol formation (red line in Figure 2.6). The first indirect forcing from nitrate, including this nitric acid effect, was strongest over the North Pacific storm track, given its dependence on both changes in CDNC and the spatial distribution of clouds.

2.5 Summary

This chapter summarises the existing research on nitrate aerosol and its effects on air quality and climate. It is found that nitrate aerosol remains relatively understudied overall compared to other aerosol species, such as sulphate aerosol, partly as a result of complexity and expense associated with

representing its semi-volatile nature in global atmospheric models. Conventionally, thermodynamic equilibrium models have been applied to simulate nitrate aerosol formation. However, this approach has been found to overestimate coarse mode aerosol formation, at the expense of the fine mode, and 'hybrid' approaches have therefore been developed to simulate the size-resolved nitrate aerosol formation more realistically (see Section 2.4.1). Furthermore, the latest AeroCom Phase III intercomparison exercise found wide variability in present day nitrate aerosol concentrations simulated by global aerosol models (see Section 2.4.2).

Changes in precursor aerosol emissions over recent decades have had regional implications for surface level $PM_{2.5}$ and $PM_{2.5}$-attributable mortality (see Sections 2.4.3 and 2.4.4). However, as a result of its omission from long term modelling studies, the impact of historical emission changes on nitrate aerosol concentrations is less well understood (see Section 2.4.5). As a component of $PM_{2.5,}$ changes in nitrate aerosol concentration could influence the number of deaths associated with long-term exposure to $PM_{2.5}$ (see Section 2.4.7). Finally, nitrate aerosol acts as a climate forcing agent and its indirect influence on the radiative budget via modification of the cloud albedo, in particular, is severely understudied (see Section 2.4.8).

Having summarised the existing research on nitrate aerosol, the next chapter, Chapter 3, will describe the methods used to address the aims outlined in Chapter 1.

3. Methods

3.1 Introduction

The primary research tool used for all model experiments in this thesis is the "nitrate-extended" version of the UM-UKCA community composition-climate model. The UM-UKCA model couples the UK Met Office's Unified Model (MetUM; Brown et al., 2012) with the UK Chemistry and Aerosol sub-model (UKCA). The UKCA sub-model includes a range of alternative chemistry schemes (e.g. Morgenstern et al., 2009; O'Connor et al., 2014) and the modal version of the Global Model of Aerosol Processes (GLOMAP-mode) aerosol microphysics module (Mann et al., 2010). Whereas the standard configurations of GLOMAP-mode only simulate the one-way transfer of extremely low-volatility (condensable) material to the particle phase, here the "nitrate-extended" version of GLOMAP is applied incorporating a hybrid "dissolution solver" (HyDiS-1.0). This solver additionally represents the size-resolved partitioning of semi-volatile inorganic gases, such as nitric acid and ammonia, into and out of the aerosol particle aqueous phase (Benduhn et al., 2016).

Section 3.2 gives a comprehensive description of this configuration of the UM-UKCA composition-climate model including the atmosphere model (3.2.1), chemistry scheme (3.2.2) and microphysical processes simulated within nitrate-extended GLOMAP-mode (3.2.3) including the HyDiS-1.0 inorganic dissolution solver (3.2.4). Section 3.3 describes the methodology applied in Chapter 5 to calculate the contribution of nitrate aerosol to $PM_{2.5}$ and associated health impacts arising from long-term exposure to $PM_{2.5}$. Section 3.4 describes the 'SOCRATES' Suite of Community Radiative Transfer codes, based on Edwards and Slingo (1996) and cloud droplet number concentration (CDNC) calculations, used offline in Chapter 6 to calculate PD nitrate aerosol radiative effects via cloud albedo perturbations (i.e. PD first aerosol indirect radiative effect).

In Chapter 4, UM-UKCA-simulated nitrate, ammonium and sulphate aerosol fields are compared with those simulated by the 9 participating models of the AeroCom Phase III nitrate intercomparison exercise (Bian et al., 2017). Section 3.5 presents an overview of these models and the protocol for the AeroCom

Phase III nitrate experiment. Surface, aircraft, ship and satellite-based observations applied to evaluate the model in Chapters 4, 5 and 6 are described in Section 3.6 of this methods chapter, with Section 3.7 explaining the statistical metrics used for model-observation comparisons.

3.2 Description of nitrate-extended UM-UKCA

This section describes the dynamics, chemistry and microphysics of the host general circulation model, UM-UKCA, the GLOMAP-mode aerosol module and the nitrate extension to the GLOMAP-Mode module, HyDiS-1.0.

3.2.1. Unified Model configuration and dynamics

The Met Office's Unified Model (MetUM; Brown et al., 2012) is hereafter referred to as "the UM" in this thesis. The coupled UM-UKCA model is run in an atmosphere-only configuration for this thesis because the science is focussed on atmospheric aerosol and its health and radiative effects. In the atmosphere-only configuration, the ocean and sea ice model components are switched off, with time-varying sea-surface temperatures and sea-ice extent prescribed from the second Atmosphere Model Intercomparison Project (www-pcmdi.llnl.gov/projects/amip). The simulations are all within version 1.1 of the 3rd generation of the "atmosphere model" of the Hadley Centre Global Environmental Model (HadGEM3-A-v1.1) described by Hewitt et al. (2011). The UM-UKCA simulations here use the winds, temperature, humidity, clouds and precipitation from HadGEM3-A-v1.1, which are calculated online and provided each timestep to the UM-UKCA sub-model as applied by Morgenstern et al. (2009) and O'Connor et al. (2014).

Large-scale advection, convective uplift and boundary layer mixing of the UM-UKCA gas and aerosol tracers are calculated by other component sub-models within the HadGEM3-A-v1.1 framework (Davies et al., 2005; Gregory and Rowntree, 1990; Lock et al., 2000; Martin et al., 2006; Priestley, 1993). These dynamical processes are integrated on the dynamical atmosphere-model timestep of 20 minutes, along with UM-UKCA emissions. Chemistry and aerosol processes are integrated on a 1-hour timestep, i.e. once every three dynamical timesteps.

All results in this thesis are simulated at N96L63 resolution (1.25° latitude x 1.875° longitude) with 63 vertical levels up to 40km. The upper bounds of the lowest model levels are located at ~15m, ~50m, ~90m, ~150m, ~220m, ~300m, 395m and ~505m.

In order to represent aerosol properties consistently with the meteorological conditions within the particular year being simulated, the "nudging" functionality has been applied for all simulations (Telford et al., 2008). For meteorological nudging in UM-UKCA, simulated horizontal winds and potential temperatures are relaxed toward the ERA-Interim reanalyses (Dee et al., 2011) at 6 hourly intervals. The nudging is applied at full strength between levels 21 (~3.2km) and 56 (~25km), with a buffer zone (two levels below and four levels above) in which the strength of the nudging is linearly decreased to zero.

3.2.2 Tropospheric chemistry scheme

For this work, gas and aerosol precursor chemistry is simulated online using the "tropospheric chemistry with isoprene" ("TropIsop") chemistry scheme. The chemical equation set is identical to that described and evaluated in O'Connor et al. (2014), with equations in the setup here being solved within the "ASAD" framework (Carver et al., 1997) and integrated using a Newton-Raphson solver as implemented in Squire et al. (2014). The TropIsop chemistry scheme simulates tropospheric oxidative capacity online in UM-UKCA and comprises a core tropospheric chemistry scheme with an additional isoprene oxidation scheme following the Mainz Isoprene Mechanism (Pöschl et al., 2000), see O'Connor et al. (2014). In total, 56 chemical species are modelled, including reactions of inorganic odd oxygen (O_x), nitrogen (NO_y), hydrogen (HO_x) and hydrocarbons, including carbon monoxide (CO), and degradation schemes for methane, ethane, propane and other volatile organic compounds (VOCs). Features of the tropospheric chemistry scheme are summarised in the following sub-sections.

3.2.2.1 Aerosol precursor chemistry

The TropIsop chemistry scheme is extended here to include gas and aqueous phase oxidation of sulphur compounds and a lumped monoterpene tracer to account for biogenic secondary organic aerosol (SOA) formation, following the

setup for the 50-year UM-UKCA aerosol hindcasts of Turnock et al. (2015) and Butt et al. (2017). This aerosol chemistry extension ("achem") to TropIsop implements the same aerosol precursor chemistry equation set as developed by Spracklen et al. (2005; 2006) for TOMCAT-GLOMAP (Toulouse Off-line Model of Chemistry and Transport; see Table 3.1). These reactions are included to allow coupling with the aerosol scheme. The added sulphur reactions include gas phase oxidation of dimethyl sulphide (DMS) and sulphur dioxide (SO_2) and aqueous phase oxidation of SO_2. Sulphate aerosol is formed from the gas-phase oxidation of SO_2 by OH and by aqueous H_2O_2 and O_3 oxidation in low-level clouds.

Table 3.1 *Summary of gas and aqueous phase reactions of sulphur and monoterpene in UM-UKCA tropospheric chemistry scheme. Monoterpene is treated as alpha-pinene with secondary organic aerosol product yield of 13%.*

Reaction	**Reference**
Gas phase reactions	
DMS + OH → SO_2 + CH_3O_2 + HCHO	(Pham et al., 1995)
DMS + OH → 0.6SO_2 + 0.4DMSO + CH_3O_2	(Pham et al., 1995)
DMSO + NO_3 → SO_2 + HNO_3 + CH_3O_2 + HCHO	(Pham et al., 1995)
SO_2 + OH → H_2SO_4 + HO_2	(Pham et al., 1995)
MONOTERPENE + OH → 0.13SOA	(IUPAC; Spracklen et al., 2006)
MONOTERPENE + O_3 → 0.13SOA	(IUPAC; Spracklen et al., 2006)
MONOTERPENE + NO_3 → 0.13SOA	(IUPAC; Spracklen et al., 2006)
Aqueous phase reactions	
HSO_3^- + H_2O_2 → SO_4^{2-}	(Kreidenweis et al., 2003)
HSO_3^- + O_3 → SO_4^{2-}	(Kreidenweis et al., 2003)
SO_3^{2-} + O_3 → SO_4^{2-}	(Kreidenweis et al., 2003)

SOA is produced at a yield of 13% from the products of monoterpene and is assumed to condense onto existing aerosols, enabling UM-UKCA to automatically include biogenic secondary organic aerosol formation within the GLOMAP-mode aerosol module (Spracklen et al., 2006; Kelly et al., 2018). As described later in

Section 3.2.4, the nitrate-extended aerosol microphysics scheme also requires the gas phase HNO_3 and NH_3 concentrations to be passed between the chemistry and aerosol scheme.

3.2.2.2 Tropospheric heterogeneous chemistry

The UM-UKCA chemistry scheme contains a dedicated module to represent heterogeneous reactions on aerosol particles. This tropospheric heterogeneous chemistry module ("TropHet") is activated for all simulations in the thesis, with the contribution of this chemistry to seasonal nitrate aerosol formation investigated in Chapter 4. The default scheme included within UM-UKCA has two heterogeneous reactions: the conversion of dinitrogen pentoxide (N_2O_5) to nitric acid and self-reaction of the hydroperoxyl radical, HO_2. The aerosol surface area is calculated online by the GLOMAP-mode aerosol module using the aerosol number concentration, the wet diameter from each mode and the modal geometric standard deviation.

The reaction probabilities of N_2O_5 are dependent on the aerosol composition and on the ambient temperature and relative humidity, with the heterogeneous rate coefficients also calculated using the aerosol surface area and wet radius. The reaction probabilities for N_2O_5 onto sulphate, black carbon and organic carbon are estimated using the equations reported in Evans and Jacob (2005). For reaction on sea-salt, γN_2O_5 = RH x 0.0005 (RH < 62%) or considered constant at 0.03 (RH ≥62%). For this thesis, the reaction probability of N_2O_5 onto ammonium nitrate has been added to the default subroutine and is calculated based on the International Union of Pure and Applied Chemistry (IUPAC) recommended studies of Hallquist et al. (2003), Wahner et al. (1998) and Davis et al. (2008). In practice, this was coded by calculating the nitrate and sulphate uptake based on rates for ammonium sulphate and ammonium nitrate. The TropHet module links directly to the GLOMAP-mode diagnostics, so reactions on dust are not included here because dust is handled by the separate bin-resolved Woodward (2011) scheme, as explained in Section 3.2.3.1. Since the thesis focuses mainly on nitrate aerosol influences within polluted industrialised regions, this omission is not considered to change the results substantially. The reaction probabilities for the HO_2 self-reaction are estimated for the same surfaces using the equations summarised in Mao et al. (2010).

3.2.2.3 Photolysis

Photolysis rates are calculated online based on the distribution of cloud, ozone and aerosol layers using the Fast-J interactive scheme (Wild et al., 2000). The photolysis rates are calculated every UM-UKCA timestep (i.e. at hourly intervals), allowing UM-UKCA to represent additional chemistry-aerosol interaction effects. In the current implementation within UM-UKCA, sulphate aerosol load from the CLASSIC scheme is passed through to Fast-J because the codebase has not yet been updated to enable interaction with GLOMAP simulated aerosol. Nitrate aerosol effects assessed in this thesis therefore do not include influences on photolysis.

3.2.2.4 Dry deposition

The interactive dry deposition scheme for tropospheric gas-phase species is implemented, whereby a resistance based approach is used to calculate deposition velocities across 9 surface types: broadleaf trees, needleleaf trees, C3 grass, C4 grass, shrub, urban, water, bare soil and ice. The scheme follows that of Wesely (1989) and is briefly described in O'Connor et al. (2014), with full descriptions of the approach given in Seinfeld and Pandis (2006) and Smith et al. (2000).

3.2.2.5 Wet deposition

The wet deposition scheme for the tropospheric gas-phase species is the same as that implemented and validated in the TOMCAT chemical transport model (CTM; Giannakopoulos et al., 1999). The wet deposition rates are parameterised as first order loss rates, calculated as a function of the model convective and large-scale precipitation. The scheme was originally developed by Walton et al. (1988). Removal rates are also dependent on the effective Henry's law co-efficient for each species, where the effective Henry's coefficient considers the effects of dissociation and complex formation on species' solubility.

3.2.2.6 Top boundary conditions

The tropospheric chemistry scheme prescribes O_3 concentrations above a threshold vertical level with concentrations from Dall'Amico et al. (2010). In these simulations, the threshold level is the 3rd level above the tropopause.

Stratospheric sources and sinks of NO_y and CH_4, respectively, into the troposphere are deactivated in these simulations. Given that the focus of this PhD is on lower tropospheric aerosol and that downward transport from the stratosphere is relatively slow, this approach is considered acceptable for the short 16 month simulations in this thesis.

3.2.3 GLOMAP-mode aerosol microphysics module

GLOMAP-mode is the modal version of the original bin-resolved Global Model of Aerosol Processes (GLOMAP-bin, e.g. Spracklen et al., 2005) developed specifically for UM-UKCA. The modal scheme was initially developed and evaluated (Mann et al., 2010) in the 3D global offline chemistry transport model, TOMCAT (Chipperfield, 2006). GLOMAP-mode parameterizes the size distribution into several log-normal modes, representing the main parts of the particle size range (nucleation, Aitken, accumulation and coarse), with two distinct types of each mode resolved (insoluble and soluble).

Both versions of GLOMAP (mode and bin) share the same or similar representations of microphysical processes that influence the multi-component, size-resolved aerosol mass and number and its evolution. As well as representing aerosol microphysical processes (nucleation, condensation, coagulation, hygroscopic growth, cloud-processing and particle ageing), the models also include size-resolved representations of primary emissions, dry deposition and wet deposition by impaction and nucleation scavenging.

Mann et al. (2010) provide a comprehensive description of the aerosol model and its implementation in TOMCAT, in which the module is shown to perform well against a range of observations. The modal settings were revised in Mann et al. (2012) to maximise the fidelity of GLOMAP-mode predictions compared to GLOMAP-bin.

Turnock et al., (2015) evaluated simulated trends in SO_4^{2-}, particulate matter, aerosol number, aerosol optical depth (AOD) and surface solar radiation (SSR) over Europe against observations from 1960 to 2010 using a very similar configuration of UM-UKCA to that applied here, but without the nitrate extension to GLOMAP-mode. The study found in general that aerosol trends over Europe are well simulated by the model. Summertime sulphate concentrations are

generally underestimated compared to observations earlier in the period but are in better agreement from around the year 2000 onwards. Wintertime sulphate concentrations are generally underestimated by the model over Europe. Turnock (2016) later showed that adjusting the cloud water pH remedies some of this low bias.

Table 3.2 describes the aerosol components and size ranges that are carried by nitrate-extended GLOMAP-mode with the additional components associated only with this GLOMAP version (Section 3.2.4) shown underlined. As with the standard non-nitrate extended version of GLOMAP, log-normal modes represent aerosols in 4 size ranges: nucleation (D_g < 10 nm), Aitken (10 nm < D_g < 100 nm), accumulation (100 nm < D_g < 1000 nm) and coarse (D_g > 1000 nm). The simulations here apply the revised modal parameters from Mann et al. (2012), with a narrower accumulation mode corresponding to σ_g=1.40 (originally 1.59) and the coarse mode covering particles down to 500 nm dry diameter (D_g).

Table 3.2 *Standard aerosol configuration for GLOMAP-mode, with additional components included for nitrate-extended GLOMAP-mode underlined, adapted from Mann et al. (2010).*

Mode	Size range	Components	Soluble	σ_g
Nucleation soluble	D_g < 10 nm	SO_4^{2-}, $\underline{NO_3^-}$, $\underline{NH_4^+}$	Yes	1.59
Aitken soluble	10 nm < D_g < 100nm	SO_4^{2-}, $\underline{NO_3^-}$, BC, OC, $\underline{NH_4^+}$	Yes	1.59
Accumulation soluble	100 nm < D_g < 500nm	SO_4^{2-}, $\underline{NO_3^-}$, BC, OC, Na^+, $\underline{NH_4^+}$, $\underline{Cl^-}$	Yes	1.40
Coarse soluble	D_g > 500 nm	SO_4^{2-}, $\underline{NO_3^-}$, BC, OC, Na^+, $\underline{NH_4^+}$, $\underline{Cl^-}$	Yes	2.0
Aitken insoluble	10 nm < D_g < 100 nm	BC, OC	No	1.59

In its standard, non-nitrate-extended configuration, GLOMAP-mode carries 5 aerosol components (sulphate, black carbon, organic carbon - including secondary organic aerosol - and sea salt) in four soluble modes and one insoluble Aitken mode, yielding a total of 19 tracers (14 aerosol mass and 5 number). The

nitrate extension adds an extra 10 aerosol tracers through the addition of nitrate and ammonium across four soluble modes and the separation of sea salt, present in the soluble accumulation and coarse modes, into sodium and chloride ions. The HyDiS-1.0 dissolution module, which constitutes the main component of nitrate-extended GLOMAP is described comprehensively in Benduhn et al. (2016), and a brief overview is provided in Section 3.2.4.

The following sub-sections give an overview of the precursor gas and primary aerosol emissions included in GLOMAP-mode, including the MACCity (MACC and CityZen project) emission inventory (Granier et al., 2011) and the model implementation of key aerosol microphysical processes.

3.2.3.1 Precursor gas and aerosol emissions

Emission inputs to the UM-UKCA simulations in this thesis are either based on pre-computed fluxes (offline) or are linked to UM meteorological variables simulated during model run time (online), for example lightning NO_x, sea salt and dust.

All simulations in this thesis use monthly varying anthropogenic and biomass burning emissions of SO_2, NO_x, NH_3, BC, OC, CO and speciated VOCs from the MACCity inventory (Granier et al., 2011). The dataset covers 50 years from 1960 to 2010 with emissions based on the Atmospheric Chemistry and Climate Model Intercomparison Project (ACCMIP) inventory (Lamarque et al., 2010) between 1960 and 2000 and on the RCP 8.5 emission pathway from 2000 onward (van Vuuren et al., 2011). The inventory is sector-specific and includes, for example, emissions from agriculture, agricultural waste, residential use, energy production, shipping and land transportation. The inventory provides emissions for each species and sector at a yearly resolution by interpolating from the decadal mean ACCMIP and RCP 8.5 datasets and a seasonal cycle applied to give monthly mean emissions at 0.5° x 0.5° resolution. In the case of biomass burning, the MACCity inventory includes annual mean carbon emissions from the Global Fire Emissions Database (GFED; van der Werf et al., 2010) to account for large inter-annual variability in emissions.

The majority of MACCity emissions are emitted into the lowest model level, with the exception of some SO_2, aircraft NO_x and biomass burning emissions.

Anthropogenic SO_2 is separated into surface and elevated sources, with elevated sources emitted between 100 and 300m above the surface to represent stack emission heights while surface emissions are emitted into the lowest model level. Year-varying 3D aircraft NO_x emissions and monthly-varying 3D biomass burning emissions of SO_2, BC and POM were re-gridded onto the N96L63 UM-UKCA grid and applied to the model as a 3D emissions source. Emissions of SO_2, BC and OC from biomass burning are distributed uniformly over the lowest 3km of the model. Biofuel and fossil fuel carbonaceous particles are emitted into the lowest model level.

To represent sub-grid sulphate particle formation, e.g. nucleation in SO_2 plumes from power plants and volcanoes, the UM-UKCA simulations match AeroCom recommendations (Dentener et al., 2006) in emitting 2.5% of all gas-phase SO_2 emissions as primary sulphate emissions. Such primary sulphate particles are included from anthropogenic, volcanic and biomass burning sources of SO_2, with the emitted aerosol number derived from the sulphate mass emission based on the grid-scale particle source having a log-normal emissions size distribution, following size recommendations from Stier et al. (2005).

DMS emissions are calculated depending on seawater concentration fields and a wind speed dependent air-sea exchange parameterisation (Kettle and Andreae, 2000; Liss and Merlivat, 1986). A climatological volcanic SO_2 source from continuous (passively degassing) and explosive (tropospheric-injecting) eruptions are included from 3D emission files, combining the Andres and Kasgnoc (1998) and Halmer et al. (2002) inventories, with AeroCom-recommended injection heights (Dentener et al., 2006).

Lightning NO_x emission is calculated online using a parameterised lightning flash frequency of $3.44 \times 10^{-5} H^{4.9}$ per minute over land and $6.4 \times 10^{-4} H^{1.73}$ per minute over ocean, where H is cloud depth, combined with a latitude dependent cloud-to-cloud and cloud-to-ground flash ratio (Price and Rind, 1992; 1993). Lightning NO_x formation is set to occur in clouds with a depth of 5km or over.

The source of secondary organic aerosol and influence on oxidising capacity from monoterpene emissions is included in the simulations by applying the single-stage oxidation scheme from Spracklen et al. (2006). Climatological

monthly varying 2D surface monoterpene emissions from vegetation follow the Global Emissions InitiAtive database (Guenther et al., 1995) in this thesis.

Monthly varying emissions of anthropogenic carbonaceous particles (emitted as internally mixed black carbon and primary organic matter particles) are included from the MACCity fossil fuel and biofuel sources. They are emitted with a modified log-normal size distribution based on AeroCom recommendations of Dentener et al. (2006), with modifications from Stier et al. (2005). Primary biomass and biofuel emissions are given a geometric mean diameter of 150 nm while primary fossil fuel emissions are set to 60 nm, with both distributed with a geometric standard deviation of 1.59.

Sea salt emission fluxes are calculated using the surface wind speed parameterisation of Gong (2003). Size-resolved sea-spray fluxes are calculated over a 20 bin size range and then fed into either the accumulation or coarse soluble modes of GLOMAP-mode.

Mineral dust aerosol is simulated using a separate six-bin scheme developed by Woodward (2001, 2011) which simulates the mass of dust particles with a dry radius between 0.03 and 30 μm. The dust emissions flux is largely controlled by wind speed, with uplift of particles occurring over erodible bare soil when wind speeds exceed a threshold value. The threshold is defined based on surface soil type.

3.2.3.2 Aerosol Microphysics

Although the main topic of research in this thesis investigates changes simulated by the nitrate-extension to GLOMAP-mode, global variations in the underlying particle size distribution and abundance stem from the processes simulated in the core GLOMAP-mode module. The following section therefore describes how these processes are represented by GLOMAP-mode in the UM-UKCA model applied for the simulations in this thesis.

3.2.3.2.1 New particle formation

New particle formation occurs via nucleation, i.e. the formation of tiny particles, initially from clusters of molecules of sulphuric acid and water vapour, in combination also with other nucleating gas phase species. In the free

troposphere (FT), new particle formation occurs principally by the binary homogeneous nucleation of H_2SO_4-H_2O to form sulphate aerosol. In TOMCAT-GLOMAP, 35% of CCN (0.2%) in global low-level clouds were found to originate in the free troposphere (Merikanto et al., 2009). The nucleation rate parameterization of Kulmala et al. (1998a) is applied, with particles forming when the gas-phase sulphuric acid concentration surpasses a critical threshold concentration. In the simulations here new particle formation occurs only via FT nucleation, although the full range of boundary layer nucleation mechanisms in GLOMAP-mode (see Reddington, 2012), including the organic-mediated rates, are included in later (non nitrate-extended) configurations of the UM-UKCA codebase.

3.2.3.2.2 Coagulation

GLOMAP-mode represents coagulation of particles from collisions both within (intra-modal) and between (inter-modal) modes. The coagulational growth process acts to conserve particle mass while reducing particle number (increasing average particle size). The model represents coagulation as occurring via Brownian diffusion, which is a reasonable approximation in most conditions. The rate of coagulation among particles is strongly size dependent and intra-modal coagulation (the coagulation of 2 particles in the same mode) is only effective for the sub-micron aerosol size modes.

In the version of GLOMAP-mode applied here, intra-modal coagulation occurs only within soluble modes. Freshly nucleated particles (i.e. those in the nucleation mode) coagulate effectively with other similar-sized particles (i.e. with those in the same mode) and also coagulate with particles in larger size modes, both soluble and insoluble. Intra-modal coagulation of particles in the smallest modes is an important growth mechanism for atmospheric aerosol, with larger insoluble particles also acting as a sink for younger nucleated particles. In this version of GLOMAP-mode, insoluble particles can only coagulate with larger soluble mode particles. More details are provided in Mann et al. (2010; 2012).

3.2.3.2.3 Condensation

GLOMAP-mode simulates condensation of H_2SO_4 and SOA precursor vapours (Table 3.1) onto all aerosol modes, with the rate of condensation determined by particle size and molecular composition following Fuchs and Sutugin (1971). Condensation acts to increase the particle mass and size while conserving particle number through condensational growth of particles. In GLOMAP-mode, condensational growth is simulated by moving a proportion of the aerosol mass up to the adjacent larger mode if needed, while the particle number remains unchanged. In doing so, growth occurs (particle size increases), with "mode-merging" checking the mode mean size is still within the limits for that mode and moving a proportion of aerosol mass to the adjacent larger mode if needed (Table 3.2).

Prior to the development of nitrate-extended GLOMAP, only one-way gas-particle condensation processes were represented, whereby condensable vapours are transferred to the particle phase with an assumed zero vapour pressure. The model calculates this gas-particle transfer kinetically with the vapour transport rate calculated for each size mode. Competition for the available condensable vapours arises between the processes of condensation and nucleation, which the model resolves by integrating each process sequentially on a number of shorter competition sub-timesteps within each GLOMAP timestep (Spracklen et al., 2005).

The condensation of H_2SO_4 and SOA precursor vapours contributes to condensation ageing, whereby previously water-insoluble aerosol can become soluble during transport. Condensation ageing also occurs by inter-modal coagulation of smaller soluble particles onto larger insoluble particles. In GLOMAP-mode, this is represented by first calculating, from the total soluble material, how many insoluble particles would be coated. A proportion of the mode's particles are then deemed to be hydrophilic and are transferred to the corresponding soluble mode once 10 monolayers of soluble material have accumulated on the particle surface (Mann et al., 2010). The number of monolayers influences the flux of insoluble carbonaceous aerosol to the soluble modes and therefore influences its rate of removal by nucleation scavenging (Section 3.2.3.2.6).

3.2.3.2.4 In-cloud oxidation and cloud processing

In the presence of low-level (e.g. stratocumulus) clouds, aqueous phase oxidation of SO_2 can occur in the model through reaction with H_2O_2 and O_3 to form sulphate aerosol. In UM-UKCA, the instantaneous cloud fraction, cloud liquid and cloud ice water contents are available at each timestep. In this version of UM-UKCA, low level cloud is identified using the liquid cloud fraction, with an additional criterion requiring that the cloud liquid water content of a grid box exceeds 0.2 g m^{-3}. SO_2 is incorporated into cloud droplets rapidly (Warneck, 2000) and the model therefore follows an effective Henry's law equilibrium approach in the standard GLOMAP-mode setup. The dissociation of dissolved SO_2 in the cloud water leads to the formation of HSO_3^- and SO_3^{2-} (via equations 3.1 and 3.2) and subsequently to sulphate aerosol formation via dissolved H_2O_2 and O_3 oxidation, proceeding via the reactions in Table 3.1.

$$SO_2 \rightleftharpoons H^+ + HSO_3^- \quad (3.1)$$

$$HSO_3^- \rightleftharpoons H_+ + SO_3^{2-} \quad (3.2)$$

SO_2 oxidation by H_2O_2 is the dominant pathway for most conditions and occurs independently of rain water pH. However, SO_2 aqueous oxidation by O_3 is highly sensitive to aqueous aerosol particle pH with order-of-magnitude differences in rates under different conditions (Seinfeld and Pandis, 2006). In UM-UKCA, the current default approach involves specifying a fixed cloud water pH of 5.0, with Turnock (2016) identifying how assuming a more acidic pH of 4.0 strongly affected simulated European wintertime surface sulphate in the model. The cloud pH of 5.0 chosen for aqueous phase reactions is considered to be representative of the 'effective' bulk pH of cloud droplets based on observations (Benedict et al., 2012; Collett et al., 1993; Murray et al., 2013).

Cloud processing in GLOMAP-mode is defined as the growth of aerosol particles through the uptake and chemical reaction of gases while particles exist as water droplets in low-level clouds (Mann et al., 2010). The growth of particles within the cloud results in differential growth between activated and non-activated particles, leading to the minimum in the size distribution between the Aitken and accumulation modes (the Hoppel gap, e.g. Hoppel et al., 1994). In this version of

the model, a globally representative bulk value of 37.5 nm is assumed for the activation dry radius, corresponding to a 0.2% cloud supersaturation typical of marine stratocumulus clouds (Mann et al., 2010; Spracklen et al., 2005).

In GLOMAP-mode, cloud processing is represented as a two-step process. First, the fraction of Aitken mode particle mass and number larger than the activation diameter is transferred to the soluble accumulation mode. Larger particles within the Aitken mode are therefore able to become activated and cloud processed while still representing the minimum in the size distribution between the soluble Aitken and accumulation modes. Second, sulphate mass produced by in-cloud oxidation of SO_2 is portioned between the soluble accumulation and coarse modes according to their fractional contribution to the total particle number concentration of the two modes (Mann et al., 2010).

3.2.3.2.5 Dry deposition

Aerosol particles are removed to the surface via both dry deposition and sedimentation, following the resistance-based approach described in Spracklen et al. (2005) and Mann et al. (2010). An overall dry deposition velocity is calculated for each of the GLOMAP size modes, based on the gravitational settling velocity and the aerodynamic and surface resistances following Slinn (1982). The rate of dry deposition is dependent on the particle size, land surface type and wind speed along with collection efficiencies for Brownian diffusion, impaction and interception set following the 16 surface types of Zhang et al. (2001) mapped onto 9 UM land-surface categories.

3.2.3.2.6 Wet deposition

Wet removal of aerosol particles in GLOMAP-mode occurs via nucleation (or in-cloud) scavenging (also known as rainout) and impaction (or below-cloud) scavenging (also known as washout).

Nucleation scavenging rates are dependent on rainfall rates and calculated for both large-scale and convective-scale precipitation (Kipling et al., 2013; Mann et al., 2010). All soluble accumulation and coarse mode particles in the cloudy fraction of each grid box are assumed to be activated and scavenged by large scale precipitation. Aerosols in convective scale rainfall are removed in a similar way, but assuming a cloud fraction of 30%. The removal rate by both large scale

and convective scale precipitation is set to proceed at the same rate as the large-scale precipitation scheme converts cloud water to rain water (i.e. the large-scale autoconversion rate). This approach differs from subsequent versions of UM-UKCA, where a size threshold approach is used to determine which aerosol are nucleation scavenged (Mann et al., 2012).

The approach for impaction scavenging in GLOMAP-mode is the same in the UM-UKCA model as in the TOMCAT model (Mann et al., 2010; Slinn, 1984). The scavenging rate is derived from the rain rates of large-scale and convective-scale precipitation combined with look-up tables for raindrop-aerosol collection efficiencies (Mann et al., 2010). The terminal velocity of raindrops is calculated using Easter and Hales (1983). The collision efficiencies are based on the modal geometric mean dry radius and a modified Marshall-Palmer raindrop size distribution that accounts for rainfall intensity (Sekhon and Srivastava, 1971).

3.2.4. Nitrate-extended GLOMAP-Mode

The nitrate-extended GLOMAP-mode module simulates the size-resolved inorganic nitrate-sulphate-ammonium-sodium-chloride system via the hybrid inorganic dissolution solver, HyDis-1.0. The solver calculates the partitioning of NH_3 and HNO_3 into NH_4^+ and NO_3^- components within each soluble mode. A comprehensive description of the solver and its implementation in the TOMCAT chemistry transport model can be found in Benduhn et al. (2016) and a summary of its implementation in UM-UKCA (as applied here) is given in this sub-section.

The term “partitioning” is preferred in this thesis to describe the two-way gas-particle exchange of the semi-volatile gases, where Benduhn et al. (2016) used the term ”dissolution”. The process combines the initial transfer of the gas and its subsequent dissociation within the aerosol particle aqueous phase. The term “condensation” is reserved in this thesis for one-way gas to particle transfer, for example of sulphuric acid, where the GLOMAP-mode routines assume the vapour condenses irreversibly into the particle phase. To re-iterate, “dissolution” or “partitioning” are used here specifically to describe two-way gas-particle transfer of semi-volatile gases, including only the inorganic species NH_3, HNO_3 and HCl. The chemistry involves the NH_3 reacting with H_2O to form NH_4OH, which then dissociates in the aerosol aqueous phase along with acidic species

HNO_3 and HCl. These gases may re-evaporate from the aerosol particle phase (de-gas) depending on ambient temperature and chemical composition (Benduhn et al., 2016).

In terms of model structure, the nitrate-extended configuration carries 10 additional aerosol mass tracers through 1) the addition of nitrate and ammonium components across four soluble modes and 2) the separation of sea salt into sodium and chloride ions (see Table 3.3). The solver also requires that gas phase tracers for HNO_3 and NH_3, which are already included within all of the UM-UKCA chemistry schemes, are made readable into GLOMAP-mode in UM-UKCA.

Table 3.3 *Overview of solutes that are subject to dissolution and dissociation in the HyDiS-1.0 solver (Benduhn et al., 2016; Kapadia et al., 2016).*

Species	**Reaction**
Nitric acid ($HNO_{3(g)}$)	$HNO_{3(g)} = H^+_{(aq)} + NO_3^-{}_{(aq)}$
Hydrochloric acid ($HCl_{(g)}$)	$HCl_{(g)} = H^+_{(aq)} + Cl^-_{(aq)}$
Sulfuric acid ($HSO_4^-{}_{(aq)}$)	$HSO_4^-{}_{(aq)} = H^+_{(aq)} + SO_4^{2-}{}_{(aq)}$
Ammonium sulphate ($(NH_4)_2.SO_{4(s)}$)	$(NH_4)_2.SO_{4(s)} = 2NH_4^+{}_{(aq)} + SO_4^{2-}{}_{(aq)}$
Ammonium nitrate ($NH_4.NO_{3(s)}$)	$NH_4.NO_{3(s)} = NH_{3(g)} + HNO_{3(g)}$
Ammonium chloride ($NH_4Cl_{(s)}$)	$NH_4Cl_{(s)} = NH_{3(g)} + HCl_{(g)}$
Sodium sulphate ($Na_2SO_{4(s)}$)	$Na_2SO_{4(s)} = 2Na^+_{(aq)} + SO_4^{2-}{}_{(aq)}$
Sodium nitrate ($NaNO_{3(s)}$)	$NaNO_{3(s)} = Na^+_{(aq)} + NO_3^-{}_{(aq)}$
Sodium chloride ($NaCl_{(s)}$)	$NaCl_{(s)} = Na^+_{(aq)} + Cl_{(aq)}$

Chemically, the solver accounts for the gas and aqueous phase equilibria during dissolution and dissociation of several solutes. Table 3.3 shows the solutes that are included in dissolution and dissociation reactions in the HyDiS-1.0 (Benduhn et al., 2016; Kapadia, 2015; Zhang et al., 2000).

The formation of solid phase salts at low ambient relative humidity below the deliquescence relative humidity is implicitly challenging to simulate because of hysteresis behaviour in hygroscopic growth and is not represented in the scheme. The implementation of HyDiS-1.0 in GLOMAP-mode described in Benduhn et al. (2016) does not yet consider semi-volatile organic species.

As described in Section 2.4.1, large-scale models often represent gas-particle partitioning as an equilibrium process, principally as a result of issues of numerical instability and computational expense. Dynamic approaches are also available but the numerical stiffness of the underlying equations means accurate solution requires an adaptive/dynamical timestep. Such schemes are often deemed too computationally expensive for use in global model simulations (see Section 2.4.1 and discussion in Capaldo et al., 2000). 'Hybrid' partitioning schemes seek to overcome the limitations of the two approaches by combining them and using decision criteria to determine whether an equilibrium or dynamic treatment is applied.

While Benduhn et al. (2016) give a full description of the solver and its implementation in GLOMAP-mode, the main features of the solver are summarised here. The main element of the nitrate-extension to GLOMAP-mode is a hybrid partitioning solver (HyDiS-1.0) which applies a time and size-dependent decision criteria, to determine whether an equilibrium or dynamic formulation is applied when solving the partitioning of semi-volatile inorganic species into the aqueous aerosol particle phase. With this hybrid approach, an accurate representation of the chemical, thermodynamic and microphysical influences on dissolution dynamics is obtained at a relatively low computational cost.

The solver combines several methods applied within existing numerical methods in combination with novel methods developed specifically for coupling to the GLOMAP size-resolved aerosol module, with the principal one being the hybrid decision criteria (Benduhn et al., 2016). For example, the dynamic dissolution formulation uses the semi-implicit and semi-analytical integration method of Jacobson (1997). The equilibrium sub-solver applies the analytical approach of Nenes et al. (1998), with a mixed time integration method following

Zhang and Wexler (2006) and Zaveri et al. (2008). The dynamic and equilibrium sub-solvers are described in Benduhn et al. (2016).

In the solver, the main distinction criterion determines whether gas-particle paritioning is carried out with the equilibrium or dynamic sub-solvers, and also specifies regimes within them (e.g. pseudo-transition). The gas-particle partitioning of an aerosol size class is treated using the equilibrium formulation (i.e. it is solved iteratively assuming equilbrium) if it meets the following two distinction criteria:

1. Equilibration time criterion. An aerosol size class is placed in the equilibrium mode if its equilibration time is much shorter than the mode time step.

   The time distinction criterion, κ_{teq}, with respect to size class, i, and species, j, can be stated as:

   $$\kappa_{teq}^{i,j} = a \cdot t_c^{i,j}$$

   Where a is an ad hoc proportionality constant, equivalent to the number of acceptable internal timesteps. Particles of size i, and species, j, are therefore deemed to be in equililbrium when $\kappa_{teq}^{i,j} < \Delta t$, where Δt is the overall model timestep.

2. Mass balance criterion. In addition to an aerosol size class needing to meet the main "time distinction criterion" above, an additional criterion is applied to optimise the operation of the scheme. This is required because some size classes are in equilibrium while others are solved kinetically and because rapid chemical interactions occur within the different sized aqueous particles. Optimal co-operation of the methods therefore requires that the influence of the equilibrium size classes on the progressing mass balance is kept to a minimum. In practice, this is achieved by an additional "mass distinction criterion" assessing the magnitude of the parameter $\kappa_{meq}^{i,j}$,

   $$\kappa_{meq}^{i,j} = \frac{\left| c_{eq}^{i,j} - c_{i,j} \right|}{c_{tot}^{j}}$$

where $c_{eq}^{i,j}$ is the equilibrium particle molecular concentration, $c_{i,j}$ is the particle molecular concentration and c_{tot}^{j} is the total particle molecular concentration (sum over all size classes). An aerosol size class is treated assuming equilibrium when $\kappa_{meq}^{i,j} < 0.1$.

An aerosol size class is treated assuming equilibrium if it meets the two criteria above with respect to all of the dissolving species in that size range. Size classes that remain in the dynamic mode are re-checked against the time criterion after every internal solver timestep. The time criterion is adapted to the remaining fraction of the timestep, such that the criterion is met when $\kappa_{teq}^{i,j} < \Delta t - \delta t$, where δt is the time accumulated by the internal time steps so far.

Benduhn et al. (2016) also present a series of sensitivity experiments to test its operation within a box model framework, including validating the equilibrium solver by comparing to the benchmark AIM-III chemical equilibrium solver (Clegg et al., 1998). The paper also evaluated its application within the global 3D TOMCAT chemistry transport model framework. The box model experiments validate that the hybrid solver achieves numerically accurate results under a wide range of atmospheric conditions. When implemented in the global modelling environment the solver was found (1) to be in good agreement with observed surface NO_3^- and NH_4^+ concentrations in Europe, North America and East Asia, (2) to capture the size partitioning of nitric acid and ammonia into the aerosol Aitken mode and (3) to have modest computational expense compared to a fully equilibrium approach. Kapadia (2015) further evaluates the TOMCAT implementation of nitrate-extended GLOMAP, comparing to vertical profile measurements from aircraft observations. The nitrate-extended GLOMAP-mode module was implemented into UM-UKCA at the start of this thesis and the evaluation of its simulated annual and seasonal mean concentrations of inorganic aerosol and precursor gas species is the first part of this PhD thesis (Chapter 4).

3.3 Aerosol health effects

In Chapter 5, the contribution of nitrate aerosol to $PM_{2.5}$ and cause-specific premature mortality is estimated. The calculations in this thesis only consider

the health impacts from long-term exposure to $PM_{2.5}$. The methods applied in Chapter 5 are described in the following sub-section.

3.3.1 Estimation of $PM_{2.5}$ and nitrate aerosol fraction

Dry $PM_{2.5}$ mass concentrations were calculated offline by summing the mass concentrations of sub-2.5 micron nitrate, sulphate, ammonium, sea salt (sodium and chloride ions), organic carbon and black carbon (BC). The $PM_{2.5}$ contribution from dust is included from a separate UM-UKCA aerosol climatology (Turnock, via correspondence). Figure 3.1 shows the regions over which $PM_{2.5}$ composition (plus mortality and emissions) are averaged for the analysis in Chapter 5.

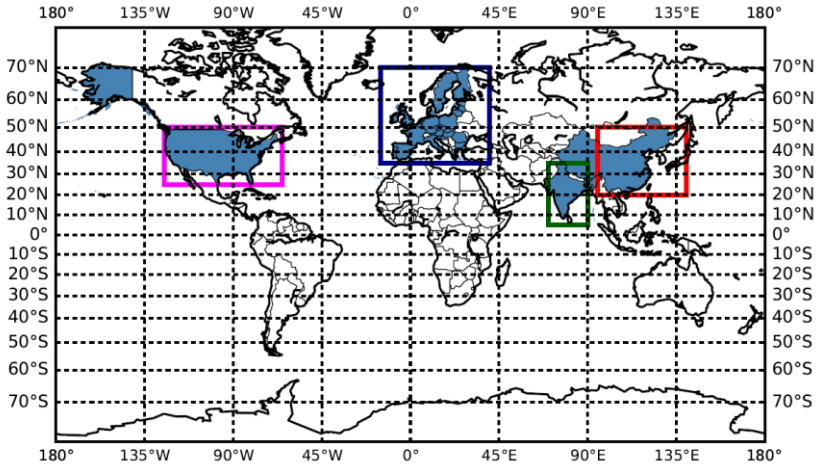

Figure 3.1 *Regional domains used in Chapter 5 analysis of 1980 to present day emission changes (solid boxes). Shaded areas show the regions over which $PM_{2.5}$ composition and mortality are calculated, including the USA, European Union (comprising the 28 current member states), India and China.*

The fractional contribution of nitrate aerosol to the $PM_{2.5}$ is estimated via two methods, which this thesis (Chapter 5) terms the 'speciation' approach and the 'subtraction' approach. The differences in resulting nitrate aerosol fraction of $PM_{2.5}$ from each approach are discussed in Section 5.3.2. The 'speciation' method takes the speciated sub-2.5 μm nitrate mass concentration and divides by the total ambient $PM_{2.5}$. The 'subtraction' method requires two simulations, which are run with and without nitrate aerosol formation. Nitrate aerosol formation is de-activated in simulations by switching off the gaseous nitric acid uptake into the particle phase. The difference between the two $PM_{2.5}$ fields then gives the

nitrate mass in addition to changes from associated aerosol (e.g. ammonium and sodium) and microphysical processes (i.e. aerosol growth and removal). This is then divided by the total ambient $PM_{2.5}$.

In Chapter 5, a bias correction factor is applied to the raw model $PM_{2.5}$ prior to the mortality calculations. Depending on the region, either ground-based observations or satellite-derived $PM_{2.5}$ (Section 3.6.3) are used to calculate the model bias. The resulting bias-corrected $PM_{2.5}$ fields are evaluated in Section 5.3.1.2.

The regional mean bias over the European Union and the USA is calculated with respect to ground-based observations as the ratio of regional mean modelled $PM_{2.5}$ to regional mean observed $PM_{2.5}$ at ground-based site locations. The bias correction factors for each region are then calculated as the inverse of the regional biases.

In order to make a same year (2008) comparison of modelled and observed $PM_{2.5}$ in the absence of adequate ground-based observations, the bias correction factor over India and China is calculated with respect to year 2008 satellite-derived surface $PM_{2.5}$ observations. The UM-UKCA $PM_{2.5}$ concentrations are first re-gridded to the resolution of the satellite-derived $PM_{2.5}$ fields. The regional mean bias is calculated as the ratio of regional mean modelled $PM_{2.5}$ to the regional mean satellite-derived $PM_{2.5}$, as averaged over each satellite resolution grid square per region.

3.3.2 Exposure-response functions

The health burden of long-term exposure to $PM_{2.5}$ is estimated in terms of annual mean premature mortality (number of premature deaths). The integrated exposure-response (IER) functions of Burnett et al. (2014) are used to estimate the relative risk of mortality from five disease endpoints linked to $PM_{2.5}$ exposure. The IERs are defined for five causes of death in adults ≥ 25 years: ischemic heart disease (IHD), stroke, chronic obstructive pulmonary disease (COPD) and lung cancer and in infants ≤ 5 years: acute lower respiratory infection (LRI). The IER functions define the relative risk from a global range of ambient annual mean $PM_{2.5}$ concentrations by integrating available information on relative risk from studies of ambient air pollution, active and second hand

tobacco smoking and household solid fuel pollution. The same IER functions were used for the 2015 Global Burden of Disease Study (GBD 2015; Forouzanfar et al., 2016; Cohen et al., 2017).

The $PM_{2.5}$ concentration, C, is used in the IERs to determine the relative risk, RR, using equation 3.3:

$$For\ C\ \geq\ C_o,\ RR(C) = 1\ +\ \alpha[1 - e^{-\beta(C-C_o)^{\gamma}}] \qquad (3.3)$$

$$For\ C\ \leq\ C_o, \qquad RR = 1$$

Where 1+ α is the maximum risk, β is the ratio of IER between low and high concentrations, γ is the power of the $PM_{2.5}$ concentration (C) and C_o is the theoretical minimum risk exposure level (TMREL) below which no excess risk above the base value of 1 is assigned. The TMREL is assigned a uniform distribution of 2.4 to 5.9 μg m^{-3}, bounded by the minimum and 5th percentiles of exposure distributions from the available outdoor air pollution cohort studies. The range represents uncertainty in adverse effects of low-level $PM_{2.5}$ exposure (Burnett et al., 2014).

The parameters α, β and γ determine the shape of the exposure-response function for each disease. As in Apte et al. (2015), Turnock et al. (2016), Butt et al. (2017), the values are collated into look up tables but updated here to use parameter combinations defined in the GBD 2015 study e.g. as in Conibear et al. (2018). Values are included in the look up table for each disease using the mean estimated RR for 0.1 μg m^{-3} increments in $PM_{2.5}$ concentration between 0 and 300 μg m^{-3}. The 5th and 95th percentile of the estimated RRs is also used to define the uncertainty range for each disease. The uncertainty in RR is considered alongside the uncertainty in background disease rates but the uncertainty range defined here does not consider uncertainty in aerosol concentrations.

Figure 3.2 shows the IERs for each disease end-point. They are sub-linear, with lower sensitivity of relative risk to changes in $PM_{2.5}$ at higher concentrations (Pope et al., 2009; Pope et al., 2011). This is true, in particular, for cardiovascular ischemic heart disease, stroke and lower respiratory infection.

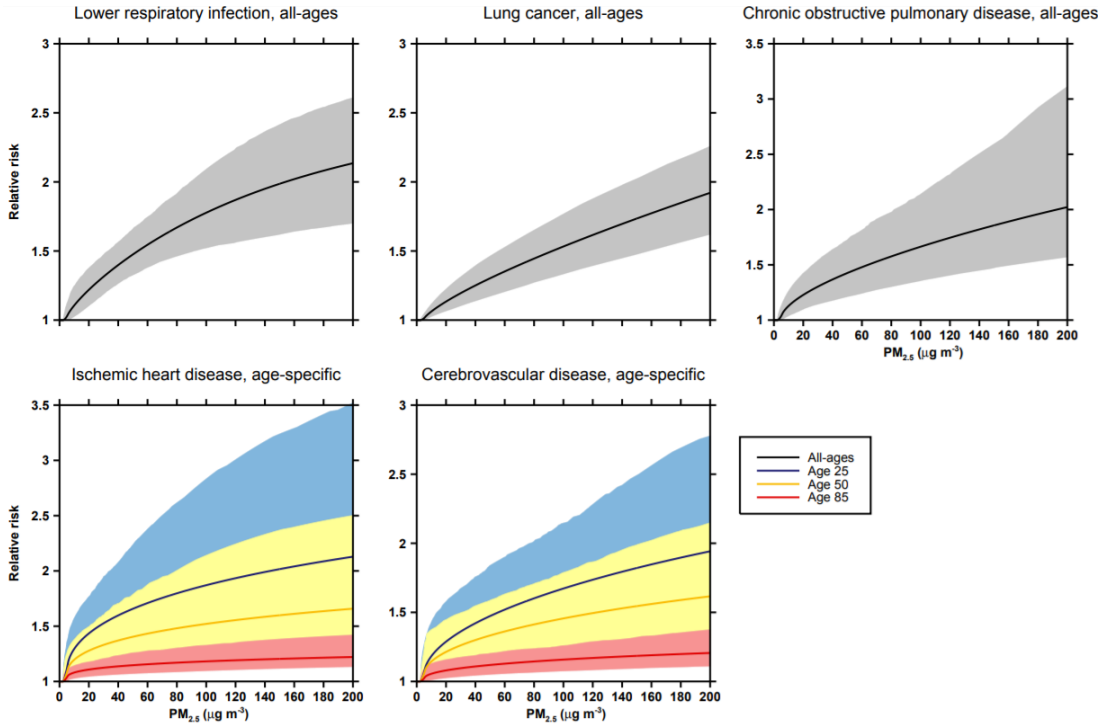

Figure 3.2 GBD 2015 integrated exposure-response (IER) functions relating $PM_{2.5}$ concentrations to the relative risk of premature mortality from five disease endpoints. These are a) lower respiratory infection, b) lung cancer, c) chronic obstructive pulmonary disease, d) ischemic heart disease and e) cerebrovascular disease (stroke). IERs are shown for ages 25, 50 and 85 years for ischemic heart disease and cerebrovascular disease, with others showing relationships based on all ages. From Butt (2018).

3.3.3 Background and demographic disease data

For present day (year 2008) estimates of $PM_{2.5}$-attributable mortality, gridded population count totals for the year 2010 at 0.25° x 0.25° (~ 30 km x 30 km) resolution are applied from the United Nations UN (United Nations)-adjusted Gridded Population of the World v4 (GPWv4.10) dataset (CIESIN, 2017).

To produce population count data for the year 1980, national level population totals are taken from the GBD 2015 (IHME, 2016) for the year 1980 and are distributed in each country according to the year 2000 spatial distribution of population from GPWv4.10. Year 2000 is used as the earliest year included in the GPW4.10 dataset. National-level population age group fractions are also applied from the GBD 2015 and are readily available for both the years 1980 and 2016 (IHME, 2016). It is assumed that there is no uncertainty from the GPWv4.10 and

UN population or demographic data because uncertainty bounds are not provided. However, sources of error are documented elsewhere for GPWv3 (e.g. Deichmann et al., 2001).

National-level age-specific background mortality rates from each disease endpoint for the year 2008 are taken from the cause of disease visualisation tool hosted by Health Metrics and Evaluation (IHME, 2018). The dataset provides upper and lower uncertainty bounds in background mortality rates which are incorporated into the defined uncertainty range of mortality rates calculated in Chapter 5. In the absence of reported background disease mortality rates for the year 1980 from this dataset, these are estimated by linearly extrapolating from year 1990 national level rates based on the rate of change in disease rates between 1990 to 2000.

3.3.4 Attributable mortality calculation

The number of attributable deaths is calculated at the spatial resolution of the gridded population count data (~30 km). The attributable-fraction type relationship of Apte et al. (2015) is used to calculate the number of premature deaths (mortality), $M_{i,j,z}$, per grid cell (i) from disease (j) in age group (z) at annual mean grid cell $PM_{2.5}$ concentration (C_i) (eq. 3.4).

$$M_{i,j,z} = P_{i,z} \times \hat{I}_{j,z,k} \times \left(RR_{j,z}(C_i) - 1\right), \tag{3.4}$$

$$\text{where, } \hat{I}_{j,z,k} = \frac{I_{j,z,k}}{\overline{RR}_{j,k}} \text{ and } \overline{RR}_{j,z,k} = \frac{\sum_{i=1}^{N} P_{i,z} \times RR_{j,z(C_i)}}{\sum_{i=1}^{N} P_{i,z}}$$

Here, $P_{i,z}$ is the population of grid cell i, $I_{j,z,k}$ is the background rate of disease j in age group z for country k, C_i represents the annual mean $PM_{2.5}$ concentration in grid cell i, $RR_{j,z,k}(C_i)$ is the relative risk for disease end point j at concentration C_i and $\overline{RR}_{j,z,k}$ is the average population-weighted RR from disease j in country k. $\hat{I}_{j,z,k}$ therefore represents the hypothetical baseline mortality rate for each disease per age group per country if $PM_{2.5}$ concentrations are reduced to the TMREL.

The 'nitrate-associated' mortality is calculated using an additional simulation in which nitrate aerosol formation is switched off. The change in mortality that arises when nitrate aerosol formation is excluded is then calculated by

subtracting the mortality calculated from the perturbed simulation from the baseline estimated mortality. This is equivalent to applying the following relationship (equation 3.5) based on Apte et al. (2015):

$$M_{i,j,z} = P_{i,z} \times \hat{I}_{j,z,k} \times \left(RR_{j,z}(C_i) - RR_{j,z}(C^*)\right) \quad (3.5)$$

Where, C_i is the baseline annual mean $PM_{2.5}$ concentration and C* is the perturbed annual mean $PM_{2.5}$ concentration. The approach used in this thesis has been termed the 'subtraction' or 'zero out' approach in the literature (Silva et al., 2016; Kodros et al., 2016; Chambliss et al., 2014) and defines the *reduction* in mortality when nitrate aerosol is removed from the ambient $PM_{2.5}$. The subtraction approach is chosen for this thesis over alternative approaches (e.g. attribution approaches) because it is more policy relevant in considering the *removal* of nitrate aerosol from the ambient $PM_{2.5}$ and because it also considers changes in associated aerosol (e.g. ammonium) and microphysical impacts of nitrate aerosol formation. The choice of method, however, can give a different indication of the change in mortality that would arise from an individual source of $PM_{2.5}$ (e.g. Kodros et al., 2016; Conibear et al., 2018).

Years of life lost (YLL) due to $PM_{2.5}$-attributable premature deaths are estimated by multiplying the national (or regional for European Union) age-specific mortality rate from all disease endpoints by the life expectancy remaining at the age of death. Life expectancies are applied from the standard reference life table from the 2015 Global Burden of Disease (IHME, 2016). The YLLs in each age group are then summed to give the regional total YLL.

The relative risks calculated from each disease end point are functions of the total $PM_{2.5}$ inhaled, with toxicity of $PM_{2.5}$ dependent on the mass (exposure) and not the composition of $PM_{2.5}$. The toxicity of different components of $PM_{2.5}$ may vary. However, there is insufficient epidemiological and toxicological knowledge to quantify their relative toxicity in these calculations. The toxicity of nitrate aerosol has been discussed in Section 2.4.7.

3.3.5 Decomposition of change in cause-specific mortality

In Chapter 5, $PM_{2.5}$-attributable and nitrate-associated mortality calculated from a present day (year 2008) emissions scenario are compared with those estimated under a 1980 scenario. The overall change in mortality with time is controlled by four factors: population growth, population ageing, background mortality rates (independent of $PM_{2.5}$ exposure) and exposure to ambient $PM_{2.5}$. The contribution to mortality change from each of these factors is estimated following the decomposition analysis approach of Cohen et al. (2017). The contribution from each factor is estimated incrementally with the increase due to population size (population growth) estimated first, before the contributions from change in population structure (age), change in background disease rates (changes in rate with access to care, treatment and non-$PM_{2.5}$ factors) and, finally, from the change in $PM_{2.5}$ exposure are estimated. The approach is described in detail in the supplementary material of Cohen et al. (2017).

3.4 Aerosol cloud albedo radiative effect

Present day aerosol cloud albedo effects are calculated offline in this thesis from simulated 3D monthly mean aerosol fields, using the Suite of Community Radiative Transfer codes based on Edwards and Slingo (SOCRATES; Edwards and Slingo, 1996). The Edwards and Slingo radiative transfer model has 6 shortwave and 9 longwave bands, with a delta-Eddington 2 stream scattering solver at all wavelengths. The principal metric for composition radiative effects is the net (shortwave + longwave) top-of-atmosphere (ToA) change in radiative balance. In this thesis, the term “radiative effect” is used to represent the radiative flux change compared to a zero baseline concentration with the same composition-climate setting (i.e. year 2008 conditions). Present day ToA aerosol cloud albedo radiative effects are calculated following the methodology applied in e.g. Kapadia et al. (2016), Rap et al. (2013) and Scott et al. (2014; 2018).

The cloud albedo radiative effect is determined based on perturbations to cloud droplet number concentrations (CDNC). CDNC are calculated offline from 3D monthly mean aerosol mass and number concentrations using the hygroscopicity parameter (κ) approach of Petters and Kreidenweis (2007) and

the mechanistic Nenes and Seinfeld (2003) parameterisation, with updates from Fountoukis and Nenes (2005) and Barahona et al. (2010). For these calculations, the updraft velocity is assumed to be 0.15 m s^{-1} over sea and 0.3 m s^{-1} over land, consistent with observations for low-level stratus and stratocumulus clouds (Guibert et al., 2003; Peng et al., 2005; Pringle et al., 2012). The following κ values are assigned to each simulated aerosol component: sulphate (0.61), sea salt (1.28), black carbon (0.0), particulate organic matter (0.1), nitrate (0.67) and ammonium (0.61). A multi-component κ value is then obtained by volume weighting the individual component κ values.

Monthly mean cloud fields (averaged over the period 1983 – 2008) are used from the International Satellite Cloud Climatology Project (ISCCP) D2 dataset (Rossow and Schiffer, 1999). To calculate the cloud albedo effect between a control and perturbed scenario, the cloud droplet effective radius for low and middle level clouds (up to 600 hPa) is modified. A uniform cloud droplet effective radius (r_{e1}) of 10 μm is first assumed, which maintains consistency with the ISCCP derivation of cloud liquid water path. Figure 3.3 shows the location of low and middle level clouds in the ISCCP-D2 climatology.

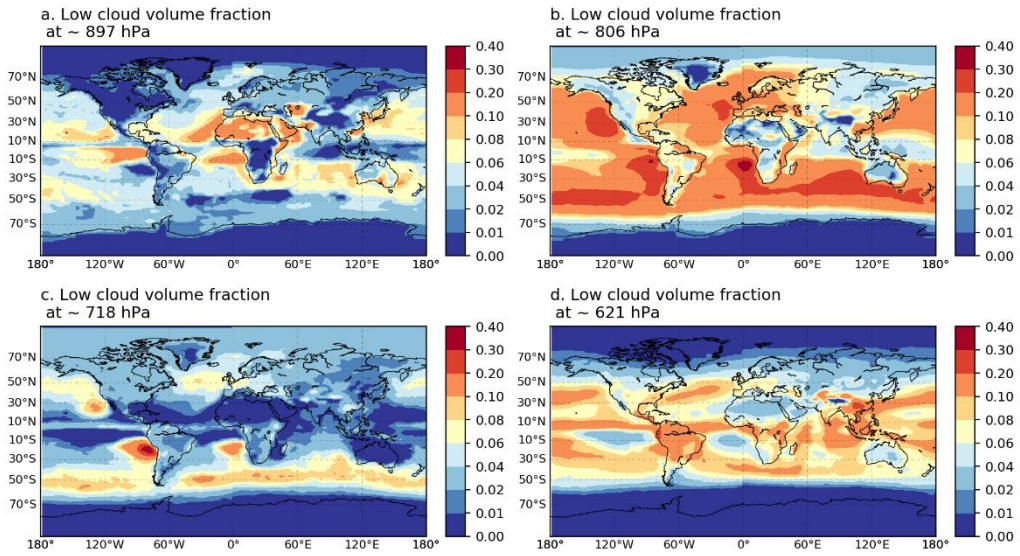

Figure 3.3 *Annual mean cloud volume fraction at a) ~897 hPa, b) ~ 806 hPa, c) ~ 718 hPa and d) ~ 621 hPa from the International Satellite Cloud Climatology Project (ISCCP) database. In nitrate CAE calculations, changes to the cloud effective radius are calculated for cloud fields below 600 hPa (lowermost 22 model levels).*

For a perturbed aerosol scenario, for example, when nitrate aerosol is excluded from simulations, the effective radius is calculated from $CDNC_1$ and $CDNC_2$ as in equation 3.6, where $CDNC_1$ represents a control simulation that includes nitrate aerosol and $CDNC_2$ represents a simulation with no nitrate aerosol.

$$r_{e2} = r_{e1} \times \left[\frac{CDNC_1}{CDNC_2}\right]^{\frac{1}{3}} \quad (3.6)$$

The cloud albedo radiative effect from nitrate aerosol is then derived by comparing the net radiative flux using re_2 with that of the control simulation with fixed re_1.

3.5 AeroCom Phase III setup

For the Chapter 4 assessment of semi-volatile inorganic aerosol, UM-UKCA simulations are placed in context by comparison to the co-ordinated nitrate experiment (Bian et al., 2017) within the AeroCom international modelling community. Nine global aerosol models have participated in the nitrate experiment of AeroCom Phase III and the individual models are described in detail in Bian et al. (2017). The models are CHASER, EMAC, INCA, GISS-MATRIX, GISS-OMA, EMEP, GMI, OsloCTM2 and OsloCTM3 and their configurations are summarised in Table 3.4. The AeroCom Phase III experiment design specified that all models run with emissions and meteorology for the year 2008, following an initial one-year spin-up period. The former 5 models in the list (GCMs) above simulated chemical fields with nudging to meteorological re-analyses, whereas the latter 4 models (CTMs) ran with meteorological fields taken directly from the re-analyses. The majority of models, except for EMAC and GISS-MATRIX, use a bulk aerosol treatment for nitrate that doesn't resolve changes in particle size and number with gas-particle transfer nor represent other aerosol microphysical processes such as new particle formation and coagulation. All of the participating models apply thermodynamic equilibrium models to represent the gas-particle partitioning of nitrate aerosol (see Table 3.4). CHASER, EMEP, GMI, INCA, GISS-MATRIX and GISS-OMA call the thermodynamic equilibrium

models only once for fine-mode aerosol particles. OsloCTM2 and OsloCTM3 consider a bimodal aerosol size distribution and calculate gas-aerosol partitioning for the fine mode before the coarse mode. EMAC calculates the gas phase species available for condensation within the model timestep and then redistributes the mass between the gas and aerosol phase assuming instant equilibrium (Pringle et al., 2010).

Other specifications for the multi-model experiment involve simulations applying harmonized anthropogenic emissions, including year-specific monthly-varying sources of SO_2, NO_x, CO, BC, OC, CH_4 and non-methane volatile organic compounds (NMVOCs) from the Hemispheric Transport of Air Pollution (HTAP) v2 database (Janssens-Maenhout et al., 2015). Other tropospheric ozone precursor gas phase tracers that were not provided by HTAP v2, including some volatile organic compounds, were taken from the CMIP5 RCP8.5 scenario following linear interpolation from the year 2005. Biomass burning emissions, e.g. of NO_x, SO_2, BC, OC, for the year 2008 were included from GFED3 (van der Werf et al., 2010). Oceanic NH_3 emissions were included from the GEIA inventory (Bouwman et al., 1997), with other NH_3 emissions sectors from HTAPv2. Natural emissions of dimethylsulfide (DMS), dust, sea salt and nitrogen oxide from lightning were included based on each modelling group's preferred approach.

All 9 AeroCom nitrate experiment models use gas phase O_3-NO_x-HO_x chemistry to produce HNO_3 and also all include tropospheric heterogeneous N_2O_5 hydrolysis on aerosol surfaces in their treatment of HNO_3 formation. The representation of nitric acid production by heterogeneous N_2O_5 hydrolysis, however, differs between the participating models, reflecting differences in the way aerosol type information is considered (relating also to the sophistication of the host model aerosol scheme) and in the sensitivity of the aerosol uptake coefficient to temperature and relative humidity. One of the 9 models (CHASER) also includes N_2O_5 conversion to HNO_3 on liquid cloud particles. Table 3.4 describes the nitrate chemical mechanisms between the AeroCom models, with details of the nitrate-extended UM-UKCA base model setup included for comparison.

Table 3.4 *Nitrate chemical mechanisms and physical properties of UM-UKCA and AeroCom models, adapted from Bian et al. (2017).*

Model	CHEM-EQM	HNO_3 chemical mechanism	N_2O_5 hydrolysis	CHEM dust	CHEM sea salt	Aerosol microphysics, bins for nitrate	Model name, type, resolution	References
UM-UKCA	HyDiS-1.0 (GLOMAP-mode)	UKCA TropIsop (O'Connor et al., 2014)	γ^b (STA[d],T, RH), STA: BC, OC, SO_4^{2-}, DU, SS (Evans and Jacob, 2005), NO_3^- (Hallquist et al., 2003; Wahner et al., 1998; Davis et al., 2008)	No	Yes	Microphysical, four log-normal modes: nucleation, Aitken, accumulation, coarse	HadGEM3-UKCA, GCM, 1.25 ° 1.875 ° x L63	(Mann et al., (2010), Turnock et al. (2015), Benduhn et al., 2016)
CHASER	ISORROPIA-I	CHASER (Sudo et al., 2002)	γ^b (0.1 for SO_4^{2-}, NO_3^-, OC, DU and SS, and 0.05 for liquid cloud particles) (Dentener and Crutzen, 1993)	No	No	Bulk, fine mode	MIROC, GCM, 2.8 ◦ × 2.8 ◦ × L64	(Watanabe et al., 2011)
EMAC	ISORROPIA-II (stable state[c])	MESSy2 (Jöckel et al., 2010)	γ(STA), STA: climatological aerosol in Aitken, accumulation and coarse soluble modes (Jöckel et al., 2010)	Yes	Yes	Microphysical, Four bins: nucleation, Aitken, accumulation, coarse	ECHAM5, GCM, 2.8 ◦ × 2.8 ◦ × L31	(Karydis et al., 2016)
EMEP	MARS	EMEP EmChem09 (Simpson et al., 2012)	γ(STA,T, RH), STA: NH_4^+, SO_4^{2-}, NO_3^- (Evans and Jacob, 2005; Davis et al., 2008)	Yes	Yes	Bulk, fine and coarse	ECMWF-IFS, CTM, 0.5 ◦ × 0.5 ◦ × L20	(Simpson et al., 2012)
GMI	RPMARES (stable state)	GMI (Strahan et al., 2007)	γ(STA,T, RH), STA: BC, OC, SO_4^{2-}, DU, SS (Evans and Jacob, 2005)	Yes	Yes	Bulk, three bins: D < 0.1, 0.1–2.5, > 2.5 μm)	MERRA2, CTM, 2.5◦ × 2 ◦ × L72	(Bian et al., 2009)
INCA	INCA (stable state)	INCA tropospheric chemistry (Hauglustaine et al., 2004)	γ(STA, T, RH), STA: BC, SO_4^{2-}, DU, SS (Evans and Jacob, 2005)	Yes	Yes	Microphysical, two bins : (D < 1 and 1–10 μm)	LMD-v4, GCM, 1.9 ◦ × 3.75 ◦ × L39	(Hauglustaine et al., 2014)
GISS-MATRIX	ISORROPIA-II (stable state)	MATRIX (Bauer et al, 2008) and tropospheric chemistry (Shindell et al., 2003)	γ(STA), STA: SO_4^{2-} (Dentener and Crutzen, 1993)	No	No	Microphysical, distributed over all mixing states, e.g., size distributions	NASA GISS-E2,GCM, 2 ◦ × 2.5 ◦ × L40	(Schmidt et al., 2014)
GISS-OMA	EQSAM_v03d (metastable[e])	OMA (Bauer et al., 2007) and tropospheric chemistry (Shindell et al., 2003)	γ(STA), STA: SO_4^{2-} (Dentener and Crutzen, 1993)	Yes	No	Bulk, fine mode	NASA GISS-E2, 2 GCM, ◦ × 2.5 ◦ × L40	(Schmidt et al., 2014)
OsloCTM2	EQSAM_v03d (metastable)	OsloCTM2 (Berntsen and Isaksen, 1997)	γ(STA), STA: climatology aerosol (Dentener and Crutzen, 1993; Søvde et al., 2012)	Yes	No	Bulk, two bins: fine and coarse mode	ECMWF, CTM, 2.8 ◦ × 2.8 ◦ × L60	(Myhre et al., 2006)
OsloCTM3	EQSAM_v03d (metastable)	OsloCTM2 (Berntsen and Isaksen, 1997)	γ(STA), STA: climatology aerosol (Dentener and Crutzen, 1993; Søvde et al., 2012)	Yes	No	Bulk, two bins: fine and coarse mode	ECMWF, CTM, 2.25 ◦ × 2.25 ◦ × L60	(Myhre et al., 2006)

a ChemDUSS: chemistry reaction on dust and sea salt particles. b γ : the dimensionless uptake coefficient. c Stable state: where salts precipitate once the aqueous phase becomes saturated. d STA: surface of tropospheric aerosols. e Metastable: where the aerosol is composed only of a supersaturated aqueous phase.

Figure 3.4 shows the difference between the NO_x emissions used in the AeroCom experiments and the MACCity emissions applied to UM-UKCA simulations in this thesis, for the year 2008. Globally, the total NO_x emissions used in the AeroCom experiments are 13% higher than those from the MACCity inventory used in the UM-UKCA simulations.

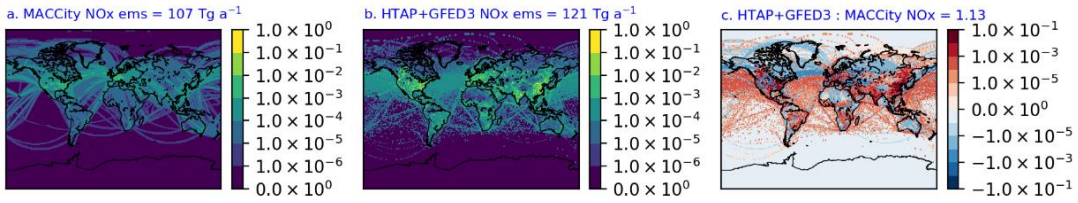

Figure 3.4 *Global fields of column NO_x emissions (kg m^{-2} a^{-1}) from a) the MACCity inventory used in UM-UKCA simulations, b) the HTAP and GFED3 inventory emissions used in the AeroCom simulations and c) the absolute difference between AeroCom and UM-UKCA NOx emissions (AeroCom minus UM-UKCA). Total global emissions are given above each panel, with the ratio of total global AeroCom to UM-UKCA NOx emissions shown above panel c.*

In Chapter 4, simulated nitrate, ammonium and sulphate concentrations from the AeroCom models are also compared to surface observations, to give context for UM-UKCA model-observation comparisons (described in Section 3.6). Monthly-mean simulated values from the lowest level are collated into seasonal or annual mean concentrations for each AeroCom model and are linearly interpolated to each measurement location from the four adjacent grid squares.

UKCA-simulated surface and zonal mean nitrate, ammonium and sulphate concentrations are also compared to the local (per grid cell) AeroCom multi-model mean and 25th to 75th percentile ranges. Simulated surface concentrations from the AeroCom models were re-gridded to a common 1° x 1° horizontal grid, and zonal means re-gridded to 1° and to the 20 vertical levels of the coarsest vertical resolution AeroCom submission (the EMEP model). The same re-gridding is also applied to the UM-UKCA concentrations to give a common model resolution for comparison.

3.6 Observations

The observations used for model validation in this thesis are described in the following sub-sections.

3.6.1 Ground-based gas and aerosol

Table 3.5 provides a summary of the surface aerosol observations included in the model evaluation of Chapter 4. Measurements of nitrate aerosol, ammonium aerosol, sulphate aerosol, total nitrate (nitric acid + nitrate aerosol) and total ammonium (ammonia + ammonium) are included from four aerosol monitoring networks: the European Monitoring and Evaluation Programme (EMEP; http://www.nilu.no/projects/ccc/index.html), Clean Air Status and Trends (CASTNET; https://www.epa.gov/castnet), Interagency Monitoring of Protected Visual Environments (IMPROVE; http://vista.cira.colostate.edu/Improve/) and Acid Deposition Monitoring Network in East Asia (EANET; http://www.eanet.asia/index.html). Ammonia observations were also collated from the Ammonia Monitoring (AMoN) network (http://nadp.sws.uiuc.edu/amon/).

Table 3.5 *Summary of surface filterpack observations included in annual and seasonal model-observation comparison of Chapter 4.*

	NO_3^-	NH_4^+	SO_4^{2-}	tNO_3	tNH_x	Reference
EMEP	29	37	46	41	42	http://www.nilu.no/projects/ccc/index.html
CASTNET	82	82	82	80	-	https://www.epa.gov/castnet
IMPROVE	166	-	166	-	-	http://vista.cira.colostate.edu/Improve/
EANET	22	23	29	5	14	http://www.eanet.asia/index.html
AMoN	-	-	-	-	18 (NH_3)	http://nadp.sws.uiuc.edu/amon/

Filterpack instruments can be prone to several artefacts when measuring nitrate and ammonium aerosol, which arise from both the aerosol volatility (evaporation from the filters) and the reactivity of nitric acid (condensation onto

the filters) (Slanina et al., 2001; Schaap et al., 2004; Vecchi et al., 2009). The magnitude of the artefact is dependent on the filter material and on ambient temperature and relative humidity (Chow, 1995; Hering and Cass, 1999). For this reason, filterpack measurements of total nitrate (TNO_3 i.e. nitrate aerosol + nitric acid) and total ammonium (TNH_x, i.e. ammonium aerosol + ammonia) were included in the Chapter 4 evaluation of simulated inorganic aerosol where available. The locations of surface observation sites are shown in Figures 4.1 to 4.6 of Chapter 4. Sites at altitudes above 1.5km were removed from the dataset to allow a more representative comparison against simulated surface concentrations.

For comparison to surface/ground-based observations in Chapter 4, monthly-mean simulated values from the lowest model level are collated into seasonal or annual mean concentrations and linearly interpolated to each measurement location from the four adjacent grid squares.

3.6.2 Aircraft aerosol

Table 3.6 summarises the year 2008 field campaigns used in this study for the evaluation of NO_3^-, NH_4^+ and SO_4^{2-} mass concentrations. The NO_3^-, NH_4^+ and SO_4^{2-} aircraft observations are those used in Heald et al. (2011) and Kapadia (2015), and were taken over flight tracks marked in Figure 3.5. Observations are included from the following projects: Appraising the Direct Impacts of Aerosol on Climate (ADIENT), European Integrated Project on Aerosol Cloud Climate and Air Quality Interactions (EUCAARI), Arctic Research of the Composition of the Troposphere from Aircraft and Satellites (ARCTAS-Spring and Summer), Oxidant and Particulate Photochemical Processes Above a South East Asian Rainforest project (OP3) and the VAMOS Ocean-Cloud-Atmosphere-Land Regional Experiment (VOCALS-UK).

Observations were taken using aerosol mass spectrometer (AMS) instruments (see Table 3.6), which optimally measures particles up to 1 μm in diameter. Only the simulated s*ubmicron* aerosol mass is therefore compared to these observations (i.e. the coarse mode is emitted from these comparisons). The aircraft observations are reported in standard temperature and pressure (STP:

Table 3.6 *Field campaign aircraft data used to evaluate simulated nitrate, ammonium and sulphate vertical profiles – adapted from Heald et al. (2011)*

Campaign	Location	Date	Conditions	Technique	Reference
ADIENT	Europe/Atlantic	18/12/07-25/09/08	Polluted (mid-latitudes)	C-ToF-AMS	(Morgan et al., 2010a)
EUCAARI	Northern Europe	06/05/08 – 22/05/08	Polluted (mid-latitudes)	C-ToF-AMS	(Morgan et al., 2010a)
ARCTAS Spring	Arctic/ N. USA	01/04 – 20/04/08	Fire (high-latitudes)	HR-ToF-AMS	(Cubison et al., 2011)
ARCTAS Summer	Arctic/ N. USA	18/06 – 13/07/08	Fire (high-latitudes)	HR-ToF-AMS	(Cubison et al., 2011)
OP3	Borneo	10/07 – 20/07/08	Remote (tropical)	C-ToF-AMS	(Robinson et al., 2011
VOCALS-UK	SE. Pacific	27/10 – 13/11/08	Remote (tropical)	C-ToF-AMS	(Allen et al., 2011)

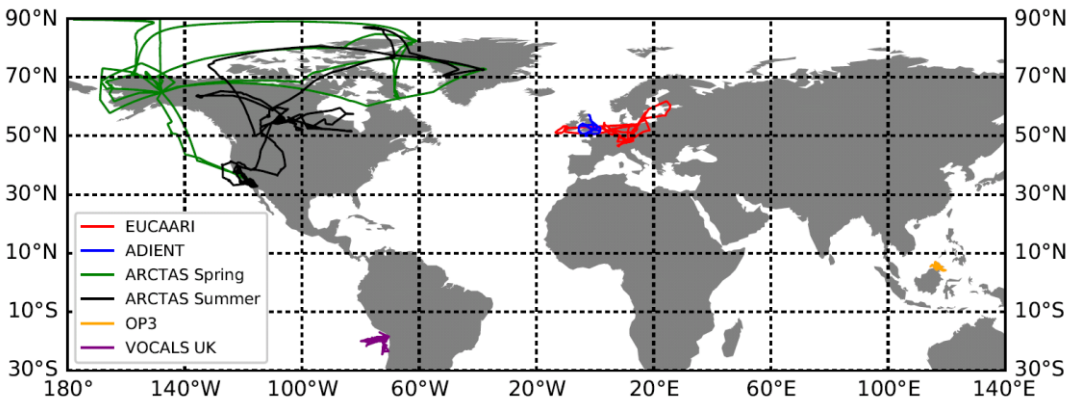

Figure 3.5 *Flight tracks from year 2008 field campaigns used for evaluation of simulated NO_3, NH_4 and SO_4 vertical profiles - adapted from Heald et al. (2011).*

298K, 1 atm) so the simulated concentrations of submicron NO_3^-, NH_4^+ and SO_4^{2-} have been converted to standard temperature and pressure. For the comparison in Chapter 4, simulated monthly-mean vertical profiles of nitrate, ammonium

and sulphate mass concentration at STP were compared for months in which observations were recorded. The model vertical profiles were linearly interpolated to the longitude and latitude locations of the aircraft observations and averaged (arithmetic mean) to give a one-dimensional vertical profile representative of the flight track locations. In order to match the methodology in the aircraft observations, the simulated mass concentrations were converted to mass concentration at standard temperature and pressure before being stratified into 0.5 km vertical bins.

3.6.3 $PM_{2.5}$

In Chapter 5, simulated $PM_{2.5}$ concentrations are evaluated against ground-based observations and satellite-derived $PM_{2.5}$. These measurements are described in the following sub-sections.

3.6.3.1 Ground-based $PM_{2.5}$

Table 3.7 describes the ground-based $PM_{2.5}$ observations included in this thesis. The locations of surface sites are shown in Chapter 5 (Figure 5.2). European and North American surface $PM_{2.5}$ observations are included from the EMEP and IMPROVE monitoring networks, respectively, as collated for the Global Aerosol Synthesis and Science Project (GASSP) aerosol database (Browse et al., 2019 in prep. in prep.) Daily mean surface observations were filtered for flagged data and averaged into monthly means. In this thesis, they are further collated into DJF, JJA and annual mean concentrations. Observations are relatively dense over Europe and the USA. However, the location of many of these sites near urban centres (to monitor human exposure to particulate matter) means that concentrations are likely to be underestimated by the model, which uses a global resolution grid (1.25° latitude x 1.875° longitude). Ground-based $PM_{2.5}$ observations are used to apply a regional bias correction over Europe and the USA, in order to offset this low urban bias and other potential sources of low bias in simulated $PM_{2.5}$, as described in Chapter 5.

Due to a lack of observations in the year 2008, observations from the years 2016 and 2014 are included for India and China, respectively, to evaluate the spatial model correlation with observations. Year 2016 observations over India at hourly resolution were obtained from the Central Pollution Control Board of the

Ministry of Environment and Forests (Government of India, 2016) and collated into seasonal and annual mean concentrations by Conibear et al. (2018). Over China, year 2014 observations at hourly resolution were obtained from the China National Environmental Monitoring Center (http://www.cnemc.cn/). Measurements were downloaded from PM2.5.in (http://pm25.in/) and collated into daily mean values by researchers at Emory University (e.g. Archer-Nicholls et al., 2016). These were collated into DJF, JJA and annual means for the evaluation in Chapter 5.

Table 3.7 *Summary of surface-based $PM_{2.5}$ measurements included in the model evaluation of Chapter 5.*

Region (data source)	Measurement year	Number of observations	Reference
Europe (EBAS)	2008	30	https://www.nilu.no/projects/ccc/index.html
N. America (IMPROVE)	2008	120	http://vista.cira.colostate.edu/Improve/
India	2016	45	Conibear et al., 2018; Government of India, 2016
China	2014	561	http://www.cnemc.cn/ ; http://pm25.in/

3.6.3.2 Satellite-derived $PM_{2.5}$

Global year 2008 annual mean satellite-derived $PM_{2.5}$ data are also used in the model evaluation in Chapter 5. Satellite-derived $PM_{2.5}$ are used to apply regional bias corrections to simulated $PM_{2.5}$ over China and India, in the absence of widespread year 2008 ground-based $PM_{2.5}$ observations. The Geographically Weighted Regression (GWR) – adjusted dataset of van Donkelaar et al. (2016) is used in this thesis, which updates the dataset applied in the 2013 GBD (Brauer et al., 2016) but precedes that used in the 2015 GBD (Cohen et al., 2017). To derive the dataset, van Donkelaar et al. (2016) first retrieved aerosol optical depths from a combination of satellite products, including MODIS (Moderate Resolution Imaging Spectroradiometer), MISR (Multi-angle Imaging

SpectroRadiometer) and SeaWIFS Deep Blue (Sea-Viewing Wide Field-of-View Sensor) as in van Donkelaar et al.(2015). The total column AOD retrievals were combined from each satellite dataset and converted to surface $PM_{2.5}$ fields based on the spatiotemporally varying relationship of AOD to $PM_{2.5}$ simulated by the GEOS-Chem chemical transport model. The satellite-derived $PM_{2.5}$ field was then bias-adjusted using GWR based on ground-based monitor observations. The satellite-derived $PM_{2.5}$ fields have a grid resolution of 6 arc-minutes, equivalent to 0.1 degrees, and cover the global land surface between 70° North and 55° South.

The GWR-adjusted satellite-derived $PM_{2.5}$ dataset correlates well with global direct $PM_{2.5}$ observations ($R^2 = 0.85$). However the within-region uncertainty is greater in parts of Asia, where observations are sparser, than over Europe and North America. Ford and Heald (2016) estimated that uncertainty in satellite-derived surface $PM_{2.5}$ fields is approximately 20% due to uncertainty in the AOD-to-surface-$PM_{2.5}$ relationship and 10% due to satellite observational uncertainty.

3.6.4 Aerosol number concentrations

In Chapter 6, simulated surface level number concentrations of particles with dry diameter greater than 50 nm (N_{50}) are compared against observations from continental and marine cruise-based field campaign for the year 2008.

The surface level N_{50} observations from the European Supersites for Atmospheric Aerosol Research (EUSAAR) and German Ultrafine Aerosol Network (GUAN) networks were collected and collated by Asmi et al. (2011) and processed into annual mean concentrations for the model-observation comparison of Turnock et al. (2015). Annual mean N_{50} are compared at the same 17 low altitude measurement sites as in Mann et al. (2014) and Turnock et al. (2016). The locations of these sites are shown in Figure 6.5.

In addition to surface station data, simulated N_{50} are compared to those observed during the International Chemistry Experiment in the Arctic LOwer Troposphere (ICEALOT) ship cruise campaign (Russell et al., 2010; Frossard et al., 2011). These observations were collated by the Global Aerosol Synthesis and Science Project (GASSP; Reddington et al., 2017). The ICEALOT campaign ran from March

to April 2008. Observations are compared to simulated concentrations at the locations show in Figure 6.5.

3.7 Model evaluation methods

Model-observation comparisons are made in Chapters 4, 5 and 6. The spatial linear relationship between modelled values and observations is determined using the Pearson correlation coefficient (R) (equation 3.7). The normalised mean bias (NMB) is calculated to represent the model bias relative to the observations (equation 3.8). The NMB is chosen to not be overly influenced by low observed concentrations.

$$R = \frac{\sum_{i=1}^{n}(M_i - \bar{M})(O_i - \bar{O})}{\sqrt{\sum_{i=1}^{n}(M_i - \bar{M})^2}\sqrt{\sum_{i=1}^{n}(O_i - \bar{O})^2}} \quad (3.7)$$

$$NMB = \frac{\sum_{i=1}^{n}(M_i - O_i)}{\sum_{i=1}^{n} O_i} \quad (3.8)$$

Where M_i and O_i are the modelled and observed values at each measurement site, respectively. $\bar{M}$ and $\bar{O}$ are the mean of the modelled and observed values, respectively, and i=1,n denotes the sum over the n measurement sites.

4. Evaluation of annual and seasonal mean nitrate aerosol concentrations in the UM-UKCA model

4.1 Introduction

This chapter comprises a comprehensive evaluation of size-resolved nitrate, ammonium and sulphate concentrations on seasonal and annual mean timescales as simulated by the UM-UKCA model with the HyDiS-1.0 inorganic dissolution solver. This work furthers the recent model evaluations by Benduhn et al. (2016), in which HyDiS-1.0 is implemented in GLOMAP-mode within the TOMCAT CTM, and by Turnock et al. (2015), in which simulated European trends in sulphate and aerosol properties are evaluated from the non-nitrate-extended version of the UM-UKCA model. Furthermore, UM-UKCA-simulated aerosol concentrations are placed in context with the recent multi-model AeroCom Phase III nitrate experiment of Bian et al. (2017).

Simulated aerosol concentrations are first compared against surface and aircraft observations from the year 2008. The surface comparison focusses on three regions: Europe, North America and East Asia, where observations are available from monitoring networks. Comparisons are then made to aircraft observations from several field campaigns which represent different aerosol loading regimes. The evaluation of UM-UKCA-simulated nitrate, ammonium and sulphate concentrations is then furthered by comparing global burdens, mean surface concentrations and zonal mean concentrations with the latest AeroCom Phase III multi-model results.

Finally, two sensitivity runs with the UM-UKCA model are included to assess the influence of heterogeneous N_2O_5 hydrolysis and a simpler 'equilibrium' assumption for the thermodynamic partitioning of semi-volatile inorganic species on simulated, size-resolved nitrate aerosol concentrations. The nitrate aerosol extension to GLOMAP-mode and tropospheric heterogeneous chemistry represent developments that are not included in the UM-UKCA model's tropospheric chemistry configuration as standard. The chapter concludes with recommendations for simulations of nitrate aerosol in the UM-UKCA model and future related research.

4.2 UM-UKCA sensitivity runs

The control and sensitivity simulations in this chapter have been performed with the UM-UKCA model. For all simulations, UM-UKCA is run at N96 resolution (1.875° x 1.25°) for the year 2008, following a 4-month spin-up period. The UM-UKCA model has been described in previous Section 3.2 and so only specifics of the UM-UKCA sensitivity runs performed in this chapter are described here.

All simulations are summarised in Table 4.1. The control simulation (HYB) applies the hybrid gas-particle partitioning configuration and includes tropospheric heterogeneous N_2O_5 hydrolysis. In a second simulation (EQU), the inorganic dissolution solver is run in an equilibrium configuration to assess the influence of the gas-particle partitioning assumption on size-resolved NO_3^- and NH_4^+ aerosol concentrations, while heterogeneous N_2O_5 chemistry remains included. Finally, the hybrid simulation is repeated with the tropospheric heterogeneous N_2O_5 hydrolysis rates set to zero (HYB-NoHet).

Table 4.1 Table 4.1. Summary of UM-UKCA sensitivity runs, 'X' indicates feature is included.

Sensitivity Runs	Hybrid partitioning	Equilibrium partitioning	Heterogeneous N_2O_5 hydrolysis on	Nitric acid partitioning to nitrate aerosol
HYB	X		X	X
EQU		X	X	X
HYB-NoHet	X			X

The AeroCom Phase III multi-model experiment design and observations used in this chapter are described in Sections 3.5 and 3.6, respectively.

Observations and AeroCom Phase III models are compared to the HYB simulation in Sections 4.3.1, 4.3.2 and 4.3.3. HYB is treated as the 'control' configuration for the work in this thesis.

4.3 Results

4.3.1 Comparison to surface observations

4.3.1.1 Nitrate aerosol and total nitrate

Figure 4.1 shows annual (ann) and seasonal mean (DJF and JJA) simulated surface nitrate aerosol concentrations over the regions of Europe, North America and East Asia, with observations overplotted from the EMEP, CASTNET/IMPROVE and EANET observation networks, respectively. Figure 4.2 is identical to Figure 4.1 but shows total nitrate concentrations (the sum of gaseous nitric acid and particulate phase nitrate). Both nitrate aerosol and total nitrate concentrations peak over regions of Asia, Europe and North America as a result of high regional precursor gas emissions and relatively short aerosol atmospheric lifetime. The seasonal and annual mean model observation comparison is summarised in Table 4.2.

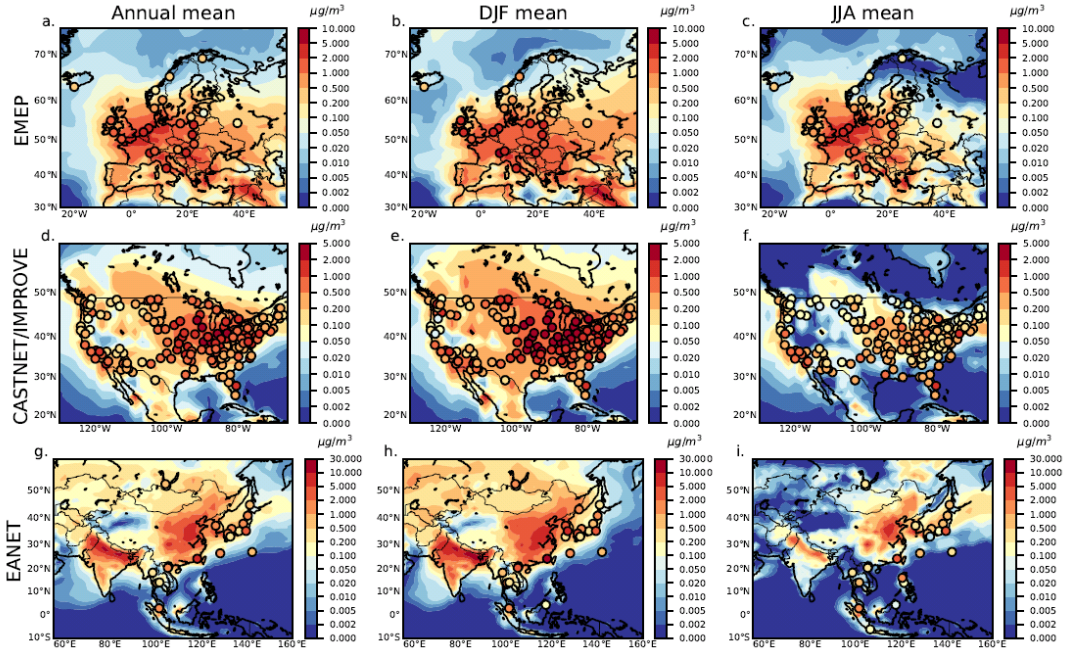

Figure 4.1 *Annual (first column), DJF (centre column) and JJA (right column) seasonal mean simulated fields of surface nitrate aerosol mass concentration for the year 2008, with filterpack observations overplotted from the EMEP (a-c), IMPROVE (d-f), CASTNET (d-f) and EANET (g-i) networks. 'DJF' and 'JJA' refer to the December, January and February and to the June, July and August seasonal mean concentrations, respectively.*

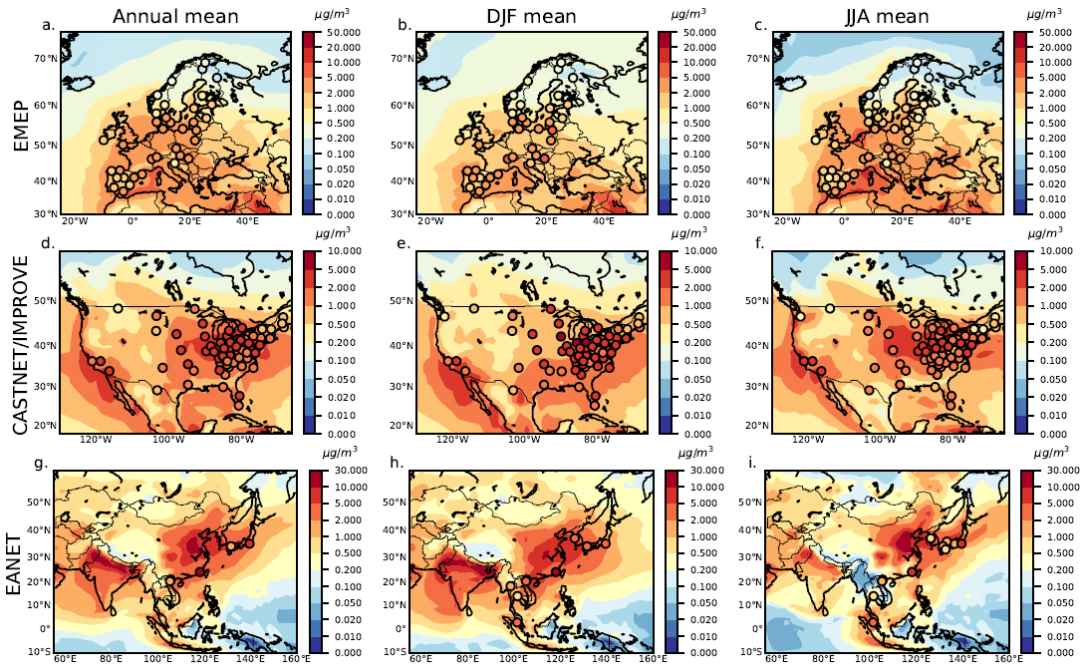

Figure 4.2 *Same as Figure 4.1 for total nitrate (tNO_3, sum of gaseous nitric acid and nitrate aerosol) concentrations. USA observations are from CASTNET network only.*

Figure 4.3 shows the annual mean model-to-observation comparisons, separated by species and observation network. In Europe, modelled nitrate aerosol concentrations correlate well with observations (ann R = 0.697, DJF R = 0.738, JJA R = 0.676; Table 4.2), though annual mean concentrations are underestimated by approximately 35% (NMB = -0.342). The low bias is greater in winter than in summer (DJF NMB = -0.581, JJA NMB = -0.167) although the Pearson correlation coefficient indicates that the model captures the spatial distribution of nitrate aerosol well in both seasons and slightly more accurately in the winter months. The largest underestimations in European nitrate aerosol concentration occur in Northern and Arctic regions with the greatest annual mean underestimation located at the Arctic site in Svalbard, Norway.

In North America, the model also correlates well with observations on annual mean timescales (ann. CASTNET R = 0.696, ann. IMPROVE R = 0.616) for nitrate aerosol but the low bias is greater than over Europe (ann. CASTNET NMB = -0.605, ann. IMPROVE NMB = -0.581). The model simulates the spatial distribution of nitrate well in winter (DJF CASTNET R = 0.671, DJF IMPROVE R = 0.564), despite being biased low (CASTNET NMB = -0.699, IMPROVE NMB = -

Table 4.2 *Table 4.2. Statistical summary of annual and seasonal mean model-observation comparison from HYB simulation.*

Component	Season	Network									
		EMEP (Europe)		CASTNET (USA)		IMPROVE (USA)		AMON (USA)[a]		EANET (E. Asia)	
		R	NMB	R	NMB	R	NMB	R	NMB	R	NMB
NO_3^-	Annual	0.697	-0.342	0.696	-0.605	0.616	-0.581	-	-	0.088	-0.487
	DJF	0.738	-0.581	0.671	-0.699	0.564	-0.636	-	-	0.373	-0.617
	JJA	0.676	-0.167	0.169	-0.702	0.323	-0.764	-	-	0.003	-0.311
tNO_3	Annual	0.796	-0.173	0.779	-0.229	-	-	-	-	0.278	-0.207
	DJF	0.679	-0.549	0.088	-0.606	-	-	-	-	0.421	-0.190
	JJA	0.684	0.435	0.446	0.001	-	-	-	-	-0.233	0.804
NH_4^+	Annual	0.859	-0.337	0.794	-0.592	-	-	-	-	0.366	-0.417
	DJF	0.828	-0.597	0.687	-0.735	-	-	-	-	0.449	-0.554
	JJA	0.842	-0.011	0.779	-0.595	-	-	-	-	0.538	-0.285
tNH_x	Annual	0.427	0.801	-	-	-	-	0.159	-0.168	0.206	-0.400
	DJF	0.357	0.433	-	-	-	-	-	-	0.483	-0.645
	JJA	0.455	0.582	-	-	-	-	-	-	0.193	-0.388
SO_4^{2-}	Annual	0.733	-0.593	0.785	-0.595	0.872	-0.510	-	-	0.517	-0.579
	DJF	0.737	-0.759	0.467	-0.777	0.434	-0.700	-	-	0.565	-0.719
	JJA	0.671	-0.392	0.837	-0.555	0.838	-0.500	-	-	0.414	-0.468

a. Statistics are calculated for AMoN gas-phase NH_3, not total NH_x

0.636). However, the model does not reproduce the spatial variability in nitrate aerosol well in JJA, correlating best against the rural IMPROVE observations (IMPROVE R = 0.323) but underestimating concentrations by approximately 70 – 76% across both networks. Elevated coastal nitrate aerosol concentrations are captured well by the model under the influence of local NO_x and NH_3 emission sources and availability of sea salt to form sodium nitrate.

Over Asia, statistical tests indicate that there is little correlation between modelled and observed nitrate and that concentrations are underestimated by approximately 50% on average over the region (R = 0.088, NMBF = -0.487). However, there is a high density of observations over Japan and the comparison may be disproportionately weighted to this region. The largest underestimations of NO_3^- occur at small island sites, while the greatest overestimates occur at several sites in Southern Japan. Emissions of precursor gases are more uncertain

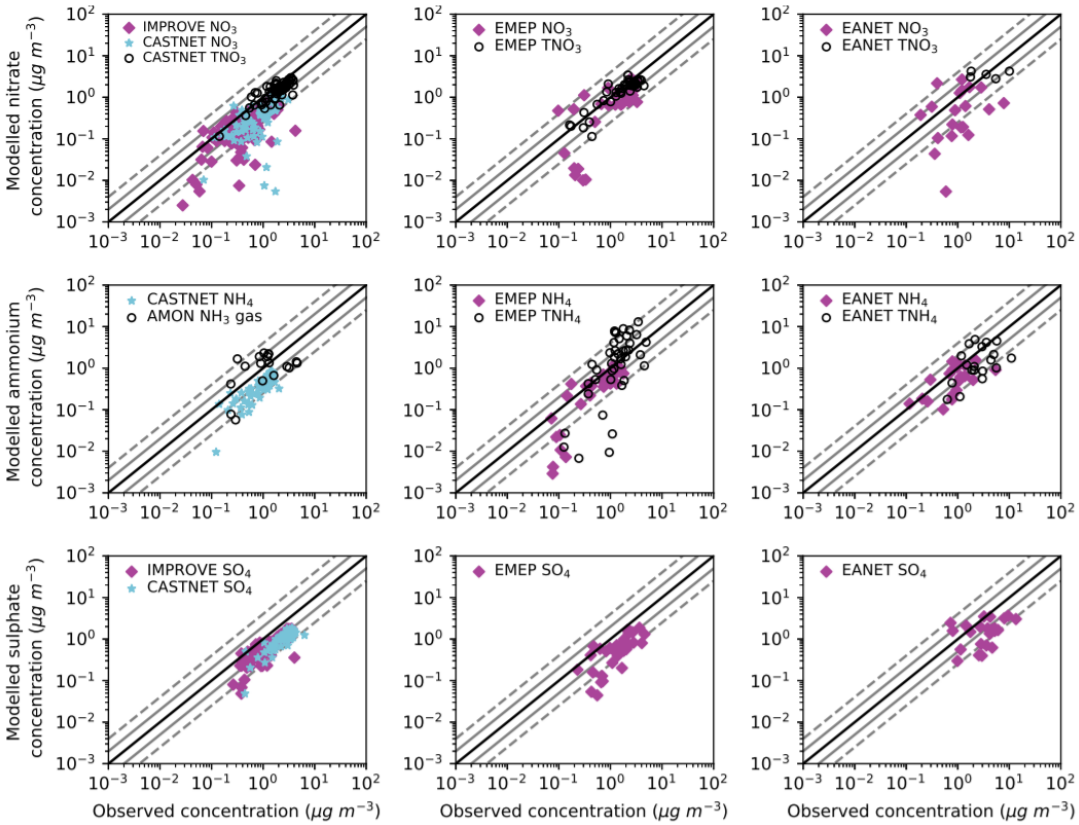

Figure 4.3 *Comparison of simulated and observed annual mean nitrate and total nitrate (top row), ammonium, ammonia and/or total ammonium (middle row) and sulphate (bottom row) aerosol concentrations for the year 2008 for N. America (left column), Europe (middle column), and E. Asia (right column). Year 2008 observations are shown from the CASTNET, IMPROVE, EANET and EMEP networks. 1:1 (black solid), 2:1 (grey solid) and 4:1 (grey dashed) lines are shown.*

over East Asia than over Europe and the USA and the limitations of resolving complex topography at global model resolution may be apparent here. Reliable observations are not available over India and much of China for this analysis and future work should focus on model evaluation in these regions.

Model underestimations in surface nitrate aerosol concentration may have several causes. Firstly, the model doesn't account for heterogeneous nitrate aerosol formation on dust, which is known to be an important pathway for coarse mode nitrate aerosol formation (Bian et al., 2017; Karydis et al., 2016). Secondly, aerosol wet deposition may be artificially high in this version of the model, particularly in the high latitudes, as a result of over-enhanced occurrence

of drizzle precipitation in this model version (Walters et al., 2011; Turnock et al., 2015). The lack of stratospheric-tropospheric exchange of nitric acid in these simulations may also be partly responsible for underestimations in nitrate aerosol.

Simulated total nitrate concentrations compare very well with the EMEP (Europe) and CASTNET (USA) observations on annual mean timescales. The model correlation against EMEP and CASTNET total nitrate is higher than those for nitrate aerosol at 0.796 and 0.779, respectively, with only a small low bias (EMEP NMB = -0.173, CASTNET NMB = -0.229). The better model-observation agreement for annual mean total nitrate indicates that the remaining low bias in nitrate aerosol in these regions is more likely to have arisen from insufficient partitioning of nitric acid to the particle phase, rather than from insufficient availability of nitric acid. The spatial variability of total nitrate is represented consistently well over the seasons in Europe (DJF R = 0.679, JJA R = 0.684), although seasonality in the magnitude of total nitrate concentrations is captured less well: total nitrate is underestimated in winter (NMB = -0.549) and overestimated in summer (NMB = 0.435), indicating that wintertime removal of tNO_3 is too high, or that wintertime formation of nitric acid is too low in the model. The role of heterogeneous N_2O_5 hydrolysis in reducing wintertime bias in nitrate aerosol is discussed later in Section 4.3.5.

Over the USA, the model simulates annual mean total nitrate concentrations very well in terms of spatial distribution and bias, as mentioned above. In winter, however, the spatial variability in total nitrate concentrations is poor (R = 0.088, NMB = -0.606). Comparison of Figure 4.1 (nitrate aerosol) and 4.2 (total nitrate) suggests that the model simulates too little wintertime nitric acid in the north-eastern USA, where the CASTNET observations are dense. The model skill is higher in summer, however, with the model capturing the magnitude of total nitrate concentrations particularly well over the USA (R = 0.446, NMB = 0.001).

Annual mean total nitrate measurements are only available from five EANET sites. A limited comparison indicates that the model doesn't reproduce the spatial variability of annual mean total nitrate well (R = 0.278) but captures the magnitude of total nitrate reasonably well over the region (NMB = -0.207). The

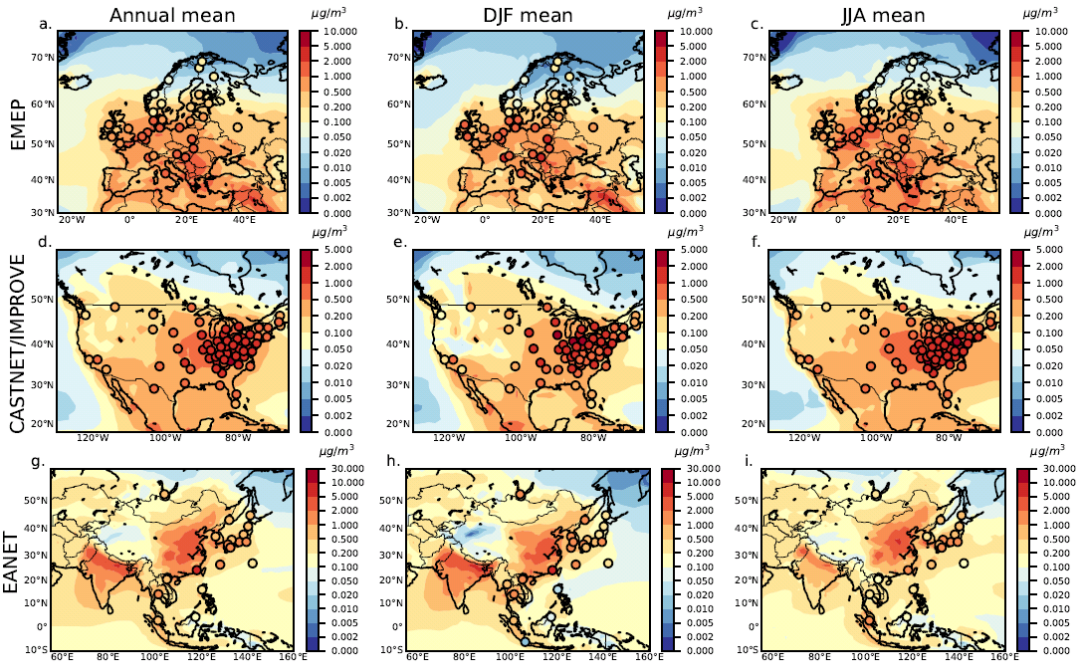

Figure 4.4 *Same as Figure 4.1 for ammonium aerosol.*

model skill is better in DJF (DJF R = 0.421, NMB = -0.190) and poorest in summer (JJA R = -0.233, NMB = 0.804) in particular as a result of model overestimation over Japanese sites, which represent half of the available sites with reliable observations. As with nitrate aerosol, there are few or no sites in India and China and the observation sites are located in marine influenced regions.

4.3.1.2. Ammonium aerosol and total ammonium

Figures 4.4 and 4.5 show the simulated surface ammonium aerosol (particulate), total ammonium (sum of gaseous ammonia plus particulate ammonium) and gaseous ammonia concentrations, respectively, with observations from Europe, the USA and eastern Asia. Annual mean ammonium and total ammonium (or gas-phase ammonia for the USA) concentrations are also compared in Figure 4.3. Similar to nitrate aerosol, ammonium concentrations are greatest over continental regions where emissions of NH_3 are high and HNO_3 and H_2SO_4 are available to neutralise NH_4^+ ions.

European annual mean ammonium concentrations are underestimated overall (NMB = -0.337), with the greatest underestimations in remote coastal and Arctic sites, but otherwise correlate very well with observations (R = 0.859). The high spatial correlation with observed concentrations is maintained through other

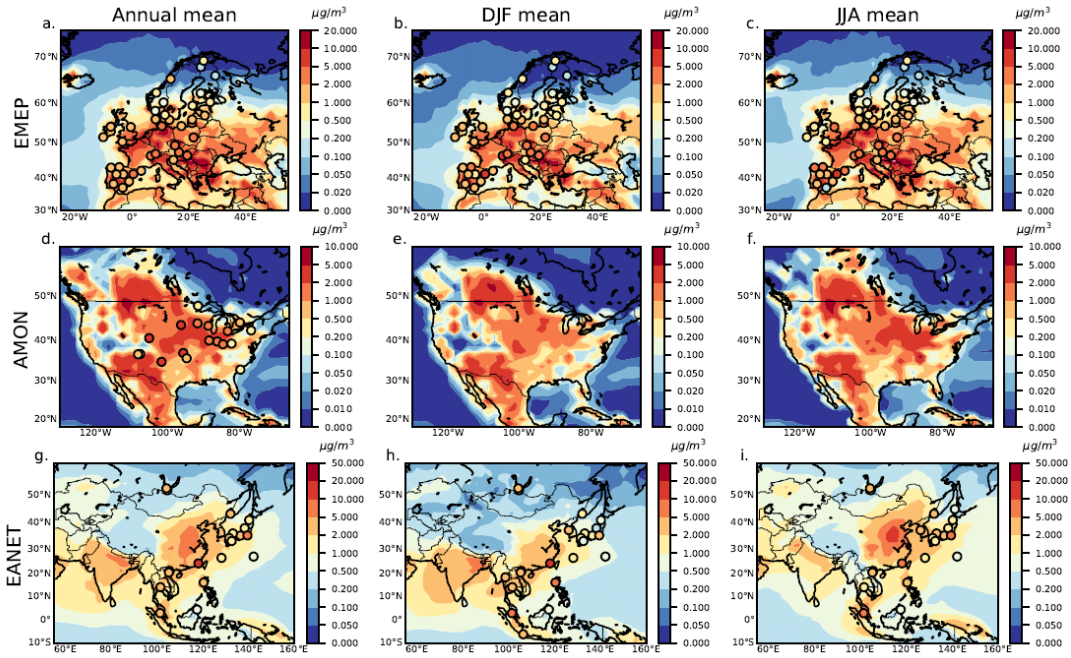

***Figure 4.5**. Same as Figure 4.1 for total ammonium (tNH_x, sum of gaseous ammonia and ammonium aerosol) concentrations in Europe (top row) and Asia (bottom row). USA maps (central row) show simulated gas-phase NH_3 only, with annual mean NH_3 observations overplotted (panel d) from the AMoN network.*

seasons (DJF R = 0.828, JJA R = 0.842). The model underestimates NH_4^+ in winter (DJF NMB = -0.597) but performs very well in summer (JJA NMB = -0.011). European annual mean total ammonium (gas + aerosol) concentrations correlate less well with observations (R = 0.427) and are overestimated by approximately 80%, implying that ammonia gas is overestimated by the model. Simulated ammonium aerosol formation is therefore limited by the availability of sulphuric and nitric acid precursor gases over much of Europe, rather than by a lack of available ammonia in these simulations. The moderate model performance is relatively consistent between winter and summer, although the greatest model overestimation occurs in spring (not shown in Table 4.2). Model overestimations may be partly driven by uncertainty in the NH_3 emission inventory. The four most important contributions to uncertainty in the MACCity NH_3 inventory (derived from EDGAR v4) are nitrogen excretion rates, NH_3 emission rates for manure in animal houses and storage, the grazing time of ruminants and non-agricultural use of manure (Beusen et al., 2008). The sub-grid variability in these factors mean that NH_3 emissions can be challenging to reproduce at the spatial

and temporal resolution required for atmospheric models. UM-UKCA also only considers the uni-directional dry deposition of NH_3 to the surface when, in reality, the air-surface exchange of NH_3 is bi-directional.

In North America, ammonium concentrations correlate well with CASTNET observations (R = 0.794) but, as with nitrate, tend to be biased low (NMB = -0.592) on annual mean timescales. The spatial correlation is relatively consistent between seasons (DJF R = 0.687, JJA R = 0.779), while the model underestimation of values is lower in summer (DJF NMB = -0.735, JJA NMB = -0.595). Figure 4.4 shows that the low bias in North American NH_4^+ is more apparent at sites measuring higher concentrations, the majority of which are located in North East USA. However, NH_4^+ aerosol concentrations in central and West USA are less biased. The greatest model underestimation, by a factor of 9, occurs at the remote site in Alaska, suggesting that, like over Europe, transport of ammonium or precursor gases from high emission regions is insufficient or that regional emissions of precursor species are too low.

The magnitude of annual mean gas-phase ammonia concentrations over the USA is captured well by the model on average with a normalised mean bias score of -0.168. The spatial distribution of NH_3, however, is not reproduced by the model (R = 0.159). Again, the model discrepancy may be partly caused by variability in NH_3 emissions, which can be uncertain given that sub-grid scale heterogeneity arises between local emission sources. The relatively well simulated magnitude of NH_3 concentrations suggests that underestimations in ammonium aerosol are driven by too low partitioning from the gas to aerosol phase.

In Asia, the model comparisons to ammonium observations are more scattered than over Europe and North America (R = 0.366, NMB = -0.417), with the greatest overestimations at coastal sites surrounding the South China Sea and Gulf of Thailand and underestimations at other marine influenced sites in Japan and East China. By contrast, total ammonium concentrations are either represented well or underestimated at sites around the South China Sea and Gulf of Thailand but are overestimated at other sites, with the greatest overestimations at sites in central Japan. The regional model skill for NH_4^+ is greater in JJA (JJA R = 0.538, NMB = -0.233) than in DJF (DJF R = 0.421, NMB = -0.554).

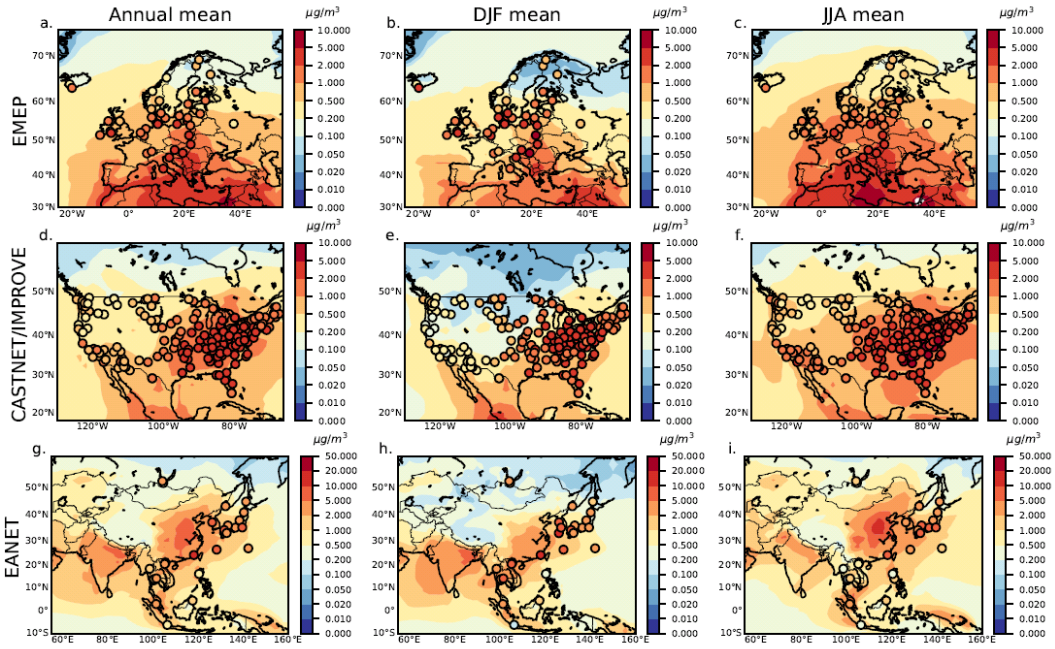

Figure 4.6 *Same as Figure 4.1 for sulphate aerosol.*

4.3.1.3 Sulphate aerosol

Figure 4.6 shows the simulated surface sulphate aerosol concentrations for Europe, the USA and Asia with observations overplotted. The greatest SO_4^{2-} concentrations are found over continental regions and downwind of regions where SO_2 emissions are highest. The annual mean spatial distribution of sulphate aerosol is well represented in the model (R > 0.7) over Europe and the USA but concentrations are prone to a systematic low bias in all three regions (NMB between -0.5 and -0.6).

Over Europe the model captures the spatial distribution of annual mean sulphate aerosol well (annual R = 0.733) but values are biased low by approximately 60% (NMB = -0.593). Similarly, the spatial distribution of sulphate is represented well in DJF and JJA (DJF R = 0.737, JJA R = 0.671) but the underestimation varies between approximately 80% in wintertime (DJF NMB = -0.759) to 40% in summertime (JJA NMB = -0.392). Annual mean concentrations are overestimated by a factor of up to 2.45 at a couple of sites in Eastern and Central Europe. As with the other species described in this study, the greatest underestimations relative to EMEP observations occur at remote coastal sites in Northern Europe and the Arctic.

The model performance is best for annual-mean sulphate over North America, with good correlations to observations (CASTNET R = 0.785, IMPROVE R = 0.872) but with similar low biases as over Europe (CASTNET NMB = -0.595, IMPROVE NMBF = - 0.510). The low bias is greatest at remote sites in Alaska and coastal sites in Eastern USA. The spatial distribution of sulphate is captured less well in DJF with R values of 0.467 and 0.434 and NMB scores of -0.777 and -0.700 for CASTNET and IMPROVE observations, respectively. The model skill is higher in JJA with R values of 0.837 and 0.838 and model biases of -0.555 and -0.500 for CASTNET and IMPROVE observations, respectively.

Of the three regions, simulated annual mean sulphate concentrations compare least well over Asia (R = 0.517, NMB = -0.579). Sulphate is underestimated by over a factor of 5 at 4 EANET sites, located in Northern Japan and Southern Russia. As seen over Europe and the USA, the model is more strongly negatively biased in wintertime (DJF NMB = -0.719, JJA NMB = -0.468).

Model underestimates of SO_4^{2-} aerosol have been reported previously and may have arisen due to an underestimation in oxidant availability or oxidation (Berglen et al., 2007; Manktelow et al., 2007; Mann et al., 2012; Turnock, 2016; Turnock et al., 2015). For example, Turnock (2016) found that the use of a fixed cloud-water pH in UM-UKCA may have artificially suppressed SO_4^{2-} formation by aqueous phase O_3 oxidation (Kreidenweis et al., 2003), particularly at high latitudes and in the wintertime. Finally, as with other aerosol components, enhanced drizzle may have contributed to overestimates in aerosol wet deposition.

4.3.2 Comparison to aircraft observations

4.3.2.1 Nitrate aerosol

Figure 4.7 shows simulated submicron nitrate aerosol vertical profiles compared against field campaign observations over (4.7a and b) Europe, (4.7c and d) the Arctic, (4.7e) South America and (4.7f) Borneo. Model skill and bias metrics are printed in each panel, based on comparisons to observations in the lowest 4 km to focus on model performance in the lower troposphere.

Over Europe (EUCAARI and ADIENT), the model represents nitrate vertical variability well (R = 0.75 and 0.93). Concentrations are biased low in the lower

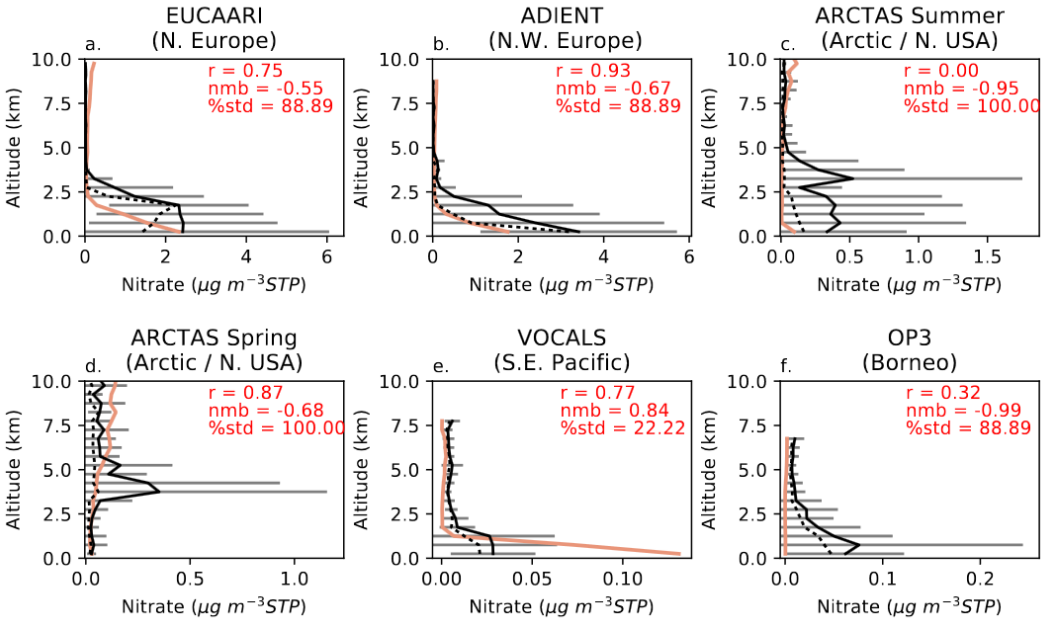

Figure 4.7 *Simulated nitrate vertical profiles (orange, μg sm^{-3}), compared against mean (black solid), median (black dashed) and standard deviation (grey error bars) observations from year 2008 aircraft field campaigns, as collated by Heald et al. (2011). Simulated monthly-mean profiles are averaged to align with respective field campaign months. Pearson correlation coefficient (r), normalised mean bias (nmb) and the percentage of modelled concentrations within one standard deviation of observed concentrations (%std) are printed for each comparison, as calculated based on the lowermost 4km of the atmosphere.*

troposphere (NMB = -0.55 and -0.67) but are within the standard deviation of the observations (%std) over most of the lowermost 4 km (88.9% for both). Nitrate concentrations compare particularly well to the median observed profile in the ADIENT campaign above 0.5km. Although the vertical variability compares well overall against EUCAARI observations, the model does not reproduce enhanced nitrate concentrations observed up to 2km altitude.

The ARCTAS-Spring campaign covered high-latitude Arctic regions while the ARCTAS-Summer campaign flew closer to mid-latitude industrial regions and local boreal biomass burning over North America. The model is biased low on average in the lower troposphere compared to the observed mean concentrations in both campaigns (NMB = -0.95 and -0.68). However, the bias is relatively small in absolute terms and the simulated values are within the standard deviation at all levels below 4 km across both campaigns.

Underestimations in the mean observed concentrations for ARCTAS-Spring are only prominent above 3.5 km, indicating that there may be missing transport processes at this level in the model. Comparing to the same ARCTAS campaigns, Bian et al. (2017) reported that the transport of aerosol between approximately 2 and 7km to Polar regions was also not captured by any of the AeroCom Phase III nitrate models. The model compares particularly well to the median observed profile in the ARCTAS-Spring campaign and also shows high correlation to the mean observed values (R = 0.87). Despite being within the standard deviation of the mean observed values, there is negative linear correlation between the model and ARCTAS-Summer observed values because peaks in the observed vertical profile are underestimated.

The model overestimates nitrate concentrations in the lowest 1km in the South-East Pacific (Fig 4.7e) and although the overestimation is low in absolute terms this contributes to a normalised mean bias of 0.84 in the lower troposphere. Only 22.2% of the mean model values lie within the standard deviation of VOCALS observations due to large overestimations below 1km and smaller underestimations above 2km but the correlation with observations is high at 0.77. Simulated concentrations are low relative to OP3 observations in the vicinity of Borneo (NMB = -0.99) with low correlation (R = 0.32) but 88.9% of the mean modelled values in the lower troposphere are within one standard deviation of those observed.

4.3.2.2 Ammonium aerosol

Figure 4.8 shows the vertical profile comparisons for ammonium aerosol for the same six aircraft campaigns. Over Europe (EUCAARI and ADIENT), the model skill is similar for ammonium as was found for nitrate. The vertical variability is captured very well by the model (R = 0.80 and 0.89) in the lower troposphere, with simulated values at most levels up to 4 km falling within the observed standard deviation (88.9 and 77.8%). Despite this, concentrations are again biased low in the lowermost 4 km (NMB = -0.62 and -0.68).

The observed ammonium vertical profile from ARCTAS-Summer aligns closely with the observed nitrate vertical profile and is reproduced more accurately by

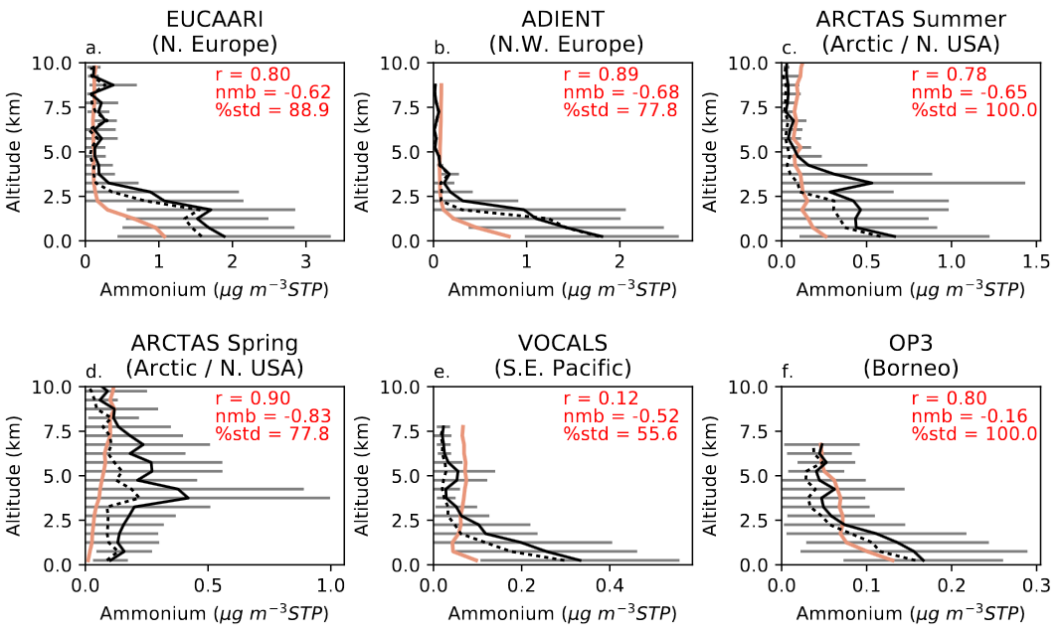

Figure 4.8 *Same as Figure 4.7 for ammonium aerosol.*

the model than the nitrate profile. Simulated concentrations at all levels below 4 km are within the standard deviation of observations, with good correlation (R = 0.78) but are biased low on average (NMB = -0.65). As with nitrate, the model does not reproduce the 3.5 - 4 km peak in ammonium concentrations observed during ARCTAS-Spring but does correlate well overall with observations (R = 0.90), capturing a general increase in ammonium concentration with height in this region. Simulated values underestimate those observed (NMB = -0.83) but are within the standard deviation at 77.8% of levels below 4 km. In both ARCTAS campaigns, the underestimations in ammonium are small in terms of absolute concentrations.

The VOCALS observations are reproduced least well by the model in terms of simulated NH_4^+ (R = 0.12, NMB = -0.52 and %std = 55.6). The simulated NH_4^+ profile is too uniform with height relative to the observations, and underestimates NH_4^+ near the surface. The vertical profile in ammonium observed during the OP3 campaign is reproduced very well by the model with high correlation (R = 0.80), low model bias (NMB = -0.16) and all simulated concentrations below 4 km (and above) within the observed standard deviation.

As mentioned, it is likely that insufficient ammonium formation is driven by insufficient nitric acid or sulphuric acid variability, rather than from a lack of gas-

phase ammonia. The underestimation of several aerosol species could also infer that aerosol deposition processes are too strong in the model. The nitrate-extended GLOMAP-mode has been implemented into a development version of UM-UKCA and changes have subsequently been made in later configurations of UM-UKCA to improve simulated precipitation processes, with implications for the wet scavenging rates of aerosol.

4.3.2.3 Sulphate aerosol

Figure 4.9 shows the vertical profile comparisons for sulphate aerosol. The simulated sulphate vertical profiles correlate well with the European observations (EUCAARI and ADIENT) below 4 km with Pearson correlation coefficient values of 0.84 and 0.93. The model also simulates values that are within the standard deviation of observations over 77.8% of lower levels for both campaigns. In general, simulated sulphate concentrations are higher at 1km altitude over the Northern European flight tracks (EUCAARI) but this feature was not observed during the campaign. Over the lowest 4 km, the model bias is moderately low at a NMB value of -0.26. Simulated sulphate concentrations are more uniform with height than those observed over the ADIENT flight track with a higher normalised mean bias score of -0.62.

The sulphate vertical profile from the ARCTAS-Summer campaign is reproduced very well by the model, with high correlation (R = 0.83), low model bias (NMB = -0.16) and with all mean simulated concentrations below 4 km within the standard deviation of the mean observed profile. However, the model systematically underestimates sulphate concentrations through the lower and mid troposphere, by 83% on average, in the ARCTAS-Spring campaign.

For VOCALS, simulated and observed SO_4^{2-} are weakly anti-correlated and the normalised mean bias is low through the lowermost 4 km at +5% because of under- and over-estimations in sulphate concentration below and above 1.5km, respectively. Simulated sulphate concentrations are within the observed standard deviation at 55.6% of levels below 4 km.

Simulated values correlate well with the OP3 observations (R = 0.92) below 4 km with 66.7% of levels within the standard deviation of observations. Concentrations in the lowermost 1.5km are represented particularly well.

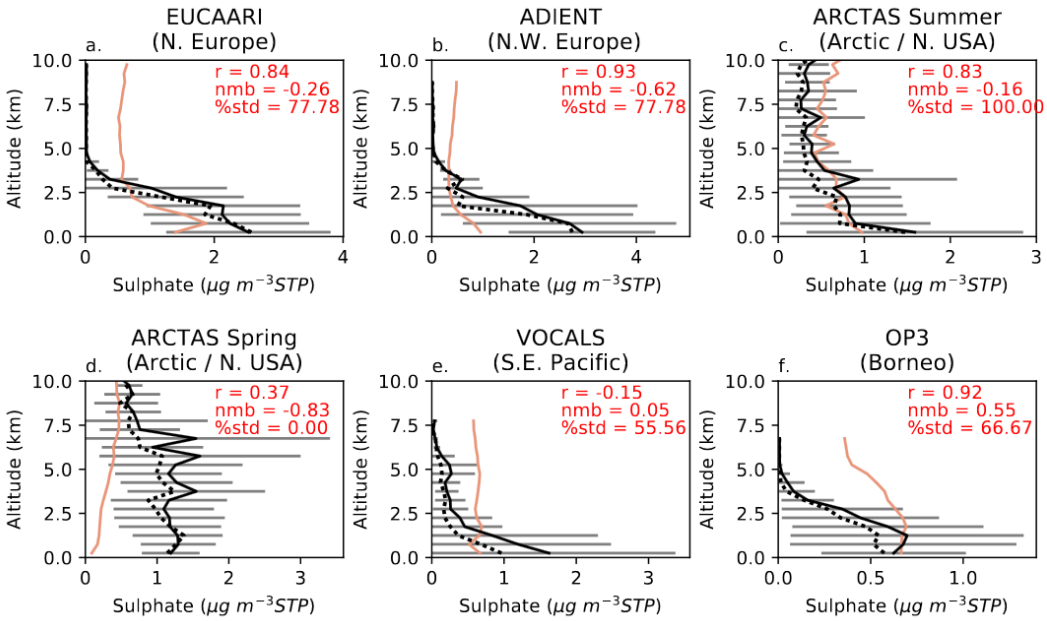

Figure 4.9 *Same as Figure 4.7 for sulphate aerosol.*

However, the model overestimates concentrations by 55% on average between the surface and 4 km, with an apparent overestimation of up to around 0.4 μg sm^{-3} continuing to higher levels.

Model overestimation of sulphate in the mid to upper troposphere is apparent in the SE Pacific, Borneo and over Europe. Sulphate is also overestimated in the free troposphere over Europe in Kapadia et al. (2016) where GLOMAP-mode is implemented in the TOMCAT CTM, but isn't overestimated in that study over the SE Pacific and SE Asia. The upward tendency in simulated sulphate aerosol concentration above approximately 4 km also exists in non-nitrate extended configurations of this UM-UKCA version. This may be a presentation of a known limitation that was subsequently amended in later configurations of the model by incorporating an in-plume convective scavenging scheme (Kipling et al., 2013; Kipling et al., 2016).

4.3.3 Comparison to AeroCom multi-model ensemble

4.3.3.1 Global burden and surface concentrations

Tables 4.3 and 4.4 show the annual, global-mean NO_3^-, NH_4^+, SO_4^{2-}, NH_3 and HNO_3 burden and surface concentrations, respectively, compared to the AeroCom multi-model mean values. The annual mean global NO_3^- burden of 0.145 Tg from

the HYB simulation is lower than the AeroCom Phase III (AP3) mean of 0.63 Tg and just within the range simulated by individual models in the AeroCom ensemble (0.14 to 1.88 Tg). The simulated annual mean global surface NO_3^- aerosol concentration of 0.082 μg kg^{-1} (0.095 μg m^{-3}) is also low relative to the AeroCom multi-model mean concentration of 0.23 μg kg^{-1}, but lies within the range of values simulated by the AeroCom models (0.05 to 0.47 μg kg^{-1}).

UKCA HYB simulates a nitric acid burden of 1.160 Tg, which is within the AeroCom range of 0.66 to 5.7 Tg. The global-mean surface nitric acid concentration simulated by UM-UKCA HYB is greater than that from any of the AeroCom models, at 0.381 μg kg^{-1} compared to the AeroCom range of 0.04 to 0.32 μg kg^{-1}. The higher nitric acid concentrations relative to the AeroCom range suggest that differences in NO_x emissions (Section 3.5, Figure 3.4), i.e. in HNO_3 availability, are not solely responsible for lower nitrate aerosol concentrations in UM-UKCA. It is more likely that UM-UKCA simulated concentrations are lower because they do not treat nitrate aerosol formation on dust, which Bian et al. (2017) and Karydis et al. (2016) found to be an important pathway for coarse mode nitrate formation.

Table 4.3 *Simulated global annual-mean burdens from UM-UKCA sensitivity runs compared with the AeroCom mean, minimum and maximum burdens (Bian et al., 2017). These are total atmospheric burdens, except for HNO_3 where the tropospheric burden up to 100 hPa is given, as in Bian et al. (2017).*

(Tg)	**NO_3^-**	**NH_4^+**	**SO_4^{2-}**	**NH_3**	**HNO_3**
HYB	0.145	0.345	2.28	0.068	1.160
EQU	0.139	0.333	2.26	0.066	1.138
HYB-NoHet	0.127	0.348	2.32	0.070	1.147
AeroCom mean [min - max]	0.63 [0.14 -1.88]	0.32 [0.17 - 0.75]	1.8 [0.83 - 3.3]	0.20 [0.05 - 0.85]	2.5 [0.66 - 5.7]

Table 4.4 *Simulated annual-mean, global-mean surface concentrations from UM-UKCA sensitivity runs compared with the AeroCom mean, minimum and maximum global-mean surface concentrations (from Bian et al., 2017). UM-UKCA values are given in μg kg^{-1} first for consistency with units of Bian et al. (2017) and μg m^{-3} in parentheses '()' for consistency with model observation comparisons in section 4.3.1.*

μg kg^{-1} (μg m^{-3})	**NO_3^-**	**NH_4^+**	**SO_4^{2-}**	**NH_3**	**HNO_3**
HYB	0.082 (0.095)	0.139 (0.161)	0.463 (0.536)	0.302 (0.337)	0.381 (0.444)
EQU	0.080 (0.094)	0.140 (0.163)	0.462 (0.532)	0.230 (0.333)	0.371 (0.432)
HYB-NoHet	0.048 (0.056)	0.131 (0.152)	0.468 (0.542)	0.308 (0.343)	0.356 (0.414)
AeroCom mean [min - max]	0.23 [0.05 - 0.47]	0.18 [0.08 - 0.44]	0.63 [0.34 - 1.72]	0.49 [0.25- 1.39]	0.14 [0.04 - 0.32]

The annual mean global NH_4^+ burden of 0.345 Tg is just above the mean AeroCom burden of 0.32 Tg and within the AeroCom multi-model range of 0.17 to 0.75 Tg. The annual mean global NH_4^+ surface concentration was 0.139 μg kg^{-1} (0.161 μg m^{-3}) which places it just below the AeroCom mean value of 0.18 μg kg^{-1} and within the multi-model range of 0.08 to 0.44 μg kg^{-1}. UM-UKCA simulates a global ammonia burden of 0.068 Tg, which falls within the range simulated by the AeroCom models (0.05 Tg to 0.85 Tg). The UM-UKCA annual global mean surface NH_3 concentration of 0.302 μg kg^{-1} also falls between the AeroCom model range of 0.25 to 1.39 μg kg^{-1}.

The UM-UKCA-simulated global-mean surface sulphate aerosol concentration of 0.463 μg kg^{-1} is below the AeroCom mean but within the range simulated by AeroCom models, despite appearing to be systematically biased low when previously compared to observations. The UM-UKCA SO_4^{2-} burden of 2.28 Tg places UM-UKCA between the AeroCom multi-model mean and upper estimates of 1.8 Tg and 3.3 Tg, respectively.

4.3.3.2 Distribution of surface NO_3^-, NH_4^+ and SO_4^{2-}

Figure 4.10 compares the spatial distribution of surface nitrate aerosol concentration from UM-UKCA simulation HYB with the 25th, 50th and 75th percentile concentrations from the AeroCom multi-model ensemble. It has been shown already that the UM-UKCA global mean surface nitrate concentration of 0.082 μg kg^{-1} (0.095 μg m^{-3}) is below the AeroCom mean but within the range simulated by individual models.

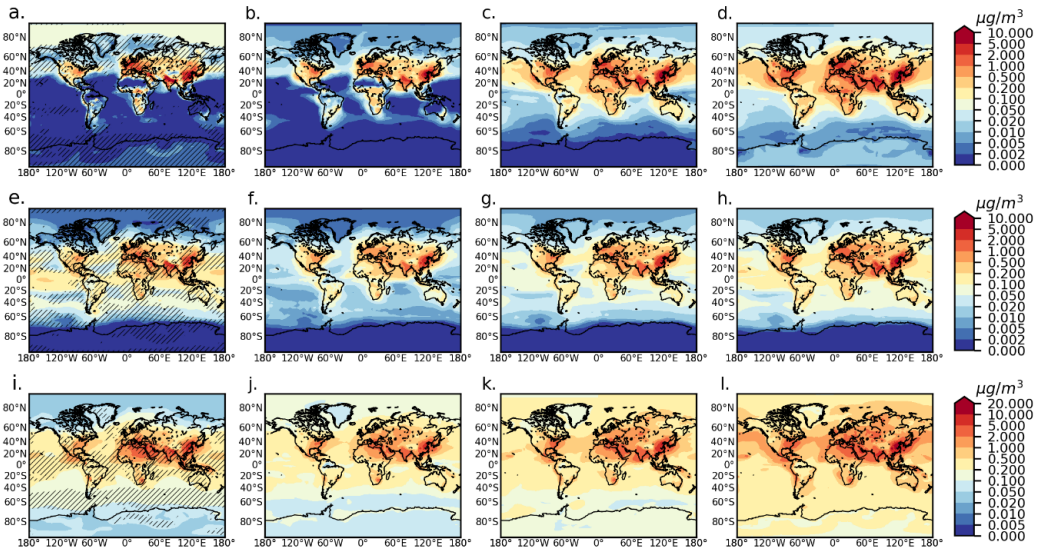

Figure 4.10 *Annual mean simulated surface NO_3^- (top row), NH_4^+ (middle row) and SO_4^{2-} aerosol from UM-UKCA HYB (1st column), compared with 25th (2nd column), 50th (3rd column) and 75th (4th column) percentile concentrations from 9 participating AeroCom Phase III models. Hatching indicates regions where UM-UKCA-simulated concentrations are within the AeroCom interquartile range.*

Regions of highest surface nitrate concentrations (Europe, USA, China and India) in UM-UKCA correspond with those simulated by the AeroCom models. Regions of lower nitrate concentration over Africa, South America, and Australia, however, may be indicative of the lack of nitrate formation on dust by UM-UKCA because 5 of the 9 AP3 models represent this process. UM-UKCA surface nitrate concentrations are within the AP3 interquartile range (IQR) over much of Europe and Eastern China but are underestimated relative to the AP3 25th percentile in eastern North America. Marine concentrations in the Northern Hemispheric mid-latitudes are largely within the AP3 IQR but fall below the 25th percentile over much of the Tropics and Southern Hemispheric mid-latitudes.

UM-UKCA concentrations in the Arctic exceed the AP3 75th percentile yet still underestimate observed concentrations in this region (Figs. 4.1 and 4.7).

As with nitrate, regions of highest ammonium concentrations are located over continental and outflow regions and correspond well with the regions simulated by the AeroCom models. Comparison to the AeroCom models varies with region over the continents, where UM-UKCA simulates ammonium levels around either the 50th or 25th AeroCom percentile values. UM-UKCA values in the remote marine regions are generally in the third and upper quartile of those simulated by the AeroCom models, with the exception of the Arctic Circle where UM-UKCA concentrations are lower than the AeroCom median. UM-UKCA and most AeroCom models are in agreement that concentrations are low (below 0.002 μg m^{-3}) over the Antarctic.

Regions of highest surface sulphate aerosol in UM-UKCA are similarly located over continental and outflow regions, as in the AP3 models. SO_4^{2-} concentrations are below the AP3 25th percentile in Western Europe and eastern North America and also below the 25th percentile in the polar and mid-latitude marine regions. Unlike NO_3^-, SO_4^{2-} concentrations exceed the 75th percentile over much of northern sub-Saharan Africa.

4.3.3.3 UM-UKCA and AeroCom multi-model skill versus observations

Figures 4.11 and 4.12 compare the UM-UKCA model skill (Pearson correlation coefficient and normalised mean bias) against the range of model skill in the AeroCom Phase III simulations. This study therefore determines not only how simulated UM-UKCA concentrations compare to the AeroCom multi-model range, but also how well UM-UKCA compares to observations relative to other models.

Figure 4.11 compares the Pearson correlation coefficients from each of the AeroCom models against those from UM-UKCA. Over Europe, both UM-UKCA and the AeroCom models represent the spatial variability in annual mean nitrate, ammonium and sulphate aerosol well and consistently, as demonstrated by median R values above 0.6. The UM-UKCA Pearson correlation coefficient is within the AP3 interquartile range in terms of model skill in DJF and remains above 0.6 on annual and JJA timescales despite falling below the AP3 skill range

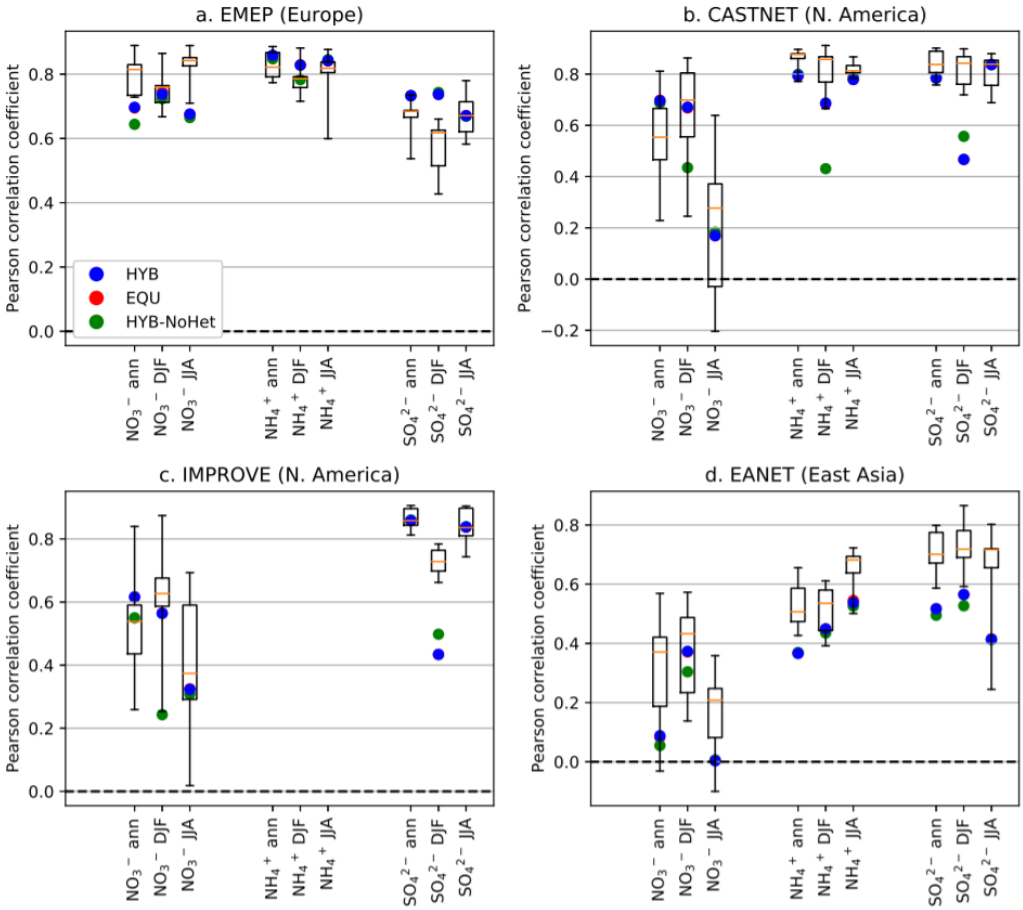

Figure 4.11 *UM-UKCA (HYB, blue marker) and AeroCom Phase III (box plot) Pearson correlation coefficients for annual and seasonal mean surface NO_3^-, NH_4^+ and SO_4^{2-} aerosol concentrations, from comparisons against (a) EMEP, (b) CASTNET, (c) IMPROVE and (d) EANET observations. Boxes mark the interquartile range and median (orange) of the AeroCom model coefficients with whiskers denoting the maximum and minimum of the multi-model range. Pearson correlation coefficients from UM-UKCA simulations EQU and HYB-NoHet are indicated by the red and green markers, respectively.*

in the latter periods. The UM-UKCA correlation coefficients for NH_4^+ and SO_4^{2-} in all seasons are greater or equal to the AP3 median scores, indicating that UM-UKCA outperforms some or all other AeroCom models in terms of reproducing the spatial distribution of those species over Europe. The Pearson coefficients in this analysis of the annual mean AeroCom concentrations are higher than those reported by Bian et al. (2017; e.g. AP3 NO_3^- comparison to EMEP ranges from R = 0.393 to 0.585) potentially because annual mean concentrations are compared in this thesis, whereas Bian et al. (2017) compared the models to observations on shorter temporal timescales.

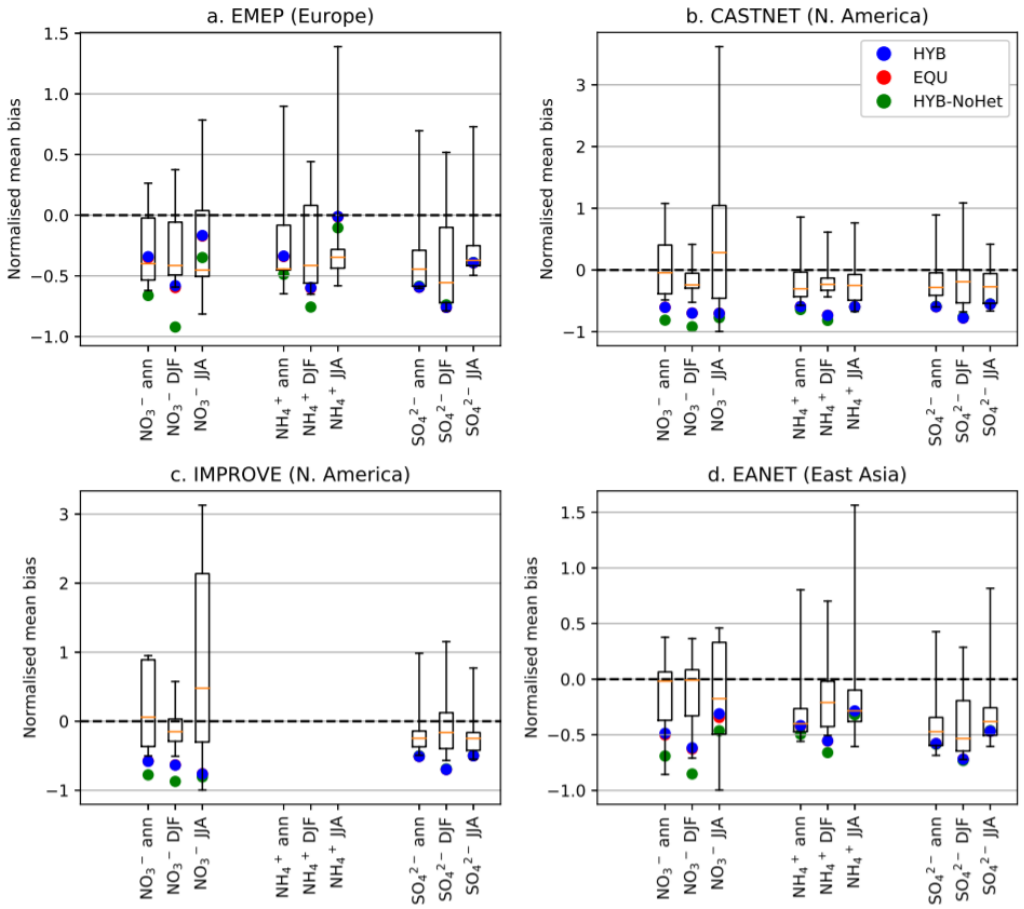

Figure 4.12 *UM-UKCA (HYB, blue marker) and AeroCom Phase III (box plot) normalised mean bias scores for annual and seasonal mean surface NO_3^-, NH_4^+ and SO_4^{2-} aerosol concentrations, from comparisons against (a) EMEP, (b) CASTNET, (c) IMPROVE and (d) EANET observations. Boxes mark the interquartile range and median (orange) of the AeroCom model biases with whiskers denoting the maximum and minimum of the multi-model range. Normalised mean bias scores from UM-UKCA simulations EQU and HYB-NoHet are indicated by the red and green markers, respectively.*

Over the USA, the wider range of Pearson correlation coefficients for each of the AeroCom models compared to CASTNET and IMPROVE networks suggests that the multi-model skill for nitrate aerosol is more varied over the USA than over Europe. UM-UKCA ranks within the upper quartile of the AP3 correlation coefficients on annual mean timescales and within the AP3 multi-model correlation range in DJF and JJA relative to US observation networks. As in UM-UKCA, the skill of other AeroCom models is also reduced in JJA (median R of 0.2-0.4 for both networks) and the UM-UKCA Pearson coefficient remains within the

multi-model interquartile range. The lower model skill in JJA across models may indicate that the gas-particle partitioning of nitric acid is more uncertain across models at higher temperatures or that the spatial variability of precursor emissions is less certain in summer.

Ammonium concentrations in the US are monitored by the CASTNET network, but not IMPROVE. The AeroCom model correlation coefficients are consistently high in the three time periods and the UM-UKCA correlation coefficients for NH_4^+ over the USA are below the AeroCom interquartile range, but within the multi-model range for each period. UM-UKCA is within the AP3 multi-model range of correlation scores for sulphate in JJA and on annual mean timescales. However, the UM-UKCA model correlation for sulphate aerosol is below that of any other AeroCom model in DJF.

Compared to East Asian observations, the UM-UKCA model correlation coefficient for nitrate is within the AP3 range across annual and seasonal time periods here and within the interquartile range in DJF. The correlation coefficients are generally lower at less than 0.6 for all AeroCom models in any time period. As seen for UM-UKCA, the AP3 correlation to NO_3^- observations is also lower in JJA on average. The UM-UKCA correlation coefficients for NH_4^+ and SO_4^{2-} in East Asia are below the AP3 range on annual mean timescales. UM-UKCA NH_4^+ is within the AP3 range in DJF and JJA and UM-UKCA SO_4^{2-} is within the range in JJA but lower than other AeroCom values in DJF.

Figure 4.12 compares the normalised mean bias among AeroCom models against the UM-UKCA simulated values. Over Europe, the median AeroCom model, in terms of magnitude of model bias, is biased low for NO_3^-, NH_4^+ and SO_4^{2-} against annual, DJF and JJA mean observations. The negative bias in UM-UKCA annual mean surface nitrate reported in Section 4.3.1.1 is smaller than the median annual and JJA mean AP3 bias. However, the UM-UKCA NO_3^- bias is approximately equal to that of the lowest AP3 model in DJF. The UM-UKCA NH_4^+ bias over Europe is within the multi-model bias range for all seasons shown here, and outperforms the AP3 interquartile range in JJA. UM-UKCA shows a stronger negative bias in European SO_4^{2-} than the AP3 median but is just within the AP3 multi-model range in all seasons here.

Over the USA, the regional average UM-UKCA low bias in NO_3^-, NH_4^+ and SO_4^{2-} is greater than most of the AP3 models for the time periods analysed, although the normalised mean bias for each aerosol species is within the AP3 multi-model range in JJA. Over East Asia, the UM-UKCA normalised mean bias is within those from the AP3 range for each species and season, with the exception of NH_4^+ in DJF when the UM-UKCA bias is greater than that of any other AP3 model.

The low bias in UM-UKCA-simulated SO_4^{2-} is just within the range of AP3 annual and DJF mean scores, and within the interquartile range and close to the median JJA mean NMB. The low surface SO_4^{2-} bias across the AP3 models is less expected, given that sulphate has traditionally received more attention in modelling studies, and is also seen in the evaluation of Bian et al. (2017).

4.3.3.4 Zonal mean NO_3^-, NH_4^+ and SO_4^{2-} concentrations

It has already been shown in Table 4.3 that the UM-UKCA-simulated nitrate aerosol burden is below the mean but within the AeroCom multi-model range. Figure 4.13 shows the annual zonal mean distribution of NO_3^-, NH_4^+ and SO_4^{2-} in the UM-UKCA control simulation, compared against the AeroCom Phase III median and interquartile range.

UKCA simulates the highest zonal mean nitrate concentrations (> 0.1 μg kg^{-1}) in the lowermost 200 hPa between 25 and 65° N (Fig 4.13a). Zonal mean concentrations in this region are largely near but below those of the AeroCom 25th percentile, though lower concentrations (0.02 – 0.1 μg kg^{-1}) between ~ 50° N an 70° N are within the AP3 IQR. Broadly, there are three regions where the UM-UKCA simulated zonal mean NO_3^- concentrations vary from those of the AP3 IQR. These are: the Northern Hemisphere polar latitudes; much of the mid-troposphere (~ 800 - 400 hPa) between 40° S and 50° N; and the lower troposphere (from the surface to ~ 800hPa) between 60° S and 50° N. UM-UKCA places more nitrate at the poles than other AP3 models. Comparisons to ARCTAS-Spring in Section 4.3.2.1 indicated that UM-UKCA nitrate was within the standard deviation of observations with a moderate low bias, which together with this zonal mean analysis suggests that UM-UKCA has higher skill than other AP3 models in this region despite being outside of the IQR.

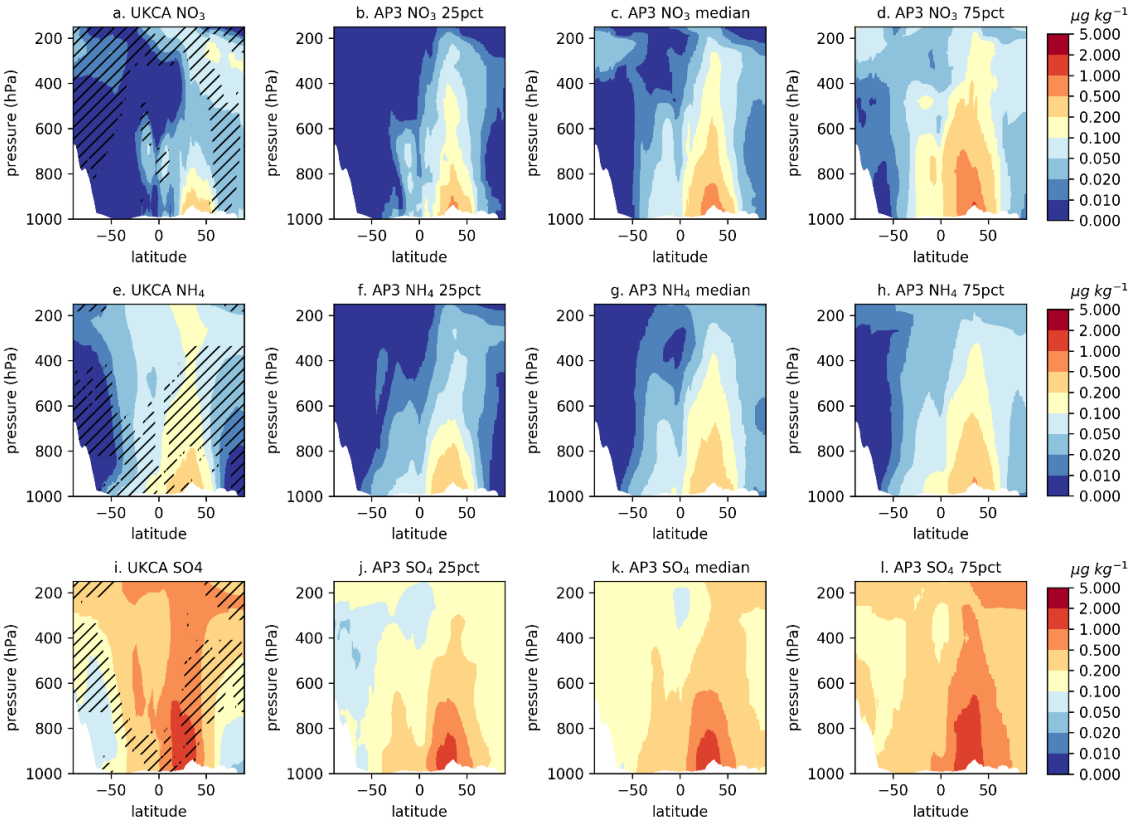

Figure 4.13 *Annual mean simulated zonal mean NO_3 (top row), NH_4 (centre row) and SO_4 aerosol from UM-UKCA HYB (1st column), compared with 25th (2nd column), 50th (3rd column) and 75th (4th column) percentile concentrations from the 9 participating AeroCom Phase III (AP3) models. Hatching indicates regions where UM-UKCA-simulated concentrations are within the AP3 interquartile range.*

The lower nitrate concentrations simulated by UM-UKCA in the northern hemispheric mid-latitudes may be attributable in part to lower NO_x emissions in UM-UKCA compared to other AeroCom models (see Figure 3.4). Lower zonal mean concentrations may be driven by lower nitrate formation associated with dust and sea salt in northern Africa, South America and the southern hemispheric oceans. Lower concentrations in remote regions are indicative of lower precursor availability or shorter aerosol lifetime. Lower nitrate concentrations in warmer equatorial regions may result from uncertainty in the temperature sensitivity of nitrate aerosol formation, encouraging partitioning to gas phase nitric acid. In the mid-troposphere, nitrate aerosol formation is elevated sulphate concentrations could also have suppressed nitric acid partitioning to nitrate aerosol.

As at the surface, the spatial distribution of zonal mean UM-UKCA simulated ammonium (Fig 4.10e.) maps closely to nitrate and sulphate concentrations. UM-UKCA-simulated ammonium aerosol is greatest in the near-surface northern hemispheric mid-latitudes (below 800 hPa and between ~10° N and 50° N), with slightly elevated concentrations (0.1-0.2 μg kg^{-1}) extending into the upper troposphere between approximately 30 and 40° N. Ammonium in the mid-to-upper troposphere is associated with sulphate aerosol.

UKCA zonal mean ammonium concentrations are within the AP3 IQR for much of the Northern Hemisphere mid-troposphere (~ 350 to 800 hPa) and Southern Hemisphere mid-troposphere in the mid-to-high latitudes (~ 50° S to 90° S). Lower tropospheric NH_4^+ concentrations are largely within the AP3 IQR in the Southern Hemisphere but fall below the IQR in the Northern Hemisphere (~ 15° N to 80° N). Secondary peaks in nitrate and ammonium concentrations in the upper troposphere at the poles are simulated by UM-UKCA and several other AeroCom models.

Zonal mean sulphate concentrations are largely within the AP3 interquartile range in the low to mid latitudes of the Northern Hemisphere (below 800 hPa). Sulphate concentrations in the lower troposphere are below the AP3 IQR and were found to be low compared to the ARCTAS Spring vertical profiles (Figure 4.9). Lower zonal mean sulphate concentrations simulated by UM-UKCA in Polar regions are likely to be partly driven by overestimated wet deposition and underestimated formation by in-cloud O_3 oxidation (e.g. Turnock, 2016; Turnock et al., 2015). However, concentrations in the mid-troposphere (~750 to 400 hPa) at high latitudes (> 50° N/S) are within the AP3 IQR. Sulphate concentrations in the mid to upper troposphere in the low and mid-latitudes (50° S to 50° N) exceed the AP3 IQR and it is recognised, in combination with comparison to aircraft observations (Figure 4.9), that sulphate is biased high by UM-UKCA in this region.

4.3.4 Influence of gas-particle partitioning assumption

In this section, the response of semi-volatile inorganic aerosol concentrations and size to the model treatment of gas-particle partitioning complexity is investigated. The two simulations compared in this section are identical in

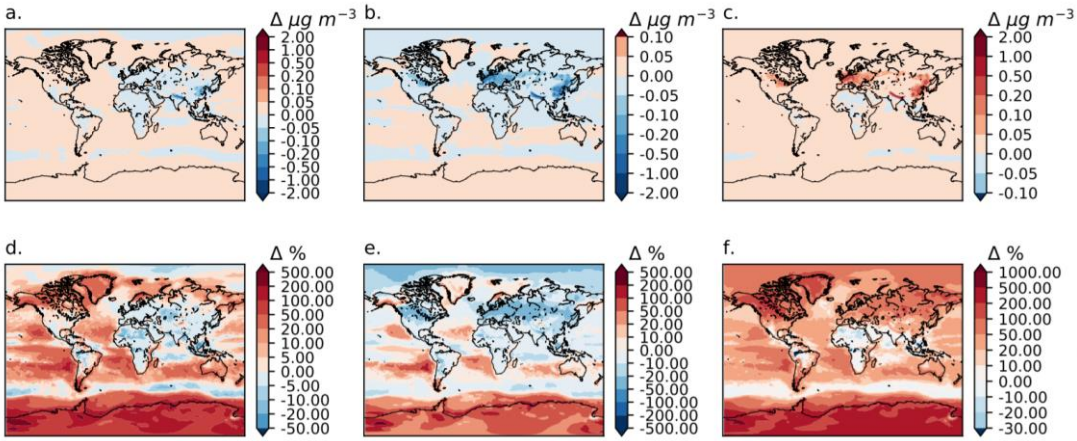

Figure 4.14 *Absolute (top row) and relative (bottom row) changes in annual mean surface (a+d) nitrate aerosol, (b+e) fine mode nitrate and (c+f) coarse mode nitrate mass concentration when switching from a hybrid (HYB) to equilibrium (EQU) configuration.*

configuration except for the treatment of semi-volatile inorganic aerosol formation. HYB has been evaluated in preceding sections of this chapter and applies a hybrid approach to treat the gas-particle partitioning of nitric acid to nitrate aerosol. Simulated nitrate aerosol concentrations are compared with those simulated in EQU, which applies an equilibrium approach (see Section 3.2.4 and 4.2). The HYB case represents the more physically realistic representation of semi-volatile inorganic aerosol partitioning of the two approaches and is considered to give the best-case representation of the size-resolved semi-volatile aerosol concentrations.

Switching to the equilibrium configuration has the overall effect of redistributing nitrate from the fine mode (comprising aerosol with dry diameter below 1 μm) to the coarse (supermicron) mode. Switching to the equilibrium scheme reduces the fine mode atmospheric nitrate burden by 9.8% from 0.115 Tg to 0.104 Tg. The coarse nitrate burden is increased by 21.3% from 0.029 Tg to 0.036 Tg. The global mean fine nitrate surface concentration is decreased by 15.2% (from 0.071 μg m^{-3} to 0.060 μg m^{-3}) while the mean coarse nitrate surface concentration is increased by 36.4% (from 0.025 to 0.034 μg m^{-3}). This redistribution of mass in EQU arises as a result of faster mass transfer from the gas phase to the coarse

mode when the assumption of thermodynamic equilibrium is applied for the larger size range. This depletes the gaseous nitric

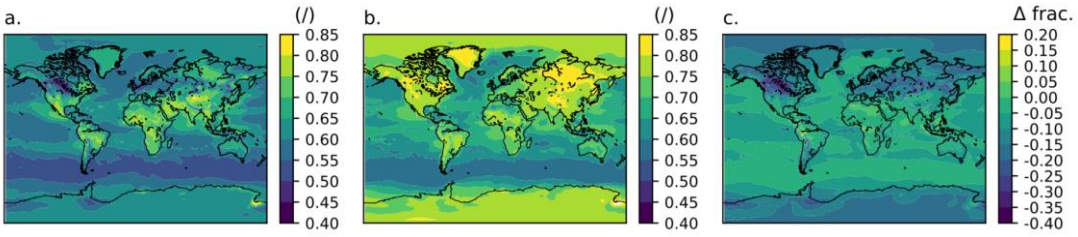

Figure 4.15 *Annual mean surface fine mode nitrate aerosol fraction in (a) EQU, (b) HYB and (c) absolute change in fine mode nitrate aerosol fraction (EQU minus HYB).*

acid available to partition into the fine mode and results in underestimations of the fine mode nitrate aerosol relative to using the more physically realistic hybrid approach.

Figure 4.14b, c, e and f show differences in the fine and coarse mode surface nitrate aerosol concentrations when switching from the hybrid to equilibrium scheme. The greatest absolute changes in fine and coarse mode nitrate concentration (up to ±1 μg m^{-3}) largely occur over polluted continental regions, exceeded only by regional changes of over ±2 μg m^{-3} over northern India. Increases in coarse mode nitrate are at least partly compensated by decreases in fine mode nitrate over most regions with the main exception of several tropical trade wind influenced marine regions and the Antarctic. Here, both fine and coarse mode concentrations increase in EQU, resulting in a small but locally important increase in surface nitrate concentration. Fine mode decreases in EQU exceed the corresponding increases in coarse mode nitrate over areas of remote central Asia, the Arctic and marine regions e.g. the Indian Ocean and Southern Ocean, while decreases in both fine and coarse mode nitrate occur over isolated regions of South America, Africa and marine regions off India and South-East Asia. In these regions, the removal of nitrate aerosol has been promoted by switching to the equilibrium scheme.

Figure 4.15 shows the fine mode fraction of nitrate aerosol simulated for EQU and HYB and the absolute difference in fine mode fraction when moving from the hybrid to the equilibrium scheme. The hybrid scheme places over 65% of the

nitrate mass in the fine mode over most continental regions. The fine mode fraction in the hybrid run also exceeds 75% over much of the Arctic and some regions of the Antarctic and exceeds 50% over other marine regions. When switching to the equilibrium scheme, the fine mode nitrate fraction decreases from over 65% down to as low as 40% over regions in the continental Northern Hemisphere and the Arctic Circle. The greatest underestimations in fine mode fraction by the equilibrium approach, relative to the hybrid approach, occur over much of the continental Northern Hemisphere and Polar regions with widespread absolute changes in fine mode fraction of approximately -0.15 between the HYB and EQU runs.

Within the GLOMAP-defined aerosol modes, nitrate mass is largely redistributed to the coarse mode from the accumulation mode, and from the Aitken mode to a lesser extent, when switching from the hybrid to the equilibrium approach (Appendix Fig A1). The results here corroborate the findings of Benduhn et al. (2016) who implemented the same GLOMAP-mode Hy-DiS-1.0 equilibrium and hybrid solvers in the TOMCAT chemical transport mode, except they found the greatest decrease in surface nitrate mass occurred in the Aitken mode when applying the equilibrium approach. This may result from the presence of boundary layer nucleation processes in the GLOMAP-Mode configuration of Benduhn et al. (2016), which produces liquid aerosol in the nucleation and Aitken modes on which nitric acid uptake can occur. The implications of using a hybrid partitioning scheme for Aitken mode nitrate, and therefore CCN concentrations, may be larger in future configurations of UM-UKCA that also include GLOMAP-mode boundary layer nucleation (e.g. Spracklen et al., 2006).

Feng and Penner (2007), referenced hereafter as FP07, provide the other main comparison of the global, size-resolved nitrate aerosol burden using a hybrid versus an equilibrium partitioning scheme. FP07 also concluded that use of a hybrid dynamical approach resulted in a redistribution of nitrate mass to the finer size range. They found that the Umich/Impact model placed 25% less nitrate mass in the fine mode when switching from a hybrid dynamical to equilibrium scheme. Their equilibrium and hybrid runs simulated total global fine mode nitrate fractions of 28% and 48%, respectively. The findings in this thesis support the hypothesis of FP07 that direct forcing estimates based on

aerosol fields simulated with an equilibrium scheme will be lower and are likely to be underestimated compared to those calculated using a hybrid dynamical approach. From the results in this chapter, it can be hypothesised that the size partitioning approach is important for aerosol indirect radiative effects, where using an equilibrium assumption may lead to an underestimation in the number concentration of nitrate aerosol that can act as CCN by disproportionately partitioning nitric acid to less numerous larger nitrate aerosol particles. This will be investigated in Chapter 6. The results in this chapter appear to contradict those found by Trump et al. (2015) who simulated increases in surface coarse mode nitrate concentration when using a hybrid approach to simulate hourly resolution aerosol concentrations over Europe. It is not clear why the results of Trump et al. (2015) differ from those of this study, Benduhn et al. (2016) and FP07.

Global annual-mean nitrate and ammonium burdens in UM-UKCA are slightly underestimated by the equilibrium approach relative to applying the hybrid approach, decreasing to 0.139 Tg (-4.1%) and 0.333 Tg (-3.5%) respectively when switching to the equilibrium scheme, as summarised in Table 4.3. The nitric acid burden decreases to 1.138 Tg (-1.9%), while total nitrate (nitric acid + nitrate aerosol) decreases by 2.1% to 1.277 Tg. Switching to the equilibrium scheme also has a modest influence on surface concentrations, as described in Table 4.4. Figures 4.11 and 4.12 shows that the influence of the equilibrium scheme on model-observation comparisons is negligible in the regions analysed compared to the equivalent hybrid simulation.

The results of FP07 suggest that changing to an equilibrium approach should influence nitrate aerosol concentrations more than was found in this work. Their study resulted in a 26% increase in nitrate aerosol burden, but an 8% decrease in total nitrate burden (gas plus aerosol), when using the equilibrium scheme compared to the hybrid dynamical approach. They attributed this to a much larger dry deposition and moderately higher wet deposition of nitrate aerosol using the equilibrium approach, following faster partitioning to larger sized aerosol. FP07 simulated a higher coarse fraction of nitrate aerosol, which may explain why the effect of changing particle size and the subsequent influence on aerosol scavenging rates were higher in their sensitivity study. The partitioning

approach may have a greater influence on nitrate aerosol removal rates and airborne concentrations if nitric acid uptake onto dust were included, through larger modification of deposition rates.

The left-most column of Figure 4.14 shows the absolute and relative differences in total (particle phase) surface nitrate concentration between the HYB and EQU simulations. Implementation of the equilibrium partitioning assumption leads to decreases in annual mean surface nitrate concentration of up to 0.1 μg m^{-3} compared to EQU over large regions of Europe and South and East Asia, with the greatest increases of up to 2 μg m^{-3} over eastern regions of China and the north of India. More modest decreases (up to 0.05 μg m^{-3}) occur over the Arctic, parts of the USA and central Africa. By contrast, low magnitude increases in nitrate concentration of up to 0.05 μg m^{-3} occur over regions of the US, Canada, Australia, South America and global ocean, including Antarctica.

The greatest changes in surface nitrate concentration relative to HYB-simulated concentrations are seen over remote regions. Surface nitrate concentrations are decreased by at least 10% over widespread oceanic regions when switching from the hybrid scheme. Small absolute changes of less than ± 0.001 μg m^{-3} occur over several regions and can represent large changes regionally, relative to low concentrations simulated by the EQU. Nitrate concentrations are decreased by 50% and upward to over 200% over some regions of the Antarctic when moving to the equilibrium scheme, although with low background concentrations this represents an absolute increase of less than 0.05 μg m^{-3}. Seasonally, the choice of partitioning has a greater influence on NO_3^- concentrations in this region in June, July and August (Appendix Fig. A2).

As a final point of discussion, the fine fraction of the nitrate aerosol burden from EQU and HYB are compared to those simulated by the 9 AP3 models. The global fine nitrate burden fractions in EQU and HYB are 74% and 80%, respectively. At the surface, the global mean fine fraction is 64% in the equilibrium sensitivity, increasing to 74% in the hybrid configuration. Bian et al. (2017) reports that the AP3 fine mode fraction varies between 100% (CHASER and GISS-OMA) to approximately 50% (EMAC, GMI and INCA), 20% (EMEP and OsloCTM2) and 3% (OsloCTM3). fine nitrate fractions ranging from 10 to 100% have been simulated

in studies prior to AP3 (e.g. Adams et al., 2001; Bauer et al., 2007; Jacobson, 2001).

Overall, comparisons to the AP3 size distributions indicate that UM-UKCA overestimates the nitrate fine fraction. Like UM-UKCA, the OsloCTM models also exclude nitrate aerosol formation on dust. However, their treatment of nitrate aerosol formation on sea salt using an equilibrium partitioning approach results in low fine nitrate fractions (Bian et al., 2017). The scavenging of sea salt may be too low in OsloCTM3, contributing further to high coarse aerosol concentrations (Lund et al., 2018). The EMAC, GMI and INCA models represent nitrate formation on both dust and sea salt, yielding lower fine fractions than both the EQU and HYB UM-UKCA configurations. Similarly, previous studies applying a dynamic approach to the gas-particle partitioning (including formation on sea salt and dust) have simulated fine mode nitrate fractions of between 40 and 60% (Feng and Penner, 2007; Xu and Penner, 2012). Therefore, it follows that the high fine mode fraction in UM-UKCA is likely to largely result from the lack of heterogeneous nitrate formation on dust.

The lower coarse nitrate fraction and nitrate burden in UM-UKCA, relative to the other AP3 models, is indicative of the missing dust source but does not indicate that the hybrid approach itself is inappropriate for simulating the size-resolved aerosol. The hybrid approach to partitioning would be expected to have a more profound impact on nitrate size partitioning in future configurations that consider nitric acid uptake onto dust, where the rates of partitioning to the coarse mode are likely to be overestimated if using a purely equilibrium approach.

4.3.5 Influence of heterogeneous N_2O_5 hydrolysis

Heterogeneous N_2O_5 hydrolysis is switched off in the HYB-NoHet simulation. The removal of this reaction results in changes to the global atmospheric burden (Table 4.3) of nitrate, ammonium and sulphate aerosol to 0.127 Tg (-12.4%), 0.348 Tg (+ 0.9%) and 2.32 Tg (+1.8%), respectively, compared to HYB. Annual-mean, global, surface concentrations of nitrate aerosol are decreased substantially by 42% from 0.082 to 0.048 μg m^{-3} when tropospheric heterogeneous N_2O_5 hydrolysis is removed (Table 4.4). Heterogeneous N_2O_5

chemistry therefore has a substantial influence on simulated nitrate aerosol concentrations.

Figure 4.16 shows the spatial changes in annual and seasonal mean surface nitrate concentration when heterogeneous N_2O_5 hydrolysis is removed. The greatest decreases in annual mean, surface nitrate aerosol concentrations occurred in the mid-to-high latitudes of the Northern Hemisphere. Annual mean nitrate aerosol concentrations are decreased by between 0.01 and 1 μg m^{-3} over much of North America, Europe and Asia when the heterogeneous chemistry is removed, with maximum regional decreases of up to 5 μg m^{-3} over East China and North India. These reductions correspond to relative decreases in nitrate aerosol concentration of at least 10% over the majority of the above continents and maximum reductions, relative to HYB concentrations, of over 80% over regions of Russia. A few regions undergo increases in nitrate aerosol of up to 1 μg m^{-3} when N_2O_5 hydrolysis is omitted. Low magnitude (<0.001 μg m^{-3}) but regionally important increases by up to 40% also occur over large marine areas, although these changes don't exert a large influence on global-mean surface nitrate concentrations.

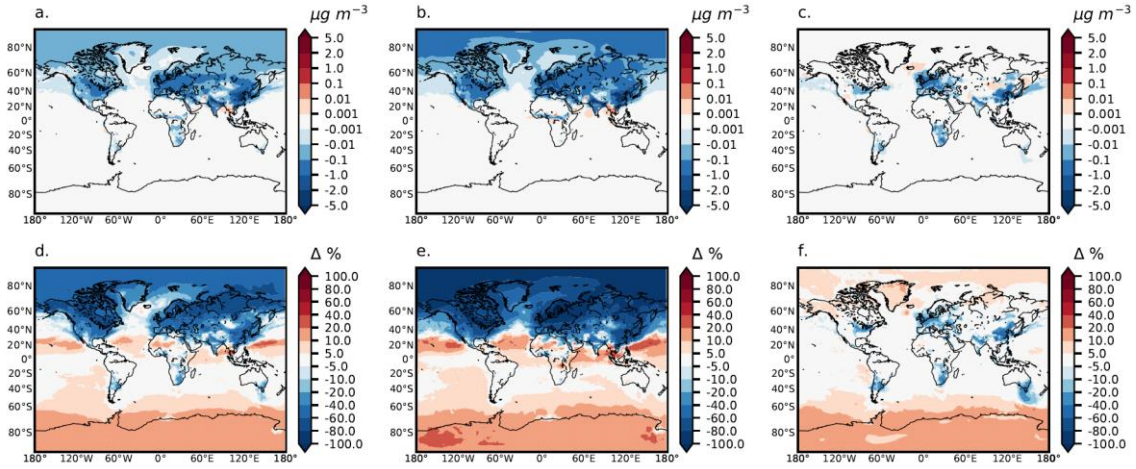

Figure 4.16 *Absolute (top row) and percentage (bottom row) changes in annual (left), DJF (centre) and JJA (right) mean surface nitrate concentrations when removing heterogeneous N_2O_5 hydrolysis i.e. HYB-NoHet minus HYB.*

Reductions in surface nitrate aerosol concentration in the Northern Hemisphere are more widespread in wintertime, where decreases of up to 1 μg m^{-3} (> 80%)

extend over the Arctic Circle. The reaction rate of heterogeneous N_2O_5 hydrolysis is a function of the reaction rate coefficient, which is itself dependent on the uptake probability γ_{N2O5} and wet aerosol surface area, and the ambient N_2O_5 concentration. In HYB, γ_{N2O5} varies globally and seasonally between 0.0320 and 0.0341. The higher reaction rate coefficient in the Arctic in wintertime, arising more from higher aerosol surface area than from γ_{N2O5}, coupled with higher N_2O_5 concentration results in the wider influence of the N_2O_5 reaction on wintertime nitrate (Fig. A3). The locations of maximum γ_{N2O5} and aerosol surface area can differ. For example, summertime reaction rate coefficients over China are elevated by higher aerosol surface area despite lower γ_{N2O5} values, while higher γ_{N2O5} values and aerosol surface area over Europe both work to increase the reaction rate coefficient in Winter.

Figures 4.11 and 4.12 statistically summarise the comparison of HYB-NoHet with observations. The removal of heterogeneous chemistry results in a greater low model bias in surface nitrate concentrations. Without heterogeneous N_2O_5 hydrolysis, the nitrate aerosol model-to-observation NMB values (Figure 4.12, green circles) are decreased to -0.662, -0.812, -0.777 and -0.691 against the annual mean EMEP, CASTNET, IMPROVE and EANET observations, respectively. The nitrate aerosol formation over most of these regions is nitric-acid limited and nitrate concentrations therefore respond strongly to the removal of nitric acid. Wintertime increases in model-observation low bias are greater than increases in the summertime bias when N_2O_5 hydrolysis is excluded. The removal of N_2O_5 hydrolysis also partly exacerbates the model underestimation of ammonium aerosol because less nitric acid is newly available to react with the ammonia and form ammonium nitrate. These changes have relevance for future UM-UKCA simulations of nitrate aerosol because heterogeneous N_2O_5 chemistry is not included in the standard model configuration.

Relatively few studies have focussed on the impacts of heterogeneous N_2O_5 hydrolysis on nitrate aerosol formation. Lowe et al. (2015) found that heterogeneous N_2O_5 hydrolysis is important for improving WRF-Chem model agreement with observed NO_3^- under high relative humidity conditions. In particular, night-time N_2O_5 hydrolysis increased night time nitrate aerosol formation in polluted regions and improved representation of the diurnal cycle

in nitrate aerosol. Stone et al. (2014) had previously also found improvements in box model simulations of night-time NO_3^- and N_2O_5 from N_2O_5 hydrolysis. In UM-UKCA, the uptake of N_2O_5 had a greater impact on night-time concentrations of nitrate aerosol in UM-UKCA for a short test case over Cabauw, the Netherlands (not shown).

The presence of nitrate in aerosol has been observed to reduce the uptake of N_2O_5 over north western Europe (Morgan et al., 2015), California, USA (Riedel et al., 2012) and Colorado, USA (Wagner et al., 2013). Prior to this, several laboratory studies also observed a suppression of N_2O_5 uptake by nitrate-containing aerosol (e.g. Bertram and Thornton, 2009; Griffiths et al., 2009; Mentel et al., 1999). The presence of chloride enhances uptake and produces $ClNO_2$ (Bertram and Thornton, 2009; Osthoff et al., 2008), while field and laboratory observations show that uptake can also be suppressed when an organic film is present on aerosol (Bertram et al., 2009; Brown and Stutz, 2012). The parameterisation for N_2O_5 uptake in UM-UKCA is limited in that it does not account for the above effects. Future work could investigate the influence of chloride and organic suppression on the rate of heterogeneous N_2O_5 hydrolysis, and further explore the self-limiting impact of nitrate in aerosol on the rate of N_2O_5 uptake. Riemer et al. (2003) describe such a scheme, which accounts for the self-limiting nitrate effect, as does Davis et al. (2008). Morgan et al. (2015) define a parameterisation based on the ratio of particulate water to nitrate aerosol that yields good agreement with observations in north western Europe if enhancement by chloride is neglected.

It is beyond the scope of this study to assess the influence of N_2O_5 hydrolysis on gas-phase species in detail. However the changes in mass mixing ratio of N_2O_5, HNO_3, NO_2, NO, O_3 and HO_2 have been the subject of several studies and are included in supplementary Figure A4 for the interested reader. Widespread increases in NO_2, NO and N_2O_5 when heterogeneous N_2O_5 hydrolysis is deactivated reinforce that nitric acid formation via N_2O_5 hydrolysis provides an important sink for NO_x, which in turn influences O_3 and HO_2 formation as found in e.g. Evans and Jacob (2005), Pope et al. (2015), Riemer et al. (2003) and Stone et al. (2014). O'Connor et al. (2014) found NO_x concentrations in UM-UKCA to be

high relative to observations and other models, potentially due to the lack of heterogeneous N_2O_5 hydrolysis.

4.4 Summary and Conclusions

This study presents the first evaluation of nitrate, ammonium and sulphate aerosol concentrations in the UM-UKCA model simulated using the nitrate-extended version of the GLOMAP-mode aerosol microphysics scheme. The control run (HYB) treats inorganic aerosol partitioning using a hybrid approach, whereby smaller aerosol particles are assumed to be in equilibrium with the gas phase while larger particles are treated dynamically. Simulated nitrate, ammonium and sulphate aerosol concentrations from HYB have been evaluated for the year 2008, with comparison to surface observations from the EMEP (Europe), CASTNET (USA), IMPROVE (USA), AMoN (USA) and EANET (East Asia) monitoring networks, and against observations collected during six aircraft field campaigns. HYB-simulated global burdens, surface concentrations, zonal mean profiles and surface model skill are compared to the AeroCom Phase III (AP3) multi-model ensemble. Finally, the influence of the gas-particle partitioning assumption and heterogeneous N_2O_5 hydrolysis for size-resolved nitrate aerosol concentrations has been quantified via additional sensitivity simulations.

Comparisons to annual mean surface observations show that the spatial distribution of nitrate, ammonium and sulphate aerosol concentrations are reproduced well (R = 0.62 - 0.87) by UM-UKCA over Europe and North America. However, aerosol concentrations are biased low on average. Total nitrate (nitric acid plus nitrate aerosol) is simulated well in these regions. The spatial distributions of annual mean NO_3^-, NH_4^+ and SO_4^{2-} are captured less well over East Asia and concentrations are again biased low. However, observations in large regions of Asia, including China and India, are sparse and this analysis should be repeated as more observational data becomes available.

Seasonally, the UM-UKCA model captures the spatial distribution of NO_3^-, NH_4^+, SO_4^{2-}, tNO_3 and tNH_x over Europe consistently between DJF and JJA, though the model tends to underestimate wintertime concentrations of NO_3^-, NH_4^+, SO_4^{2-} and tNO_3 over Europe. In the USA, the model-observation spatial correlation for NO_3^- is greater in DJF while SO_4^{2-} and tNO_3 correlation against observations is highest

in JJA. Model underestimation of NO_3^- over the US is consistent between DJF and JJA, while model underestimation of tNO_3, SO_4^{2-} and NH_4^+ is greater in DJF than JJA. Over East Asia, the model correlates better with observed NO_3^-, NH_4^+, SO_4^{2-} and tNO_3 in DJF than JJA and with similar skill for NH_4^+ in both seasons. The model is more strongly negative biased for all species in DJF, and overestimates tNO_3 in JJA. It is beyond the scope of this analysis to evaluate the model representation of diurnal variability in nitrate aerosol concentration, though this would be an interesting avenue for future model evaluation.

Vertical variability in NO_3^- and NH_4^+ concentrations in the lower troposphere are reproduced well compared to the aircraft campaigns analysed. As seen in surface comparisons, the model tends to underestimate NO_3^- and NH_4^+ concentrations but more than 70% of modelled values sit within the standard deviation of observations in the lowermost 4 km for most campaigns, excluding VOCALS. Modelled SO_4^{2-} vertical profiles generally compare well to the aircraft observations below 4 km. Over 55% of modelled values sit within the standard deviation of observations for all campaigns except the Arctic-based ARCTAS-Spring campaign, where the model is biased low. However, above 4 km sulphate concentrations are overestimated by the model compared to the European, the South-East Pacific and Borneo-based campaigns.

Comparison to AeroCom Phase III indicates that the UM-UKCA-simulated nitrate aerosol burden of 0.145 Tg is below the mean but within the AP3 multi-model range of burdens. The UM-UKCA ammonium and sulphate aerosol burdens of 0.345 Tg and 2.28 Tg, respectively, are within 10% and ~ 25% of the AeroCom multi-model mean. The annual, global-mean surface NO_3^-, NH_4^+ and SO_4^{2-} UM-UKCA concentrations of 0.082 $\mu g\,kg^{-1}$, 0.139 $\mu g\,kg^{-1}$ and 0.463 $\mu g\,kg^{-1}$ respectively are below the AeroCom mean but within the range simulated by models. Spatially, annual mean UM-UKCA surface nitrate aerosol concentrations are within the AP3 IQR over most of Europe, East China, western USA and Antarctica. UM-UKCA surface SO_4^{2-} and NH_4^+ concentrations are within the AP3 IQR over most of China, India, western USA and eastern Europe, but are below the AP3 25^{th} percentile over western Europe, eastern USA and Polar regions. Overall, the ability of UM-UKCA model to reproduce the spatial distribution and magnitude

of ground-based NO_3^-, NH_4^+ and SO_4^{2-} observations is reasonable compared to model-observation comparisons with the 9 AeroCom Phase III models.

The underestimation of nitrate concentrations may arise because heterogeneous nitrate aerosol formation onto dust isn't represented, or from artificially high aerosol wet deposition and a lack of stratospheric nitric acid source in this model configuration (Walters et al., 2011; Turnock et al., 2015). Lower nitrate concentrations in UM-UKCA relative to other AeroCom models might also result from lower NO_x emissions in the UM-UKCA setup (see Section 3.5, Figure 3.4). UM-UKCA underestimation of surface SO_4^{2-} aerosol has been reported previously and partly explained by underestimations in oxidant availability (Berglen et al., 2007; Manktelow et al., 2007) or cloud pH (Turnock et al., 2015; Turnock, 2016). Overestimation of sulphate in the free troposphere may be related to the convective scavenging (Kipling et al., 2016; Kipling et al., 2013). NH_4^+ concentrations are closely related to those of SO_4^{2-} and NO_3^-, being limited by H_2SO_4 and HNO_3 availability and also subject to overestimated wet deposition. Overall, the UM-UKCA model, using the HyDiS-1.0 nitrate aerosol extension to GLOMAP-mode and MACCity anthropogenic emissions, is a suitable tool for use in further investigation of nitrate aerosol impacts in the lower troposphere, with consideration of the known limitations above.

Following this work, it is recommended that nitrate aerosol formation on dust aerosol be accounted for in future UM-UKCA simulations in order to evaluate its importance for simulated nitrate aerosol concentrations. Other models have also identified adding nitrate formation on dust as an avenue for future development (GISS-MATRIX; Mezuman et al., 2016). This might be achieved using an assumption of linear uptake on dust aerosol surface area or by developing the model to simulate dust ionic composition (e.g. K^+, Ca^+, Mg^+) and include reactions with these ions within nitrate-extended GLOMAP-mode (as already done for sea salt as Na^+ and Cl^-). At present such a parameterisation is not available in UM-UKCA and so other results in this thesis are also derived from simulations that exclude nitrate formation on dust.

Size-resolved nitrate aerosol concentrations simulated using the hybrid aerosol partitioning approach (HYB) have been compared to a sensitivity run, EQU, in which inorganic aerosol partitioning occurs assuming thermodynamic

equilibrium. The hybrid approach provides a more physically realistic representation of the aerosol partitioning because it considers differential rates of uptake of nitric acid across the aerosol size distribution, though most global atmospheric models apply an equilibrium approach (e.g. Bian et al., 2017). Overall, the annual mean global fine mode nitrate aerosol burden is underestimated by approximately 9.8% and the coarse mode overestimated by approximately 21.3% when the equilibrium approach is applied, compared to applying the hybrid approach. Similarly, the annual global mean surface concentration of fine mode nitrate is decreased by 15.2% in EQU compared to HYB. This change in size distribution arises as a result of an overall faster mass transfer from the gas phase to the coarse mode when the partitioning to larger aerosol is assumed to be in equilibrium, at the expense of nitric acid transfer to the fine mode. The results here corroborate the findings of Feng and Penner (2007) and Benduhn et al. (2016) in that reverting to an equilibrium scheme overestimates coarse mode nitrate concentrations compared to a hybrid approach. This change in the aerosol size distribution is expected to have implications for nitrate aerosol radiative effects, which will be investigated in Chapter 6.

The influence of heterogeneous N_2O_5 hydrolysis on nitrate aerosol formation has been quantified through comparison to a sensitivity run (HYB-NoHet) in which N_2O_5 uptake onto aerosol is set to zero. The exclusion of heterogeneous N_2O_5 hydrolysis decreases the annual global mean surface nitrate aerosol concentration by 42% and the annual mean global nitrate aerosol burden by 12.4%. Formation of nitric acid via heterogeneous N_2O_5 hydrolysis therefore represents a major formation pathway for nitrate aerosol. Heterogeneous N_2O_5 hydrolysis is most important for nitrate aerosol formation in the northern hemisphere mid- and high-latitudes, particularly in the winter months when longer nights enable greater nitric acid formation via the N_2O_5 hydrolysis pathway. Inclusion of the reaction is essential to partially correct wintertime underestimations in surface nitrate aerosol concentration over Europe, the USA and East Asia, therefore improving model representation of the nitrate seasonal cycle. It is recommended that future UM-UKCA simulations treating nitrate aerosol formation include representation of heterogeneous N_2O_5 hydrolysis,

given that it is not currently included as standard. Future work could develop the parameterisation for N_2O_5 uptake to investigate the self-limiting impacts of nitrate in aerosol on uptake, in addition to enhancement of uptake by chloride and the suppression of uptake in the presence of organic species. The implications for night-time NO_3^- aerosol formation could be investigated further, as could the influence on gaseous species such as NO_x and O_3.

5. Quantifying the changing impact of nitrate aerosol on air quality and human health

5.1 Introduction

Long-term exposure to ambient concentrations of particulate matter with an aerodynamic dry diameter of less than 2.5 μm ($PM_{2.5}$) is a major cause of regional and global premature mortality, contributing also to morbidity and lowered life expectancy (Dockery et al., 1994). Ambient (outdoor) air pollution is estimated to cause 4.2 million premature deaths worldwide (Cohen et al., 2017). Long-term exposure to $PM_{2.5}$ is associated with adverse health impacts including respiratory (lower respiratory infection, chronic obstructive pulmonary disorder, lung cancer), cardiovascular (ischemic heart disease) and cerebrovascular disease (stroke).

In the previous chapter, simulated size-resolved nitrate, ammonium and sulphate aerosol concentrations were evaluated from the UM-UKCA model, using the recently developed nitrate-extended version of GLOMAP-mode. In this chapter, the same model configuration will be used to estimate the impact of nitrate aerosol on air quality and human health in four regions – China, India, Europe and the USA – which have the highest surface nitrate concentrations globally (e.g. as seen in Chapter 4). The present day (year 2008) nitrate-associated premature mortality (the reduction in number of $PM_{2.5}$-attributable premature deaths when nitrate aerosol formation is omitted) is calculated, along with changes in the contribution of nitrate to mortality resulting from years 1980 to 2008 changes in aerosol and precursor gas emissions.

Observations have indicated that nitrate aerosol is a driving component of elevated particulate matter in high pollution episodes over Europe (Crosier et al., 2007; Yin and Harrison, 2008; Morgan et al., 2010a; Vieno et al., 2016) and also contributes to haze episodes over China (Pan et al., 2016; Yang et al., 2017). Furthermore, several studies have identified that sectors associated with nitrate aerosol precursor emissions, such as NH_3 from agriculture and food cultivation, make a major contribution to global and regional $PM_{2.5}$ concentrations (e.g. Bauer et al., 2016; Lelieveld et al., 2015). In this work, the specific contribution

of nitrate aerosol to present day ambient $PM_{2.5}$ and mortality will be assessed. The analysis will enable the identification of regions where emission reductions can most effectively reduce present day $PM_{2.5}$ and mortality through the removal of nitrate aerosol and any associated response in other aerosol species, e.g. ammonium aerosol.

Many regions have undergone substantial emission changes in the past few decades. The combined effects of air quality legislation, technological advances and economic influences have led to significant decreases in key pollutants (NO_x, SO_2, BC and OC) in Europe and North America in the past few decades (Vestreng et al., 2007; Lamarque et al., 2010; Granier et al., 2011; Hoesly et al., 2018). Meanwhile, economic growth and limited environmental regulation have led to widespread increases in emissions over China and India between 1980 and 2010 (the period of interest in this study), with decreases in emissions, including NO_x, from China subsequently emerging only since 2010 (e.g. Liu et al., 2016). NH_3 emissions, however, have remained relatively level or increased in all regions as a result of continued use largely in the agricultural industry. Li et al. (2017) found nitrate aerosol to be the second most dominant driving component, after organic aerosol, of increases in global population-weighted $PM_{2.5}$, through its influence over populous regions of South Asia, East Asia, Western Europe and North America. However, relatively few studies have investigated historical trends in long-term $PM_{2.5}$–attributable mortality (e.g. Wang et al., 2017; Butt et al., 2017; Cohen et al., 2017) and, of these, none have isolated the influence of nitrate aerosol on mortality changes.

In the first part of this chapter (Section 5.3.1), the spatial distribution of UM-UKCA-simulated $PM_{2.5}$ will first be compared to surface and satellite-derived $PM_{2.5}$ observations, with both observational datasets then used to regionally bias correct the simulated $PM_{2.5}$ for its application to premature mortality calculations. Secondly, the contribution of nitrate aerosol to simulated present day $PM_{2.5}$ fields over the European Union (EU28; current 28 member states), the USA, India and China will be quantified in Section 5.3.2. In Section 5.3.3, the influence of nitrate aerosol formation on present day premature mortality will then be assessed. Finally, the influence of post-1980 emission changes on the

contribution of nitrate aerosol to regional $PM_{2.5}$ and to premature mortality will be quantified (Section 5.3.4).

5.2 Model Setup and Methods

$PM_{2.5}$ is defined in this work as the mass concentration of particulate matter with an aerodynamic dry diameter below 2.5 μm. Figure 3.1 (Chapter 3) shows the regional domains used in this chapter. Sections 5.3.1 to 5.3.3 compare simulated $PM_{2.5}$ (and associated mortality) from two year 2008 UM-UKCA simulations with nitrate aerosol formation included and excluded. The term 'nitrate aerosol formation' in this thesis refers just to the gas-particle partitioning of nitric acid. Nitrate aerosol formation is excluded from simulations by deactivating the uptake of gas phase nitric acid to the aerosol particle phase. Section 5.3.4 compares simulated $PM_{2.5}$ concentrations from the two year 2008 UM-UKCA runs to two additional sensitivities with year 1980 emissions, population and background disease rates (again, with and without nitrate aerosol formation). As in Chapter 4, all simulations are nudged to year 2008 meteorological reanalyses and apply either year 2008 or year 1980 anthropogenic MACCity emissions of NO_x, SO_2, NH_3, OC and BC. The approach applied to calculate the mortality (number of premature deaths per year) associated with long-term exposure to $PM_{2.5}$ and nitrate aerosol is described in Chapter 3 (Section 3.3).

The evaluation in Sections 5.3.1.1 and 5.3.1.2 focusses on the spatial distribution of $PM_{2.5}$, with comparison to ground-based and satellite-derived $PM_{2.5}$ observations (described in Section 3.6.3). Ground based observations are included for the years 2008, 2008, 2016 and 2014 over Europe, the USA, India and China, respectively, while the satellite-derived $PM_{2.5}$ observations (van Donkelaar et al., 2016) are representative of the year 2008 in all regions. The satellite-derived climatology used in this study succeeds the dataset used for the 2013 Global Burden of Disease assessment and precedes that used for GBD 2015. Model underestimation of $PM_{2.5}$ was expected based on previous evaluations of the standard non-nitrate extended configuration of UM-UKCA (Turnock et al., 2015; Turnock et al., 2016; Butt et al., 2017) and the TOMCAT-GLOMAP chemistry transport model (Butt, 2018). Potential causes of model underestimation are described in Section 5.3.5.

To address the expected low model bias, four additional sensitivities are included in the mortality calculations presented representing the same two 2008 (Sections 5.3.4 and 5.3.5) and two 1980 emission cases (Section 5.3.4) but with regional bias corrections applied to the simulated raw model $PM_{2.5}$. The bias correction is calculated based on regional mean year 2008 surface-based observations over Europe and the USA and on year 2008 satellite AOD-derived $PM_{2.5}$ over India and China in the absence of adequate year 2008 surface-based observations. The resulting bias-corrected $PM_{2.5}$ fields are evaluated in Section 5.3.1.2.

5.3 Results

5.3.1 Evaluation of simulated surface $PM_{2.5}$

In the following section, UM-UKCA-simulated $PM_{2.5}$ fields are compared to ground-based $PM_{2.5}$ observations and satellite-derived $PM_{2.5.}$ The evaluation focuses on the spatial distribution of simulated $PM_{2.5}$ and changes in spatial model skill when nitrate aerosol formation is included in simulations. Surface-based and satellite-derived $PM_{2.5}$ observations are then used to bias-correct for an expected $PM_{2.5}$ low bias in the model (as described in Section 5.2).

5.3.1.1 Spatial variability in simulated $PM_{2.5}$

Figure 5.1 compares annual mean year 2008 UM-UKCA-simulated $PM_{2.5}$ concentrations (with and without nitrate formation) to ground-based observations over Europe, the USA, India and China. Ground-based observations over Europe and the USA are from the year 2008, in line with the model simulation year, whereas ground-based observations over India and China are from years 2016 and 2014, respectively, because observational coverage was poor in these latter regions over the year 2008.

Table 5.1 summarises the annual mean UM-UKCA skill for representing the spatial distribution of $PM_{2.5}$ when nitrate aerosol formation is included and excluded from simulations. Comparison to ground-based observations indicate that the spatial correlation of simulated annual mean $PM_{2.5}$ with ground-based observations is relatively low ($R = 0.35$) but is improved by the inclusion of nitrate aerosol (from $R = 0.23$ without nitrate). The inclusion of nitrate aerosol

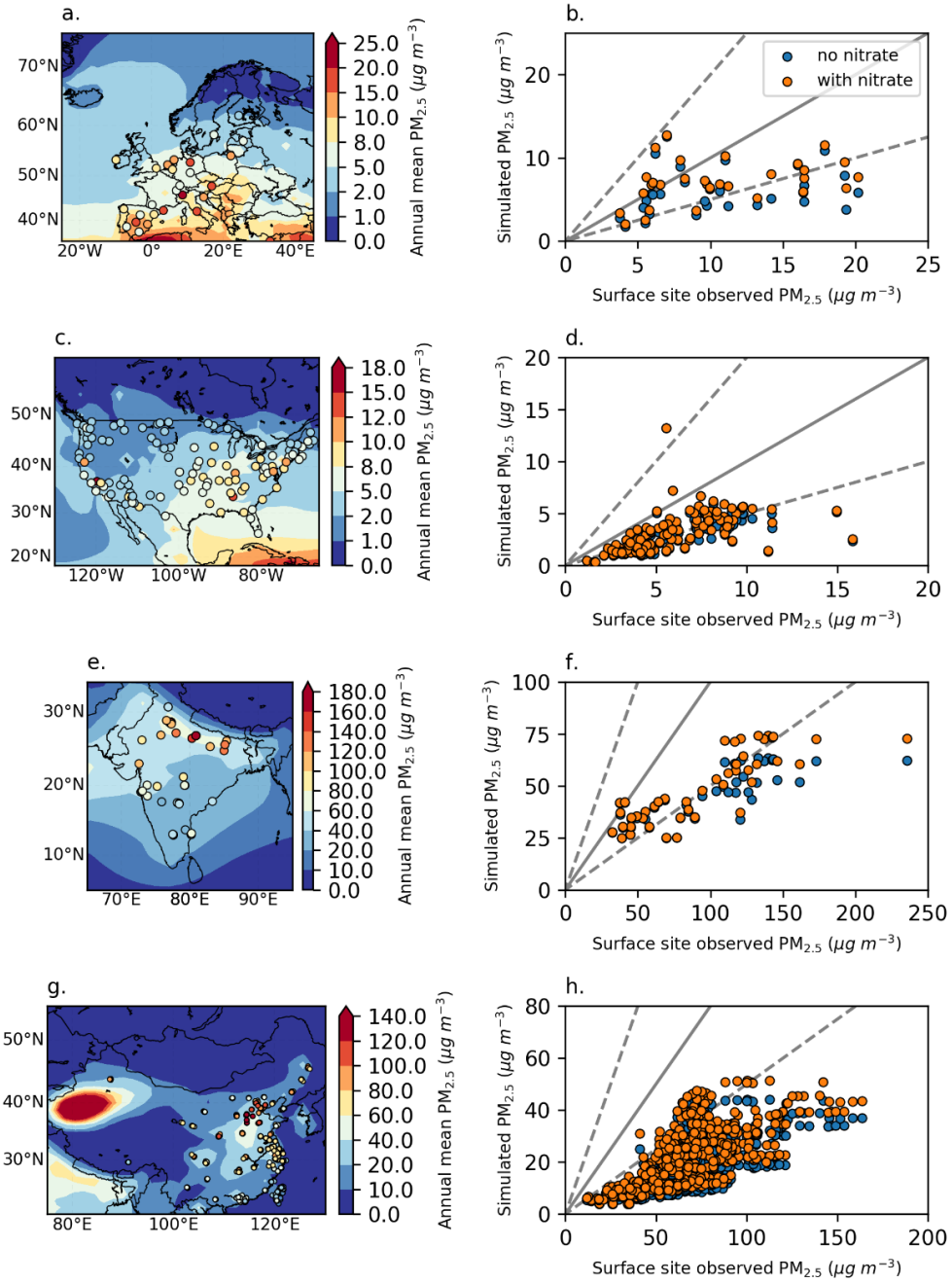

Figure 5.1 *(a+b) Simulated annual mean surface $PM_{2.5}$ concentrations, with nitrate aerosol formation included, with observations overplotted over a) Europe and b) the USA. (c+d) Scatter plot comparisons of observed and simulated $PM_{2.5}$ concentrations. Simulated $PM_{2.5}$ from sensitivity runs with (orange) and without (blue) nitrate aerosol formation included are shown. 1:1 (solid grey), 1:2 and 2:1 (dashed grey) lines are shown. European and USA observations are from the EMEP and IMPROVE networks, respectively. Simulated and observed concentrations are both from the year 2008.*

Table 5.1 *Pearson correlation coefficients between annual mean simulated $PM_{2.5}$ and $PM_{2.5}$ from ground-based and satellite-derived observations. Comparisons from simulations including and excluding nitrate aerosol formation are shown.*

Region	Observational method	Pearson correlation coefficient (R)	
		With NO_3^-	Without NO_3^-
Europe	Ground-based (2008)	0.35	0.23
	Satellite-derived (2008)	0.71	0.61
USA	Ground-based (2008)	0.59	0.56
	Satellite-derived (2008)	0.77	0.72
India	Ground-based (2016)	0.83	0.80
	Satellite-derived (2008)	0.82	0.76
China	Ground-based (2014)	0.71	0.68
	Satellite-derived (2008)	0.70	0.68

also improves the simulated spatial distribution of seasonal mean $PM_{2.5}$ for DJF and JJA (see Appendix Table B1), although $PM_{2.5}$ concentrations on annual mean timescales are considered for calculating long term health effects in this thesis. The linear correlation over Europe is greater between the model and annual mean satellite-derived $PM_{2.5}$ than found with ground-based observations as a result of variability between the two observational datasets. As found in the comparison to ground-based observations, the correlation to satellite-derived $PM_{2.5}$ is again reduced, from R = 0.71 to R = 0.61, when nitrate aerosol formation is removed from simulations.

Over the USA, the spatial distribution of annual mean $PM_{2.5}$ is better captured by the model than over Europe compared to both ground-based and satellite-derived observations, with Pearson correlation coefficients of 0.59 and 0.77, respectively. The removal of nitrate aerosol formation reduces the spatial correlation with annual mean ground-based observations to 0.56 and with satellite-derived $PM_{2.5}$ to 0.72, suggesting that nitrate aerosol improves model skill but is less important for modelled $PM_{2.5}$ over the USA than over Europe.

Over India, the spatial distribution of annual mean $PM_{2.5}$ is simulated very well compared to both ground-based (R = 0.83) and satellite-derived (R = 0.82) observations. The removal of nitrate aerosol results in a small reduction of the

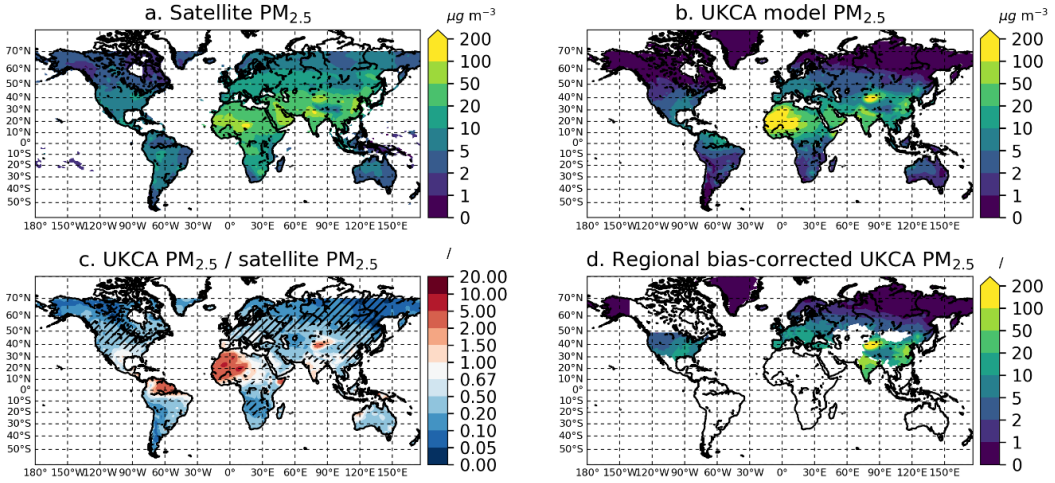

Figure 5.2 *Annual mean surface $PM_{2.5}$ concentrations from (a) satellite-derived estimates and (b) UM-UKCA simulation with nitrate formation included (NO_3 on), given in μg m^{-3}, (c) model bias calculated as UM-UKCA divided by satellite $PM_{2.5}$ concentrations. (d) Regional bias-corrected annual mean UM-UKCA surface $PM_{2.5}$ field. Hatching in (c) shows regions where the inclusion of nitrate partitioning both increases $PM_{2.5}$ by greater than 10% and reduces model bias.*

spatial correlation with annual mean observed concentrations, to 0.80 compared to ground-based and to 0.76 compared with satellite-derived concentrations. The spatial distribution of $PM_{2.5}$ is also simulated well (R > 0.70) over China on annual mean timescales compared to both observational datasets. The spatial correlation of simulated $PM_{2.5}$ with observations is slightly reduced, to 0.68 against both ground-based and satellite-derived observations, when nitrate aerosol formation is removed.

Figure 5.2 shows the global distribution of simulated $PM_{2.5}$ (Fig. 5.2a), satellite-derived surface level $PM_{2.5}$ (Fig 5.2b) and the ratio between the two (Fig. 5.2c). Overall, the model reproduces the global variability in surface $PM_{2.5}$ well (R = 0.65). The hatched regions in Figure 5.2c show where including nitrate aerosol formation has increased $PM_{2.5}$ concentrations by at least 10% and where this has increased the percentage of modelled $PM_{2.5}$ within a factor of 2 of satellite-derived $PM_{2.5}$ observations. The greatest improvements to simulated $PM_{2.5}$ as a result of accounting for nitrate aerosol can be seen over much of Europe and across Northern Europe into east China. The $PM_{2.5}$ underestimation is also reduced in northeast US into Canada and parts of Southern Africa when nitrate

formation is included. The improvement of model skill in populated regions reinforces the importance of including nitrate aerosol in simulations.

5.3.1.2 Evaluation of regional bias correction for $PM_{2.5}$

Section 5.3.1.1 showed that the spatial distribution of $PM_{2.5}$ is represented reasonably well and that the inclusion of nitrate aerosol formation in UM-UKCA acts to improve the spatial model skill compared to ground-based and satellite-derived observations of $PM_{2.5}$. Here, a regional bias correction is applied to the simulated $PM_{2.5}$ using year 2008 *ground-based* observations over Europe and the USA and using year 2008 *satellite-derived* $PM_{2.5}$ over India and China, as described in Section 3.3.1. This results in regional bias correction factors of 1.48 over Europe, 1.89 over the USA, 1.22 over India and 1.42 over China being applied.

Figure 5.2d shows the regional UM-UKCA simulated $PM_{2.5}$ fields after these bias corrections have been applied. In Sections 5.3.3 onwards, mortality estimates are primarily calculated from these regionally bias-corrected simulated $PM_{2.5}$ fields, though results calculated without the bias correction are also presented. The IER functions are non-linear, resulting in a greater sensitivity of the relative risk to changes in $PM_{2.5}$ exposure at lower $PM_{2.5}$ concentrations. Application of the bias correction to $PM_{2.5}$ fields therefore aims to avoid over-estimating the relative mortality response to the removal of nitrate aerosol.

Figure 5.3 compares the bias-corrected $PM_{2.5}$ with ground-based observations for each region of interest. Table 5.2 summarises the normalised mean bias scores calculated between annual mean modelled and observed (ground-based and satellite-derived) $PM_{2.5}$, when nitrate aerosol formation is both included and excluded from simulations, prior and subsequent to the bias correction being applied. Prior to the bias correction, model underestimation of $PM_{2.5}$ occurred in all four study regions compared to both the ground-based and satellite-derived observational datasets, though the magnitude of the model underestimation differed depending on whether the model was compared to ground-based observations or satellite-derived $PM_{2.5}$. Differences in the calculated model bias arose because of discrepancies between the satellite-derived $PM_{2.5}$ and ground-

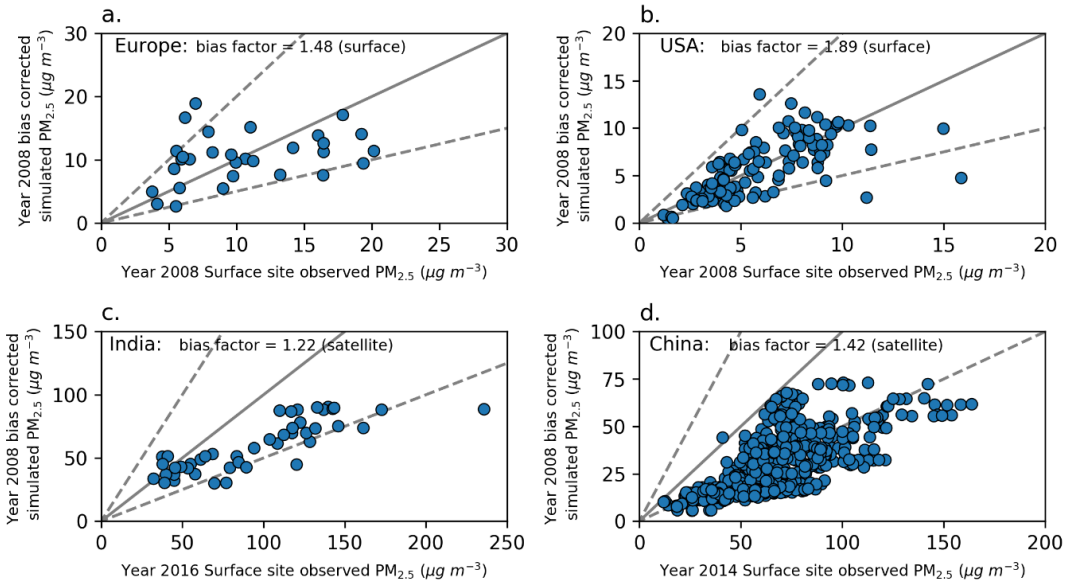

Figure 5.3 *Comparison of bias-corrected $PM_{2.5}$ against surface observed $PM_{2.5}$ over a) Europe, b) USA, c) India and d) China. The present day bias-corrected field with nitrate aerosol included is shown. Regional mean bias correction factors are shown for each region along with the observation technique used to calculate the regional bias (surface or satellite).*

based observations, in addition to differences in the observational year between datasets over India and China (Appendix Table B2).

Table 5.2 shows that application of the bias correction factors successfully correct the model biases (to NMB ≈ 0) with respect to ground-based observations over Europe and USA and with respect to satellite-derived $PM_{2.5}$ over India and China. Over Europe and the USA, the remaining underestimation in the bias-corrected model $PM_{2.5}$ calculated with respect to satellite-derived $PM_{2.5}$, of approximately 20%, results largely from differences between the ground-based observations (used for the bias correction) and satellite-derived observations (Table B2). The discrepancy therefore doesn't reflect a limitation in the bias correction approach itself. Ground-based observations were deemed more appropriate for deriving the bias correction factors over Europe and the USA than the satellite-derived $PM_{2.5}$, given that they provide direct same year observations of $PM_{2.5}$ in these regions. Given the discrepancy between satellite and ground-based observations described above, the application of satellite-derived bias correction factors (Europe: 1.86; USA: 2.31) would have overcorrected the bias in these regions relative to ground-based observations.

Table 5.2 *Statistical summary of normalised mean bias (NMB) values calculated between simulated $PM_{2.5}$ and $PM_{2.5}$ from ground-based and satellite-derived observations. NMB values are shown prior and subsequent to the regional bias correction being applied, alongside the regional bias correction factor. The observational dataset used to calculate the bias correction factors for each region are shown in bold.*

Region	Observational method	NMB (raw model)		Bias correction factor	NMB (after regional bias correction)
		With NO_3^-	Without NO_3^-		With NO_3^-
Europe[a]	**Ground-based (2008)**	-0.33	-0.44	**1.48**	**-0.01**
	Satellite-derived (2008)	-0.47	-0.56	-	-0.22
USA[a]	**Ground-based (2008)**	-0.47	-0.52	**1.89**	**0.00**
	Satellite-derived (2008)	-0.56	-0.60	-	-0.18
India[b]	Ground-based (2016)	-0.48	-0.53	-	-0.37
	Satellite-derived (2008)	-0.18	-0.23	**1.22**	**0.00**
China[b]	Ground-based (2014)	-0.68	-0.72	-	-0.54
	Satellite-derived (2008)	-0.29	-0.33	**1.42**	**0.01**

a. Regional mean bias correction factor based on ground-based observations is applied.
b. Regional mean bias correction factor based on satellite-derived observations is applied.

Low model bias remains over India and China with respect to ground-based $PM_{2.5}$ observations after the regional bias correction (based on satellite-derived $PM_{2.5}$) has been applied. Separate analysis (Table B2) shows that the satellite-derived $PM_{2.5}$ datasets underestimate ground-based $PM_{2.5}$ observations by approximately 27% and 21% over India and China, respectively, as a result of both discrepancies between the satellite and ground based observations and from differences in observational year. After considering these factors, the remaining underestimation between the regional bias-corrected UM-UKCA $PM_{2.5}$ and the ground based observations over India and China is indicative of limitations in the regional bias-correction method. Alternative bias correction factors of 1.75 and 3.12 would have been applied over India and China respectively if calculated with respect to the available ground-based observational datasets. However, the bias correction method based on satellite-derived observations over India and China is still considered acceptable for this

Table 5.3 *Table 5.3 Mass concentration (μg m^{-3}) and fractional contribution (in parentheses) of each $PM_{2.5}$ component, calculated from UM-UKCA for the present day emissions scenario. Total and speciated $PM_{2.5}$ are shown as calculated using the speciation method, in addition to the nitrate aerosol contribution to $PM_{2.5}$ calculated using the subtraction method.*

Component	EU28	USA	India	China
	Speciation method			
Nitrate	0.80 (13.4%)	0.19 (7.3%)	1.81 (4.9%)	1.05 (4.8%)
Ammonium	0.50 (8.3%)	0.20 (7.7%)	1.27 (3.5%)	0.76 (3.5%)
Sulphate	0.85 (14.2%)	0.53 (20.3%)	2.38 (6.5%)	1.73 (8.0%)
Sea salt	0.34 (5.6%)	0.11 (4.3%)	0.22 (0.6%)	0.04 (0.2%)
Black carbon	0.27 (4.5%)	0.09 (3.2%)	1.37 (3.7%)	1.05 (4.8%)
Organic carbon	0.85 (14.2%)	0.26 (9.9%)	8.49 (23.0%)	3.72 (17.2%)
Dust	2.37 (39.8%)	1.24 (47.2%)	21.3 (57.9%)	13.3 (61.4%)
Total $PM_{2.5}$	5.95	2.62	36.9	21.6
	Subtraction method			
Nitrate	0.97 (16.3%)	0.22 (8.5%)	2.21 (6.0%)	1.26 (5.8%)

work given the scarcity of same year 2008 ground-based observations in these regions. This approach also improves consistency in these regions with the methodology of the Global Burden of Disease assessments which use satellite-derived $PM_{2.5}$ to inform calculations of $PM_{2.5}$-attributable mortality.

By its design, the regional bias correction does not affect the simulated $PM_{2.5}$ composition. The Chapter 4 comparison of simulated annual mean NO_3^-, NH_4^+ and SO_4^{2-} concentrations to ground-based observations is repeated and finds that the bias correction reduces underestimations in nitrate, ammonium and sulphate aerosol relative to observations in Europe and the USA. Compared to the evaluation of non-bias corrected concentrations in Table 4.2, the normalised mean bias against annual mean EMEP measurements is reduced in magnitude to

-0.03, -0.02 and -0.39 for nitrate, ammonium and sulphate, respectively. The normalised mean bias compared to CASTNET observations is reduced to -0.25, -0.23 and -0.23 for the same species, respectively. Compared to IMPROVE, the normalised mean bias for nitrate and sulphate are reduced to -0.47 and -0.38, respectively. Bias-corrected secondary inorganic aerosol concentrations weren't compared over China and India, where speciated aerosol observations for the year 2008 aren't available.

5.3.2 Nitrate contribution to present day $PM_{2.5}$ concentrations

Having compared the simulated $PM_{2.5}$ fields against surface observations and satellite-derived $PM_{2.5}$ concentrations, the fractional contribution of nitrate aerosol to present day (year 2008) surface $PM_{2.5}$ will be assessed using both a 'speciation' and 'subtraction' approach (described in Section 3.3.1).

5.3.2.1 Speciation method

Table 5.3 shows the annual regional area weighted mean (AWM) $PM_{2.5}$ (from raw model concentrations i.e. without bias adjustment) and fractional contributions from each $PM_{2.5}$ component in the present day year 2008 simulation, as calculated using the speciation approach. Over the EU28, nitrate contributes 13.4% of the AWM $PM_{2.5}$ and is the fourth most dominant aerosol after dust (39.8%) and just after organic carbon and sulphate (each 14.2%). Ammonium contributes 8.3% of $PM_{2.5}$ on average, followed by sea salt (5.6%) and black carbon (4.5%). Nitrate is less dominant over the USA, contributing 7.3% of the AWM $PM_{2.5}$ on average. It is the 5th most dominant AWM $PM_{2.5}$ component in this region after dust (47.2%), sulphate (20.3%), organic carbon (9.9%) and ammonium (7.7%).

Over India, the average regional nitrate fraction of AWM $PM_{2.5}$ is 4.9%, though, of the four regions, its absolute mean concentration is highest in this region at 1.81 μg m^{-3}. Dust is, again, the most dominant $PM_{2.5}$ component (57.9%), followed by organic carbon (23%), sulphate (6.5%), nitrate (4.9%), ammonium

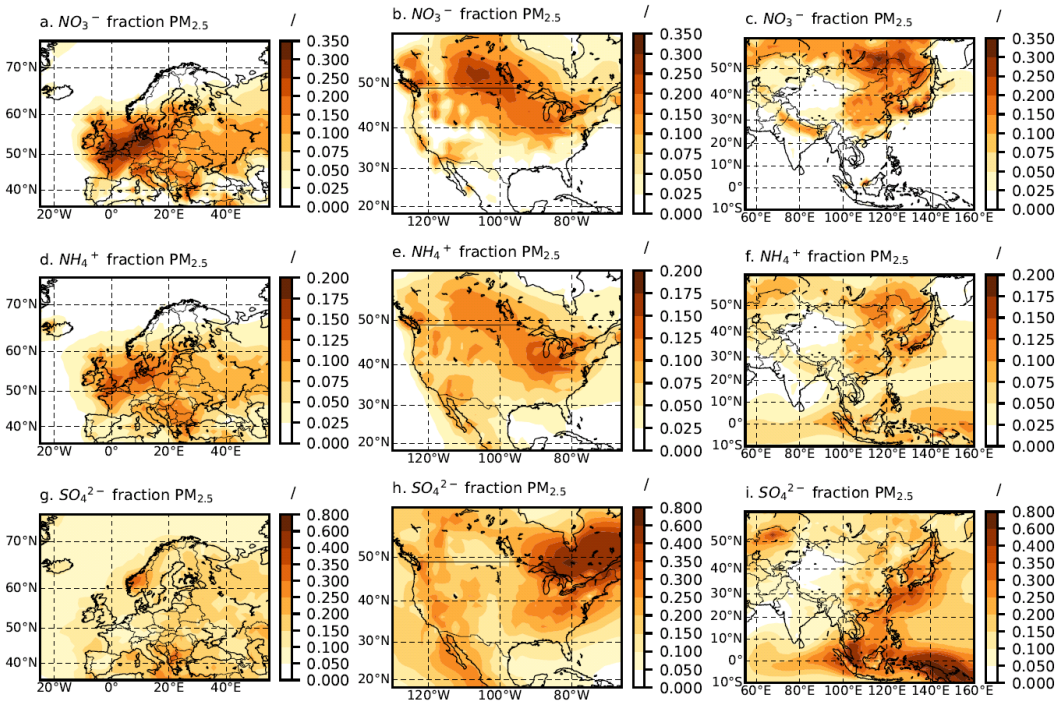

Figure 5.4 *Fractional contribution of nitrate (top row), ammonium (middle row) and sulphate (bottom row) aerosol to annual mean surface $PM_{2.5}$ concentrations over Europe (left column), the USA (middle column) and East and South Asia (right column), calculated via the speciation method. Note that different scales are used for each species.*

(3.5%), black carbon (3.7%) and sea salt (0.6%). Nitrate represents 4.8% of $PM_{2.5}$ on average over China. It is the 5th most dominant $PM_{2.5}$ component after dust (61.4%), organic carbon (17.2%) and sulphate (8%). The contribution of nitrate to the regional AWM $PM_{2.5}$ is near equivalent to that of black carbon (also 4.8%) and greater than that of ammonium (3.5%) and sea salt (0.2%).

Figure 5.4 shows the fractional contribution of nitrate, ammonium and sulphate aerosol to simulated annual mean surface $PM_{2.5}$ concentrations over Europe, the USA and Asia, as calculated using the speciation approach described above. Of the three regions, the greatest local contribution to $PM_{2.5}$ from nitrate, of up to 35%, occurs over regions of Western Europe. Nitrate contributes at least 5% of the total $PM_{2.5}$ over most of Europe, with the exception of Northern Scandinavia, Portugal and regions of Spain. Over Europe, the nitrate fraction is highest in the northwest, where it contributes between 15 and 35% of simulated $PM_{2.5}$. The nitrate fraction exceeds 15% over France, the Netherlands, Belgium, Germany and the UK and peaks at up to 35% over Northern Germany. There is also a

substantial contribution from nitrate (> 15%) over Northern Italy. In these regions where nitrate exceeds 15%, its contribution exceeds those of ammonium and sulphate, which each represent between 5 and 15% of $PM_{2.5}$.

The European ammonium fraction peaks between 12.5 and 15% over the UK, Northern Germany and Denmark. The fractional ammonium contribution to $PM_{2.5}$ maps closely to that of nitrate, also exceeding 5% over most of Europe with the exception again of northern Scandinavia, Portugal and Spain. The sulphate fraction of $PM_{2.5}$ peaks at up to 35% over Norway. Its contribution to $PM_{2.5}$ exceeds 5% over all of Europe and exceeds 15% over several regions, most notably Scandinavia, Eastern Europe and Southern Italy.

The nitrate fraction of $PM_{2.5}$ is generally lower over the USA than over Europe. Nitrate contributes over 5% of $PM_{2.5}$ for much of northern USA and the west coast but only over Arizona and New Mexico in the South. Nitrate is most important for simulated $PM_{2.5}$ (up to 25%) around the Great Lakes and into the northern Great Plains. However, the nitrate contribution to $PM_{2.5}$ is higher over Canada, at up to 30%.

Nitrate generally exceeds ammonium concentrations in the Northern USA, where ammonium contributes up to 15% of the $PM_{2.5}$. However, ammonium aerosol is more widespread and its $PM_{2.5}$ fraction exceeds 5% over almost all of the USA, excluding some regions that border the Gulf of Mexico. Overall, sulphate is the most dominant of the three secondary inorganic species, contributing over 5% of $PM_{2.5}$ everywhere in the USA and dominating particularly strongly in the northeast with fractional contributions up to 40%. Its importance in eastern Canada is higher still at up to 80%.

The nitrate fraction exceeds 5% over most of eastern China and peaks at up to 20% of $PM_{2.5}$. Ammonium contributes between 5 and 15% of $PM_{2.5}$ over the same regions, with the highest contribution in northeast China as for nitrate. Sulphate is also most important for simulated $PM_{2.5}$ over east China, although the regions where sulphate contributes at least 5% of the $PM_{2.5}$ extends farther to the west than for nitrate and ammonium. As in the USA, sulphate is the most dominant of the three SIA components, contributing at least 15% over large regions of southeast and northeast China.

In terms of their relative contribution to $PM_{2.5}$, neither SIA is particularly important over India. Nitrate aerosol contributes 5 – 10% in a northern geographical band extending from Punjab and northern Rajasthan to Bihar and West Bengal. Ammonium contributes 5 – 10% to $PM_{2.5}$ over and east of Uttar Pradesh in the same geographical band. Sulphate has a more widespread influence, contributing at least 5% over much of India, except for the north-western coast, and up to 15% in some north eastern regions.

5.3.2.2 Subtraction method

Table 5.3 also shows the nitrate aerosol contribution to AWM $PM_{2.5}$ calculated using the subtraction method. By this method, the regional AWM nitrate fractions of $PM_{2.5}$ calculated are 16.3%, 8.5%, 6.0% and 5.8% in the EU28, USA, India and China, respectively.

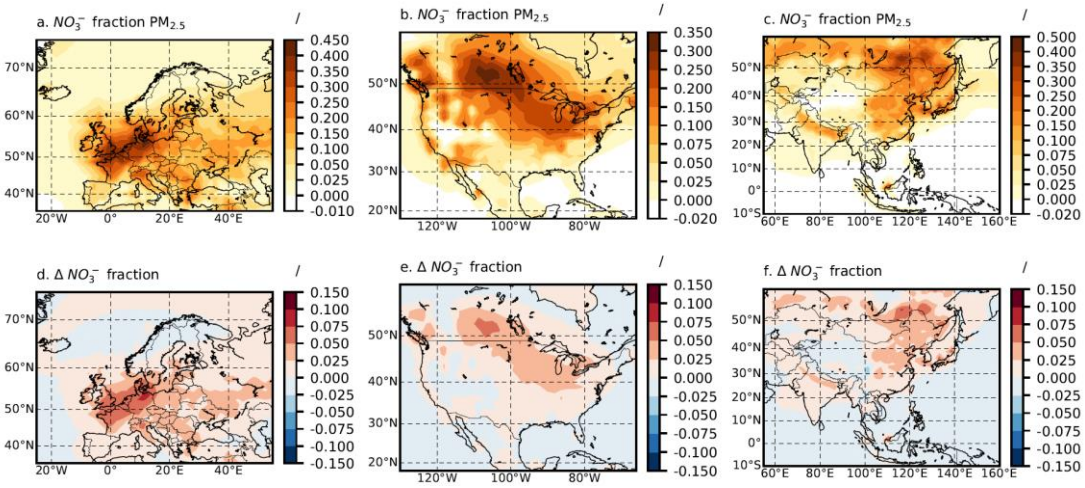

Figure 5.5 *(a-c, top row) Nitrate aerosol fractions calculated via the subtraction method. (d-f, bottom row) Absolute difference in nitrate fraction calculated using the subtraction method, compared to the speciation method (subtraction minus speciation).*

Figure 5.5 shows the fraction of annual mean $PM_{2.5}$ associated with nitrate aerosol formation, as calculated using the subtraction method, and the absolute difference in nitrate-associated $PM_{2.5}$ fractions calculated using the subtraction and speciation methods. The spatial distribution of the nitrate-associated $PM_{2.5}$ fraction calculated using the subtraction method is visually similar to that calculated using the speciation method (shown in Figure 5.4). The magnitude of

the calculated nitrate contribution to $PM_{2.5}$ differs between the two methods, however.

The nitrate-associated fraction of $PM_{2.5}$ is greater over much of Europe when calculated using the subtraction method, with the exception of northern Europe. The nitrate-associated fraction represents at least 10% of the total $PM_{2.5}$ over most of western, central and eastern Europe, with an absolute change in $PM_{2.5}$ fraction of +2.5 to 5% compared to those calculated using the speciation method. The subtraction-derived nitrate fraction of $PM_{2.5}$ is greatest over northern Germany and peaks at up to 45%, compared to up to 35% when calculated using the fraction approach. These higher $PM_{2.5}$ fractions are indicative of increased ammonium formation that occurs when nitrate aerosol formation is included in simulations.

Over northern Europe, the nitrate-associated $PM_{2.5}$ fraction is slightly lower (Δ –2.5%) than that calculated using the fraction approach. This arises where the partitioning of nitric acid into the aerosol results in reductions in $PM_{2.5}$ through its influence on microphysical processes, such as aerosol growth and removal. A feature of the subtraction approach for calculating the nitrate-associated $PM_{2.5}$ fraction is that a negative fraction is defined where this increased aerosol removal exceeds the increase from additional nitrate and associated aerosol mass. This can be seen, for example, in Figure 5.5b over the western USA and Figure 5.5c over western China. These are regions identified in Chapter 4 as having low nitrate aerosol concentrations. The decreases are small in magnitude but show, counter-intuitively, that nitrate aerosol formation could have a slight health benefit in these regions.

Over the USA, the nitrate-associated fraction peaks at up to 30% (and up to 35% over Canada), compared to up to 25% in the north of the country calculated using the fraction method. The nitrate fraction is higher by 2.5 to 5% over much of the Midwest and northern prairies using the subtraction approach but remains within ±2.5% of the fraction method-calculated $PM_{2.5}$ fraction over most of the country.

Over India, the nitrate-associated fraction of $PM_{2.5}$ is highest in the north and peaks at just over 25%. The subtraction-calculated nitrate fraction is 2.5 – 5%

higher in the north of the country, but is otherwise within 2.5% of the fraction calculated using the speciation approach. Similarly, over China the nitrate fraction of $PM_{2.5}$ is greatest in the north and east of the country and is up to 5% higher when using the subtraction approach over most of this region.

5.3.3 Present day health impacts of nitrate aerosol formation

The number of premature deaths associated with exposure to $PM_{2.5}$ and nitrate aerosol is calculated using integrated exposure-response functions. The mortality calculations are primarily presented as calculated from regionally bias corrected $PM_{2.5}$ (validated in Section 5.3.1.2). The influence of nitrate on mortality is estimated using a subtraction, or zero out, approach, similar in

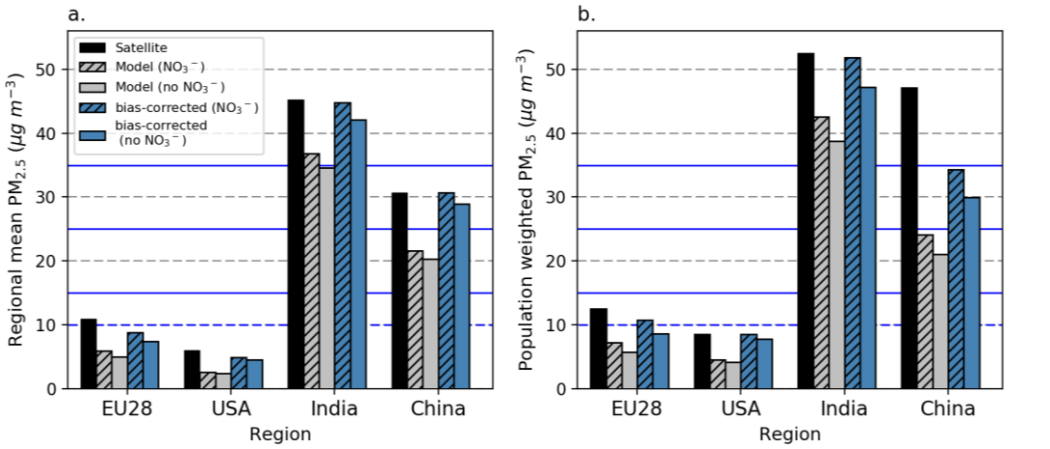

Figure 5.6 Annual mean *(a) regional area-weighted and (b) population-weighted mean surface $PM_{2.5}$ concentrations from satellite (black), raw UM-UKCA model fields (grey) and bias-corrected UM-UKCA model fields (blue). Hatched bars indicate $PM_{2.5}$ concentrations when nitrate aerosol formation has been included in simulations, with unhatched bars indicating $PM_{2.5}$ concentrations excluding nitrate aerosol.*

theory to that applied in Section 5.3.2.2. The subtraction approach gives the change in $PM_{2.5}$-attributable mortality when nitrate aerosol formation is removed from the ambient $PM_{2.5}$. Figure 5.6a shows regional AWM $PM_{2.5}$ concentrations from the raw model and bias-corrected simulations, alongside $PM_{2.5}$ fields from simulations with nitrate aerosol formation excluded.

The calculated change in long-term mortality when nitrate aerosol formation is switched off is described as the 'nitrate-associated mortality' in this thesis. The mortality calculated from the total ambient $PM_{2.5}$ (including nitrate aerosol

formation) is given as the '$PM_{2.5}$-attributable mortality' and is provided to indicate the relative importance of nitrate-associated mortality.

5.3.3.1. Population weighted mean $PM_{2.5}$

Weighting the $PM_{2.5}$ average by population density gives the average annual mean human exposure to $PM_{2.5}$. Figure 5.6b shows annual mean population-weighted $PM_{2.5}$ concentrations calculated from the satellite product, raw model and bias-corrected $PM_{2.5}$ fields (for simulations with and without nitrate aerosol formation). For all regions here, the annual year 2008 population-weighted mean $PM_{2.5}$ concentrations are higher than the regional 'area-weighted' means because the spatial distribution of population and $PM_{2.5}$ concentrations are correlated.

The population weighted mean satellite-derived $PM_{2.5}$ values are 12.5 μg m^{-3}, 8.6 μg m^{-3}, 52.5 μg m^{-3} and 47.1 μg m^{-3} over the EU28, USA, India and China, respectively. The population weighted mean $PM_{2.5}$ calculated from the bias corrected $PM_{2.5}$ are 10.7 μg m^{-3}, 8.6 μg m^{-3} , 51.8 μg m^{-3} and 34.3 μg m^{-3} over the same regions, respectively. These are within 2% of those calculated from the satellite data over the USA and India, respectively. Over the European Union and China, the population weighted $PM_{2.5}$ concentrations are approximately 15% and 27% lower than the satellite-derived population-weighted mean $PM_{2.5}$. Resulting mortality calculations may therefore underestimate the number of premature deaths resulting from ambient $PM_{2.5}$ exposure in these regions.

The removal of nitrate aerosol formation leads to decreases in regional population-weighted mean $PM_{2.5}$ of 2.1, 0.8, 4.6 and 4.3 μg m^{-3} in the EU28, USA, India and China, respectively, when calculated from the regional bias-corrected $PM_{2.5}$ fields. The nitrate-associated fraction of population-weighted mean $PM_{2.5}$ is calculated at 20%, 8.9%, 8.9% and 12.7%, respectively, over the same regions. The nitrate-associated population-weighted mean $PM_{2.5}$ is lower when calculated from the unscaled model fields, at 1.4, 0.4, 3.9 and 3.0 μg m^{-3} for the EU28, USA, India and China, respectively. The relative contribution of nitrate to the total population-weighted mean $PM_{2.5}$ remains the same over all regions when the bias-correction is removed.

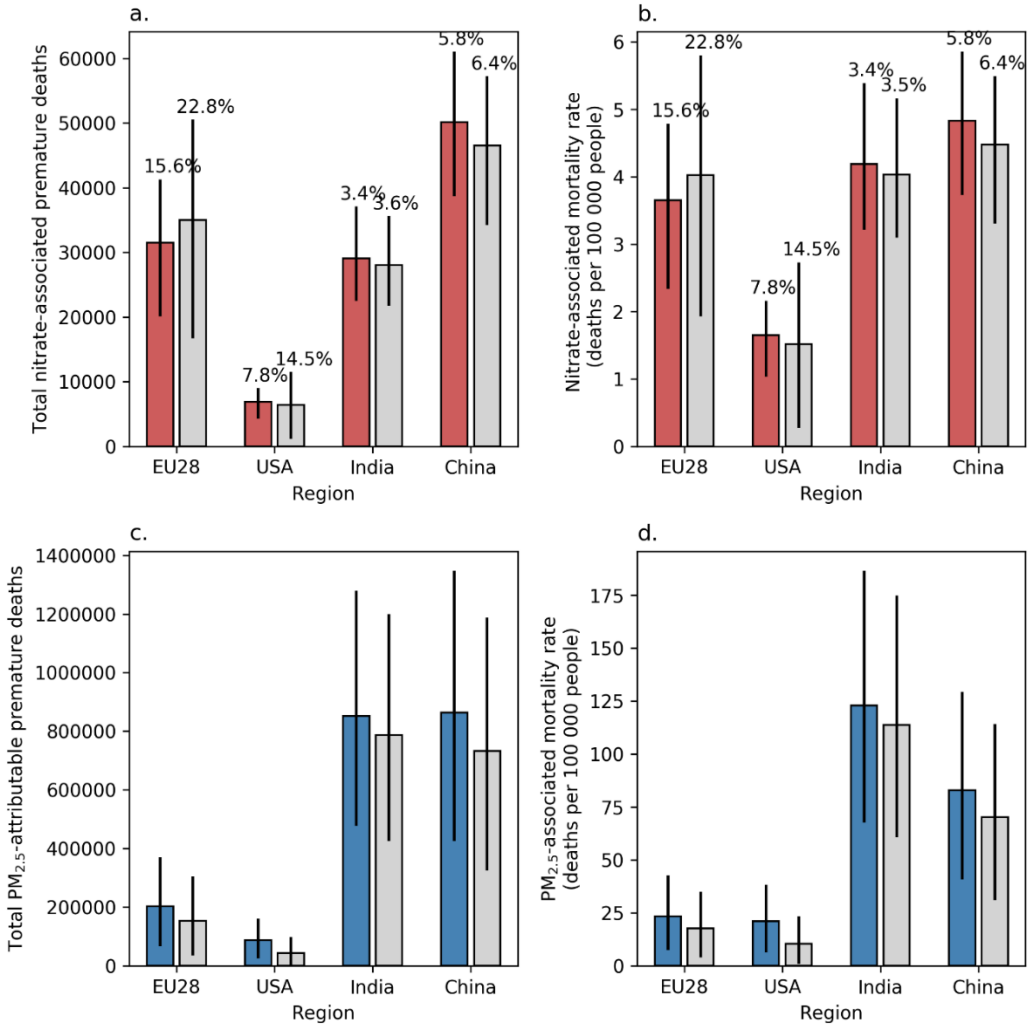

Figure 5.7 *(Left column) Total number of deaths (a) associated with nitrate aerosol formation and (c) attributable to ambient $PM_{2.5}$, as calculated from regional bias-corrected $PM_{2.5}$ fields (coloured bars) and model $PM_{2.5}$ fields with no bias correction (grey bars). (Right column) Age standardised mortality rate, or number of deaths per 100,000 people (c) associated with nitrate aerosol formation and (d) attributable to ambient $PM_{2.5}$. Error bars denote the 5^{th} to 95^{th} percentile uncertainty range. The relative magnitude of reductions in mortality and mortality rates associated with nitrate, compared to total $PM_{2.5}$-attributable mortality and mortality rates, are given as percentages in (a) and (b).*

The population scaling factor (PSF) can be defined as the ratio of population weighted mean $PM_{2.5}$ to the regional mean $PM_{2.5}$ (Wang et al., 2017). The PSF gives an indication of the correlation between population and simulated $PM_{2.5}$. The $PM_{2.5}$ PSF is 1.22, 1.73, 1.16 and 1.11 for the EU28, USA, India and China, respectively. The nitrate-associated $PM_{2.5}$ yields a PSF of 1.50, 1.82, 1.70 and 2.42 indicating a stronger correlation between population exposure and nitrate-

associated $PM_{2.5}$ than between population and the ambient $PM_{2.5}$. This is indicative of nitrate aerosol being associated with anthropogenic precursor sources and therefore present in populated regions where it can impact on human health.

5.3.3.2 Nitrate-associated mortality

Figure 5.7 shows regional premature mortality estimates for the EU28, USA, India and China associated with long-term exposure to nitrate aerosol, as calculated using the subtraction method, and ambient total $PM_{2.5}$. Table 5.4 shows values for the nitrate-associated and $PM_{2.5}$-attributable premature mortalities per region. The results here are calculated from the regional bias corrected $PM_{2.5}$ concentrations unless otherwise stated. In the European Union, long-term ambient $PM_{2.5}$ exposure results in ~ 203,000 (65,800 – 371,000) premature mortalities per year. The removal of nitrate aerosol formation results in a decrease in mortality of 31,500 (20,100 – 41,300) deaths per year. The number of nitrate-associated premature deaths over the EU28 therefore equates to 15.6% of the total $PM_{2.5}$–attributable mortality. In other words, removing nitrate aerosol would result in a 15.6% reduction in $PM_{2.5}$-attributable mortality. The EU28 age-standardised mortality rate attributed to ambient $PM_{2.5}$ exposure is 23.4 (7.62 – 42.7) mortalities per 100,000 persons. The age-standardised mortality rate is reduced by 3.65 (2.33 – 4.79) deaths per 100,000 persons when nitrate aerosol is removed, equivalent to 15.6% of the ambient $PM_{2.5}$ – attributable mortality rate over the European Union.

Figure 5.8 (a and b) shows the mortality and age standardised mortality rates per year that are associated with nitrate aerosol for individual countries in the European Union. It can be seen that the greatest number of nitrate-associated deaths per year occur in Germany (7,269 deaths), followed by the United Kingdom (7,161 deaths), France (2,782 deaths), Poland (2,271 deaths) and Italy (2,183 deaths). However, the number of nitrate-associated premature deaths per 100,000 people (age-standardised mortality rate) is greatest in Denmark (7.69), followed by Latvia (6.96), the UK (6.74), Belgium (6.19) and the Netherlands (5.85). The lowest nitrate-associated mortality (< 1 death) and

Table 5.4 *Reduction in regional premature mortality and age-standardised mortality rate per year when removing nitrate aerosol formation, compared with $PM_{2.5}$-attributable premature mortality and age-standardised mortality rates calculated from this study and the year 2010 GBD estimates from GBD 2015. Results are shown for regional bias-corrected and for unscaled model $PM_{2.5}$ fields. The $PM_{2.5}$-attributable mortality calculated from satellite fields is also shown.*

		Number of premature deaths ($x10^3$)			
		Nitrate-associated (this study)	$PM_{2.5}$-attributable (this study)	$PM_{2.5}$-attributable (Satellite, this study)	Year 2010 $PM_{2.5}$-attributable (GBD)
EU28	Bias-corrected	31.5 (20.1 – 41.3)	203 (65.8 - 371)		
	Unscaled	34.9 (16.7 - 50.6)	154 (35.2 -306)	227 (83.6 – 399)	225 (186 – 267)
USA	Bias-corrected	6.90 (4.3 - 9.0)	88.2 (26.2– 161)		
	Unscaled	6.40 (1.1 – 11.5)	44.0 (3.7 - 97.8)	92.2 (29.2 - 165)	80 (63.3 – 98.5)
India	Bias-corrected	29.0 (22.5 - 37.1)	851 (476 – 1,280)		
	Unscaled	28.0 (21.8 - 35.6)	787 (426 - 1,200)	847 (472 - 1,270)	888 (767 – 1,010)
China	Bias-corrected	50.2 (38.7 – 61.0)	865 (425 – 1,350)		
	Unscaled	46.5 (34.3 - 57.2)	733 (325 – 1,190)	1,010 (539 - 1,520)	1,070 (931 – 1,220)
		Age-standardised mortality rate (number of premature deaths per 100,000 people)			
		Nitrate-associated	$PM_{2.5}$-attributable	$PM_{2.5}$-attributable (Satellite, this study)	Year 2010 $PM_{2.5}$-attributable (GBD)
EU28	Bias-corrected	3.65 (2.33 - 4.79)	23.4 (7.62 - 42.7)		
	Unscaled	4.02 (1.93 - 5.80)	17.7 (4.07 - 35.1)	26.18 (9.70 - 46.0)	25.3 (21.2 – 29.8)
USA	Bias-corrected	1.65 (1.03 - 2.16)	21.1 (6.30 - 38.4)		
	Unscaled	1.52 (0.23 - 2.73)	10.5 (0.90 - 23.3)	22.06 (7.02 - 39.37)	18.6 (14.7 – 22.9)
India	Bias-corrected	4.19 (3.21 - 5.39)	123 (67.8 - 187)		
	Unscaled	4.04 (3.09 - 5.17)	114 (60.6 - 175)	122 (67.2 - 186)	123 (104 – 142)
China	Bias-corrected	4.83 (3.73 - 5.86)	83.0 (40.9 - 129)		
	Unscaled	4.48 (3.31 - 5.49)	70.3 (31.2 - 114)	96.7 (51.8 - 146)	97.2 (83.9 – 112)

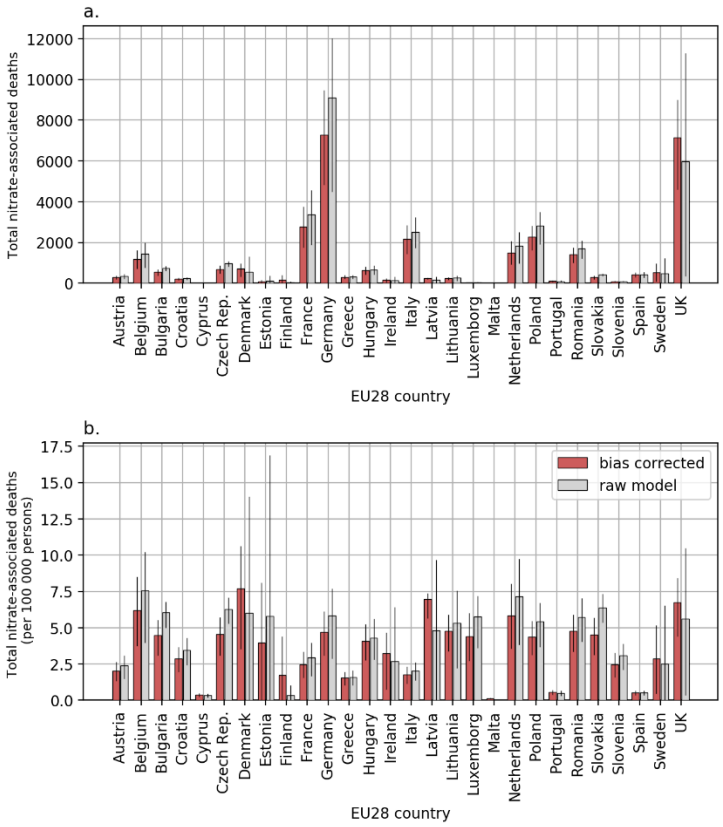

Figure 5.8 *(a) Total number of nitrate-associated deaths and (b) age-standardised mortality rate (number of nitrate-associated deaths per 100,000 people) per individual EU28 country. Values are shown as calculated from regional bias-corrected $PM_{2.5}$ fields (red) and model $PM_{2.5}$ fields with no bias correction (grey). Error bars show the 5th to 95th percentile uncertainty range.*

age-standardised mortality rate (0.13 deaths per 100,000 people) per year in the EU28 occurs in Malta.

Table 5.4 and Figure 5.7 also show the estimates for mortality from the raw model (unscaled) $PM_{2.5}$ fields. The total premature mortality attributed to long term ambient $PM_{2.5}$ exposure over Europe is 24% lower when calculated using the unscaled $PM_{2.5}$ fields, at around 154,000 (35,200 – 306,000) deaths per year. However, the removal of nitrate aerosol results in a slightly greater decrease in premature mortality, of ~ 34,900 (16,700 – 50,600), when calculated from raw model concentrations. The relative contribution of nitrate to total $PM_{2.5}$-attributable mortality is therefore higher when calculated from the raw model

concentrations, at 22.8%. The bias-correction of $PM_{2.5}$ fields is also important for mortality estimates at the national level within Europe (Figure 5.8).

Over the USA, the ambient $PM_{2.5}$–attributable mortality is ~ 88,200 (26,200 – 161,000), with an age-standardised mortality rate of 21.1 (6.30-38.4) deaths per 100,000 persons. Removing nitrate aerosol results in a decrease of ~ 6,900 (4,300 – 9,000) premature deaths and reduction in age-standardised mortality rate of 1.65 (1.03 – 2.16). Nitrate aerosol exposure therefore makes a more moderate relative contribution of ~ 7.8% to the total number of $PM_{2.5}$–attributable mortalities and to the age-standardised $PM_{2.5}$–attributable mortality rate in the USA than is calculated for the EU28.

As seen over Europe, ambient $PM_{2.5}$–attributable mortality over the USA is lower, by approximately 50%, when calculated from the raw model $PM_{2.5}$ fields. However, the number of premature mortalities associated with nitrate aerosol exposure in the USA is only ~ 7% lower in the raw model case compared to the bias-corrected case. Nitrate aerosol contributes to ~ 6,400 (1,100 – 11,500) premature deaths per year when calculated from the raw model $PM_{2.5}$ fields although the uncertainty range estimated from the non-bias-corrected $PM_{2.5}$ is larger and the relative contribution of nitrate aerosol to total $PM_{2.5}$-attributable mortality is greater at 14.5%. Similarly, age-standardised premature mortality rates associated with ambient $PM_{2.5}$ exposure are 50% lower in the raw model sensitivity, while the age-standardised nitrate-associated mortality rate is reduced by ~ 20% to 1.52 (0.23 – 2.73) deaths per 100,000 persons. Therefore, in the raw model case, the reduction in mortality when removing nitrate is greater relative to the ambient $PM_{2.5}$-attributable mortality.

Over India, approximately 851,000 (476,000 – 1,280,000) premature deaths are attributed to long-term, ambient $PM_{2.5}$ exposure. Nitrate aerosol exposure in India is associated with 29,000 (22,500 – 37,100) deaths equating to a 3.4% reduction in total $PM_{2.5}$-attributable deaths in this region. Despite its relatively low importance compared to the total $PM_{2.5}$-attributable mortality, the total number of nitrate-associated deaths is within 10% of those in the EU28. The age-standardised mortality rate attributable to total $PM_{2.5}$ exposure is the highest of the regions in this analysis, at 123 (67.8 – 187) premature deaths per 100,000

people, with the nitrate associated mortality rate of 4.19 (3.21 – 5.39) deaths per 100,000 people equating to ~ 3.4% of the total $PM_{2.5}$-attributable mortality rate.

Over India, both the ambient $PM_{2.5}$-attributable and nitrate-associated premature mortality and mortality rates are reduced by ~ 9.7% in the raw model sensitivity, relative to the estimates above from bias-corrected $PM_{2.5}$ fields. The number of deaths related to nitrate aerosol contributes a similar 3.6% to the total $PM_{2.5}$-attributable mortality as in the bias-corrected estimate because the relative risk is less sensitive to changes in $PM_{2.5}$ concentration in the IERs at higher ambient concentrations, such as over India.

Over China, long term ambient $PM_{2.5}$ exposure results in approximately 865,000 (425,000 – 1,350,000) premature deaths per year. Nitrate-associated premature deaths total ~ 50,200 (38,700 – 61,000) per year and are greatest over China, from the four regions studied. The nitrate-associated mortality rate in China is 4.83 (3.73 – 5.86) premature deaths per 100,000 people per year and also the highest of the four regions studied. Removing nitrate aerosol would result in a ~ 5.8% reduction in $PM_{2.5}$-attributable mortality and age-standardised mortality rate over China. As over India, both the ambient $PM_{2.5}$–attributable and nitrate-associated premature mortality and mortality rates are lower in the raw model sensitivity than in the bias-corrected sensitivity over China. Again, both the nitrate and total $PM_{2.5}$ mortality are reduced when calculated from the unscaled $PM_{2.5}$ field because the exposure-response relationships are less sensitive to changes in $PM_{2.5}$ at higher ambient concentrations.

5.3.3.3 Years of life lost from nitrate-associated aerosol exposure

With knowledge of the premature mortality and remaining life expectancy per age group, the number of years of life lost to nitrate aerosol exposure can be estimated for each region as described in Section 3.3. Appendix Fig. B1 shows the mean age distribution of mortalities for each region. Table 5.5 indicates the years of life lost (YLL) from long-term exposure to nitrate aerosol and $PM_{2.5}$ in the four study regions. In the EU28 region, nitrate aerosol exposure results in approximately 432,000 (278,000 – 564,000) years of life lost in the EU28 region per year. This represents ~ 15.7% of the 2,760,000 (913,000 – 5,000,000)

Table 5.5 *Years of life lost (YLLs) associated with exposure to nitrate and ambient $PM_{2.5}$ calculated in this study, compared with $PM_{2.5}$-attributable YLLs calculated from satellite fields and for 2010 by GBD 2015 (which applied the same IERs as this study). Results are shown for regional bias-corrected and for unscaled model $PM_{2.5}$ fields.*

	Years of life lost (x 10^3)			
	Regional bias-corrected $PM_{2.5}$			
	Nitrate-associated (this study)	$PM_{2.5}$-attributable (bias-corrected field, this study)	$PM_{2.5}$-attributable (satellite, this study)	Year 2010 $PM_{2.5}$-attributable (GBD, 2016)
EU28	432 (278 – 564)	2,760 (913 – 5,000)	3,100 (1,170 – 5,420)	3,450 (2,910 -4,040)
USA	104 (65.8 – 134)	1,330 (404 – 2,400)	1,390 (450 – 2,460)	1,350 (1,070 – 1,650)
India	906 (726 – 1,117)	25,200 (15,100 – 36,500)	25,100 (14,900 – 36,500)	27,200 (24,000 – 30,700)
China	929 (726 – 1,122)	15,800 (7,900 – 24,400)	18,500 (10,000 – 27,600)	21,200 (18,800 – 23,700)
	Raw model $PM_{2.5}$ (unscaled)			
EU28	470 (231 – 668)	2,080 (487 – 4,100)		
USA	95.1 (17.5 – 168)	664 (58.0 – 1,460)		
India	882 (720 – 1,068)	23,200 (13,400 – 34,100)		
China	862 (644 – 1,051)	13,400 (6,000 – 21,500)		

years of life lost due to total $PM_{2.5}$ exposure in EU28. Nitrate aerosol exposure leads to greater lost years of life in the raw model simulation at approximately 470,000 (231,000 – 668,000) years and contributes a higher 22.6% to the total number of $PM_{2.5}$ related YLL.

In the USA, nitrate exposure results in ~ 104,000 (65,800 – 134,000) years of life lost, such that removing nitrate aerosol would reduce the $PM_{2.5}$-attributable years of life lost by 7.8%. From raw model $PM_{2.5}$ fields the number of nitrate-associated years of life lost is reduced at 95,100 (17,500 – 168,000) years, but

still contributes a higher 14.3% to the total $PM_{2.5}$-attributable YLL because the total $PM_{2.5}$-attributable mortality is much lower.

Over India, nitrate aerosol exposure results in ~ 906,000 (726,000 to 1,117,000) YLL in the bias-corrected simulation, equivalent to 3.6% of the total YLL from $PM_{2.5}$ exposure. Nitrate aerosol exposure makes a similar contribution of 3.8% (~ 882,000 YLL) to total $PM_{2.5}$-affiliated YLLs in the raw model case. In China, nitrate aerosol exposure results in ~ 929,000 (726,000 to 1,122,000) YLLs, or 5.8% of ambient $PM_{2.5}$-attributable YLL. Nitrate-associated YLL are lower in the raw model case, at ~ 862,000 years but contribute a slightly enhanced 6.4% of the total $PM_{2.5}$-attributable YLL.

5.3.4 Post-1980 emission driven changes in $PM_{2.5}$-attributable and nitrate-associated mortality

Having examined the contribution of nitrate to present day $PM_{2.5}$ and health in Section 5.3.3, this section will assess the influence of post-1980 emission changes on the relative importance of nitrate for $PM_{2.5}$ composition and human health. Figure 5.9 shows the changes in regional mean emissions between the year 1980 and 2008 over Europe, the USA, India and China from the MACCity inventory (Granier et al., 2011). The period 1980 to 2008 has been characterised by decreases in emissions of NO_x, SO_2, BC and OC over Europe and the USA as a result of air quality mitigation strategies and technologies. The MACCity inventory reports, however, that NH_3 emissions have increased since 1980, dominated by the agricultural sector and also influenced by road transport emissions as a result of uptake in use of catalytic converters. Conversely, emissions of all species in Figure 5.9 have increased over the Indian and Chinese regional domains since 1980 as a result of population growth and economic development in these regions. Previous studies show that these emission changes have contributed to decreases (Europe and the USA) and increases (India and China) in $PM_{2.5}$-attributable mortality (e.g. Butt et al., 2017; Turnock et al., 2016). However, the contribution of nitrate aerosol to these mortality trends were not included in these studies.

Figure 5.10a and 5.10b shows the influence of post-1980 emission changes on regional mean AWM and PWM $PM_{2.5}$. Reflecting the above changes in post-1980

emissions, two patterns of change in regional mean $PM_{2.5}$ emerge: reductions in the regional mean ambient $PM_{2.5}$ over the EU28 and USA and increases over India and China. AWM ambient $PM_{2.5}$ concentrations undergo regional changes of -33.9% (Δ 4.53 μg m^{-3}), -27.5% (Δ 1.88 μg m^{-3}), +23.0% (Δ 8.37 μg m^{-3}) and +14.7% (Δ 3.94 μg m^{-3}) in the EU28, USA, India and China, respectively. PWM ambient $PM_{2.5}$ is changed by –37.6% (Δ 6.48 μg m^{-3}), -35.8% (Δ 4.79 μg m^{-3}), +31.1% (Δ 12.3 μg m^{-3}) and +39.5% (Δ 9.71 μg m^{-3}) over the same regions, respectively.

Figure 5.10c and 5.10d show changes in the $PM_{2.5}$-attributable age-standardised mortality rate and mortality that arise from changes in post-1980 emissions, demography and background disease rates in each region. Table 5.6 shows $PM_{2.5}$-attributable mortality and mortality rates calculated for the 1980 case.

Age-standardised $PM_{2.5}$-attributable mortality rates are decreased in all regions between the bias-corrected 1980 and 2008 cases but the absolute number of mortalities increases over India and China. Figure 5.11 shows how change in

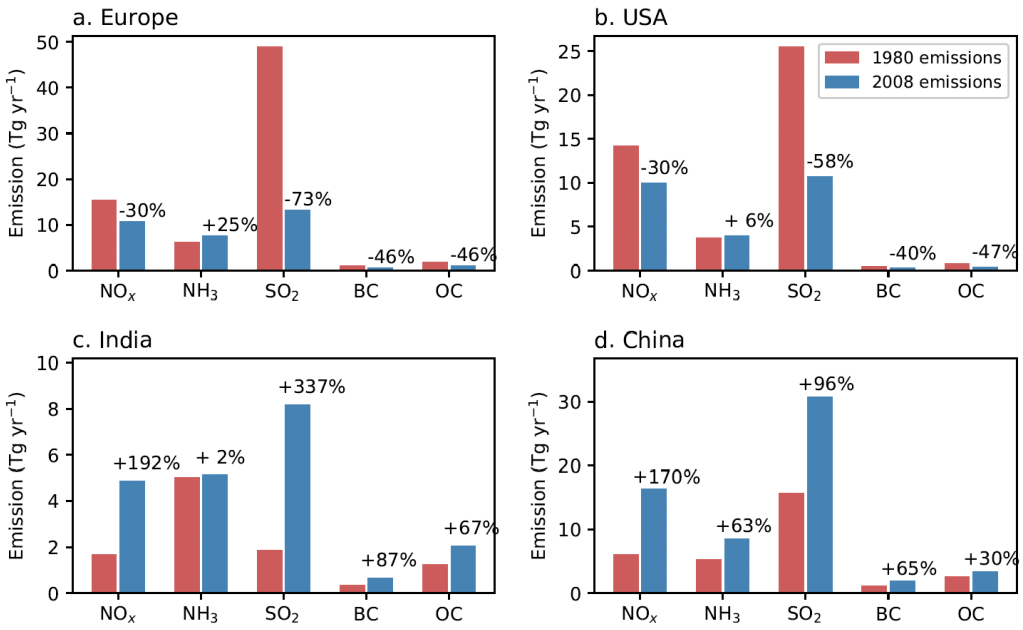

Figure 5.9 *Total emissions of gas phase aerosol precursor and primary aerosol species for the year 1980 and 2008 for regional domains over a) Europe, b) USA, c) India and d) China. Percentages above the blue 2008 emission bars show the change in emissions relative to a 1980 baseline. Regional domains are defined in Figure 5.1. Monthly-mean emissions are taken from the MACCity inventory (Granier et al., 2011).*

$PM_{2.5}$ exposure, population growth, population ageing and changes in background mortality rates contribute to the net change in number of $PM_{2.5}$-attributable deaths between the 1980 and 2008 case. It can be seen that upward trends in absolute mortality over India and China are also driven strongly by population growth and ageing. Therefore, although age-standardised mortality rates fall in India and China, the decreases are offset by increased population growth and population ageing in these regions. In the EU28 and USA, reductions in $PM_{2.5}$ exposure and background mortality rates are substantial enough to offset the countering effects of population growth and ageing between the 1980 and 2008 case. Both mortality and mortality rates therefore decline over the EU28 and USA.

Figure 5.10e to 5.10h shows the changes in nitrate-associated AWM $PM_{2.5}$, PWM $PM_{2.5}$, age-standardised mortality rate and absolute mortality arising from post-1980 changes in emissions (plus changes in demography and background disease for mortality estimates).

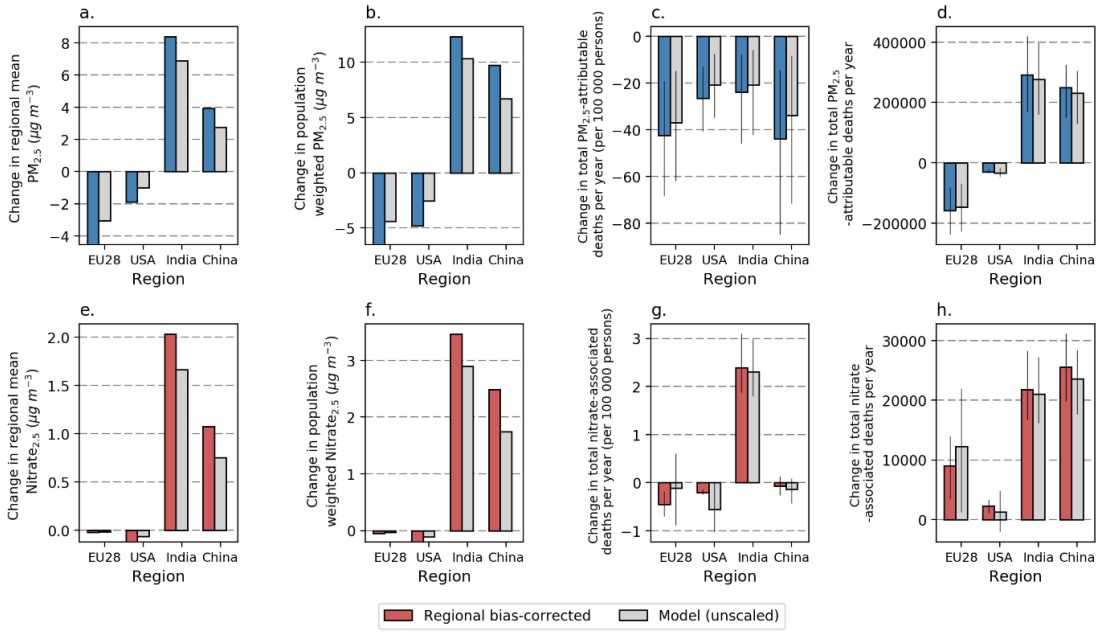

Figure 5.10 *Change in (a) regional mean $PM_{2.5}$, (b) population-weighted mean $PM_{2.5}$, (c) $PM_{2.5}$-attributable age-standardised mortality rate (premature deaths per 100,000 people per year) and (d) number of $PM_{2.5}$-attributable premature deaths per year when emissions of NO_x, NH_3, SO_2, BC and OC are changed from 1980 to 2008 levels. (e-h) the same for sub-2.5 µm nitrate aerosol concentrations ($Nitrate_{2.5}$) and nitrate-associated mortality rates and mortality. Year 1980 and 2008 emissions are shown in Figure 5.9.*

Table 5.6 *Nitrate-associated and $PM_{2.5}$ attributable mortality and mortality rates calculated in this study for a year 1980 emissions scenario (shown in Figure 5.10). Results are shown for regional bias-corrected and for unscaled raw model $PM_{2.5}$ fields.*

Number of premature deaths ($x10^3$)			
		Nitrate-associated	$PM_{2.5}$-attributable
EU28	Bias-corrected	22.5 (16.6 - 27.4)	361 (147 - 609)
	Unscaled	22.7 (15.4 – 28.6)	300 (104 - 533)
USA	Bias-corrected	4.6 (3.2 - 5.7)	118 (46.9 - 195)
	Unscaled	5.1 (3.2 – 6.7)	77.3 (20.9 – 143)
India	Bias-corrected	7.2 (5.7 - 8.8)	559 (306 - 859)
	Unscaled	7.0 (5.6 - 8.3)	510 (266 – 801)
China	Bias-corrected	24.6 (18.8 - 29.9)	614 (276 - 1,020)
	Unscaled	22.9 (16.6 - 28.7)	502 (194 - 882)
Age-standardised mortality rate (number of premature deaths per 100,000 people)			
		Nitrate-associated	$PM_{2.5}$-attributable
EU28	Bias-corrected	4.10 (3.04 - 4.97)	65.7 (26.7 - 111)
	Unscaled	4.13 (2.81 - 5.19)	54.5 (18.8 - 97.0)
USA	Bias-corrected	1.86 (1.29 - 2.31)	47.6 (19.0 - 79.0)
	Unscaled	2.07 (1.29 - 2.71)	31.3 (8.43 – 58.0)
India	Bias-corrected	1.79 (1.34 - 2.29)	147 (75.6 - 232)
	Unscaled	1.73 (1.30 - 2.18)	135 (66.3 - 217)
China	Bias-corrected	4.89 (3.60 - 6.12)	127 (55.1 - 214)
	Unscaled	4.61 (3.22 - 5.92)	104 (39.3 - 186)

Over the EU28, sub-2.5 μm nitrate aerosol concentrations remain relatively stable between the 1980 and present day emissions scenario, decreasing only slightly from 1.46 μg m^{-3} to 1.44 μg m^{-3} (-1.4%). Similarly the population-weighted mean NO_3^- concentrations show little downward trend, decreasing from 2.19 μg m^{-3} to 2.15 μg m^{-3} (-2.0%).

The relatively small downward trend in nitrate aerosol concentration over Europe compared to NO_x emission reductions could be driven by decreased competition from sulphuric acid (following reduced SO_2 emissions of 73%) for the available ammonia and increases in ammonia emission (e.g. Fagerli and Aas, 2008). Fagerli and Aas (2008) found non-significant trends in observations of airborne nitrate between 1990 and 2003. Despite nitrate aerosol concentrations undergoing a weak decline over Europe between the 1980 and present day emission scenario, the nitrate fraction of $PM_{2.5}$ is increased from 10.9% to 16.3% between 1980 and 2008, reflecting the fall in ambient $PM_{2.5}$ concentrations while nitrate-associated $PM_{2.5}$ concentrations remain relatively stable. Similarly, the nitrate-associated fraction of population-weighted $PM_{2.5}$ has increased from 12.7% to 20.0%.

The nitrate-associated age-standardised mortality rate has decreased by 11.0% (Δ 0.45 premature deaths per 10^5 of population per year) over the EU28 between the 1980 and present day emission scenarios. However the nitrate-associated mortality increases overall by 40% from 22,500 (16,600 – 27,400) deaths in 1980 to 31,500 (20,100 – 41,300) deaths per year in the present day, showing that decreases in $PM_{2.5}$ exposure and background disease rates are not substantial enough to offset increased mortality from population growth and ageing. Removing nitrate aerosol formation reduces $PM_{2.5}$-attributable mortality by a higher 15.6% in the present day case, compared to a 6.2% reduction in 1980. The higher nitrate-associated mortality, relative to $PM_{2.5}$-attributable mortality, under present day emissions is indicative of nitrate representing a larger fraction of the ambient $PM_{2.5}$ composition and is also increased because the integrated exposure-response functions are more sensitive to changes in $PM_{2.5}$ at the lower present day total $PM_{2.5}$ concentrations.

Over the USA, area weighted mean sub-2.5 μm nitrate concentrations are reduced by 22.0% from 0.54 μg m^{-3} to 0.42 μg m^{-3} under the influence of post-1980 emission changes, with population weighted concentrations reduced by 20.5% from 0.96 μg m^{-3} to 0.77 μg m^{-3}. The fraction of $PM_{2.5}$ associated with nitrate has increased slightly from 7.9% to 8.5%, while the population-weighted mean $PM_{2.5}$ nitrate fraction is also increased from 7.2 to 8.9%. The nitrate-associated age-standardised mortality rates are reduced by 11.4% between the

1980 and present day emission regime from 1.86 to 1.65 (1.03 – 2.16) mortalities per 10^5 of population per year. The change in nitrate associated mortality is much lower (by 6,755 mortalities, or 25%) over the US than over Europe in absolute terms but increases by ~ 2,300 deaths (50.0%) from 4,600 (deaths between the 1980 and PD emission scenarios. The number of nitrate-associated premature deaths is equivalent to 3.9% of total ambient $PM_{2.5}$-attributable deaths under 1980 emissions, increasing to 7.8% under the present day scenario.

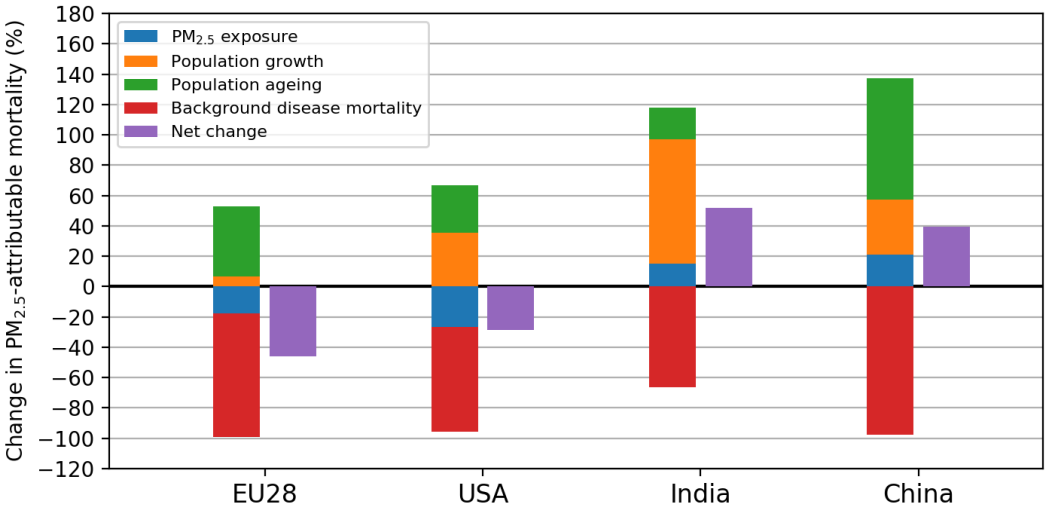

Figure 5.11 *Change in the relative contribution of $PM_{2.5}$ exposure, population growth, population ageing and background disease rates to total $PM_{2.5}$-attributable mortality between the bias-corrected 1980 case and 2008 emission cases.*

Over India and China, regional nitrate concentrations have increased as a result of post-1980 changes in emissions. Over India, the regional area-weighted mean sub-2.5 μm nitrate aerosol concentration increases from 0.67 μg m^{-3} to 2.70 μg m^{-3} (303%), while the population weighted mean increases from 1.13 μg m^{-3} to 4.59 μg m^{-3} (by 307%). The nitrate fraction of regional mean $PM_{2.5}$ increases from 1.8% to 6.0%, with the nitrate fraction of population weighted $PM_{2.5}$ also increasing from 2.9% under 1980 emissions to 8.9% under present day emissions. Unlike in other regions, the nitrate-associated age-standardised mortality rate increases substantially, by 133%, from 1.79 to 4.19 premature

deaths per 100,000 people between the 1980 and present day emissions sensitivity. Increased nitrate aerosol exposure contributes to increased death rates from all disease endpoints, whereas the $PM_{2.5}$-attributable death rate decreased driven by reductions in mortality rates associated with COPD, LRI and stroke. Overall, the number of deaths per year associated with nitrate aerosol exposure increase by 303% from 7,200 in the 1980 scenario to 29,000 under present day emissions. Removing nitrate aerosol in 1980 reduces $PM_{2.5}$-attributable mortality by 1.3% under 1980 emissions, increasing to only 3.4% in the present day scenario.

In China, the regional area-weighted mean sub-2.5 μm nitrate aerosol concentration increases from 0.73 μg m^{-3} under 1980 emissions to 1.80 μg m^{-3} (+148.6%) under the present day emission scenario. Removing nitrate aerosol under 1980 emissions results in a 2.7% reduction in regional mean $PM_{2.5}$, compared to 5.9% under present day emissions. The population weighted mean nitrate concentration is 134.2% higher in the present day scenario, increasing from 1.86 μg m^{-3} to 4.34 μg m^{-3}. The nitrate aerosol fraction of the population weighted ambient $PM_{2.5}$ is 7.5% under 1980 emissions, compared to 12.7% in the present day emissions scenario. The nitrate-associated age-standardised mortality rate decreases by 1.4% from 4.89 to 4.83 premature deaths per 100,000 people between the 1980 and present day scenario. Decreases in age-standardised nitrate-associated mortality rates from COPD and LRI are offset by increasing rates of nitrate-associated death from stroke, IHD and lung cancer, reducing the magnitude of decline in total nitrate-associated mortality rate. Overall, approximately 25,600 (104%) more nitrate-associated deaths occur per year under the present day emission regime in China, compared to a 1980 baseline of 24,600 (18,800 – 29,900) deaths per year. Removing nitrate aerosol under the 1980 emissions scenario reduces $PM_{2.5}$-attributable mortality by 4.0%, compared to 5.8% in the present day.

Figure 5.10 also shows changes in $PM_{2.5}$ and nitrate-associated $PM_{2.5,}$ age-standardised mortality rates and mortality derived from the raw model fields. In the unscaled simulation, post-1980 changes in AWM (PWM) nitrate concentration are smaller in magnitude by 25.4% (38.5%), 46.8% (45.4%), 17.9% (16.2%) and 29.7% (30%) over the EU28, USA, India and China,

respectively. Despite the smaller change in AWM and PWM sub-2.5 μm nitrate concentrations, the change in associated mortality over Europe, is approximately 35.7% higher than that calculated from bias-corrected data. Removing nitrate from the 1980 scenario has a lesser impact on the number of deaths because the IER functions are less sensitive to changes in $PM_{2.5}$ at the higher ambient $PM_{2.5}$ concentrations simulated under the 1980 emissions case. The change in number of nitrate-associated premature deaths is 44.6%, 3.5% and 7.7% lower in the USA, India and China, respectively, relative to the change calculated using bias-corrected $PM_{2.5}$ fields.

5.3.5 Study uncertainties and limitations

Uncertainty in simulated $PM_{2.5}$ arises from uncertainty in emissions, meteorology, model structure (e.g. spatial resolution) and microphysical processes. A perturbed parameter ensemble-based (PPE) study using the non-nitrate extended configuration of UM-UKCA found parametric uncertainty ranges (95^{th} uncertainty intervals) in regional PWM $PM_{2.5}$ of 5-14 μg m^{-3} , 6-12 μg m^{-3}, 20-85 μg m^{-3} and 18-58 μg m^{-3} over Europe, the USA, India and China respectively (Butt et al., 2017; Yoshioka, 2019 in prep.). The regional PWM $PM_{2.5}$ in this study are within this uncertainty range.

Model underestimation of $PM_{2.5}$ was expected based on previous evaluations of the standard non-nitrate extended configuration of UM-UKCA (Turnock et al., 2015; Turnock et al., 2016; Butt et al., 2017). Regional bias correction factors have been applied to simulated $PM_{2.5}$ based on year 2008 ground (Europe and USA) and satellite-based (India and China) observations. The resulting mortality estimates associated with long-term exposure to the bias-corrected $PM_{2.5}$ are within the uncertainty range of those from the Global Burden of Disease (IHME), 2018) over the European Union, USA and India. $PM_{2.5}$-attributable mortality estimates following the bias correction for China are below the lower limit of the GBD uncertainty range, but are within the uncertainty range (based on the IER functions) calculated for this study using satellite-derived $PM_{2.5}$ (Table 5.4).

The causes of low model bias should be investigated in future work. Model low bias may result from the relatively coarse model resolution and uncertainty in

water content (Browse et al., 2019 in prep.) in addition to known under prediction of organic aerosol at this version (see Mann et al., 2010) and potential under-representation of other $PM_{2.5}$ sources, such as re-suspension or primary biogenic aerosol particles. This configuration of UM-UKCA does not include anthropogenic secondary organic aerosol formation which could be expected to contribute up to ~2.6 μg m^{-3} in Europe, ~3.6 μg m^{-3} in the USA and ~4 μg m^{-3} over India and China (Spracklen et al., 2011b). It was established in Chapter 4 that UM-UKCA displays some systematic underestimations in surface secondary inorganic aerosol concentrations, with several potential causes (e.g. lack of heterogeneous nitrate aerosol formation on dust, over-enhanced wet removal), that may also have contributed to underestimations in $PM_{2.5}$.

The relatively coarse model resolution of UM-UKCA (approximately 140km) enables comparisons of $PM_{2.5}$ composition to be made between large regions of the globe. Previous studies have found differences in the $PM_{2.5}$-attributable mortality using different model spatial resolutions (e.g. Ford and Heald, 2016; Punger and West, 2013; Fenech et al., 2018; Li et al., 2016). Using UM-UKCA, Turnock et al. (2016) concluded that under prediction of $PM_{2.5}$ by the model (at the same spatial resolution to the configuration used here) in urban areas contributed to a low bias in mortality estimates by 13 – 16% over Europe, which was smaller than the uncertainty in the IER functions. Butt et al. (2017) found only small differences (< 4%) in population-weighted mean $PM_{2.5}$ estimated using population fields at UM-UKCA resolution (1.875° x 1.25°) and the original gridded resolution of 0.1° x 0.1°. Fenech et al. (2018) found ~±5% change in European total mortality attributable to $PM_{2.5}$ and O_3 between UM-UKCA simulations at ~140km and ~50km.

The uncertainty in mortality is presented in this work as the 5^{th} and 95^{th} percentile of mortality estimates calculated with a combination of lower, middle and upper uncertainty bounds of the IERs and national level background disease rates. The IERs are based on epidemiological evidence from Europe and North American studies and have been applied over successive Global Burden of Disease reports (e.g. Brauer et al., 2016; Forouzanfar et al., 2016; Cohen et al., 2017). There is uncertainty, however, when applying these relationships to other

regions, where patterns of $PM_{2.5}$ exposure (lifestyle), healthcare and age structures differ.

The IER functions are particularly subject to uncertainty in very clean and polluted regions because of a lack of epidemiological data on which to constrain the relative risk in highly polluted regions and these are currently defined from active and passive smoking cohort studies (Pope et al., 2009; Pope et al., 2011). Yin et al. (2017) found that the IERs may underestimate $PM_{2.5}$-attributable mortality at higher concentrations, based on a cohort study in China. Most ambient air pollution epidemiology studies have been conducted in developed countries and so the relative risk at lower concentrations is better constrained, except at very low concentrations. This study applies a lower threshold of 6 μg m^{-3} below which $PM_{2.5}$ exposure is deemed to have no health impacts, whereas some epidemiological studies have found an association between health impacts and long-term exposure to low concentrations of $PM_{2.5}$ (Crouse et al., 2012; Correia et al., 2013; Pinault et al., 2016).

Calculating the health response to $PM_{2.5}$ exposure requires the spatial and age distributions of population and background disease rates. Changes in the nitrate aerosol health burden between 1980 and 2008 are driven by both changes in total $PM_{2.5}$ and nitrate aerosol concentrations, in addition to demographic changes in population (number and age) and background disease rates, as demonstrated in Figure 5.11. The 1980 population fields have been constructed by distributing national level population totals according to the sub-national year 2000 spatial distribution. This contributes uncertainty when calculating population exposure to $PM_{2.5}$ in 1980, but particularly over India and China where large scale movement of people to urban areas has occurred in the past few decades. Rates of national level background disease have been estimated by linearly extrapolating the 1990-2000 trends in background disease rates backwards from 1990 data. Mortality estimates in 1980 could be improved if more information on historical background disease rates were known. National level background disease data and population age distribution may be important for estimates because sub-national variability is not accounted for.

The IERs are functions of total $PM_{2.5}$ concentration and neglects $PM_{2.5}$ composition, assuming that all $PM_{2.5}$ components are equally toxic to human

health. IERs, and this assumption of equal toxicity, have been applied in many studies, including assessments of $PM_{2.5}$-associated mortality from the Global Burden of Disease (e.g. Lelieveld et al., 2015; Cohen et al., 2017; Forouzanfar et al., 2016). The elicitation exercise of Tuomisto et al. (2008) has yielded agreement that combustion-derived particles are more toxic than secondary sulphate and nitrate particles. However, epidemiological and toxicological studies have yielded non-conclusive results as to the relative toxicity of nitrate aerosol over or below ambient $PM_{2.5}$ mixtures (Wyzga and Rohr, 2015.) It has been suggested that sulphate and nitrate aerosol can affect health through interactions with metallic ions and through links to the production of secondary organic matter (Reiss et al., 2007). Ultimately, there is insufficient evidence to exclude nitrate aerosol as being important for the long-term $PM_{2.5}$-attributable health risk and it has therefore been given an equal toxicity to other $PM_{2.5}$ components in this work, as in other studies of attributable mortality (e.g. Wang et al., 2017; Lelieveld et al., 2015; Turnock et al., 2016; Butt et al., 2017; Pozzer et al., 2017; Conibear et al., 2018 and others). If future toxicological research conclusively isolates any component of the $PM_{2.5}$ as being less toxic then a weighting could be applied to the IER functions (e.g. as in Lelieveld et al., 2015). Further research is needed to differentiate the health impacts from exposure to individual $PM_{2.5}$ components for each region.

5.4 Summary and Conclusions

The over-arching aim of this chapter is to ascertain the present day contribution of nitrate aerosol to $PM_{2.5}$ composition and mortality over the European Union, USA, India and China, and its changing contribution to these as a result of post-1980 emission changes. This is the first study using the UM-UKCA model in which nitrate aerosol impacts on $PM_{2.5}$ and mortality have been quantified. With consideration given to the uncertainties described in Section 5.3.5, the following summary and conclusions are presented.

Initial model validation against surface and satellite observations indicate a systematic underestimation in surface level $PM_{2.5}$ was present over the four study regions. The application of a regional bias correction is shown to reduce the low bias in each region and, importantly, to also improve the model

representation of simulated nitrate, ammonium and sulphate aerosol concentrations against observations introduced in Chapter 4. However, the underlying causes of model bias should be addressed in further study.

The nitrate fraction of regional area-weighted mean $PM_{2.5}$ is calculated and compared using a 'speciation' and a 'subtraction' approach. The latter method gives regional mean $PM_{2.5}$ nitrate fractions of 16.3%, 8.5%, 6.0% and 5.8% over Europe, USA, India and China, respectively. Nitrate aerosol formation contributes at least 10% of the total $PM_{2.5}$ over most of western, central and eastern Europe, with its greatest contribution over northern Germany at up to 45% of the total $PM_{2.5}$. In the USA, the nitrate-associated $PM_{2.5}$ fraction peaks at up to 30% in the north of the country and up to 20% elsewhere. In India, the nitrate-associated $PM_{2.5}$ fraction is greatest in the north at 25%, and over China the nitrate fraction is greatest in the north and east of the country, contributing up to 35% of the total $PM_{2.5}$.

The 'subtraction' method yields higher nitrate-associated $PM_{2.5}$ fractions than the 'speciation' method in most regions because it considers nitrate-associated ammonium aerosol formation. In some cases, however, the subtraction method results in small negative nitrate-associated fractions being calculated where the inclusion of nitrate aerosol formation decreases the total ambient $PM_{2.5}$, for example through microphysical processing and subsequently enhanced aerosol deposition. The results from this comparison suggest that changes to associated aerosol concentrations and microphysical processes should be considered when calculating the nitrate-associated mortality and when identifying policy to reduce particulate matter concentrations. The subtraction, or zero-out approach, is subsequently used to calculate the influence of nitrate-associated $PM_{2.5}$ on population weighted mean $PM_{2.5}$ and mortality.

Population-weighted mean $PM_{2.5}$ nitrate fractions of 20%, 8.9%, 8.9% and 12.7% are calculated over the EU28, USA, India and China, respectively. The higher relative contribution of nitrate aerosol to population-weighted mean $PM_{2.5}$ than to area-weighted regional mean $PM_{2.5}$ indicates that its precursor emissions are anthropogenic in origin and that it makes an important contribution to $PM_{2.5}$ in populated regions. Population scaling factors (i.e. the ratio of population-weighted to area-weighted mean $PM_{2.5}$) for each region are higher when

calculated from nitrate-associated $PM_{2.5}$ than from ambient $PM_{2.5}$, indicating a stronger correlation of population with nitrate than with ambient $PM_{2.5}$. Reducing nitrate aerosol concentrations would, therefore, be more effective in reducing human exposure to $PM_{2.5}$ than reducing total ambient $PM_{2.5}$ by the same amount (i.e. without considering the particulate composition).

The contribution of nitrate aerosol formation to premature mortality in the EU28, USA, India and China are quantified after the aforementioned regional bias correction has been applied to simulated $PM_{2.5}$. The changes in simulated (bias-corrected) $PM_{2.5}$ arising from the removal of nitrate aerosol formation are applied in integrated exposure response functions to calculate the long-term excess premature mortality from ischemic heart disease, stroke, lung cancer, chronic obstructive pulmonary disorder and lower respiratory infections in each region.

It is found that long-term exposure to nitrate aerosol results in 31,500 (20,100 – 41,300), 6,900 (4,300 – 9,000), 29,000 (22,500 – 37,100) and 50,200 (38,700 – 61,000) premature deaths per year over the EU28, USA, India and China, respectively, under a present day year 2008 emissions scenario. While the total number of nitrate-associated premature deaths is greatest in China, its relative contribution to total ambient $PM_{2.5}$-attributable deaths is highest over Europe at 15.6%. The removal of nitrate aerosol formation results in smaller 7.8%, 3.4% and 5.8% relative reductions in $PM_{2.5}$-attributable premature deaths in the USA, India and China, respectively. Age-standardised nitrate-associated mortality rates indicate that, even when the population dependency is removed from mortality estimates, the greatest number of nitrate-associated deaths still occurs in China at a rate of 4.83 deaths per 10^5 of population. It is found that long-term exposure to nitrate aerosol results in 432,000, 104,000, 906,000 and 929,000 lost years of life in the EU28, USA, India and China, respectively.

The change in nitrate-associated $PM_{2.5}$ and mortality resulting from post-1980 changes in emissions, demography and background disease rates are calculated. It is found that the nitrate-associated age-standardised mortality rate is decreased in most regions as a result of changes in nitrate-aerosol exposure and background disease rates, with the exception of India where nitrate-associated mortality from all disease endpoints is increased. The absolute number of

nitrate-associated deaths has increased between 1980 and the present day case in all regions, as has the relative contribution of nitrate to the total $PM_{2.5}$–attributable mortality in each region. The number of nitrate-associated premature deaths per year is increased by 40%, 49%, 303% and 104% between the 1980 and present day scenario over the EU28, USA, India and China, respectively.

This analysis finds that nitrate aerosol is associated with more deaths in the present day in all regions and that stringent emission controls will be required to reduce, or more effectively reduce, nitrate concentrations to overcome demographic influences on mortality, including population growth and ageing. It will be essential for future emission sensitivity studies to take changes in demography and background disease rates into account when assessing potential emission reductions in future projections of $PM_{2.5}$-attributable and nitrate-associated mortality. Emission controls may be particularly effective in Europe, where nitrate makes the greatest contribution to present-day mortality of the regions studied here and where multi-national emission controls on air quality have been shown to reduce $PM_{2.5}$ and $PM_{2.5}$-attributable mortality successfully in the past few decades (e.g. Butt et al., 2017; Turnock et al., 2016; Cohen et al., 2017; Li et al., 2017).

Further work is needed to assess how to effectively control nitrate aerosol concentrations in each region. Evaluation of nitrate aerosol dependence on atmospheric SO_2, NO_x, NH_3 concentrations and aerosol acidity remains an active area of research (e.g. Pusede et al., 2016; Vasilakos et al., 2018; Guo et al., 2018) along with sector based emission reduction modelling sensitivities (e.g. Bauer et al., 2016; Pozzer et al., 2017; Silva et al., 2016). Currently, uncertainty remains in future projections of atmospheric nitrate aerosol concentration, with some studies projecting that global mean surface nitrate concentrations will continue to increase (Bauer et al., 2007; Bellouin et al., 2011), while others project a stabilisation or decline in surface nitrate aerosol concentrations in response to reduced NO_x emissions (Bauer et al., 2016; Pusede et al., 2016; Trail, 2014).

6. Sensitivity of the simulated present day nitrate aerosol cloud albedo radiative effect to the gas-particle partitioning approach

6.1. Introduction

In Chapter 5, the contribution of nitrate aerosol to regional air quality ($PM_{2.5}$ concentrations) and cause-specific $PM_{2.5}$-related mortality was examined. As explained in Chapter 2, nitrate aerosol plays another important role in the atmospheric system as a climate forcing agent. Nitrate aerosol can alter the atmospheric radiative balance directly by scattering incoming radiation and indirectly by modifying cloud albedo and lifetime, with subsequent implications for cloud interactions with radiation. The uptake of nitric acid into the aerosol particle phase affects cloud properties by growing existing particles to create new cloud condensation nuclei (CCN) and by changing the size and composition of existing CCN. Although several studies have assessed the influence of nitrate aerosol on the global and regional radiative balance (e.g. Bellouin et al., 2011, Hauglustaine et al., 2014), very few studies (Xu and Penner, 2012) have quantified its aerosol-cloud interaction radiative effects.

Simulating the uptake of nitric acid into fine mode particles (i.e. to resolve the influence of nitrate aerosol on particle growth to CCN sizes) requires that models resolve aerosol microphysical processes, such as coagulation and condensation, and apply a size-resolved aerosol partitioning approach that accounts for variations in timescales for gas-particle partitioning to different particle sizes. The majority of global climate models that resolve nitrate aerosol apply an equilibrium approach to treat semi-volatile inorganic gas-particle partitioning, which does not recognise that larger particles necessarily have a slower rate of nitric acid uptake. The sophistication of the partitioning approach was shown by Feng and Penner (2007), Benduhn et al. (2016) and Chapter 4 of this thesis to influence the uptake of nitric acid into the aerosol fine mode. Although these studies have identified the importance of the aerosol partitioning approach for the nitrate aerosol size distribution, the implications for model predictions of the nitrate aerosol radiative forcing have not been previously investigated.

In this chapter, the influence of nitrate aerosol on the present day aerosol cloud-albedo effect, hereafter referred to simply as the "nitrate CAE", is quantified via simulations with the UM-UKCA model. The nitrate CAE is defined in this work as the change in present day TOA (SW) radiative flux resulting from changes in cloud albedo when simulated nitric acid partitions into the aerosol particle phase.

The impact of the aerosol partitioning method on simulated nitrate CAE is assessed in the first part of this chapter, comparing model experiments that apply a hybrid approach with those applying an equilibrium approach. In order to understand the magnitude and spatial distribution of the nitrate CAE, the impact of nitrate aerosol formation on aerosol number and cloud droplet number concentrations are then evaluated. Within this second part of the analysis, UM-UKCA simulated aerosol number concentrations are also compared to observations, representative of both continental and marine-influenced conditions. The results in this chapter represent the first study of nitrate aerosol radiative effects using the two-moment GLOMAP-mode aerosol microphysical scheme in the UM-UKCA model.

6.2. Model Setup

Table 6.1 shows the four simulations included in this chapter, designed to understand the influence of nitrate aerosol formation on simulated aerosol radiative effects. Simulations use either a hybrid (HYB and HYB-NoNO_3) or an equilibrium (EQU and EQU-NoNO_3) approach for gas-particle partitioning of inorganic semi-volatile aerosol so that the influence of each approach on aerosol properties and the nitrate CAE can be compared. In HYB-NoNO_3 and EQU-NoNO_3, nitrate aerosol formation is excluded by disabling the uptake of gaseous nitric acid into the particulate nitrate phase. As with all simulations in the thesis, all simulations are run for 12 months with a 4 month spin up period from September 2007. Meteorological nudging is applied to the simulations at 6 hourly intervals. Monthly-varying anthropogenic emissions from the MACCity inventory (Granier et al., 2011) are applied.

Table 6.1. Summary of simulations analysed in this chapter.

Experiment number	Experiment name	Description
1	HYB	Identical to experiment HYB, evaluated in Chapter 4.
2	EQU	Identical to experiment EQU, evaluated in Chapter 4.
3	HYB-NoNO$_3$	Identical to experiment HYB (1) but with nitrate aerosol formation disabled.
4	EQU-NoNO$_3$	Identical to experiment EQU (2) but with nitrate aerosol formation disabled.

The radiative effect of nitrate aerosol is calculated offline using SOCRATES and determined based on perturbations to cloud droplet number concentration (CDNC), via their influence on cloud effective radius. CDNC is calculated offline using 3D monthly aerosol mass and number concentrations simulated online using GLOMAP-mode in UM-UKCA. Changes in CDNC at all vertical levels between the surface and 600 hPa are considered in the calculation of the nitrate aerosol radiative effect, hence the influence of nitrate aerosol formation on low- and mid-level water clouds is quantified. More detail on the methodology is provided in Chapter 3 Section 3.4.

The GLOMAP-mode aerosol microphysics scheme treats key aerosol processes including new particle formation, particle growth by coagulation, condensation and cloud processing and wet/dry deposition, as described in Chapter 3 Section 3.2.3. The model setup applied here includes the simulation of new particle formation in the free troposphere, which is the dominant source of global CCN (e.g Merikanto et al., 2009). However, boundary layer nucleation mechanisms (e.g those evaluated in Reddington, 2012) are not implemented in this developmental configuration of the model codebase.

6.3. Results

This section quantifies the present day cloud albedo effect that arises when nitrate aerosol formation is included in simulations. The magnitude and spatial distribution of the present day nitrate CAE (with nitrate aerosol formation simulated using the hybrid approach) is compared to the more approximate prediction with an equilibrium approach. The results in this chapter have been ordered to first present the main result, i.e. the nitrate CAE (section 6.3.1), before presenting the underlying changes in aerosol properties and CDNC that drive the nitrate CAE. The analysis in this chapter will focus on changes in aerosol properties and CDNC at both low (model level 9; mean pressure of ~ 900 hPa) and middle level (model level 18; mean pressure ~ 720 hPa) clouds.

6.3.1 Present day nitrate aerosol cloud albedo effect

Figure 6.1 shows the spatial and zonal mean distribution of the UM-UKCA predicted present day annual mean nitrate aerosol CAE with the HYB and EQU simulations shown in panels a and b, respectively. Throughout this analysis, results with the hybrid partitioning scheme (HYB) represent the best-estimate prediction by the model. The equilibrium runs are used to assess the importance of resolving the size-dependent timescales for gas-particle transfer.

The model experiments show that nitrate aerosol causes a present day cloud albedo radiative effect of -0.007 W m^{-2} using the HYB approach, with stronger forcing arising in the Northern Hemisphere (mean PD CAE of -0.02 W m^{-2}). It was expected that the nitrate CAE would be negative overall. However, the experiments show that nitrate aerosol formation acts to weaken the PD aerosol radiative effect in the Southern Hemisphere (mean PD CAE of +0.008 W m^{-2}), dominated by positive radiative forcing within the tropics and over the Southern Ocean. This effect of nitrate to weaken the present day CAE is strongest in regions of the tropics, reaching a maximum magnitude of +0.1 W m^{-2} at the equator. Over the Southern Hemisphere mid-latitudes, nitrate again acts to strengthen the aerosol cloud albedo effect but causes another slight weakening effect south of approximately 50° S. The strengthening in Southern Hemisphere mid-latitude CAE arises despite surface nitrate concentrations being lower there than in the Northern Hemisphere (see Chapter 4). As in other studies of the

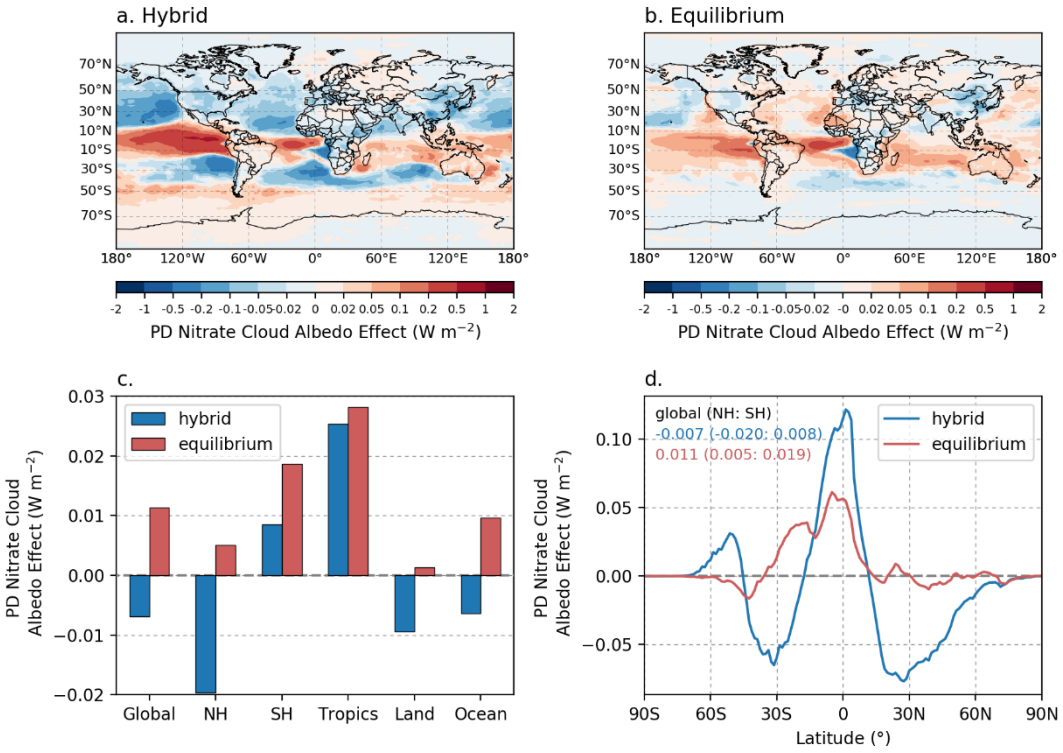

Figure 6.1 *Spatial distribution of the annual mean all-sky cloud albedo effect from nitrate aerosol formation, simulated using (a) the hybrid and (b) equilibrium partitioning approaches. (c) compares the annual mean, regional mean nitrate CAE using both partitioning approaches over the whole globe, Northern Hemisphere, Southern Hemisphere, tropics (23.5 °S – 23.5 °N), land and ocean. (d) shows zonal mean variability in the annual mean CAE simulated using both partitioning approaches, with global, Northern and Southern Hemisphere mean nitrate CAEs.*

aerosol CAE (e.g. Spracklen et al., 2011b), the radiative effects in this work are more sensitive to CDNC changes in regions with persistent marine stratocumulus cover. Furthermore, this study finds that vertical variability in the influence of nitrate aerosol formation on CDNC has implications for the radiative forcing. The changes in CDNC over these and other regions will be examined in the subsequent sections of this chapter. The mean nitrate CAE simulated using the hybrid partitioning approach is slightly stronger over land than over ocean because negative forcings over the ocean are offset by positive forcings over other oceanic regions.

For the EQU case, the global mean PD nitrate CAE is calculated to be +0.011 W m^{-2}, representing a sign reversal in global mean nitrate CAE from that calculated using the HYB assumption. The weighting of the nitrate CAE to regions with

persistent marine cloud cover is, again, evident and subsequent sections of this chapter will examine how CDNC changes in these regions contribute to the differences between the HYB and EQU nitrate CAE. Compared to the hybrid approach, the equilibrium approach under-represents the mean nitrate CAE over both Hemispheres and over both land and ocean. The equilibrium method results in a positive mean nitrate CAE in the Northern Hemisphere, compared to the negative mean CAE with the hybrid scheme. Both partitioning approaches result in a mean positive nitrate CAE in the Southern Hemisphere but with differences in spatial distribution. Nitrate aerosol formation applying the equilibrium scheme produces a weaker positive zonal mean CAE in the tropics than the hybrid approach but with this positive CAE extending further southward into latitudes where the HYB scheme produced negative CAE. Nitrate aerosol formation via the equilibrium scheme therefore produces a stronger positive CAE in the Southern Hemisphere on average compared with the hybrid approach.

The magnitude and spatial distribution of the nitrate CAE is dependent on both changes in CDNC, the horizontal and vertical location of clouds and insolation. The remainder of this chapter will therefore focus on the influence of nitrate aerosol formation on aerosol properties before the combined influences of CDNC and cloud location on the nitrate CAE are discussed.

6.3.2 Simulated total particle number concentrations

The magnitude and spatial distribution of simulated annual mean surface level N_3 (N_3; particles with dry diameter above 3 nm) is presented in this sub-section. Figure 6.2a shows the spatial distribution of surface level N_3 simulated by GLOMAP-mode in UM-UKCA, with nitrate aerosol formation included. It can be seen that aerosol number concentrations are greatest over continental regions with concentrations generally ranging, over several orders of magnitude, between 200 cm^{-3} and 20,000 cm^{-3}. The greatest concentrations of 10,000-20,000 cm^{-3} are simulated over Northern India and Eastern China, with the lowest continental concentrations (< 200 cm^{-3}) found over the remote Northern Hemisphere and Australasia. Particle number concentrations are lower in the marine boundary layer than over continental regions and range between 10 cm^{-3} and 500 cm^{-3}, with the lowest concentrations over the remote Arctic Ocean and

greatest concentrations in regions of continental outflow (e.g. the Northern Atlantic and Northern Pacific Oceans).

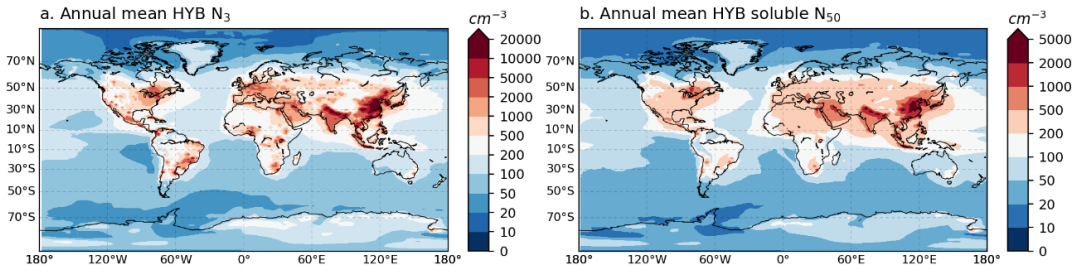

Figure 6.2 *Annual mean surface level (a) total particle number concentrations (N_3; particles with dry diameter greater than 3 nm) and (b) soluble N_{50} (particles with dry diameter greater than 50 nm), both simulated using the hybrid (HYB) partitioning approach.*

The range in continental surface N_3 in this study is larger than that simulated previously by GLOMAP-mode in the TOMCAT model (Gordon et al., 2017, Figure 2b), where N_3 ranged between 350 and 6,000 cm^{-3} over most regions. Though lower in northern Europe, UM-UKCA concentrations are generally on the same order of magnitude as those simulated by Gordon et al. (2017) over Europe (this study: 100 – 5000 cm^{-3}; Gordon: 600 – 3500 cm^{-3}) and by Merikanto et al. (2009; 1,000 – 8,000 cm^{-3}). As a result of not including boundary layer nucleation, UM-UKCA N_3 is generally substantially lower than Gordon et al. (2017) and Merikanto et al. (2009) in regions where those studies found the fraction of N_3 formed via new particle formation to be greatest, including large regions of Australasia, central/northern Asia, South and North America. Notably, peaks in UM-UKCA surface N_3 are higher than previous studies over India (this study: 2000 – 20,000 cm^{-3}; Gordon et al.: 1,000 – 3,500 cm^{-3}; Merikanto et al.: 2,000 to 6,000 cm^{-3}) and China (this study: 200 - over 20,000 cm^{-3}; Gordon et al.: 600 - > 6,000 cm^{-3}; Merikanto et al.: 1,000 to 10,000 cm^{-3}). Given that primary particle formation is a large source of particles than new particle formation in these regions (Merikanto et al., 2009), this indicates that primary particle formation is higher in this UM-UKCA study than the previous GLOMAP assessments.

The surface N_3 simulated in this study is comparable to Gordon et al. (2017) over most remote marine regions (between 20 and 600 cm^{-3}) but are lower over regions of continental outflow than in their simulations (up to 2000 cm^{-3}). Like

Gordon et al. (2017), this study has substantially lower marine N_3 than those from Merikanto et al. (2009), in which boundary layer new particle formation rates were high at relatively low sulphuric acid concentrations. Gordon et al. (2017) show that these rates were reduced when ammonia and organic-mediated boundary layer nucleation mechanisms were included in simulations. The additional mechanisms brought marine N_3 more in line with those simulated here by UM-UKCA.

6.3.3 Change in total particle concentration

This section describes the change in simulated N_3 when nitrate aerosol is formed (i.e. when nitric acid reversibly condenses onto existing particles) using the best case hybrid (HYB) and alternative equilibrium (EQU) gas-particle partitioning method.

Table 6.2 shows the global annual mean surface level N_3 simulated for each experiment and the change in N_3 when nitrate aerosol formation is included using both the hybrid and equilibrium gas-particle partitioning approaches. The inclusion of nitrate aerosol formation in the HYB case decreases annual global mean surface N_3 by 1.7%, while N_3 is reduced by less than 0.1% in the EQU sensitivity. The overall effect of nitrate aerosol formation globally is therefore to slightly decrease aerosol number concentrations at the surface. This reduction in N_3 is caused by increasing aerosol size via the condensation of nitric acid onto existing particles, which enhances the condensation sink for new particle formation and the coagulation sink for newly formed particles. The reductions in global mean N_3 are more apparent when using the hybrid partitioning approach. This occurs because the hybrid approach results in nitric acid uptake to the fine mode (as shown in Chapter 4) and therefore a greater increase in aerosol surface area. This more greatly enhances the condensation sink of potentially nucleating gases. Conversely, the equilibrium approach results in over-enhanced nitric acid uptake to the coarse mode (as found in Chapter 4) with a smaller influence on the aerosol surface area.

Table 6.2 also shows how the influence of nitrate formation on global mean N_3 varies with altitude. N_3 concentrations are lower at low cloud height than at the

Table 6.1 *Annual mean global surface, low cloud (~ 900 hPa) and middle cloud (~ 720 hPa) level N_3 and soluble N_{50}, with and without nitrate aerosol formation, as simulated using the hybrid (HYB) and equilibrium (EQU) gas-particle partitioning approaches. Relative changes are given in brackets as percentages.*

	N_3 (# cm^{-3})	**Change in N_3 (# cm^{-3})**	**N_{50} (# cm^{-3})**	**Change in soluble N_{50}**
		Surface level		
EQU-NoNO$_3$	389.5	-	145.2	-
HYB-NoNO$_3$	389.6	-	145.8	-
EQU	389.2	-0.28 (-0.07%)	147.0	1.79 (+1.23%)
HYB	383.0	-6.57 (-1.69%)	146.1	0.29 (+0.20%)
		Low cloud level		
EQU-NoNO$_3$	294.9	-	168.9	-
HYB-NoNO$_3$	294.5	-	169.2	-
EQU	294.5	-0.39 (-0.13%)	170.8	1.91 (+1.13%)
HYB	284.7	-9.82 (-3.33%)	168.8	-0.34 (-0.201%)
		Middle cloud level		
EQU-NoNO$_3$	317.3	-	182.1	-
HYB-NoNO$_3$	317.4	-	181.8	-
EQU	320.5	3.18 (+1.01%)	185.1	2.30 (+1.65%)
HYB	311.6	-5.75 (-1.81%)	186.3	4.50 (+2.47%)

surface with nitrate aerosol formation by the hybrid partitioning approach again having a larger influence (-3.3%) on global mean concentrations than the equilibrium approach (-0.13%). Global mean N_3 concentrations at middle cloud level are between the surface and low cloud level concentrations in terms of magnitude, but with the two partitioning approaches having near-comparable influences on the magnitude of global mean middle cloud level N_3, although opposite in sign. Focussing on the change in N_3 simulated using the hybrid scheme, the influence of including nitrate aerosol formation on global mean N_3

is less strongly negative at middle cloud level than at low cloud level because more nucleation mode aerosol is available for growth to longer-lived Aitken and accumulation mode particles. On the global mean scale, increases in aerosol lifetime therefore counteract the decreases in N_3 arising from the enhanced condensation sink when nitrate aerosol formation is included.

The influence of nitrate aerosol formation on total particle concentrations therefore varies spatially in the vertical and also horizontally. Figures 6.3 and 6.4 show changes in the spatial distribution of annual mean low (~ 900 hPa) and middle cloud (~ 720 hPa) level N_3, respectively, when nitrate aerosol formation is included using both gas-particle partitioning approaches. Nitrate aerosol formation is associated with increases in low cloud level N_3 of up to 100 cm^{-3} over hotspot regions in North America and Asia when both partitioning approaches are employed (Fig. 6.3a and 6.3c), representing increases of up to 20% locally (Fig 6.3b and 6.3d). The hybrid approach results in more greatly decreased low cloud level particle concentrations than the equilibrium approach over most of the global oceans, with HYB low cloud level N_3 decreasing over oceanic regions by up to 30%, as a result of the larger influence on the condensation sink. Conversely, HYB N_3 is increased by up to 10% in the North Pacific, where little (< 5%) response in EQU N_3 is seen. The choice of partitioning scheme is also relevant over the Arctic: the equilibrium approach results in larger decreases (of up to 10%) over most of the Arctic oceans, while decreases using the hybrid approach are larger in the region of the Greenland Sea and Barents Sea.

At middle cloud level (Fig 6.4), absolute changes in HYB N_3 (Fig 6.4a) tend to be greater in magnitude than at low cloud level (Fig 6.3a). Notably, HYB N_3 is increased over wider regions of the Northern Hemisphere at the higher altitude (Fig 6.4a and 6.4b), including over much of the Arctic (up to + 10%), North Atlantic Ocean (up to + 20%) and North America (up to +20%) where low cloud

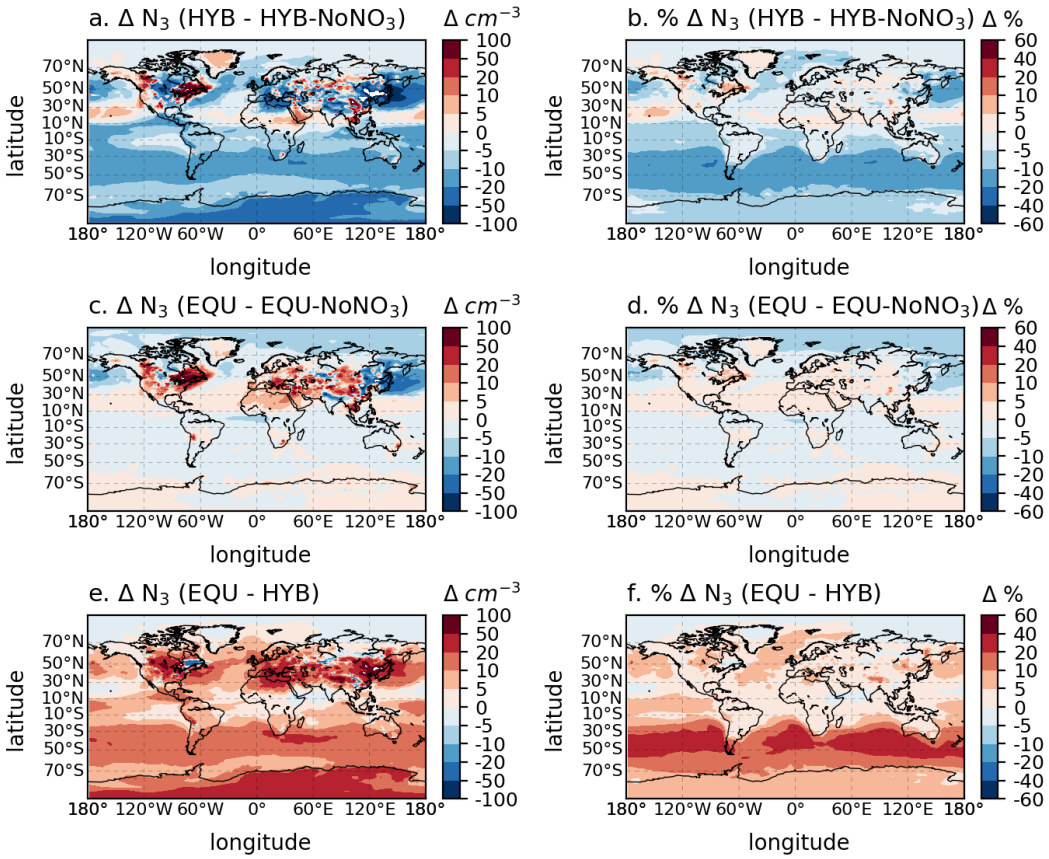

Figure 6.3 *Absolute (left column) and relative (right column) changes in annual mean low cloud level (~ 900 hPa) soluble N_3 when nitrate aerosol formation is included via HYB (top row) and EQU (middle row) partitioning approaches. Bottom row shows the absolute and relative difference (EQU – HYB) in simulated soluble N_3 between both gas-particle partitioning approaches.*

level N_3 was decreased. These increases at higher altitude could result from higher availability of nucleation mode particles than at the low cloud level/surface in these simulations, such that nitric acid uptake leads to greater aerosol growth into the more stable Aitken/accumulation modes. However, absolute HYB N_3 is decreased more strongly at middle cloud level over large regions of Europe, as are concentrations over most of the tropics and mid-to-high latitudes of the Southern Hemisphere compared to at low cloud level, showing that the effect of nitrate aerosol formation on the condensation sink is stronger at higher altitude over these regions. The greatest relative increase in HYB N_3 at middle cloud level of up to +60% is simulated over China. Using the equilibrium approach (Fig 6.4c and 6.4d), nitrate formation has a relatively small (< ± 5%) impact on middle cloud level N_3, except over and down-source of China

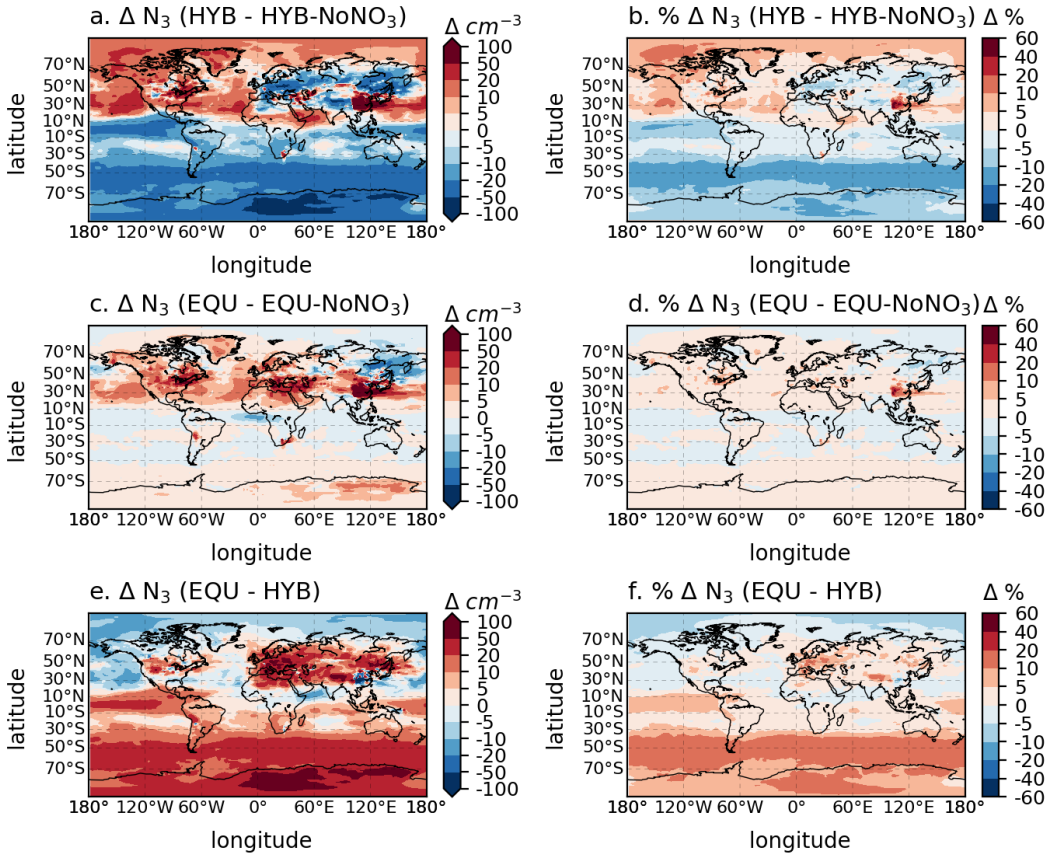

Figure 6.4. *Absolute (left column) and relative (right column) changes in annual mean middle cloud level (~ 720 hPa) soluble N_3 when nitrate aerosol formation is included via HYB (top row) and EQU (middle row) partitioning approaches. Bottom row shows the absolute and relative difference (EQU – HYB) in simulated soluble N_3 between both gas-particle partitioning approaches.*

where, as in the HYB case, concentrations are increased by up to 60%. The relatively small changes in EQU N_3 show that nitrate aerosol formation using the equilibrium approach has a smaller effect on the condensation sink and on the growth of nuclei than the hybrid approach in most regions.

Overall (panels e and f of Fig. 6.3 and 6.4), it is found that the conventionally adopted equilibrium approach underestimates total particle concentrations in the remote Northern Hemisphere high latitudes compared to using the hybrid approach. The relative underestimations in N_3 tend to be more widespread and greater in magnitude at middle cloud than at lower cloud level. The equilibrium approach overestimates N_3 over near-source continental and Southern Hemispheric marine regions compared to using the hybrid approach, with the

greatest underestimations of up to 40% found between 30° S and 40° S at low cloud level. These results demonstrate that the influence of nitrate aerosol formation on total particle concentrations vary spatially, in the horizontal and vertical, when using the equilibrium approach instead of the more realistic hybrid approach for semi-volatile gas-particle partitioning.

6.3.4 Evaluation of simulated soluble N_{50}

N_{50} is defined as the number concentration of particles with a dry diameter greater than 50 nm. In this sub-section the spatial distribution of simulated surface level soluble N_{50} (including nitrate aerosol formation) is described and total (soluble plus insoluble) N_{50} concentrations are compared to observations. Figure 6.2b shows the magnitude and spatial distribution of simulated surface level N_{50}, including nitrate aerosol simulated using the hybrid partitioning approach. The spatial distribution of surface level N_{50} concentrations corresponds with surface N_3 concentrations (Figure 6.2a), with enhanced concentrations over continental and outflow regions and the lowest concentrations over the remote marine atmosphere. As with N_3 the greatest concentrations of surface N_{50} (up to 5000 cm^{-3}) are simulated over eastern China and the northern plains of India.

Figure 6.5 compares simulated surface level N_{50} against annual mean year 2008 observations from the EUSAAR/GUAN ground based monitoring network and against ship based observations from the North Atlantic ICEALOT campaign (October to December 2008). Observations are described in Section 3.6.4 and cover regions where HYB nitrate aerosol formation was found to exert a negative present day cloud albedo forcing in Section 6.3.1. The comparison to observed concentrations indicates that UM-UKCA underestimates annual mean N_{50} at continental sites (nmb = -0.856) with moderate spatial correlation against observations (r = 0.415). Concentrations over the North Atlantic, representative of marine region influenced by continental outflow, are better represented by the model. Concentrations are underestimated by approximately 35% (nmb = -0.338) but the spatial distribution of N_{50} in continental outflow from North America, decreasing into the more remote North Atlantic, are captured particularly well by the model (r = 0.839).

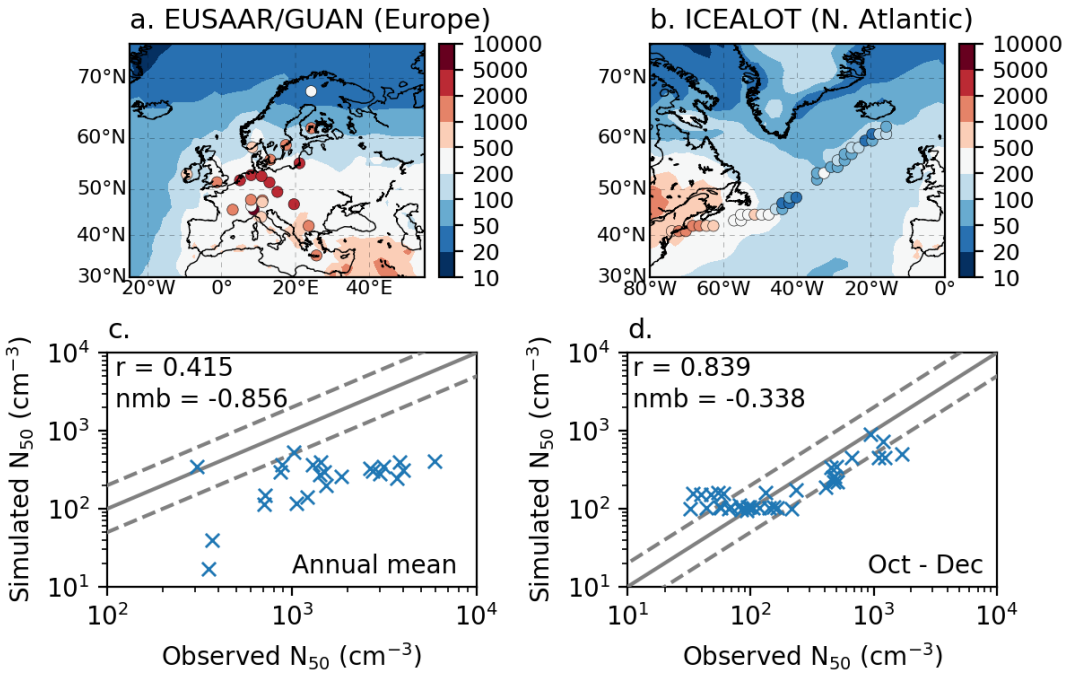

Figure 6.5 *Comparison of HYB-simulated total N_{50} (soluble + insoluble) to observed total N_{50} from (a+c) EMEP surface monitoring sites and (b+d) the ICEALOT cruise campaign in the North Atlantic Ocean. Observed and simulated N_{50} are compared for year 2008. Annual mean simulated and observed N_{50} are compared at EMEP sites, while March-April simulated mean N_{50} are compared to the ICEALOT observations to align with the campaign time period. Pearson correlation coefficients and normalised mean bias scores are given in subplots (d) to (f).*

6.3.5 Change in soluble N_{50}

6.3.5.1 Annual mean concentrations

Two main mechanisms control the magnitude and distribution of changes in N_{50} when nitrate aerosol is formed. Firstly, the uptake of nitric acid onto aerosol can grow particles to a larger size, therefore increasing the number concentration of particles in the size range above 50 nm. Conversely, as mentioned in Section 6.3.3, the enhanced surface area of particles following this growth leads to a larger uptake, or condensation sink, of gaseous sulphuric acid, therefore suppressing the H_2SO_4 available for new particle formation in the free troposphere. The growth of newly formed particles also enhances coagulational scavenging. Decreases in N_{50}, particularly in the marine boundary layer, are indicative of this being the case where 45% of CCN (at 0.2% supersaturation) are entrained from the free troposphere (Merikanto et al., 2009).

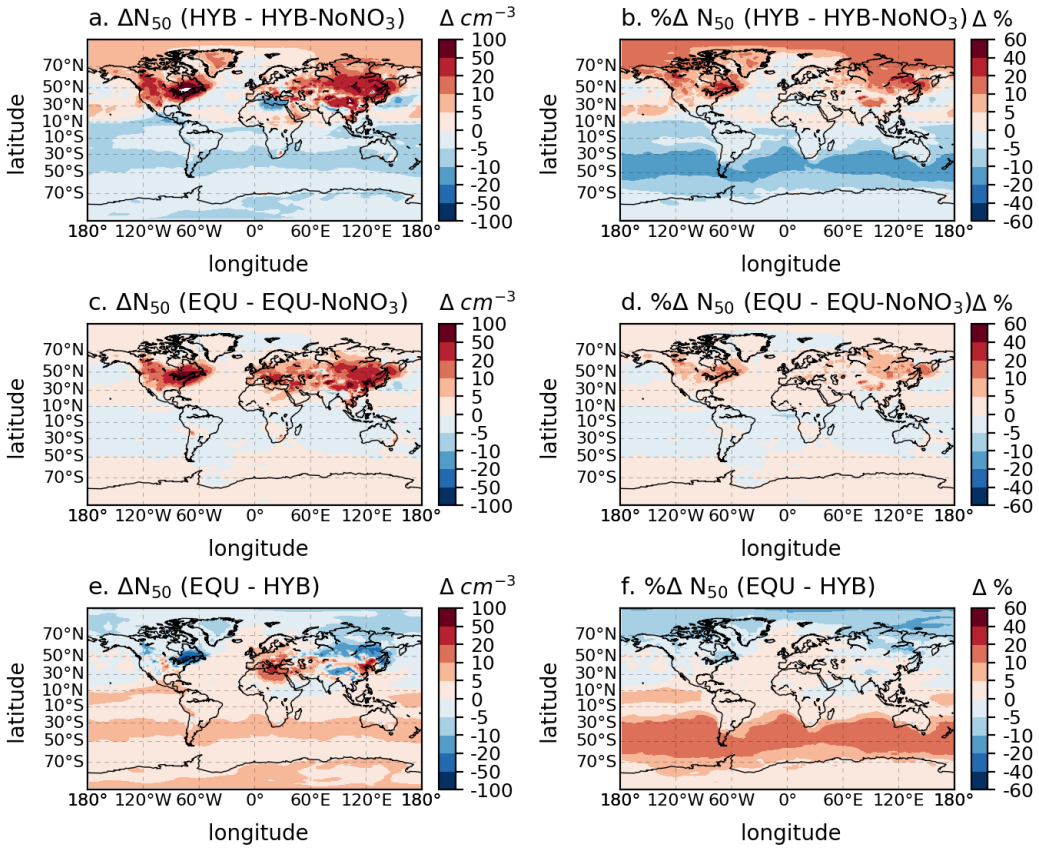

Figure 6.6 *Absolute (left column) and relative (right column) changes in annual mean low cloud level (~ 900 hPa) soluble N_{50} (number concentration of soluble particles with dry diameter greater than 50 nm) when nitrate aerosol formation is included via HYB (top row) and EQU (middle row) partitioning approaches. Bottom row shows the absolute and relative difference (EQU – HYB) in simulated soluble N_{50} between both gas-particle partitioning approaches.*

Figure 6.6 shows changes in the spatial distribution of annual mean low cloud level N_{50} when nitrate aerosol formation is included using both gas-particle partitioning approaches. When simulated using the hybrid partitioning scheme (Fig. 6.6a and 6.6b), nitrate aerosol formation results in large annual mean absolute increases in low cloud level N_{50} over the continental Northern Hemisphere, with increases peaking at up to 200 cm^{-3} over North America. These regions of increased N_{50} coincide broadly with regions of high nitrate aerosol concentration (see Figure 4.10) but also extend into more remote, nitrate-poor regions. It is in these more remote regions where the relative increase in annual mean HYB N_{50} is greatest because background N_{50} concentrations prior to nitrate formation are lower. Most notably, nitrate aerosol formation using the hybrid

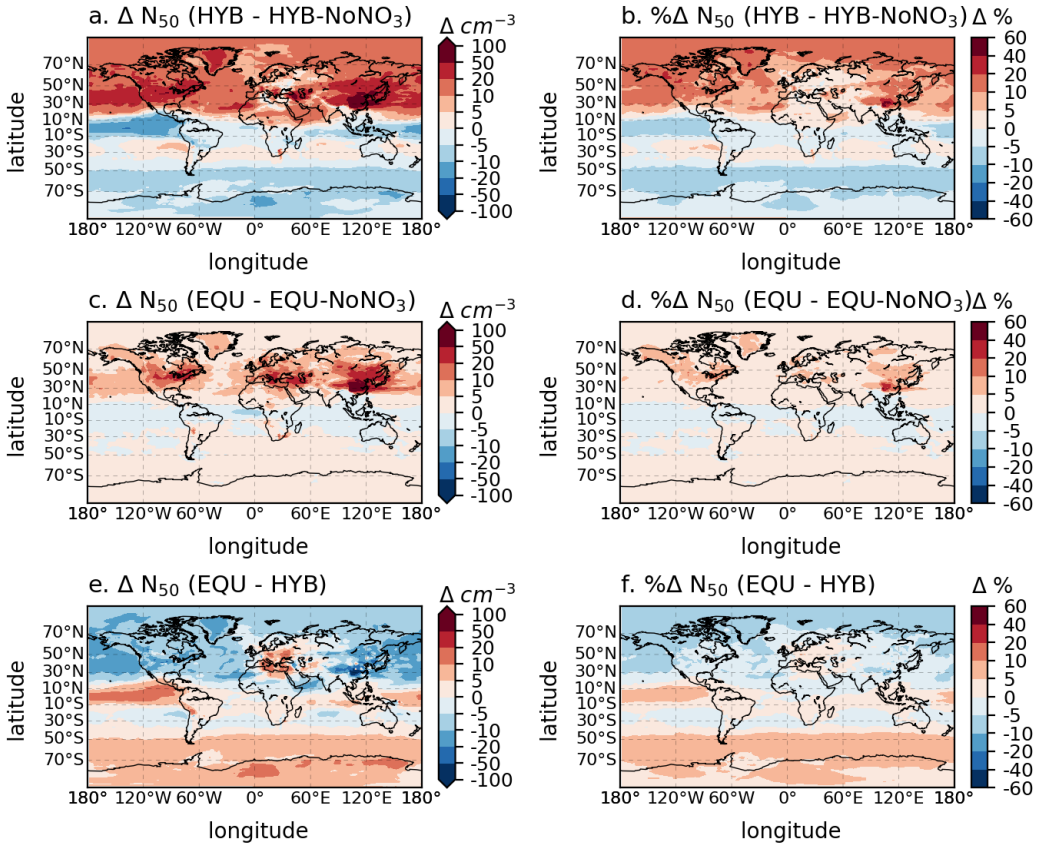

Figure 6.7 *Absolute (left column) and relative (right column) changes in annual mean middle cloud level (~ 720 hPa) soluble N_{50} when nitrate aerosol formation is included via HYB (top row) and EQU (middle row) partitioning approaches. Bottom row shows the absolute and relative difference (EQU – HYB) in simulated soluble N_{50} between both gas-particle partitioning approaches.*

partitioning approach results in widespread N_{50} increases of between 10 and 20% over the Arctic, with increases of at least 5% over large regions of Canada, Russia and parts of Asia. These latter continental regions have high particle concentrations on which nitric acid uptake can occur (Fig. 6.2) and nitrate aerosol formation promotes growth and, therefore, transport of particles from these regions and higher altitudes over the Arctic. Conversely, the formation of nitrate aerosol using the hybrid scheme results in decreases in N_{50} over most marine regions, with the exception of the Arctic and adjacent oceanic regions as mentioned and also much of the ocean between approximately 10° N and 30° N where N_{50} is increased. The decreases in low cloud level N_{50} simulated using the HYB scheme are most prominent between approximately 30° S and 50° S, where concentrations fall by up to 20%. Though nucleation mode particle

concentrations are similarly low over Southern Hemisphere marine regions as over the Arctic, the partitioning of nitric acid to particles is favourable at colder temperatures in the Arctic.

Using the equilibrium partitioning approach (Fig. 6.6c and 6.6d), nitrate aerosol formation has a smaller relative influence on N_{50} concentrations in most regions, compared to changes when the hybrid approach is applied (at low cloud level). Relative changes in EQU N_{50} are below 5% over most of the globe. Overall, low cloud level N_{50} concentrations are underestimated by up to 20% over high latitude Northern Hemisphere continents and the Arctic Ocean by the equilibrium scheme but are overestimated over much of the Southern Hemisphere, also by up to 20%, compared to those simulated using the hybrid approach (Fig 6.6e and 6.6f). Overall, regional changes in N_{50} are under-represented by the equilibrium scheme compared to changes when the hybrid scheme is applied.

Figure 6.7 shows the influence of nitrate aerosol formation on N_{50} using both partitioning approaches at middle cloud level (~ 720 hPa). At the middle cloud level, nitrate aerosol formation by the hybrid approach (Fig 6.7a and 6.7b) results in more widespread increases in N_{50} than at low cloud level over the Northern Hemisphere. Relative increases in HYB N_{50} are consistent (+10-20%) in magnitude between the low and middle cloud level over the Arctic. The response of HYB N_{50} to nitrate aerosol formation is relatively modest (< ± 5% in most regions) at middle cloud level in the Southern Hemisphere compared to changes at low cloud level. Though notably, nitrate aerosol formation results in increases in HYB N_{50} at middle cloud level centred on 30° S, whereas HYB N_{50} was strongly decreased (by up to 20%) at the lower level.

At middle cloud level, changes in Northern Hemisphere EQU N_{50} when nitrate is formed (Fig. 6.7c and 6.7d) are generally lower in magnitude than those simulated using the hybrid scheme, with the exception of Eastern Europe. Like at low cloud level, the equilibrium scheme differs from the hybrid scheme by increasing N_{50} over the Antarctic Ocean, although increases in EQU N_{50} extend further northward into the Southern Hemisphere at middle cloud level than at the low cloud level. Like at the surface, decreases in EQU N_{50} around the equator are less prominent than those simulated using the hybrid scheme. Overall,

nitrate aerosol formation applying the equilibrium scheme results in a smaller N_{50} response than is simulated using the more physically realistic hybrid gas-particle partitioning approach. Therefore at middle cloud level, the equilibrium assumption results in larger absolute under- and overestimates in N_{50} over many regions (Fig. 6.7e) compared to the hybrid simulated N_{50}. Compared to N_{50} simulated using the hybrid approach, EQU N_{50} is underestimated over many regions of the Northern Hemisphere and also between 10° S and 40° S where it was greater than HYB N_{50} at low cloud level. The magnitude of underestimations in EQU N_{50} relative to the greater HYB N_{50} are relatively less important at middle cloud level, however, while relative overestimations South of 50° S and between 10-40° S are higher than at low cloud level.

Given that emissions are identical across all the sensitivities in this Chapter, the regional differences in the magnitude and spatial distribution of N_{50} between the hybrid and equilibrium approach arise ultimately from differences in the nitric acid uptake across the aerosol size distribution. The aerosol surface area is more greatly enhanced when the hybrid approach is applied because nitric acid is partitioned more strongly into the nucleation, Aitken and accumulation modes. Conversely, the equilibrium approach partitions a larger proportion of the available nitric acid into the coarse mode, adding to the aerosol mass at the expense of partitioning of nitric acid to the nucleation, Aitken and accumulation modes (see Chapter 4 Fig. 4.14).

Changes to the aerosol size distribution resulting from nitrate aerosol formation can influence a large range of microphysical processes, including dry and wet deposition rates, nucleation rates and trace gas uptake. A process-based model evaluation, for example using a perturbed parameter ensemble and/or emulator-style (e.g. Lee et al., 2013; Sengupta, 2017; Butt et al., 2017), would therefore be required to more fully understand the mechanisms driving regional responses of N_3 and soluble N_{50} to nitrate aerosol formation. Alternatively sensitivities and feedbacks when nitrate aerosol formation is included could be investigated using an adjoint model. Such models are not available for GLOMAP-mode at present but have been developed for other inorganic aerosol solvers (Henze et al., 2007; Pye et al., 2009; Karydis et al., 2012a; Karydis et al., 2012b; Lee et al., 2014).

Table 6.2 also shows global annual mean surface, low cloud and middle cloud level soluble N_{50} from each experiment and changes in soluble N_{50} when nitrate aerosol formation is included in simulations, using both gas-particle partitioning approaches. As with N_3, the influence of nitrate aerosol formation on global mean soluble N_{50} varies with altitude. On the global mean scale, nitrate aerosol formation using the hybrid approach results in a greater change to global mean N_{50} at middle cloud level than at the surface and low cloud levels, with a net increase of +2.47% because there is higher availability of nucleation mode particles on which aerosol growth can occur at this altitude. It has been shown, however, that the choice of partitioning approach when including nitrate aerosol formation can have widely varying regional effects on N_{50}. The regional importance of the partitioning approach for changes in N_{50} isn't apparent in these global mean values because the global mean changes result from cancellations between regional increases and decreases in N_{50}. The hybrid approach, for example, results in smaller magnitude changes in global mean N_{50} (±0.2%) at lower levels than the equilibrium approach (~ +1.1%) despite having a larger effect on N_{50} in several regions.

6.3.5.2 Seasonal mean concentrations

Given that nitrate aerosol concentrations vary seasonally (Chapter 4), it is expected that its influence on N_{50} will also vary throughout the year. Figure 6.8 shows the relative changes in annual and seasonal mean surface and middle cloud level zonal mean N_{50} concentrations when nitrate aerosol is formed via the hybrid and equilibrium partitioning approaches.

The top row of Figure 6.8 shows the seasonal variability in the influence of nitrate aerosol formation on N_{50} using the *hybrid* scheme at the low cloud and middle cloud level. On annual mean timescales, nitrate aerosol formation decreases low cloud level zonal mean N_{50} at all latitudes south of approximately 40 °N. Nitrate formation causes increases in annual mean zonal N_{50} at the surface to the north of this boundary, with a peak 15% fractional increase of annual zonal mean N_{50} around 90 °N. The greatest fractional decrease in annual surface zonal mean N_{50} occurs around 40° S where marine conditions dominate. Seasonally, the relative increase in Northern Hemisphere surface N_{50} is greatest in the autumn and winter months, where colder conditions favour greater nitrate

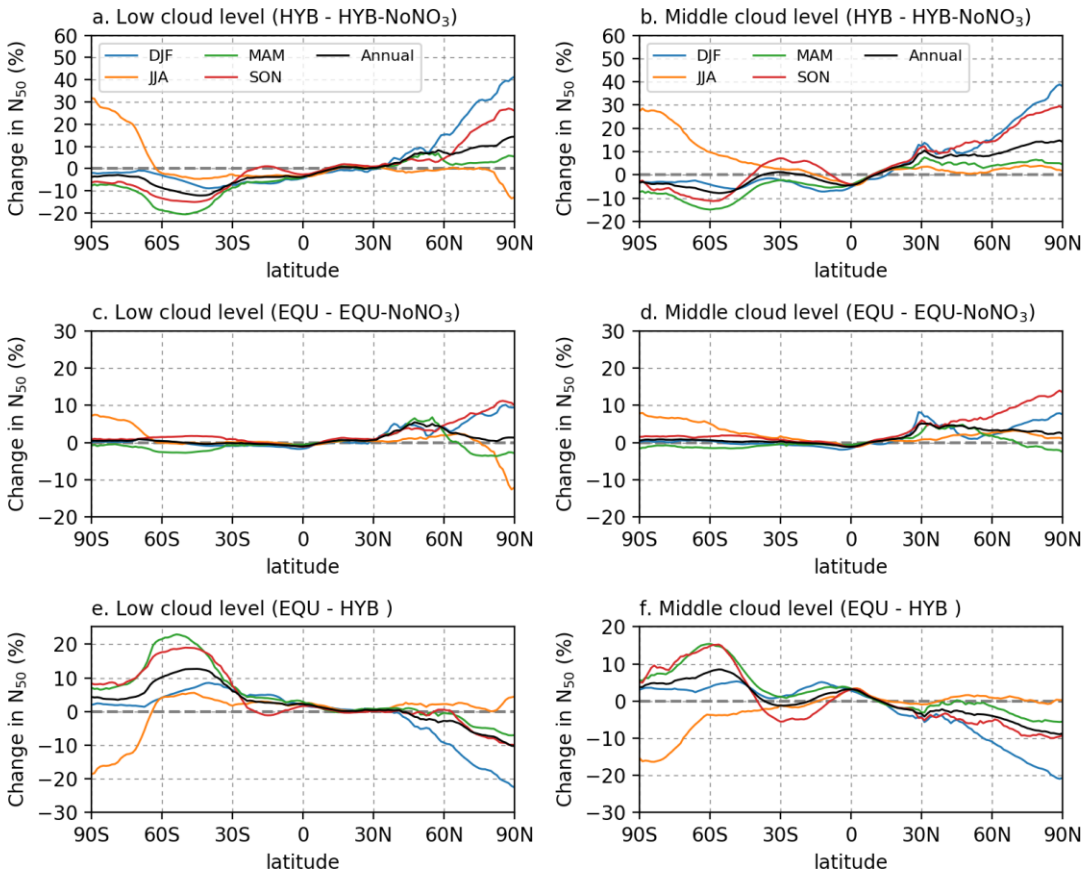

Figure 6.8 *Relative changes in annual and seasonal zonal mean soluble N_{50} at (left column) low cloud level and (right column) middle cloud level, when nitrate aerosol formation is included using the (top row) hybrid partitioning approach and (middle row) equilibrium partitioning approach. Bottom row shows the relative difference (EQU – HYB) in simulated zonal mean soluble N_{50} between both gas-particle partitioning approaches.*

aerosol formation. Wintertime zonal mean N_{50} is increased by a peak 41% at 90° N when HYB nitrate aerosol formation is accounted for. Greater relative increases in low cloud level N_{50} at higher latitudes arise as result of lower background aerosol state in this region. Conversely, in JJA, nitrate formation results in a peak seasonal mean decrease in zonal mean surface N_{50} of 13% near 90° N relative to the zero nitrate baseline, and to large increases in the Southern Hemisphere high latitudes, peaking at +32% at 90° S.

At middle cloud level (Fig. 6.8b), it can be seen again that the greater increase in global annual mean N_{50} (Table 6.2) at this level arises from more widespread increases in N_{50} over the Northern Hemisphere and smaller decreases in N_{50} over the Southern Hemisphere latitudes than at low cloud level. The patterns of

seasonal change in annual zonal mean N_{50} are broadly consistent with those simulated at low cloud level, except for larger increases (or weaker decreases) in N_{50} in the lower mid-latitudes of each Hemisphere and for changes in the JJA zonal mean N_{50}. In JJA, the response of zonal mean N_{50} is smaller in the high latitudes at middle cloud level, such that all seasons experience increases in zonal mean N_{50} north of ~ 15 °N, and increases in JJA zonal mean N_{50} are also more widespread over the Southern Hemisphere.

The second row of Figure 6.8 shows relative changes in low and middle cloud level N_{50} when nitrate aerosol is formed using the *equilibrium* partitioning approach. At both cloud levels, the fractional response of zonal mean EQU N_{50} to nitrate aerosol formation is weakened overall and is subject to lower seasonal variability than the fractional response in zonal mean HYB N_{50}. As seen for HYB N_{50}, the fractional increases in zonal mean EQU N_{50} are greatest in JJA at 90° S (~ +7-8% at both cloud levels) and in DJF and SON at ~ 90° N (~ +10% at low cloud level and up to +14% at middle cloud level), though the magnitude of the response in N_{50} is smaller than that of HYB N_{50}. Similarly, the equilibrium scheme also results in the greatest fractional decreases in zonal mean N_{50} in JJA at 90° N (-12%) at low cloud level, although the change in zonal mean N_{50} is again smaller in magnitude than changes simulated using the hybrid approach. The pattern of seasonal changes in zonal mean N_{50} are therefore more robust in these regions, with the choice of gas-particle partitioning mechanism having less of an impact on the latitudinal and seasonal distribution of changes in zonal mean N_{50}.

The final row of Figure 6.8 shows the relative under and over-estimations in soluble N_{50} simulated using the equilibrium approach, compared to using the hybrid approach. Overall (Fig. 6.8e), compared to the hybrid approach at low cloud level, the above effects result in an underestimation of MAM, SON and DJF zonal mean N_{50} at latitudes north of 40 °N. However, zonal mean N_{50} concentrations are overestimated across many seasons by the equilibrium approach, in particular over the equator and Southern Hemisphere mid-latitudes, relative to the hybrid approach. Overall, the combined influences of nitrate formation over the year result in the overestimation of annual zonal mean N_{50} by the equilibrium approach in the Southern Hemisphere, with up to a 10% underestimation of N_{50} north of 30 °N. At middle cloud level (Figure 6.8f),

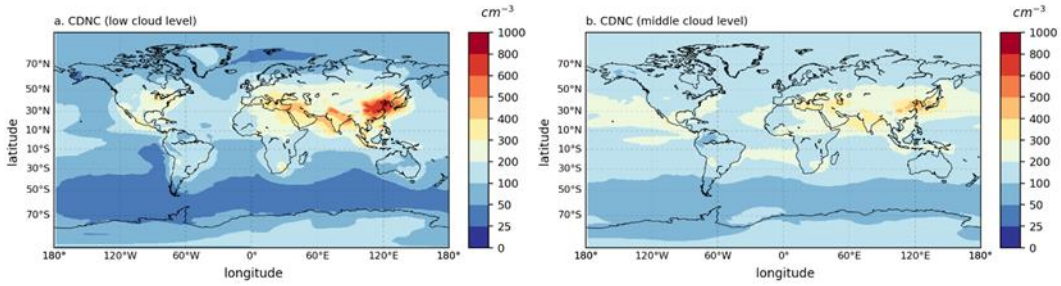

Figure 6.9 *Annual mean (a) low cloud level (~ 900 hPa) and (b) middle cloud level (~ 720 hPa) cloud droplet number concentration as simulated using the hybrid (HYB) partitioning approach.*

underestimations in middle cloud level zonal mean N_{50} by EQU are more widespread over the Northern Hemisphere than at low cloud level, with underestimations extending from approximately 10 to 90° N in most seasons.

The greatest overestimations in zonal mean EQU N50, relative to HYB N_{50}, across several seasons in the Southern Hemisphere are shifted more towards the higher latitudes at middle than at low cloud level, though the relative underestimations are lower in magnitude than at low cloud level. This southward shift results in greater agreement of the annual zonal mean N_{50} in the Southern Hemisphere mid-latitudes between the two partitioning schemes. Despite both schemes simulating increases in wintertime N_{50} at 90° N and 90° S when nitrate aerosol is formed, indicating a robust response coincident with colder temperatures which are favoured for nitrate aerosol formation, the relative underestimation of N_{50} by the equilibrium approach, compared to the hybrid approach, is particularly apparent in the high latitudes. The low background N_{50} at these latitudes results in greater relative sensitivity of N_{50} to the partitioning approach, where the hybrid approach encourages nitric acid uptake to be distributed over a higher number of smaller particles.

6.3.6 Change in cloud droplet number concentration

6.3.6.1 Annual mean concentrations

Figure 6.9 shows the spatial distribution of annual mean simulated CDNC with nitrate aerosol formation included via the hybrid partitioning approach at low and middle cloud level. The distribution of CDNC reflects the surface N_{50} distribution with the greatest concentrations distributed over polluted regions

Table 6.2 *Annual mean global low cloud (~ 900 hPa) and middle cloud (~ 720 hPa) level CDNC, with and without nitrate aerosol formation, as simulated using the hybrid (HYB) and equilibrium (EQU) gas-particle partitioning approaches. Relative changes are given in brackets as percentages.*

	CDNC (# cm^{-3})	Change in CDNC
	Low cloud level	
EQU-NoNO$_3$	126.2	-
HYB-NoNO$_3$	126.9	-
EQU	128.1	+1.86 (+1.48%)
HYB	129.0	+2.18 (+1.72%)
	Middle cloud level	
EQU-NoNO$_3$	160.0	-
HYB-NoNO$_3$	160.1	-
EQU	160.8	+0.88 (+0.56%)
HYB	164.6	+4.52 (+2.82%)

of the Northern Hemisphere. Polluted continental regions have simulated CDNC between 100 and 1000 cm^{-3} at low cloud level. Again, continental concentrations are likely to be underestimated because the simulations here don't account for boundary layer nucleation. Annual mean CDNC at low cloud level varies between 25 and 200 cm^{-3} over marine regions, with greater concentrations over regions influenced by continental outflows. Comparison to the annual mean CDNC at middle cloud level shows that CDNC over source regions tend to decrease with altitude, while CDNC is increased over many remote regions at higher levels.

Table 6.2 shows the global annual mean CDNC calculated at low and middle cloud level for each experiment and the changes in CDNC when nitrate aerosol formation is included using both the hybrid and equilibrium gas-particle partitioning approaches. The global mean CDNC increases with altitude between

these model levels, driven by increased CDNC over many remote marine regions (Fig. 6.9). At low cloud level, global mean CDNC is increased by 1.72% when nitrate aerosol formation is included using the hybrid partitioning approach. The relative influence of nitrate aerosol formation on global mean CDNC is slightly larger at middle cloud level (+2.82%) than at low cloud level using the hybrid approach. Using the equilibrium approach to treat nitrate aerosol formation yields a similar increase in global mean CDNC (+1.48%) to the hybrid approach at low cloud level. However, the influence of nitrate aerosol formation on global mean CDNC using the equilibrium approach decreases between the low and middle cloud level (to +0.56%), therefore underestimating the influence of nitrate aerosol formation on global mean CDNC compared to the hybrid approach at middle cloud level.

Figure 6.10 shows the annual mean change in CDNC distribution at *low cloud* height when nitrate aerosol formation is considered using both the hybrid and equilibrium partitioning approaches. Using the hybrid partitioning approach (Fig. 6.10a), spatial patterns in low cloud level CDNC change broadly follow changes in N_{50} (Fig. 6.6a) in the Northern Hemisphere, but with more widespread increases in CDNC than found for N_{50} in the Southern Hemisphere (e.g. over the Antarctic). Under the HYB approach, the greatest absolute and relative increases in CDNC of up to 100 cm^{-3} (up to 60%) occur in hotspot regions over China and North America (Fig 6.10a and b), along with widespread relative increases of up to 40% over the Arctic and high latitudes of the Northern Hemisphere. Absolute increases, of up to 50 cm^{-3}, arise over much of northern India, Europe, central Asia and North America. Relative to the equivalent 'no nitrate' simulation, nitrate aerosol formation results in at least a 5% increase in annual mean low cloud level CDNC over most of Europe, North America and Asia, but also results in decreases of at least 5% over much of the Southern Hemispheric oceans.

Figure 6.11 shows the annual mean absolute and relative changes in the global distribution of CDNC again, but at *middle level* cloud height. It can be seen that, like N_{50} (Fig. 6.7), the influence of nitrate aerosol formation on CDNC varies with altitude. Nitrate aerosol formation acts to increase middle level HYB CDNC over most regions, with the main exception being over equatorial oceans where CDNC in the equatorial Pacific decrease by up to 10%. Generally, relative increases in

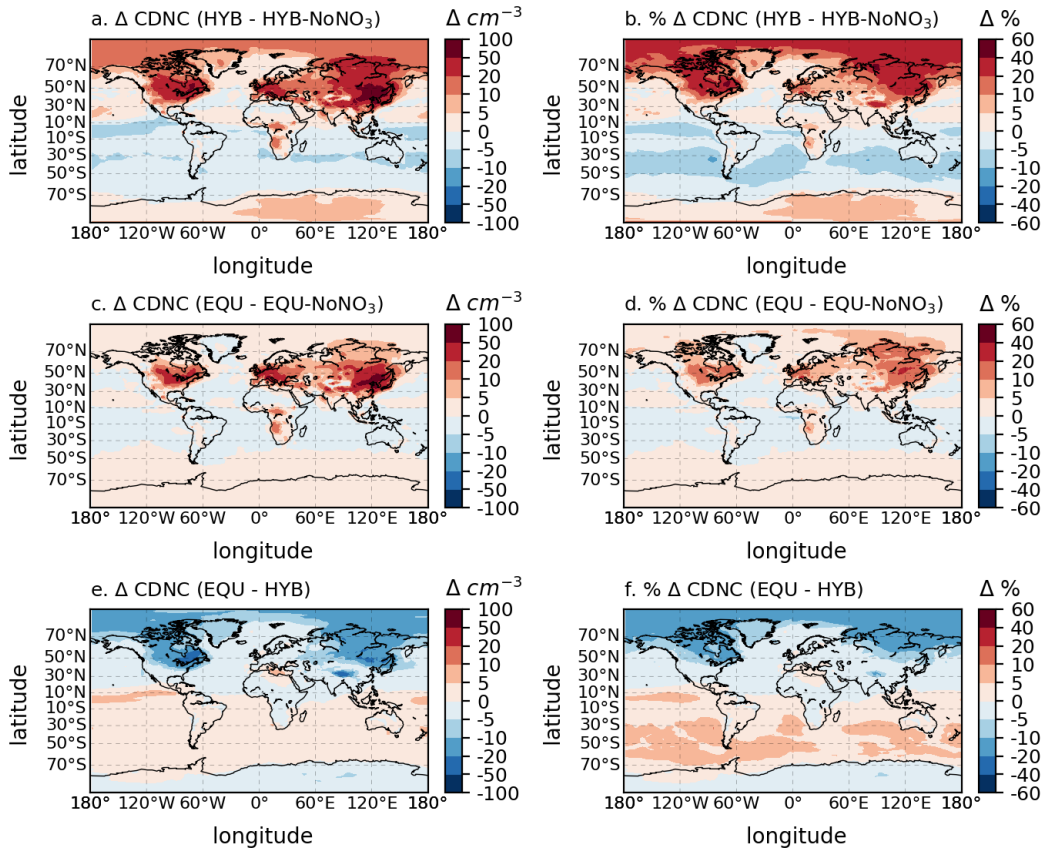

Figure 6.10 *Absolute (left column) and relative (right column) changes in annual mean low cloud level (~ 900 hPa) CDNC when nitrate aerosol formation is included via HYB (top row) and EQU (middle row) partitioning approaches. Bottom row shows the absolute and relative difference (EQU – HYB) in simulated CDNC between both gas-particle partitioning approaches.*

HYB CDNC at middle cloud level are larger over most oceanic regions but smaller over most Northern Hemispheric continental regions and the Arctic than at low cloud level. Vertical variability in HYB CDNC change is apparent over the Southern Hemisphere oceans where nitrate formation contributes to small but widespread increases of up to 10% in middle cloud level CDNC. This contrasts with changes in these regions at low cloud level, where CDNC was reduced, though subtle changes in these low background concentration regions can have large consequences for the relative change in CDNC.

As seen for N_{50}, the choice of gas-particle partitioning approach influences the change in CDNC when nitrate aerosol formation is included. At both cloud levels, the change in CDNC simulated using the equilibrium approach (Fig. 6.10c and 6.11c) broadly align with changes in N_{50}. At low cloud level, nitrate aerosol

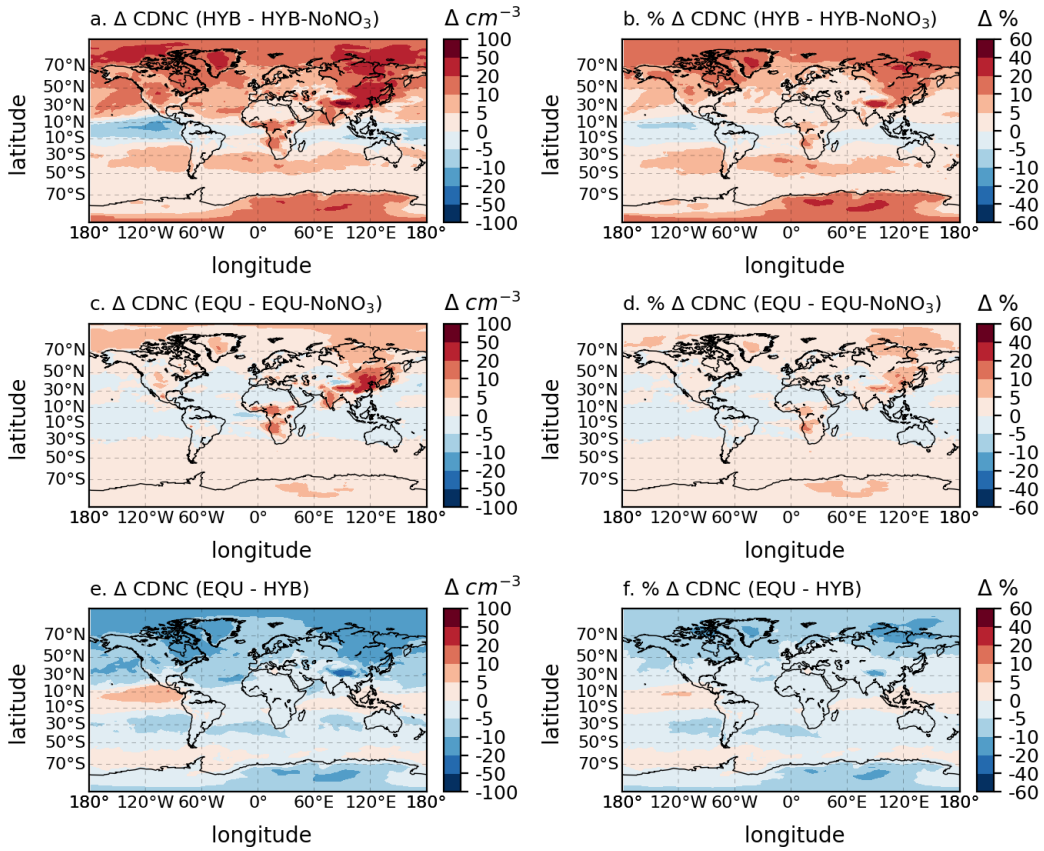

Figure 6.11 *Absolute (left column) and relative (right column) changes in annual mean middle cloud level (~ 720 hPa) CDNC when nitrate aerosol formation is included via HYB (top row) and EQU (middle row) partitioning approaches. Bottom row shows the absolute and relative difference (EQU – HYB) in simulated CDNC between both gas-particle partitioning approaches.*

formation via the equilibrium method has a more moderate influence on CDNC than the hybrid approach over most regions. Overall, comparison of the CDNC simulated using both gas-particle partitioning approaches shows that the equilibrium approach results in the underestimation of mid- and high- latitude Northern Hemisphere CDNC and of Antarctic CDNC, relative to those calculated using the hybrid approach, at both cloud levels. The use of an equilibrium partitioning approach results in overestimations of CDNC in the equatorial Pacific at both altitudes. The influence of the partitioning approach varies with altitude, however, across the mid- to high- latitudes of the Southern Hemisphere, with the equilibrium scheme tending to overestimate CDNC in this region at low cloud level and underestimate concentrations at middle cloud level relative to using the hybrid approach.

Figure 6.12 presents annual mean zonal changes in CDNC simulated using the hybrid and equilibrium approaches at both cloud levels, in addition to seasonal changes (to be discussed in Section 6.3.6.2). At low cloud level, both partitioning approaches result in annual zonal mean CDNC increases north of ~ 30 °N. At low cloud level, the greatest relative increase in annual zonal mean CDNC is 22% at 90° N by the hybrid approach and 8% around 50° N by the equilibrium approach. At middle cloud level the greatest increase in annual zonal mean CDNC arises at 90° N by both approaches, with an 18% increase in HYB CDNC and a 4% increase in EQU CDNC. It is shown again here that the equilibrium approach suppresses increases in annual mean CDNC from nitrate aerosol formation over most of the Northern Hemisphere at both cloud levels. The zonal mean comparisons reflect the tendency of the equilibrium approach to overestimate annual mean CDNC in the Southern Hemisphere mid-latitudes at low cloud level and underestimate at middle cloud level relative to the hybrid scheme. Annual zonal mean CDNC is increased south of approximately 70° S when nitrate aerosol is formed using both approaches but CDNC is underestimated by the equilibrium scheme at both levels and by up to 7% at middle cloud level.

Xu and Penner (2012) quantified the influence of nitrate aerosol formation on simulated CDNC at low cloud level (around 930 mb) using a hybrid dynamic method (Feng and Penner, 2007) in the IMPACT global chemistry transport model. The results of that study were presented in Section 2.4.8.1. Xu and Penner (2012) simulated a 2.7% increase in global mean CDNC, which is larger than that simulated using either partitioning approach at low cloud level in this thesis but highly comparable to the global mean increase of 2.8% simulated using the hybrid approach at middle cloud level. Xu and Penner (2012) simulated a peak relative increase in annual zonal mean CDNC of 20% around 50° N while nitrate aerosol formation using the hybrid approach in this study results in an increase in zonal mean low cloud level CDNC of 13% at this latitude. However, the hybrid approach in this study simulates greater increases in zonal mean CDNC at higher latitudes on the annual mean timescale than Xu and Penner (2012), with increases in CDNC peaking at 90 °N, while Xu and Penner (2012) simulated much smaller relative changes in CDNC north of 50 °N. The more substantial changes simulated in this work could result from higher nitrate concentrations in this

region, resulting in greater increases in CDNC, or could arise from a lower 'zero-nitrate' aerosol background in this study. The findings of this study are similar to Xu and Penner (2012) in simulating small decreases in zonal mean CDNC at latitudes where nitrate aerosol formation has provided an additional condensation sink for new particle formation. Decreases in CDNC simulated using the hybrid approach are more widespread than those simulated by Xu and Penner (2012) and, in this regard, the equilibrium approach produces more comparable results.

6.3.6.2 Seasonal mean concentrations

Figure 6.12 shows the seasonal variability in zonal mean CDNC simulated using both partitioning approaches. As seen for N_{50}, relative increases in the zonal mean CDNC are greatest in DJF over most of the Northern Hemisphere when nitrate aerosol formation is included using the hybrid approach (Fig. 6.12a and b), peaking at 57% and 39% near 90° N at low and middle cloud level, respectively. Relative increases in the Southern Hemispheric zonal mean CDNC peak in JJA at 69% and 59% at low and middle level cloud, respectively. The relative changes in zonal mean CDNC vary widely between seasons in the mid to high latitudes of each hemisphere, with the greatest variability found at the Poles. Here, the response in zonal mean CDNC to nitrate aerosol formation is greatest in the wintertime (and autumn at middle cloud level) and smallest in the summer months at both cloud levels. Seasonal zonal mean CDNC is increased over much of the Northern Hemisphere in DJF, MAM and SON at both cloud levels. Conversely, nitrate aerosol formation results in a decrease in zonal mean CDNC at low cloud level over DJF, SON and MAM (up to -14% in MAM around 50° S) in the Southern Hemisphere mid-latitudes, whereas zonal mean CDNC is increased over the same latitudes in several seasons, particularly JJA and SON, at middle cloud level. As conditions at these latitudes are marine dominated with high cloud cover, moderate fractional changes in CDNC can have a high impact on the nitrate CAE.

As seen with EQU N_{50} (Fig. 6.8c and d), the changes in zonal mean CDNC simulated when nitrate aerosol formation is treated using the equilibrium approach (Fig 6.12c and d) are more moderate over most seasons in comparison

to the response using the hybrid approach, at both cloud levels. In the Northern Hemisphere, fractional increases in zonal mean CDNC are greatest in MAM and

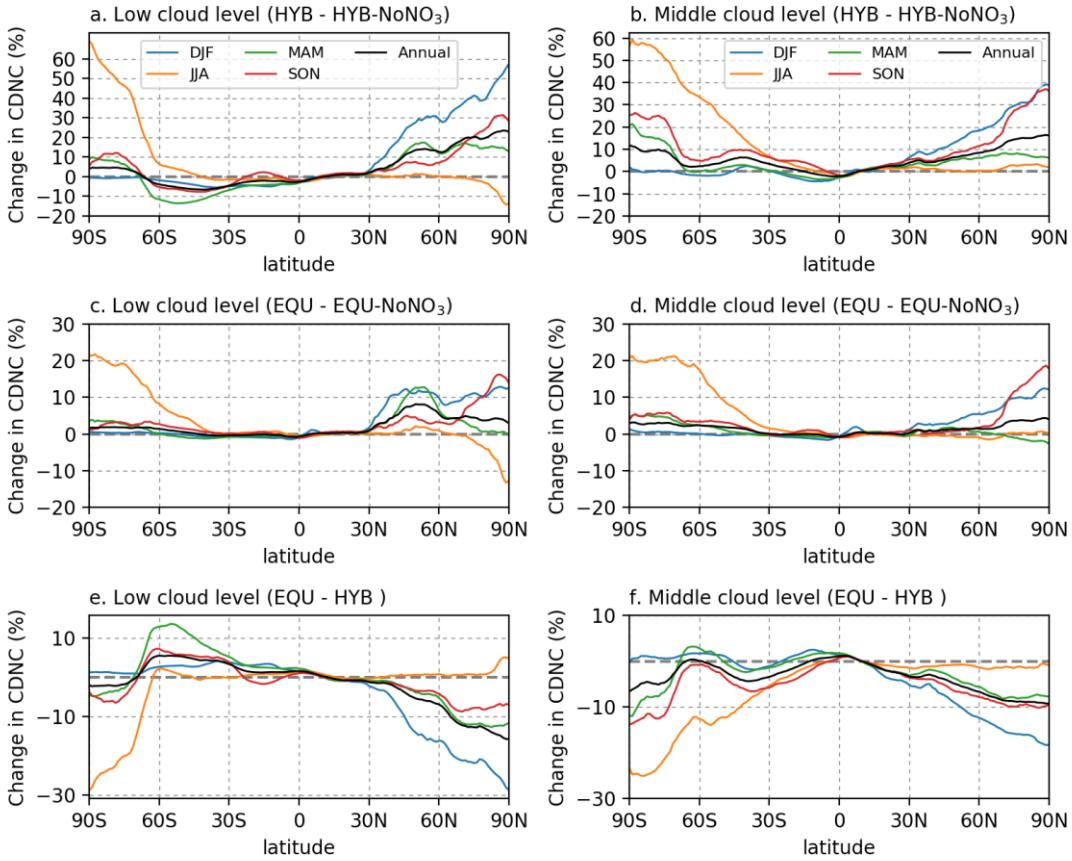

Figure 6.12 *Relative changes in annual and seasonal zonal mean CDNC at (left column) low cloud level and (right column) middle cloud level, when nitrate aerosol formation is included using the (top row) hybrid partitioning approach and (middle row) equilibrium partitioning approach. Bottom row shows the relative difference (EQU – HYB) in simulated zonal mean soluble* N_{50} *between both gas-particle partitioning approaches.*

DJF (both + 13%) in the mid-latitudes and in SON (+16%) and DJF (+ 13%) near 90° N at low cloud level as a result of nitrate aerosol formation (Fig 6.12c). At middle cloud level (Fig 6.12d), relative increases in the Northern Hemisphere zonal mean EQU CDNC peak in SON (+19%) and DJF (+12%) near 80° N. At low cloud level, the response of zonal mean EQU CDNC to nitrate formation is small (up to +4% in SON) over the Southern Hemisphere in all seasons with low seasonal variability except for JJA, where the relative change increases from around 40° S to peak at + 21% at 90° S. The magnitude of change in seasonal Southern Hemisphere zonal mean CDNC is similar at middle cloud level, except

for higher relative changes of around 20% in JJA extending further northward from 90° S to 60° S.

Overall, nitrate aerosol formation via the equilibrium approach tends to underestimate zonal mean CDNC at low cloud level in the Northern Hemisphere (Fig. 6.12e) compared to the hybrid approach, with greater underestimations in DJF (by up to 29%), MAM (up to 13%) and SON (by up to 8%). Similarly, Northern Hemisphere zonal mean CDNC at middle cloud level (Fig 6.12f) is underestimated by up to 18% (DJF), 12% (MAM) and 14% (SON) when the equilibrium approach is applied, compared to using the hybrid scheme. However, JJA mean CDNC concentrations are relatively unaffected in the Northern Hemisphere at both cloud levels by the choice of partitioning scheme. The equilibrium approach overestimates low cloud level zonal mean CDNC (Fig. 6.12e) over most of the Southern Hemisphere mid-latitudes in MAM, DJF and SON, compared to using the hybrid approach. The overestimation of MAM zonal mean CDNC peaks at 14% (~50° S), though DJF and MAM zonal mean CDNC remain within 10% of that simulated by the hybrid scheme. JJA zonal mean CDNC is relatively unaffected at low cloud level by the choice of partitioning approach in the tropics and mid-latitudes but is substantially lower by 29% at 90° S using the equilibrium approach. At middle cloud level (Fig. 6.12f), JJA zonal mean CDNC is similarly underestimated by up to 25% at 90° S relative to hybrid-simulated CDNC but, unlike at low cloud level, is underestimated over most of the Southern Hemisphere. MAM and SON zonal mean CDNC are also underestimated by up to 12% and 14%, respectively, at 90° S by the equilibrium approach, compared to the hybrid scheme, though the partitioning approach has little influence (< 10%) on mid-latitude zonal mean CDNC in these seasons, nor in DJF.

6.3.6.3 Vertical variability in CDNC response

To investigate vertical variability in the CDNC response and its relation to the simulated PD nitrate CAE (Fig. 6.1), Figure 6.13 shows the latitudinal-altitudinal changes in CDNC at longitudes of 90° W and 11° E when nitrate aerosol formation is included in simulations. Regions of strong negative and positive PD nitrate CAE (Figure 6.1a) were simulated at these longitudes using the hybrid approach, which had large influences on the zonal mean PD nitrate CAE (Figure 6.1d).

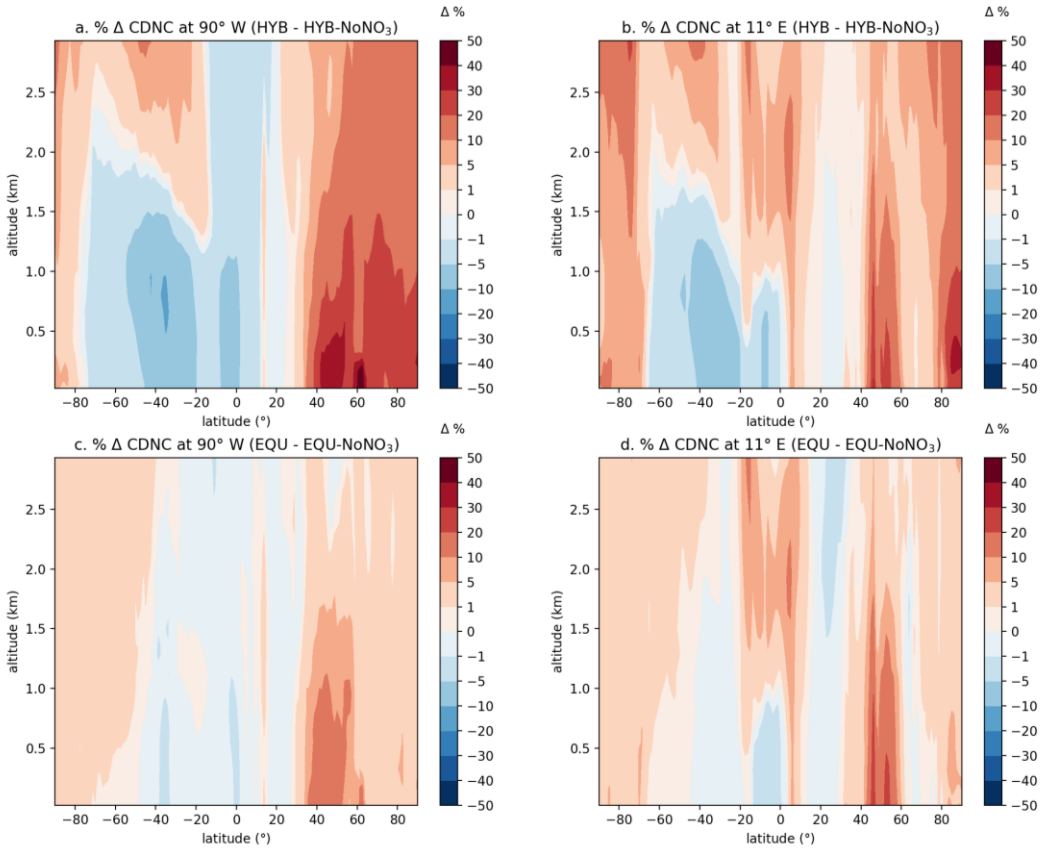

Figure 6.13 Relative changes in CDNC with altitude and latitude at (a + c) 90° W and (b + d) 11° E when nitrate aerosol formation is included in simulations using the hybrid scheme (top row) and equilibrium scheme (bottom row).

Figure 6.1a shows that relative increases in HYB CDNC persist above the surface in the mid to high latitudes of the Northern Hemisphere, with increases of at least 10% found at altitudes of 3km at 90° W. Decreases in CDNC by at least 1% also occur throughout the vertical column which, co-located with cloudy regions, contribute to the positive zonal mean PD nitrate CAE around the equator seen in Figure 6.1d. When nitrate aerosol formation is included, HYB CDNC is also decreased in the lowermost couple of kilometres in the southern hemisphere (by up to 20%) but decreases aloft (by up to 20% at 3 km). Increases in HYB CDNC aloft lead to negative PD nitrate CAE signal around 30° S. However, decreases in CDNC in the lowermost kilometres around 50° S, combined with higher cloud fraction at lower altitudes, lead to a positive CAE at this latitude. The PD nitrate

CAE is therefore sensitive to the vertical variability in CDNC response to nitrate aerosol formation, modulated by its co-dependence on cloud location.

As determined in preceding sub-sections of this chapter, Figure 6.13c again shows a generally weaker relative response of CDNC to nitrate aerosol formation using the equilibrium scheme. The resulting nitrate CAE calculated with the equilibrium approach is therefore smaller in magnitude than that calculated using the hybrid approach at this longitude (Figure 6.1b), and produces an overall weaker zonal mean CAE in turn (Figure 6.1d).

At 11° E, regions with increasing or decreasing HYB CDNC are broadly similar to those at 90° W, with the exception of the tropics where nitrate aerosol formation results in CDNC increases above cloud base. This increase in CDNC drives a strong negative PD nitrate CAE in the region, though the global zonal mean CAE (Figure 6.1d) remains positive as a result of decreasing CDNC over other regions of the tropics e.g. at 90° W. Like at 90° W, the sign of CDNC change reverses from negative to positive between low and middle cloud levels, with implications for the cloud-modulated PD nitrate CAE.

Increases in CDNC over the tropics are of similar magnitude at 11° E when the equilibrium approach is applied to treat nitrate aerosol formation, resulting in similar PD nitrate CAE with both schemes over this longitude. However, as previously ascertained (Fig. 6.10e and Fig. 6.12e), the equilibrium scheme underestimates the reduction in CDNC over the lowermost 2 km of the Southern Hemisphere mid-latitudes and also underestimates increases in CDNC over the high latitudes of both hemispheres, relative to applying the hybrid approach. The smaller reduction in EQU CDNC, relative to reductions in HYB CDNC, results in a sign reversal of the PD nitrate CAE over much of the Southern Hemisphere at 11° E, 90° W and other longitudes, between partitioning schemes. However, low wintertime insolation and relatively low cloudiness in the Polar regions meant that the PD nitrate CAE was less sensitive to the partitioning approach at higher latitudes than over the mid-latitudes.

6.3.7 Explanation of regional PD nitrate CAE

The magnitude and spatial distribution of the PD nitrate CAE described in Section 6.3.1 is explained by its co-dependency on changes in CDNC, the spatial distribution of low and middle level clouds and insolation. The regional PD nitrate CAE was sensitive to the gas-particle partitioning approach employed because of differences in the response of CDNC to nitrate aerosol formation. The influence of nitrate aerosol formation on particle concentrations and CDNC using both partitioning approaches has been examined in sub-sections 6.3.2 to 6.3.6 and the spatial distribution of clouds from the ISCCP-D2 database was shown in Chapter 3 Figure 3.3.

As in other studies (e.g. Spracklen et al., 2011b), it is seen that the distribution of the PD nitrate CAE is strongly weighted to the global distribution of clouds. For example, nitrate aerosol formation exerts a negative radiative forcing over most of the Northern Hemisphere under the HYB partitioning approach as a result of increases in low cloud height CDNC. Another clear feature of the PD nitrate CAE (particularly apparent in Figure 6.1d) is the positive CAE associated with nitrate aerosol formation in the tropics. Despite changes in HYB CDNC being relatively small on the zonal mean scale (Figure 6.12), local decreases in HYB CDNC of up to 10% over cloudy marine regions bordering the equator produce the relatively strong positive zonal mean CAE. Relative regional decreases in EQU CDNC peak at 5%, leading to an approximately 50% reduction in the peak positive zonal mean nitrate CAE compared to the hybrid approach. This again reinforces that the CAE is sensitive to small changes in CDNC over cloudy regions.

There is also a positive CAE associated with nitrate aerosol formation around 50° S when applying the hybrid approach. Unlike in previous studies, this study finds that the PD CAE is affected by vertical variability in the influence of nitrate aerosol formation on the CDNC. The positive nitrate CAE around 50° S results from decreases in CDNC at low cloud level. The cloud fraction is greater at the low cloud level than at the middle cloud level, hence the effect of decreasing CDNC at low cloud level dominates over increases at middle cloud level. Conversely, middle cloud level increases in CDNC between ~25° S and ~ 45° S result in a negative overall CAE using the hybrid approach despite CDNC having decreased at low cloud level. The nitrate CAE can therefore not be explained by

changes in CDNC at cloud base alone. Insolation also plays a role, with a weakly negative annual mean PD nitrate CAE arising over the Arctic despite nitrate aerosol formation leading to large relative increases in CDNC this region.

The equilibrium scheme produces a less strongly negative, with sometimes sign-reversed (i.e. positive), PD CAE than the hybrid scheme over the Northern Hemisphere when nitrate aerosol formation is considered. Regions of more weakly negative CAE using the equilibrium approach are attributable to the generally smaller increases in CDNC when nitrate aerosol formation is included in simulations. Another key region where the regional PD nitrate CAE is sensitive to the gas-particle partitioning approach is over the zonal band centred around 30° S, where the equilibrium approach simulates weaker increases in CDNC than the hybrid approach, coincident with regions of large middle-level cloud cover.

6.4 Summary and Conclusions

This chapter comprises the first study of nitrate aerosol radiative effects using a two-moment aerosol microphysics scheme in the UM-UKCA model. The present-day radiative effect of nitrate aerosol formation, via its influence on cloud albedo, has been quantified using a hybrid and equilibrium approach to treat the semi-volatile gas-particle partitioning of nitric acid to nitrate aerosol. The hybrid approach is considered to give the better representation of the nitrate CAE because it applies a more physically realistic representation of the uptake of the gas-particle partitioning of nitrate aerosol across the particle size distribution. The magnitude and spatial distribution of the PD nitrate CAE using both approaches has been assessed by considering the influence of nitrate aerosol formation on aerosol number concentrations (N_3 and N_{50}) and cloud droplet number concentrations.

The formation of nitrate aerosol results in a global mean radiative effect of -0.007 W m^{-2} when applying the hybrid partitioning mechanism, with a more strongly negative CAE in the Northern Hemisphere (-0.02 W m^{-2}) than in the Southern Hemisphere (+0.008 W m^{-2}). On the global mean scale, regions of negative CAE are partly offset by regions of positive CAE elsewhere, which weakens the final estimate of the global mean PD nitrate CAE. Nitrate aerosol formation strongly

affects annual mean regional N_{50} and CDNC when applying the hybrid partitioning approach. Increases in CDNC arise over most of the Northern Hemisphere when nitrate aerosol formation is included in UM-UKCA, including widespread regional increases in annual mean CDNC by up to 40% over the Arctic and high latitude continents in the Northern Hemisphere. Zonal mean CDNC is increased in most seasons, excluding JJA, over the Northern Hemisphere mid-to-high latitudes, with the greatest relative seasonal mean increases occurring in DJF.

The influence of nitrate aerosol formation on particle number concentrations and CDNC varies spatially in both the horizontal and vertical dimensions. Applying the hybrid gas-particle approach, nitrate aerosol formation has a greater relative influence on global mean CDNC at middle cloud level (+2.8%; ~ 720 hPa) than at lower cloud level (~ 900 hPa) as a result of more widespread increases in CDNC over the Southern Hemisphere and marine regions in the Northern Hemisphere at this altitude. The magnitude of change in global mean CDNC at the low cloud level is more greatly reduced by the averaging of larger positive and negative regional influences on CDNC.

Locally, the greatest negative PD nitrate radiative forcing in the Northern Hemisphere using the hybrid approach, of up to -0.5 W m^{-2}, occurs over cloudy marine regions coincident with moderate increases in CDNC. The negative radiative forcing is countered on the global scale, however, by regional forcings of up to +1 W m^{-2} arising from moderate increases in CDNC over many cloudy marine regions in the tropics. Nitrate aerosol formation can therefore have far-reaching impacts on regional radiative effects at great distances from precursor source regions. In the Southern Hemisphere, the negative local PD radiative forcing associated with nitrate aerosol formation is greatest (up to -0.5 Wm^{-2}) over marine regions with high middle level cloud fraction, where middle cloud level CDNC is increased by up to 10%. However, on the hemispheric mean scale, the local negative forcing is again countered by a positive local nitrate CAE (up to +0.5 W m^{-2}) over many equatorial regions and by positive forcing centred around 50° S, driven by decreases (by up to 20%) in low level cloud CDNC where the cloud fraction was larger than at higher altitudes.

The magnitude of the PD nitrate aerosol radiative effect is sensitive to the approach applied for the gas-particle partitioning of semi-volatile inorganic aerosol, with a positive PD global mean nitrate CAE (+0.011 W m^{-2}) calculated when the equilibrium approach is applied. Unlike with the hybrid approach, the equilibrium scheme produces a positive nitrate CAE in both hemispheres. This is because the influence of decreased CDNC in many cloudy equatorial regions dominates over the smaller increases in CDNC elsewhere. Overall, the equilibrium approach under-represents increases in CDNC in the Northern Hemisphere and at middle cloud level in the Southern Hemisphere when nitrate aerosol formation is included in simulations, compared to the changes simulated using the hybrid approach.

The response of N_3, N_{50} and therefore of CDNC to nitrate aerosol formation is complicated by changes in the aerosol size distribution, which has ramifications for most aerosol microphysical processes, including nucleation, precursor gas uptake and dry and wet deposition rates. Overall, two mechanisms are considered to be primarily responsible for the effects on CDNC found in this chapter. Firstly, the uptake of nitric acid onto existing aerosol contributes to the growth of particles to sizes that can be more readily activated to cloud droplets. Conversely, the enhanced surface area of particles leads to a larger condensational sink for potentially nucleating gases and coagulational sink of newly formed particles, resulting in decreased particle concentrations available for growth to CCN size.

The extent to which nitrate aerosol formation contributes to the mechanisms above is dependent on the approach applied for the gas-particle partitioning. The equilibrium approach overestimates the uptake of nitric acid into the coarse mode, relative to the hybrid approach, leading to an increase in the coarse mode aerosol mass at the expense of the fine mode nitrate aerosol formation (as shown in Chapter 4). Conversely, the hybrid approach partitions a greater portion of the available nitric acid into the smaller aerosol size ranges, therefore having a larger influence on the total aerosol surface area. Nitrate aerosol formation using the hybrid approach therefore results in greater enhancement of the condensation sink for potentially nucleating vapours. The hybrid approach also more effectively grows nucleation mode particles into more stable Aitken and

accumulation mode particles, with implications for the transport and deposition of nitrate aerosol.

In previous studies of speciated aerosol cloud albedo radiative effects, uncertainty ranges have been calculated by varying CDNC inputs to the radiative calculations, as defined using additional model sensitivity experiments e.g. to nucleation mechanisms, size distribution and global yields/source strengths (e.g. Scott et al., 2015; Spracklen et al., 2011b; Spracklen et al., 2011a; Scott et al., 2018; Rap et al., 2013; Butt et al., 2016). The global mean nitrate CAE is relatively small compared to the radiative effects of other aerosol species in these studies but is shown to be regionally important. Furthermore, the influence of nitrate aerosol formation on aerosol properties and PD radiative forcing is likely to be underestimated in this study because the simulations do not include representation of boundary layer nucleation. This should be addressed in future work. Comparison of the two gas-particle partitioning assumptions has given an indication of the uncertainty range arising from the size distribution of nitrate aerosol. However further sensitivities (i.e. precursor emission perturbations, with consideration given to the co-dependency of NO_x, NH_3 and SO_2 emissions) could constrain uncertainty in the nitrate CAE further. The overestimation of sulphate in the free troposphere (identified in Chapter 4) should also be considered and amended in future studies. There is considerable uncertainty in the radiative forcing calculations associated with the distribution of clouds. Uncertainty arises from ISCCP cloud retrievals and from applying a monthly-mean climatology to radiative calculations i.e. sub-grid and temporal variability in cloud cover.

Multi-model comparisons could contribute to defining the uncertainty range of the nitrate PD (and PI) CAE, though structural model differences (e.g. in representation of aerosol microphysical processes) would need to be considered. A more structurally self-consistent approach within UM-UKCA could involve adding nitrate aerosol formation to future perturbed parameter ensemble assessments of uncertainty (e.g. Yoshioka, 2019 in prep.; Fanourgakis et al., 2019).

The anthropogenic component of the nitrate CAE could be identified by repeating these simulations with a pre-industrial emissions scenario.

Furthermore, it has been hypothesised that equilibrium partitioning schemes may underestimate the direct radiative impacts of nitrate aerosol by distributing a greater portion of nitrate mass to the less optically efficient coarse mode (Feng and Penner, 2007; and supported by the results in Chapter 4). Future evaluation of the nitrate direct radiative effect would complement the results presented here.

7. Conclusions and Future Work

This thesis aimed, first, to evaluate atmospheric nitrate aerosol concentrations simulated by the UM-UKCA model with the nitrate-extended GLOMAP-mode aerosol microphysics module, with comparison to observations and modelled concentrations from the AeroCom Phase III intercomparison exercise. Second, this thesis aimed to quantify the changing contribution of nitrate aerosol to atmospheric particulate pollution and premature mortality arising from recent decadal emission changes. Finally, the thesis aimed to quantify the influence of nitrate aerosol on the present day cloud albedo radiative effect and identify the sensitivity of this effect to different gas-particle partitioning approaches. This work represents the first application and evaluation of the recently developed nitrate extension to the GLOMAP-mode microphysics scheme implemented in the UM-UKCA model. Moreover, the work in this thesis represents an advancement on many previous model-based studies of nitrate aerosol by applying a physically realistic 'hybrid' approach to represent the size-resolved partitioning of the semi-volatile inorganic aerosol system, whereas the majority of global aerosol models apply a simpler equilibrium assumption to represent this two-way gas-particle partitioning.

This chapter summarises the completion of the thesis aims outlined in Chapter 1 (Section 1.2). The following sub-sections review the main conclusions and future implications of each chapter.

7.1 Evaluation of annual and seasonal mean nitrate aerosol concentrations in the UM-UKCA model

The aim of this first results chapter was to comprehensively evaluate the surface level and lower tropospheric size-resolved nitrate aerosol concentrations on seasonal and annual mean timescales, as simulated using the nitrate-extended GLOMAP-mode aerosol module applied in the UM-UKCA model. Ammonium and sulphate aerosol concentrations were also considered, in addition to gaseous nitric acid and ammonia concentrations where observations were available. The control run consisted of a 12 month UM-UKCA simulation (after 4 month spin-

up) at N96 resolution (1.875° x 1.25°) for year 2008 conditions, applying the GLOMAP-mode HyDiS-1.0 solver to treat the two-way aerosol partitioning within the nitrate-ammonium-sulphate-sodium-chloride aerosol system. The main conclusions from this chapter are outlined here and map back to the research questions identified in Section 1.2 of Chapter 1.

7.1.1 Main Conclusions

a. The spatial distribution of annual mean surface level nitrate, ammonium and sulphate aerosol concentrations was reproduced well by the UKCA model (R between 0.62 and 0.87) over Europe and North America compared to observations, though simulated concentrations were biased low on average (NMB between -0.35 and -0.61 for NO_3^-, between -0.34 and -0.59 for NH_4^+ and between -0.51 and -0.60 for SO_4^{2-}). Total nitrate concentrations were simulated well ($R \approx 0.78$, NMB > -0.23) over Europe and North America. The spatial distributions of annual mean NO_3^-, NH_4^+ and SO_4^{2-} aerosol concentrations were captured less well over East Asia ($R < 0.52$) and the model under predicted regional annual mean concentrations (NMB values between -0.42 and -0.58).

Seasonally, the UM-UKCA model demonstrated similar skill in DJF and JJA when simulating the spatial distribution of NO_3^-, NH_4^+, SO_4^{2-}, tNO_3 and tNH_x over Europe ($\Delta R < 1$ between seasons). However, European wintertime NO_3^-, NH_4^+, SO_4^{2-} and tNO_3 concentrations tended to be more greatly underestimated than in summer. Over the USA, simulated NO_3^- aerosol correlated more strongly with observations in DJF, with SO_4^{2-} and tNO_3 being better captured spatially in JJA. UM-UKCA underestimation of NO_3^- over the USA was similar between seasons while underestimation of SO_4^{2-} and NH_4^+ was greater in winter. The magnitude of tNO_3 was captured well in the summer. The spatial distribution of NO_3^-, NH_4^+, SO_4^{2-} and tNO_3 was better captured in winter than in summer over East Asia, with similar skill for NH_4^+ in both seasons though the correlation was generally lower in this region than Europe and the USA (NMB < 0.6 for all). Model underestimation of all species was greater in DJF on average over Asia and tNO_3 was overestimated in JJA.

b. Simulated NO_3^-, NH_4^+ and SO_4^{2-} concentrations were compared against aircraft observations from year 2008 field campaigns (ADIENT, EUCAARI, ARCTAS Spring/Summer, OP3 and VOCALS-UK) in several locations globally. The vertical profiles of NO_3^- and NH_4^+ concentrations were simulated well overall, with over 70% of modelled concentrations being within one standard deviation of aircraft-based observations below 4 km altitude for most campaigns. However, the model tended to underestimate NO_3^- and NH_4^+ concentrations in the vertical, as found in the surface comparisons. Vertical variability in SO_4^{2-} concentrations compared well to aircraft observations below 4 km altitude, where over 55% of modelled values remaining within the standard deviation of observations for all campaigns except the Arctic-based ARCTAS-Spring project.

c. The annual mean global UKCA-simulated nitrate burden of 0.145 Tg was below the mean burden from the AeroCom Phase III models but within the multi-model range. The UM-UKCA ammonium aerosol burden of 0.345 Tg was within 10% of the AP3 multi-model mean, while the sulphate aerosol burden of 2.28 Tg was ~ 25% higher than the multi-model mean of 1.8 Tg. The annual global mean surface NO_3^-, NH_4^+ and SO_4^{2-} concentrations from UM-UKCA of 0.082 μg kg^{-1}, 0.139 μg kg^{-1} and 0.463 μg kg^{-1}, respectively, were below the AP3 mean concentrations but within the ranges simulated by the models. Annual mean UM-UKCA surface nitrate aerosol concentrations were within the AP3 IQR over most of Europe, East China, western USA and Antarctica, but were below the 25th percentile over India, eastern North America and the Southern Hemisphere oceans. UM-UKCA surface NO_3^- concentrations exceeded the AP3 75th percentile over the Arctic Ocean.

The statistical comparisons of annual and seasonal mean NO_3^-, NH_4^+ and SO_4^{2-} between UM-UKCA and surface observations were compared to the model-observation comparisons from the AP3 models. The majority of UM-UKCA model-observation Pearson correlation coefficients were within the range or those for AP3 indicating a good spatial model skill of UM-UKCA in the context of the AP3 models. For normalised mean bias, UM-UKCA values tended to be just within or below than the AP3 model range over the USA, indicating a larger low bias. However, the vast majority of UM-UKCA values were within the AP3 range of NMB values for NO_3^-, NH_4^+ and SO_4^{2-} over Europe and Asia.

d. Applying the equilibrium gas-particle partitioning assumption led to a 9.8% underestimation of the fine (submicron) atmospheric NO_3^- burden and 21.3% overestimation of the coarse (supermicron) NO_3^- burden compared to applying the more physically realistic hybrid approach to treat nitrate aerosol partitioning. The greatest absolute changes in surface fine and coarse nitrate concentrations of up to ±1-2 μg m^{-3}, occurred over polluted continental regions (Europe, China, North America and Northern India). However, small absolute changes in fine and coarse mode nitrate aerosol concentrations had a large relative influence on surface NO_3^- concentrations over marine regions, where low concentrations were more sensitive to changes. Decreases in the fine mode fraction of nitrate aerosol were greatest over much of the continental Northern Hemisphere and Polar regions. Despite the substantial change in the size distribution of NO_3^-, switching from the hybrid to equilibrium configuration had a small influence on the annual mean global nitrate burden (Δ -4.1%) and global mean surface nitrate concentrations (Δ -2.4%). However, small absolute changes had greater relative importance (up to Δ + 200%) in low concentration regions.

e. Nitrate aerosol concentrations from the control run (HYB) were compared to those simulated when heterogeneous N_2O_5 hydrolysis was switched off (HYB-NoHet). The exclusion of heterogeneous N_2O_5 hydrolysis decreased the annual global mean surface NO_3^- aerosol concentration by 42% and the annual mean global NO_3^- burden by 12.4%. Heterogeneous N_2O_5 hydrolysis was most important for surface nitrate aerosol concentrations in the Northern Hemisphere mid- and high-latitudes, particularly in the winter months. Annual mean surface NO_3^- concentrations were reduced by between 40% and 100% over most of this region, with the greatest absolute reductions of up to 5 μg m^{-3} in annual mean surface NO_3^- over eastern China and northern India. Removing heterogeneous N_2O_5 hydrolysis strongly exacerbated the wintertime model underestimation of surface NO_3^- concentrations and reduced the model representation of the spatial distribution of surface NO_3^- aerosol over Europe, the USA and East Asia. NH_4^+ concentrations were also more greatly underestimated, particularly in the wintertime, when heterogeneous N_2O_5 hydrolysis was removed.

7.1.2 Implications for future research

The research in Chapter 4 represents the first evaluation of nitrate and ammonium aerosol concentrations simulated in the UM-UKCA model using the nitrate extended version of GLOMAP-mode. Simulated concentrations were placed in context through comparison to regional observations and to results from the AeroCom Phase III intercomparison exercise. The chapter results therefore contribute to specific recommendations for the UM-UKCA model on its representation of nitrate aerosol (thus, addressing research question 1f from Chapter 1). Sensitivity experiments demonstrating the influence of the gas-particle partitioning complexity and heterogeneous N_2O_5 hydrolysis on nitrate aerosol concentrations have implications for the UM-UKCA simulation of nitrate aerosol in addition to having wider community implications for global model representations of nitrate aerosol.

Overall, the comparison to observations showed that the UM-UKCA model tended to underestimate NO_3^-, NH_4^+ and SO_4^{2-} aerosol concentrations. However, simulated annual global burden and global mean surface NO_3 concentrations were within the AP3 multi-model range (Bian et al., 2017) and the spatial distribution of NO_3^- compared well to ground-based observations. The UM-UKCA annual and mean model skill compared to surface observations was reasonable in the context of model-observation comparisons from the other AP3 models. This provided confidence that the UM-UKCA model, with the nitrate-extended GLOMAP-mode aerosol microphysics module, is a suitable tool to apply in determining the impacts of nitrate aerosol on air quality and radiative effects within this thesis and in future studies. However, future work should address the low model bias identified in this study.

Lower nitrate concentrations in the UKCA model may result in part from the lack of heterogeneous uptake of nitric acid onto dust (e.g. Karydis et al., 2016; Bian et al., 2017). Though this was not tested in Chapter 4, it is recommended that nitrate aerosol formation on dust aerosol be represented in future UM-UKCA simulations to ascertain its contribution to nitrate aerosol concentrations. This might be achieved by assuming linear uptake onto dust aerosol surface or by incorporating dust-associated ions (e.g. K^+, Ca^+, Mg^+) into the existing nitrate solver for GLOMAP-mode. Aerosol wet deposition may also be artificially high in

this model version as a result of enhanced drizzle in low-level clouds (Walters et al., 2011; Turnock et al., 2015). Understimation in surface SO_4^{2-} could be explained by underestimations in oxidant availability (Manktelow et al., 2007) or pH-dependent in-cloud aqueous phase oxidation (Turnock, 2016). Enabling the tropospheric input of nitric acid from the stratosphere may also enhance nitrate aerosol concentrations and could be incorporated within future model developments.

The results of Chapter 4 could be extended to evaluate nitrate aerosol concentrations on diurnal timescales (e.g. Morgan et al., 2010b; Aan de Brugh et al., 2012; Mensah et al., 2012). Preliminary comparisons found that UM-UKCA simulated characteristic diurnal cycles in NO_3^- concentration over Cabauw, the Netherlands (Figure A6). The UM-UKCA model could therefore be used to investigate drivers of diurnal variability in NO_3^- aerosol concentration.

It was found that reverting from a hybrid to an equilibrium partitioning approach (EQU) substantially changed the size distribution of nitrate aerosol in GLOMAP-mode. The findings in this thesis reinforce previous conclusions (Feng and Penner, 2007; Benduhn et al., 2016) that aerosol models applying equilibrium assumptions under represent the formation of fine mode nitrate aerosol. The implications of these results are far-reaching because the equilibrium approach remains the standard method for treating this partitioning in models, the assumption having been employed by all of the AP3 models (Bian et al., 2017). Misrepresentation of the nitrate aerosol size distribution is potentially important for assessments of the radiative impact of nitrate aerosol, though the effect of applying an equilibrium assumption on aerosol radiative effects has never been quantified against those calculated using a hybrid scheme. Community understanding of nitrate aerosol impacts could be improved further if other global aerosol models were to implement and test the importance of using a hybrid approach on size resolved nitrate aerosol concentrations and radiative effects. Following on from the findings in Chapter 4, Chapter 6 of this thesis investigated the implications of using an equilibrium versus a hybrid approach on the present day cloud albedo radiative effect of nitrate aerosol.

Comparison to a further sensitivity test (HYB-NoHet) confirmed that the formation of nitric acid via heterogeneous N_2O_5 hydrolysis represents an

essential formation pathway for nitrate aerosol, particularly in correcting Northern Hemispheric wintertime model low bias. Nitric acid formation by this reaction is not included in the standard UM-UKCA configuration and the second recommendation from this chapter is therefore to account for this in future simulations that treat nitrate aerosol formation. Relatively few studies have focussed on the influence of heterogeneous N_2O_5 hydrolysis on nitrate aerosol but the reaction has been found to be particularly important for night time NO_3^- formation, improving model representation of the diurnal cycle of NO_3^- (e.g. Lowe et al., 2015; Stone et al., 2014). The impact of heterogeneous N_2O_5 hydrolysis on NO_3^- could be investigated further as a potential driver of diurnal variability. Moreover, the results in Chapter 4 demonstrate the wider importance of heterogeneous N_2O_5 hydrolysis for NO_3^- formation on seasonal and annual mean timescales. Following inclusion of the reaction in UM-UKCA, the model parameterisation for heterogeneous N_2O_5 hydrolysis could be developed further to account for the self-limiting impacts of nitrate within the aerosol, enhancement of uptake by chloride and suppression of the reaction in the presence of organic species. Future work could also focus on the impact of N_2O_5 uptake on the NO_x sink and subsequent implications for gaseous species, including O_3 and HO_2.

7.2 Quantifying the changing impact of nitrate aerosol on air quality and human health

The second results chapter aimed to quantify the present day contribution of nitrate aerosol to $PM_{2.5}$ composition and to premature mortality over the European Union, USA, India and China. Nitrate aerosol impacts on $PM_{2.5}$ and mortality in these regions were also assessed for a year 1980 emission scenario to quantify changes in NO_3^- impacts arising from emission changes in recent decades. The main conclusions are revisited in this sub-section and correspond to the research questions outlined in Chapter 1.

7.2.1 Main Conclusions

a. The inclusion of nitrate aerosol formation in UM-UKCA improved the modelled spatial distribution and magnitude of annual mean simulated $PM_{2.5}$ compared to surface and satellite-derived observations over the four regions. Globally, the greatest improvements to the magnitude of simulated $PM_{2.5}$ following the inclusion of nitrate aerosol occurred over North America and across Northern Europe into east China. Underestimation of the surface level $PM_{2.5}$ simulated by UM-UKCA was expected over the four study regions based on previous model evaluations. To better characterise the contribution of nitrate to premature mortality, regional bias corrections were applied to the simulated $PM_{2.5}$ before mortality calculations were undertaken.

b. Using a 'subtraction' method, the annual mean contribution of nitrate aerosol to the simulated regional AWM $PM_{2.5}$ was calculated at 16.3%, 8.5%, 6.0%, and 5.8% over Europe, the USA, India and China, respectively. Within these regions, the nitrate-associated $PM_{2.5}$ fractions peaked locally at up to 45%, 30%, 25% and 35%, respectively. Compared to a 'speciation' method, the subtraction method yielded greater regional mean nitrate-associated $PM_{2.5}$ fractions because it considered changes in nitrate-associated ammonium aerosol formation. Using the subtraction method, nitrate aerosol was deemed to constitute 20% of the population-weighted mean (PWM) $PM_{2.5}$ over Europe, 8.9% over the USA, 8.9% over India and 12.7% over China.

c. Long-term exposure to sub-2.5 μm nitrate aerosol resulted in 31,500 (20,100 - 41,300), 6,900 (4,300 - 9,000), 29,000 (22,500 - 37,100) and 50,200 (38,700 - 61,000) premature deaths per year over the EU28, USA, India and China in a present day (year 2008) scenario. The relative contribution of nitrate to total $PM_{2.5}$-attributable deaths was greatest, at 15.6%, over Europe, with smaller relative contributions of 7.8% over the USA, 3.4% over India and 5.8% over China. The present day age-standardised mortality rate was reduced by 3.65 (2.33 - 4.79), 1.65 (1.03 - 2.16), 4.19 (3.21 - 5.39) and 4.83 (3.73 - 5.86) deaths per 100,000 people over the EU28, USA, India and China, respectively, when nitrate aerosol formation was removed. Long term exposure to nitrate aerosol resulted in approximately 432,000 (278,000 – 564,000) years, 104,000 (65,800 – 134,000) years, 906,000 (726,000 – 1,117,000) years and 929,000 (726,000 –

1,122,000) years of life lost in the present day scenario over the EU28, USA, India and China, respectively.

d. Over the EU28, sub-2.5 μm (bias-corrected) AWM nitrate concentrations decreased only slightly from 1.46 μg m^{-3} to 1.44 μg m^{-3} (-1.4%) as a result of post-1980 changes in emissions. Similarly, PWM nitrate concentrations decreased only by 2.0%. Over the USA, sub-2.5 μm AWM nitrate concentrations were reduced by 22.0%, and PWM nitrate by 20.5%. Over India, regional AWM and PWM sub-2.5 μm nitrate aerosol concentrations increased by 303% and 306%, respectively, following post-1980 emission changes. Over China, the AWM sub-2.5 μm nitrate aerosol concentration increased from 0.73 μg m^{-3} to 1.80 μg m^{-3} (+149%). The PWM nitrate concentration was 134.2% higher in the present day scenario over China, having increased from 1.86 μg m^{-3} to 4.34 μg m^{-3}.

The relative contribution of nitrate aerosol to simulated AWM and PWM $PM_{2.5}$ increased in all regions as a result of post-1980 emission changes. Despite simulated nitrate concentrations remaining relatively stable over the EU28, the fractional contribution of nitrate to AWM $PM_{2.5}$ increased from 10.9% to 16.3% as a result of falling ambient $PM_{2.5}$. Similarly, its contribution to PWM $PM_{2.5}$ increased from 12.7% to 21.5% over the EU28. Over the USA, the nitrate contribution to AWM and PWM $PM_{2.5}$ underwent a small increase from 7.9% to 8.5% and from 7.2% to 9.1%, respectively, between the 1980 and present day emissions case. In India, the AWM nitrate-associated $PM_{2.5}$ fraction increased from 1.8% to 6.0%, with the PWM nitrate $PM_{2.5}$ fraction also increasing from 2.9% to 9.0%. The nitrate-associated fraction of AWM $PM_{2.5}$ over China was also slightly enhanced, at 5.8% of AWM $PM_{2.5}$ in the present day compared to 2.7% in the 1980 emissions scenario. Likewise, the nitrate-associated fraction of PWM ambient $PM_{2.5}$ over China increased from 7.5% to 12.7%.

e. Absolute nitrate-associated mortality was greater in the present day scenario than in the 1980 emissions scenario by 40%, 50%, 303% and 104% over the EU28, USA, India and China, respectively. However, the age-standardised mortality rate associated with long term exposure to nitrate aerosol decreased in all regions except India. Changes in $PM_{2.5}$ were responsible for differences in total ambient $PM_{2.5}$-attributable mortality of -17.6%, -26.5%, +15.0% and +20.9% between the 1980 and present day case over the EU28, USA, India and

China, respectively, with the remainder of the mortality change driven by background disease rates, population growth and ageing. This implies that emission changes are also not the largest determinants of decadal changes in nitrate-associated mortality.

7.2.2 Implications for future research

This study was the first to apply the UM-UKCA model to quantify the impacts of nitrate aerosol on $PM_{2.5}$ and premature mortality, representing an advancement on previous studies of $PM_{2.5}$-attributable mortality using non-nitrate extended configurations of the model (Butt et al., 2017; Turnock et al., 2015; Turnock et al., 2016; Butt et al., 2017; Fenech et al., 2018). The improvement in UM-UKCA model skill for $PM_{2.5}$ when nitrate aerosol was included, particularly in populated regions where $PM_{2.5}$ exposure was high, reinforces the importance of including nitrate aerosol in future assessments of $PM_{2.5}$ and its associated health impacts.

The differences in regional nitrate-associated $PM_{2.5}$ fraction calculated with the 'speciation' and 'subtraction' approaches show that the removal of nitrate aerosol formation reduces ammonium aerosol concentrations and modifies aerosol microphysical processes. These changes should be considered when quantifying the health benefit of reducing nitrate aerosol concentrations and when identifying policy to reduce $PM_{2.5}$. The larger relative contribution of nitrate aerosol to PWM $PM_{2.5}$, compared to AWM $PM_{2.5}$, in the regions studied here further indicates the potential of targeting nitrate aerosol reductions to reduce human exposure to $PM_{2.5}$.

Of the regions studied, it was found that nitrate aerosol made the greatest fractional contribution to present day $PM_{2.5}$ and to $PM_{2.5}$-attributable mortality over the European Union member states, suggesting that models that exclude nitrate aerosol formation will substantially underestimate the $PM_{2.5}$-attributable mortality in this region. Moreover, this suggests that targeting nitrate aerosol in emission reduction strategies would be particularly effective in the EU28 for reducing the mortality associated with long-term exposure to ambient $PM_{2.5}$. Removing nitrate aerosol would result in larger absolute reductions in the $PM_{2.5}$-attributable mortality and age-standardised mortality rate over China and India. However, these decreases were relatively small compared to the total $PM_{2.5}$-attributable mortality and mortality rates in these regions, indicating that

reducing other species could be more effective in reducing the total $PM_{2.5}$-attributable mortality.

The results in Chapter 5 showed that post-1980 emission changes resulted in an increased relative contribution of nitrate aerosol to regional mean $PM_{2.5}$ and $PM_{2.5}$-attributable mortality in all regions, implying that the importance of nitrate aerosol will continue to increase in the future if effective emission controls are not established. Previous studies have indicated the importance of agricultural emissions for $PM_{2.5}$ by limiting sulphate and nitrate aerosol formation (e.g. Lelieveld et al., 2015; Pozzer et al., 2017; Brandt et al., 2013; Megaritis et al., 2013; Bauer et al., 2016). Studies of future trends in nitrate-associated mortality should take projected changes in demography and background disease rates into account, to ascertain whether more stringent emission reductions will be needed to overcome the influence of growing and ageing populations. The influence of changes in climate between 1980 and the present day on nitrate aerosol concentrations were not considered in this work but may also influence decadal trends in nitrate concentration and could be examined in future studies (Megaritis et al., 2014).

Simulated regional mean nitrate aerosol concentrations over Europe were found to remain relatively stable as a result of post-1980 emission changes. A non-linear response of nitrate aerosol concentrations to decreases in NO_x concentration has also been noted in other studies over Europe (Erisman and Schaap, 2004; Fagerli and Aas, 2008) and is thought to arise in part because of increased availability of NH_3. The relative roles of NO_x, NH_3 and SO_2 emissions in driving nitrate aerosol concentrations in UM-UKCA should be investigated further in the future and is also proposed for future study within the AeroCom Phase III framework (Bian et al., 2017). Recent studies suggest that aerosol acidity should also be considered when investigating the influence of emission changes on nitrate aerosol formation (Weber et al., 2016; Murphy et al., 2017; Guo et al., 2018).

The greatest uncertainty in this study was associated with the calculation of premature mortality. The study also assumed equal toxicity among all species and the study should be updated as more information becomes available on the

relative toxicity of $PM_{2.5}$ components. Low model bias in $PM_{2.5}$ was addressed in the mortality calculations by applying regional bias corrections. However, the mortality estimates are likely to be underestimated over China, in particular, where the bias was not fully corrected and sources of low model bias should be addressed in future work. In addition to the causes of low bias outlined in Chapter 4, there is a known under prediction of organic aerosol at this configuration (see Mann et al., 2010) and under-representation of biogenic sources of $PM_{2.5}$. The study only considers dry $PM_{2.5}$ and the model has a relatively coarse resolution.

7.3 Sensitivity of the simulated present day nitrate aerosol cloud albedo radiative effect to the gas-particle partitioning approach

The third results chapter addressed the final aim of this thesis: to quantify the radiative impact of present day nitrate aerosol formation via its influence on cloud albedo. The present day radiative effect was calculated based on the perturbation to the cloud effective radius when nitric acid partitioning to the aerosol phase was included in UM-UKCA (termed here as the "nitrate CAE"). Earlier in the thesis, the results of Chapter 4 confirmed that the complexity of the semi-volatile aerosol partitioning approach was important for the size distribution of simulated nitrate aerosol mass concentrations. This chapter furthers that analysis by investigating the influence of the size-resolved gas-particle partitioning approach on aerosol number concentrations, cloud droplet number concentrations and resulting perturbations to the global radiative budget in the present-day atmosphere. The main conclusions are summarised here and relate back to the research questions identified in Chapter 1. Results calculated using the hybrid aerosol partitioning approach, as opposed to the equilibrium approach, are presented here unless stated otherwise.

7.3.1 Main Conclusions

a) The influence of nitrate aerosol formation on total particle number concentrations (N_3) varied with altitude. At low cloud level (~ 900 hPa), nitrate aerosol formation led to a decrease in global annual mean N_3 of 3.33% as a result of widespread decreases in N_3. At middle cloud level (~720hPa), the inclusion of

nitrate aerosol resulted in N_3 increases over much of the Northern Hemisphere, including relative local increases of up to 60% over China and up to 20% over North America and remote marine regions. The increases in N_3 at middle cloud level were countered on the global mean scale by decreases in N_3 over the Southern Hemispheric oceans (by up to 20%) and other continental regions (e.g. by up to 10% over Europe and elsewhere in Asia), resulting in a smaller global mean decrease of -1.81% than at low cloud level.

b) The inclusion of nitrate aerosol formation in UM-UKCA resulted in widespread regional increases in annual mean CDNC of up to 40% over the Arctic and high latitudes of the Northern Hemisphere with smaller increases of up to 10% over most of the mid-latitudes. Conversely, nitrate aerosol formation resulted in decreases in annual mean CDNC by up to 20% over many equatorial regions. Annual mean CDNC was increased over most of the Southern Hemisphere at middle cloud level when nitrate aerosol formation was included, with increases peaking at up to 40% locally over Antarctica. At low cloud level, the annual mean CDNC was decreased over much of the Southern Hemisphere, except over Antarctica and Africa, with maximum local decreases of up to 20% over mid-latitude marine regions. Seasonally, relative increases in zonal mean CDNC were greatest in DJF over most the Northern Hemisphere, peaking at +57% and +39% over the Arctic at low and middle cloud level, respectively, when nitrate aerosol formation was included. Increases in zonal mean CDNC over the Southern Hemisphere peaked in JJA at 90° S at between 59 and 69% over both cloud levels. Spatially, changes in soluble N_{50} when nitrate aerosol formation was included were similar to changes in CDNC.

c) Nitrate aerosol formation resulted in a global mean present day radiative forcing of -0.007 W m^{-2} via its influence on cloud albedo, with a more strongly negative radiative forcing in the Northern Hemisphere (-0.02 W m^{-2}) than in the Southern Hemisphere (+0.008 W m^{-2}). The PD nitrate CAE was weakened on the global mean scale as a result of averaging over regional positive and negative forcings. Locally, the greatest negative PD nitrate CAE in the Northern Hemisphere, of up to -0.5 W m^{-2}, occurred over cloudy marine regions with moderate increases in CDNC. The negative radiative effect was partly countered, however, by local positive forcings of up to +1 W m^{-2} arising from moderate

relative decreases in CDNC over many cloudy marine regions in the tropics. In the Southern Hemisphere, the negative local PD radiative forcing associated with nitrate aerosol formation was greatest (up to -0.5 Wm^{-2}) over marine regions with high middle level cloud fraction, where middle cloud level CDNC was increased by up to 10%. However, on the hemispheric mean scale, the local negative forcing was again countered by positive local nitrate CAE (up to +0.5 W m^{-2}) over many equatorial regions and by positive forcing centred around 50° S, driven by decreases (by up to 20%) in low level cloud CDNC where the cloud fraction was larger than at higher altitudes.

d) The effects of nitrate aerosol formation on N_3, N_{50}, CDNC and PD nitrate CAE were sensitive to the choice of gas-aerosol partitioning mechanism employed. Nitrate aerosol formation using the equilibrium approach resulted in greater global mean N_3 than the hybrid approach (up to 3.4% higher) through its overall smaller influence on aerosol surface area and on the condensation sink for potentially nucleating vapours. Using the equilibrium approach, N_3 was regionally up to 40% higher than concentrations simulated using the hybrid approach.

The influence of the choice of partitioning approach on N_{50} was spatially similar to the influence on CDNC. Nitrate aerosol formation using the equilibrium approach resulted in the widespread underestimation of regional CDNC over the Northern Hemisphere compared to the hybrid approach, including underestimations of up to 20% in the high latitudes. Over the Northern Hemisphere, this resulted in a positive hemispheric mean nitrate CAE of +0.005 W m^{-2} using the equilibrium approach, where the hybrid approach produced a negative mean forcing of -0.02 W m^{-2}. Compared to the hybrid approach, the equilibrium approach under-represented increases in CDNC at middle cloud level in the Southern Hemisphere mid-latitudes, by up to 10%, resulting again in a more weakly negative radiative forcing over this region. Ultimately, the annual global mean PD nitrate CAE was calculated to be +0.011 W m^{-2} using the equilibrium approach, representing a sign reversal from that calculated using the hybrid scheme.

7.3.2 Implications for future research

For the first time, it has been shown here that the choice of semi-volatile aerosol partitioning approach leads to large variability in the effect of nitrate aerosol formation on regional total particle number concentrations and on the growth of particles to the size at which they can be activated to CCN. Most notably, compared to applying the hybrid approach, the equilibrium approach under-represented the negative forcing associated with nitrate aerosol formation over most of the Northern Hemisphere. This has implications for future assessments of nitrate aerosol radiative effects because the majority of models that account for nitrate aerosol formation apply an equilibrium approach (e.g. Bian et al., 2017). In the future, the influence of the partitioning approach on the direct radiative effects of nitrate aerosol could be investigated, though it is hypothesised that the direct effect is less sensitive to the microphysical approaches than the cloud-aerosol effect based on previous studies of natural aerosol (Rap et al., 2013; Scott et al., 2015).

The results show that nitrate aerosol formation has a complex influence on the microphysical processing of aerosol and can therefore have far-reaching impacts on the radiative forcing at distances far from precursor source regions. These effects would be under-represented by models that apply a bulk aerosol scheme (e.g. Bellouin et al., 2013). Though several mechanisms are presented in the chapter to explain the influence of nitrate aerosol formation on aerosol properties and CDNC, future work could focus on isolating the microphysical responses associated with changes in the aerosol size distribution when nitrate aerosol is formed. A perturbed parameter ensemble approach (e.g. Lee et al., 2013; Fanourgakis et al., 2019; Yoshioka, 2019 in prep.) or adjoint model (Henze et al., 2007; Pye et al., 2009; Karydis et al., 2012a; Karydis et al., 2012b; Lee et al., 2014) could be applied to achieve this, though these methods have not currently been developed to describe the nitrate-extended version of GLOMAP-mode. As an interim next step, the nitrate-extension to GLOMAP-mode could be applied in a configuration that includes boundary layer nucleation mechanisms (e.g. those evaluated in Reddington, 2012) to give a more accurate representation of particle concentrations prior to nitric acid uptake being implemented. Model

overestimation of sulphate aerosol concentrations in the free troposphere (identified in Chapter 4) should also be addressed.

Given the importance of the gas-particle partitioning approach for the simulated size-resolved nitrate aerosol mass (Chapter 4) and aerosol number concentrations (Chapter 7), it would be valuable to evaluate the nitrate aerosol size distribution against observations. This analysis would be particularly informative once nitrate formation on dust has been implemented in the model as discussed in Section 7.1.2. Monitor for AeRosol and Gases (MARGA) instruments provide high resolution, long-term observations of both size resolved nitrate aerosol and gaseous nitric acid that could be used for further model evaluation (e.g. ten Brink et al., 2007; Mensah et al., 2012; Schaap et al., 2011; Griffith et al., 2015). Other techniques for observing size-resolved nitrate concentrations include Micro Orifice Uniform Deposit Impactors (MOUDI; Marple et al., 1991; Lee et al., 2008; Plaza et al., 2011), high volume virtual impactor air samplers (e.g. Itahashi et al., 2016) and AMS instruments (e.g. Mensah et al., 2012).

The results in Chapter 6 show that nitrate aerosol formation has a regionally important influence on present day aerosol radiative effects via its modification of the cloud albedo and should not be neglected in assessments of aerosol radiative effects. This aspect of the aerosol radiative forcing has been severely understudied in the past, with a small number of dedicated global model assessments of the nitrate aerosol influence on cloud radiative properties having been previously undertaken (Bellouin et al., 2011; Xu and Penner, 2012). To enable comparison to these previous studies, a natural progression from the results in Chapter 6 would be to identify the anthropogenic component of the radiative forcing through additional pre-industrial simulations. The difference in sign of the present-day nitrate CAE calculated with the two gas-particle partitioning approaches also has potential implications for the pre-industrial to present day climate forcing by nitrate. Investigation of the future radiative effects of nitrate aerosol would be another interesting avenue for future research.

This thesis has tested and concluded that hybrid gas-particle partitioning mechanisms should be applied when modelling radiative effects associated with

nitrate aerosol-cloud interactions. The radiative effects associated with aerosol-radiation interactions are also likely to be affected by the choice of gas-particle partitioning approach, though they may be less sensitive to changes in the size distribution based on previous studies with GLOMAP-mode (Scott et al., 2015). In terms of air quality, the choice of gas-particle partitioning approach has the potential to influence ambient ultrafine particle concentrations (≤0.1 μm in diameter). However the available evidence for an association between ultrafine particle concentrations and health impacts is limited (e.g. Wittmaack, 2007; Lanzinger et al., 2016; Yin et al., 2019).

Based on the results of this thesis, it is recommended that a hybrid size-resolved approach be applied for the gas-particle partitioning of semi-volatile inorganics within global aerosol models to ensure that the size distribution of nitrate aerosol, and therefore its radiative effects, are accurately characterised.

8. Bibliography

(IHME), I.f.H.M.a.E. 2016. *Global Burden of Disease Study (GBD 2015) Reference Life Table.* Seattle, United States: Institute for Health Metrics and Evaluation (IHME).

(IHME), I.f.H.M.a.E. 2018. *GBD Compare.* [Online]. [Accessed 1 August]. Available from: https://vizhub.healthdata.org/gbd-compare/

Aan de Brugh, J.M.J., Henzing, J.S., Schaap, M., Morgan, W.T., van Heerwaarden, C.C., Weijers, E.P., Coe, H. and Krol, M.C. 2012. Modelling the partitioning of ammonium nitrate in the convective boundary layer. *Atmospheric Chemistry and Physics.* **12**(6), pp.3005-3023.

Adams, P.J., Seinfeld, J.H., Koch, D., Mickley, L. and Jacob, D. 2001. General circulation model assessment of direct radiative forcing by the sulfate-nitrate-ammonium-water inorganic aerosol system. *Journal of Geophysical Research: Atmospheres.* **106**(D1), pp.1097-1111.

Albrecht, B.A. 1989. Aerosols, Cloud Microphysics, and Fractional Cloudiness. *Science.* **245**(4923), p1227.

Alexander, B., Hastings, M.G., Allman, D.J., Dachs, J., Thornton, J.A. and Kunasek, S.A. 2009. Quantifying atmospheric nitrate formation pathways based on a global model of the oxygen isotopic composition ($\Delta^{17}O$) of atmospheric nitrate. *Atmos. Chem. Phys.* **9**(14), pp.5043-5056.

Allen, G. et al. 2011. South East Pacific atmospheric composition and variability sampled along 20° S during VOCALS-REx. *Atmospheric Chemistry and Physics.* **11**(11), pp.5237-5262.

Allen, H.M., Draper, D.C., Ayres, B.R., Ault, A., Bondy, A., Takahama, S., Modini, R.L., Baumann, K., Edgerton, E., Knote, C., Laskin, A., Wang, B. and Fry, J.L. 2015. Influence of crustal dust and sea spray supermicron particle concentrations and acidity on inorganic NO_3^- aerosol during the 2013 Southern Oxidant and Aerosol Study. *Atmospheric Chemistry and Physics.* **15**(18), pp.10669-10685.

Andres, R.J. and Kasgnoc, A.D. 1998. A time-averaged inventory of subaerial volcanic sulfur emissions. *J. Geophys. Res.* **103**(D19), pp.25251-25261.

Ansari, A.S. and Pandis, S.N. 1998. Response of Inorganic PM to Precursor Concentrations. *Environmental Science & Technology.* **32**(18), pp.2706-2714.

Ansari, A.S. and Pandis, S.N. 1999. Prediction of multicomponent inorganic atmospheric aerosol behavior. *Atmospheric Environment.* **33**(5), pp.745-757.

Apte, J.S., Marshall, J.D., Cohen, A.J. and Brauer, M. 2015. Addressing Global Mortality from Ambient PM2.5. *Environmental Science & Technology.* **49**(13), pp.8057-8066.

Archer-Nicholls, S., Carter, E., Kumar, R., Xiao, Q., Liu, Y., Frostad, J., Forouzanfar, M.H., Cohen, A., Brauer, M., Baumgartner, J. and Wiedinmyer, C. 2016. The Regional Impacts of Cooking and Heating Emissions on Ambient Air Quality and Disease Burden in China. *Environmental Science & Technology.* **50**(17), pp.9416-9423.

Asmi, A. et al. 2011. Number size distributions and seasonality of submicron particles in Europe 2008–2009. *Atmos. Chem. Phys.* **11**(11), pp.5505-5538.

Aw, J. and Kleeman, M.J. 2003. Evaluating the first-order effect of intraannual temperature variability on urban air pollution. *Journal of Geophysical Research.* **108**(D12), pp.4365-4365.

Barahona, D., West, R.E.L., Stier, P., Romakkaniemi, S., Kokkola, H. and Nenes, A. 2010. Comprehensively accounting for the effect of giant CCN in cloud activation parameterizations. *Atmos. Chem. Phys.* **10**(5), pp.2467-2473.

Basu, R., Harris, M., Sie, L., Malig, B., Broadwin, R. and Green, R. 2014. Effects of fine particulate matter and its constituents on low birth weight among full-term infants in California. *Environmental Research.* **128**, pp.42-51.

Bauer, S.E., Koch, D., Unger, N., Metzger, S.M., Shindell, D.T. and Streets, D.G. 2007. Nitrate aerosols today and in 2030: a global simulation including aerosols and tropospheric ozone. *Atmospheric Chemistry and Physics.* **7**(19), pp.5043-5059.

Bauer, S.E., Tsigaridis, K. and Miller, R. 2016. Significant atmospheric aerosol pollution caused by world food cultivation. *Geophysical Research Letters.* **43**(10), pp.5394-5400.

Beelen, R. et al. 2014. Effects of long-term exposure to air pollution on natural-cause mortality: an analysis of 22 European cohorts within the multicentre ESCAPE project. *The Lancet.* **383**(9919), pp.785-795.

Bellouin, N., Rae, J., Jones, A., Johnson, C., Haywood, J. and Boucher, O. 2011. Aerosol forcing in the Climate Model Intercomparison Project (CMIP5) simulations by HadGEM2-ES and the role of ammonium nitrate. *Journal of Geophysical Research.* **116**(D20), pp.D20206-D20206.

Bellouin, N., Mann, G.W., Woodhouse, M.T., Johnson, C., Carslaw, K.S. and Dalvi, M. 2013. Impact of the modal aerosol scheme GLOMAP-mode on aerosol forcing in the Hadley Centre Global Environmental Model. *Atmos. Chem. Phys.* **13**(6), pp.3027-3044.

Benas, N., Mourtzanou, E., Kouvarakis, G., Bais, A., Mihalopoulos, N. and Vardavas, I. 2013. Surface ozone photolysis rate trends in the Eastern Mediterranean: Modeling the effects of aerosols and total column ozone based on Terra MODIS data. *Atmospheric Environment.* **74**, pp.1-9.

Benduhn, F., Mann, G.W., Pringle, K.J., Topping, D.O., McFiggans, G. and Carslaw, K.S. 2016. Size-resolved simulations of the aerosol inorganic composition with the new hybrid dissolution solver HyDiS-1.0: description, evaluation and first global modelling results. *Geoscientific Model Development.* **9**(11), pp.3875-3906.

Benedict, K.B., Lee, T. and Collett, J.L. 2012. Cloud water composition over the southeastern Pacific Ocean during the VOCALS regional experiment. *Atmospheric Environment.*

Berglen, T.F., Myhre, G., Isaksen, I.S.a., Vestreng, V. and Smith, S.J. 2007. Sulphate trends in Europe: Are we able to model the recent observed decrease? *Tellus, Series B: Chemical and Physical Meteorology.* **59**(4), pp.773-786.

Bergström, A.-K. and Jansson, M. 2006. Atmospheric nitrogen deposition has caused nitrogen enrichment and eutrophication of lakes in the northern hemisphere. *Global Change Biology.* **12**(4), pp.635-643.

Berntsen, T.K. and Isaksen, I.S.A. 1997. A global three-dimensional chemical transport model for the troposphere: 1. Model description and CO and

ozone results. *Journal of Geophysical Research: Atmospheres.* **102**(D17), pp.21239-21280.

Bertram, T.H. and Thornton, J.A. 2009. Toward a general parameterization of N_2O_5 reactivity on aqueous particles: the competing effects of particle liquid water, nitrate and chloride. *Atmospheric Chemistry and Physics.* **9**(21), pp.8351-8363.

Bertram, T.H., Thornton, J.A., Riedel, T.P., Middlebrook, A.M., Bahreini, R., Bates, T.S., Quinn, P.K. and Coffman, D.J. 2009. Direct observations of N2O5 reactivity on ambient aerosol particles. *Geophysical Research Letters.* **36**(19), pp.1-5.

Bessagnet, B., Beauchamp, M., Guerreiro, C., de Leeuw, F., Tsyro, S., Colette, A., Meleux, F., Rouïl, L., Ruyssenaars, P., Sauter, F., Velders, G.J.M., Foltescu, V.L. and van Aardenne, J. 2014. Can further mitigation of ammonia emissions reduce exceedances of particulate matter air quality standards? *Environmental Science & Policy.* **44**, pp.149-163.

Beusen, A.H.W., Bouwman, A.F., Heuberger, P.S.C., Van Drecht, G. and Van Der Hoek, K.W. 2008. Bottom-up uncertainty estimates of global ammonia emissions from global agricultural production systems. *Atmospheric Environment.* **42**(24), pp.6067-6077.

Bian, H., Chin, M., Rodriguez, J.M., Yu, H., Penner, J.E. and Strahan, S. 2009. Sensitivity of aerosol optical thickness and aerosol direct radiative effect to relative humidity. *Atmospheric Chemistry and Physics.* **9**(7), pp.2375-2386.

Bian, H., Chin, M., Hauglustaine, D.A., Schulz, M., Myhre, G., Bauer, S.E., Lund, M.T., Karydis, V.A., Kucsera, T.L., Pan, X., Pozzer, A., Skeie, R.B., Steenrod, S.D., Sudo, K., Tsigaridis, K., Tsimpidi, A.P. and Tsyro, S.G. 2017. Investigation of global particulate nitrate from the AeroCom phase III experiment. *Atmospheric Chemistry and Physics.* **17**(21), pp.12911-12940.

Binkowski, F.S. and Roselle, S.J. 2003. Models-3 Community Multiscale Air Quality (CMAQ) model aerosol component 1. Model description. *Journal of geophysical research: Atmospheres.* **108**(D6).

Boucher, O., Randall, D., Artaxo, P., Bretherton, C., Feingold, G., Forster, P., Kerminen, V.-M., Kondo, Y., Liao, H. and Lohmann, U. 2013. Clouds and aerosols. *Climate change 2013: the physical science basis. Contribution of Working Group I to the Fifth Assessment Report of the Intergovernmental Panel on Climate Change.* Cambridge University Press, pp.571-657.

Bouwman, A.F., Lee, D.S., Asman, W.A.H., Dentener, F.J., Van Der Hoek, K.W. and Olivier, J.G.J. 1997. A global high-resolution emission inventory for ammonia. *Global Biogeochemical Cycles.* **11**(4), pp.561-587.

Bouwman, A.F., Van Vuuren, D.P., Derwent, R.G. and Posch, M. 2002. A Global Analysis of Acidification and Eutrophication of Terrestrial Ecosystems. *Water, Air, and Soil Pollution.* **141**(1), pp.349-382.

Brandt, J., Silver, J.D., Christensen, J.H., Andersen, M.S., Bønløkke, J.H., Sigsgaard, T., Geels, C., Gross, A., Hansen, A.B., Hansen, K.M., Hedegaard, G.B., Kaas, E. and Frohn, L.M. 2013. Contribution from the ten major emission sectors in Europe and Denmark to the health-cost externalities of air pollution using the EVA model system – an integrated modelling approach. *Atmospheric Chemistry and Physics.* **13**(15), pp.7725-7746.

Brauer, M., Freedman, G., Frostad, J., van Donkelaar, A., Martin, R.V., Dentener, F., Dingenen, R.v., Estep, K., Amini, H., Apte, J.S., Balakrishnan, K., Barregard, L., Broday, D., Feigin, V., Ghosh, S., Hopke, P.K., Knibbs, L.D., Kokubo, Y., Liu, Y., Ma, S., Morawska, L., Sangrador, J.L.T., Shaddick, G., Anderson, H.R., Vos, T., Forouzanfar, M.H., Burnett, R.T. and Cohen, A. 2016. Ambient Air Pollution Exposure Estimation for the Global Burden of Disease 2013. *Environmental Science & Technology.*

Brown, A., Milton, S., Cullen, M., Golding, B., Mitchell, J. and Shelly, A. 2012. Unified Modeling and Prediction of Weather and Climate: A 25-Year Journey. *Bulletin of the American Meteorological Society.* **93**(12), pp.1865-1877.

Brown, S.S. and Stutz, J. 2012. Nighttime radical observations and chemistry. *Chem. Soc. Rev.* **41**(19), pp.6405-6447.

Browse, J. et al. 2019 in prep. Evaluating a Perturbed Parameter Ensemble against global aerosol observations to constrain parametric uncertainty: Is there an ideal aerosol model?

Burnett, R.T., Pope, C.A., III, Ezzati, M., Olives, C., Lim, S.S., Mehta, S., Shin, H.H., Singh, G., Hubbell, B., Brauer, M., Anderson, H.R., Smith, K.R., Balmes, J.R., Bruce, N.G., Kan, H., Laden, F., Prüss-Ustün, A., Turner, M.C., Gapstur, S.M., Diver, W.R. and Cohen, A. 2014. An Integrated Risk Function for Estimating the Global Burden of Disease Attributable to Ambient Fine Particulate Matter Exposure. *Environmental Health Perspectives.*

Butt, E. 2018. *Impact of changes in anthropogenic emissions on particulate air quality and the attributable burden of disease*. PhD thesis, University of Leeds.

Butt, E.W., Rap, A., Schmidt, A., Scott, C.E., Pringle, K.J., Reddington, C.L., Richards, N.A.D., Woodhouse, M.T., Ramirez-Villegas, J., Yang, H., Vakkari, V., Stone, E.A., Rupakheti, M., Praveen, P.S., Van Zyl, P.G., Beukes, J.P., Josipovic, M., Mitchell, E.J.S., Sallu, S.M., Forster, P.M. and Spracklen, D.V. 2016. The impact of residential combustion emissions on atmospheric aerosol, human health, and climate. *Atmospheric Chemistry and Physics.*

Butt, E.W., Turnock, S.T., Rigby, R., Reddington, C.L., Yoshioka, M., Johnson, J.S., Regayre, L.A., Pringle, K.J., Mann, G.W. and Spracklen, D.V. 2017. Global and regional trends in particulate air pollution and attributable health burden over the past 50 years. *Environmental Research Letters.* **12**(10), pp.104017-104017.

Capaldo, K.P., Pilinis, C. and Pandis, S.N. 2000. A computationally efficient hybrid approach for dynamic gas/aerosol transfer in air quality models. *Atmospheric Environment.* **34**(21), pp.3617-3627.

Carver, G.D., Brown, P.D. and Wild, O. 1997. The ASAD atmospheric chemistry integration package and chemical reaction database. *Computer Physics Communications.* **105**(2), pp.197-215.

Chambliss, S.E., Silva, R., West, J.J., Zeinali, M. and Minjares, R. 2014. Estimating source-attributable health impacts of ambient fine particulate matter exposure: global premature mortality from surface transportation emissions in 2005. *Environmental Research Letters.* **9**(10), p104009.

Che, H.C., Zhang, X.Y., Wang, Y.Q., Zhang, L., Shen, X.J., Zhang, Y.M., Ma, Q.L., Sun, J.Y., Zhang, Y.W. and Wang, T.T. 2016. Characterization and parameterization of aerosol cloud condensation nuclei activation under different pollution conditions. *Scientific Reports.* **6**, p24497.

Chen, Y., Cheng, Y., Ma, N., Wolke, R., Nordmann, S., Schüttauf, S., Ran, L., Wehner, B., Birmili, W., van der Gon, H.A.C.D., Mu, Q., Barthel, S., Spindler, G., Stieger, B., Müller, K., Zheng, G.-J., Pöschl, U., Su, H. and Wiedensohler, A. 2016. Sea salt emission, transport and influence on size-segregated nitrate simulation: a case study in northwestern Europe by WRF-Chem. *Atmospheric Chemistry and Physics.* **16**(18), pp.12081-12097.

Chipperfield, M.P. 2006. New version of the TOMCAT/SLIMCAT off-line chemical transport model: Intercomparison of stratospheric tracer experiments. *Quarterly Journal of the Royal Meteorological Society.* **132**(617), pp.1179-1203.

Chow, J.C. 1995. Measurement Methods to Determine Compliance with Ambient Air Quality Standards for Suspended Particles. *Journal of the Air & Waste Management Association.* **45**(5), pp.320-382.

CIESIN. 2017. Gridded Population of the World, Version 4 (GPWv4): Population Count Adjusted to Match 2015 Revision of UN WPP Country Totals, Revision 10. Center for International Earth Science Information Network - Columbia University

Palisades, NY: *NASA Socioeconomic Data and Applications Center (SEDAC)*. [Online]. Available from: https://doi.org/10.7927/H4JQ0XZW

Clegg, S.L., Brimblecombe, P. and Wexler, A.S. 1998. Thermodynamic Model of the System H+−NH4+−Na+−SO42-−NO3-−Cl-−H2O at 298.15 K. *The Journal of Physical Chemistry A.* **102**(12), pp.2155-2171.

Cohen, A.J., Brauer, M., Burnett, R., Anderson, H.R., Frostad, J., Estep, K., Balakrishnan, K., Brunekreef, B., Dandona, L., Dandona, R., Feigin, V., Freedman, G., Hubbell, B., Jobling, A., Kan, H., Knibbs, L., Liu, Y., Martin, R., Morawska, L., Pope, C.A., Shin, H., Straif, K., Shaddick, G., Thomas, M., van Dingenen, R., van Donkelaar, A., Vos, T., Murray, C.J.L. and Forouzanfar, M.H. 2017. Estimates and 25-year trends of the global burden of disease attributable to ambient air pollution: an analysis of data from the Global Burden of Diseases Study 2015. *The Lancet.* **389**(10082), pp.1907-1918.

Collett, J., Oberholzer, B. and Staehelin, J. 1993. Cloud chemistry at Mt Rigi, Switzerland: Dependence on drop size and relationship to precipitation chemistry. *Atmospheric Environment. Part A. General Topics.* **27**(1), pp.33-42.

Conibear, L., Butt, E.W., Knote, C., Arnold, S.R. and Spracklen, D.V. 2018. Residential energy use emissions dominate health impacts from exposure to ambient particulate matter in India. *Nature Communications.* **9**(1), pp.617-617.

Correia, A.W., Pope, C.A., 3rd, Dockery, D.W., Wang, Y., Ezzati, M. and Dominici, F. 2013. Effect of air pollution control on life expectancy in the United States: an analysis of 545 U.S. counties for the period from 2000 to 2007. *Epidemiology.* **24**(1), pp.23-31.

Crosier, J., Allan, J.D., Coe, H., Bower, K.N., Formenti, P. and Williams, P.I. 2007. Chemical composition of summertime aerosol in the Po Valley (Italy), northern Adriatic and Black Sea. *Quarterly Journal of the Royal Meteorological Society.* **133**(S1), pp.61-75.

Crouse, D.L., Peters, P.A., van Donkelaar, A., Goldberg, M.S., Villeneuve, P.J., Brion, O., Khan, S., Atari, D.O., Jerrett, M., Pope, C.A., Brauer, M., Brook, J.R., Martin, R.V., Stieb, D. and Burnett, R.T. 2012. Risk of nonaccidental

and cardiovascular mortality in relation to long-term exposure to low concentrations of fine particulate matter: a Canadian national-level cohort study. *Environ Health Perspect.* **120**(5), pp.708-714.

Cubison, M.J., Ortega, A.M., Hayes, P.L., Farmer, D.K., Day, D., Lechner, M.J., Brune, W.H., Apel, E., Diskin, G.S., Fisher, J.A., Fuelberg, H.E., Hecobian, A., Knapp, D.J., Mikoviny, T., Riemer, D., Sachse, G.W., Sessions, W., Weber, R.J., Weinheimer, A.J., Wisthaler, A. and Jimenez, J.L. 2011. Effects of aging on organic aerosol from open biomass burning smoke in aircraft and laboratory studies. *Atmospheric Chemistry and Physics.* **11**(23), pp.12049-12064.

Dall'Amico, M., Gray, L.J., Rosenlof, K.H., Scaife, A.A., Shine, K.P. and Stott, P.A. 2010. Stratospheric temperature trends: impact of ozone variability and the QBO. *Climate dynamics.* **34**(2-3), pp.381-398.

Davies, T., Cullen, M.J.P., Malcolm, A.J., Mawson, M.H., Staniforth, A., White, A.A. and Wood, N. 2005. A new dynamical core for the Met Office's global and regional modelling of the atmosphere. *Quarterly Journal of the Royal Meteorological Society.* **131**(608), pp.1759-1782.

Davis, J.M., Bhave, P.V. and Foley, K.M. 2008. Parameterization of N_2O_5 reaction probabilities on the surface of particles containing ammonium, sulfate, and nitrate. *Atmospheric Chemistry and Physics.* **8**(17), pp.5295-5311.

Dee, D.P. et al. 2011. The ERA-Interim reanalysis: configuration and performance of the data assimilation system. *Quarterly Journal of the Royal Meteorological Society.* **137**(656), pp.553-597.

Deichmann, U., Balk, D. and Yetman, G. 2001. Transforming population data for interdisciplinary usages: from census to grid. *Washington (DC): Center for International Earth Science Information Network.* **200**(1).

Dentener, F., Kinne, S., Bond, T., Boucher, O., Cofala, J., Generoso, S., Ginoux, P., Gong, S., Hoelzemann, J.J., Ito, A., Marelli, L., Penner, J.E., Putaud, J.P., Textor, C., Schulz, M., van der Werf, G.R. and Wilson, J. 2006. Emissions of primary aerosol and precursor gases in the years 2000 and 1750 prescribed data-sets for AeroCom. *Atmospheric Chemistry and Physics.* **6**(12), pp.4321-4344.

Dentener, F.J. and Crutzen, P.J. 1993. Reaction of N2O5 on tropospheric aerosols: Impact on the global distributions of NO x, O3, and OH. *Journal of Geophysical Research: Atmospheres.* **98**(D4), pp.7149-7163.

Dockery, D.W., Pope, C.A., Xu, X., Spengler, J.D., Ware, J.H., Fay, M.E., Ferris, B.G. and Speizer, F.E. 1994. An Association between Air Pollution and Mortality in Six U.S. Cities. *New England Journal of Medicine.* **329**(24), pp.1753-1759.

Drugé, T., Nabat, P., Mallet, M. and Somot, S. 2019. Model simulation of ammonium and nitrate aerosols distribution in the Euro-Mediterranean region and their radiative and climatic effects over 1979–2016. *Atmos. Chem. Phys.* **19**(6), pp.3707-3731.

Easter, R.C. and Hales, J.M. 1983. Interpretation of the OSCAR data for reactive gas scavenging. pp.649-662.

Edwards, J.M. and Slingo, A. 1996. Studies with a flexible new radiation code. I: Choosing a configuration for a large-scale model. *Quarterly Journal of the Royal Meteorological Society.* **122**(531), pp.689-719.

Erisman, J.W. and Schaap, M. 2004. The need for ammonia abatement with respect to secondary PM reductions in Europe. *Environmental Pollution.* **129**(1), pp.159-163.

Evans, M.J. and Jacob, D.J. 2005. Impact of new laboratory studies of N_2O_5 hydrolysis on global model budgets of tropospheric nitrogen oxides, ozone, and OH. *Geophysical Research Letters.* **32**(9), pp.L09813-L09813.

Fagerli, H. and Aas, W. 2008. Trends of nitrogen in air and precipitation: model results and observations at EMEP sites in Europe, 1980--2003. *Environmental pollution.* **154**(3), pp.448-461.

Fanourgakis, G.S. et al. 2019. Evaluation of global simulations of aerosol particle number and cloud condensation nuclei, and implications for cloud droplet formation. *Atmospheric Chemistry and Physics Discussions.* pp.1-40.

Fenech, S., Doherty, R.M., Heaviside, C., Vardoulakis, S., Macintyre, H.L., amp, apos and Connor, F.M. 2018. The influence of model spatial resolution on simulated ozone and fine particulate matter for Europe: implications for health impact assessments. *Atmospheric Chemistry and Physics.* **18**(8), pp.5765-5784.

Feng, Y. and Penner, J.E. 2007. Global modeling of nitrate and ammonium: Interaction of aerosols and tropospheric chemistry. *Journal of Geophysical Research.* **112**(D1), pp.D01304-D01304.

Finlayson-Pitts, B.J. and Pitts Jr, J.N. 1999. *Chemistry of the upper and lower atmosphere: theory, experiments, and applications.* Elsevier.

Ford, B. and Heald, C.L. 2016. Exploring the Uncertainty Associated with Satellite-Based Estimates of Premature Mortality due to Exposure to Fine Particulate Matter. **16**, pp.3499-3523.

Forouzanfar, M.H. et al. 2016. Global, regional, and national comparative risk assessment of 79 behavioural, environmental and occupational, and metabolic risks or clusters of risks, 1990–2015: a systematic analysis for the Global Burden of Disease Study 2015. *The Lancet.* **388**(10053), pp.1659-1724.

Forster, P., Ramaswamy, V., Artaxo, P., Berntsen, T., Betts, R., Fahey, D.W., Haywood, J., Lean, J., Lowe, D.C. and Myhre, G. 2007. Changes in atmospheric constituents and in radiative forcing. Chapter 2. *Climate Change 2007. The Physical Science Basis.* Cambridge, United Kingdom and New York, NY, USA.: Cambridge University Press.

Fountoukis, C. and Nenes, A. 2005. Continued development of a cloud droplet formation parameterization for global climate models. *Journal of Geophysical Research.* **110**(D11).

Fountoukis, C. and Nenes, A. 2007. ISORROPIA II: a computationally efficient thermodynamic equilibrium model for K^+–Ca^{2+}–Mg^{2+}–NH_4^+–Na^+–SO_4^{2-}–NO_3^-–Cl^-–H_2O aerosols. *Atmos. Chem. Phys.* **7**(17), pp.4639-4659.

Frossard, A.A., Shaw, P.M., Russell, L.M., Kroll, J.H., Canagaratna, M.R., Worsnop, D.R., Quinn, P.K. and Bates, T.S. 2011. Springtime Arctic haze contributions of submicron organic particles from European and Asian combustion sources. *Journal of Geophysical Research: Atmospheres.* **116**(D5).

Fuchs, N.A. and Sutugin, A.G. 1971. Highly dispersed aerosols. In: Hidy, G.M. and Brock, J.R. eds. *Topics in Current Aerosol Research.* New York: Pergamon, pp.1-60.

Giannakopoulos, C., Chipperfield, M.P., Law, K.S. and Pyle, J.A. 1999. Validation and intercomparison of wet and dry deposition schemes using ^{210}Pb in a global three-dimensional off-line chemical transport model. *Journal of Geophysical Research: Atmospheres.* **104**(D19), pp.23761-23784.

Gidden, M.J., Riahi, K., Smith, S.J., Fujimori, S., Luderer, G., Kriegler, E., van Vuuren, D.P., van den Berg, M., Feng, L., Klein, D., Calvin, K., Doelman, J.C., Frank, S., Fricko, O., Harmsen, M., Hasegawa, T., Havlik, P., Hilaire, J., Hoesly, R., Horing, J., Popp, A., Stehfest, E. and Takahashi, K. 2018. Global emissions pathways under different socioeconomic scenarios for use in CMIP6: a dataset of harmonized emissions trajectories through the end of the century. *Geosci. Model Dev. Discuss.* **2018**, pp.1-42.

Gong, S.L. 2003. A parameterization of sea-salt aerosol source function for sub- and super-micron particles. *Global Biogeochemical Cycles.* **17**(4), p1097.

Gordon, H. et al. 2017. Causes and importance of new particle formation in the present-day and preindustrial atmospheres. *Journal of Geophysical Research: Atmospheres.* **122**(16), pp.8739-8760.

Government of India, I. 2016. Continuous Ambient Air Quality Monitoring (CAAQM). Central Pollution Control Board (CPCB), Ministry of Environment and Forests. [Online]. [Accessed 1st July 2016]. Available from: http://www.cpcb.gov.in/CAAQM/

Granier, C., Bessagnet, B., Bond, T., Angiola, A.D., Gon, H.D.V.D., Frost, G.J., Heil, A., Kaiser, J.W., Kinne, S., Klimont, Z., Kloster, S. and Lamarque, J.-f. 2011. Evolution of anthropogenic and biomass burning emissions of air pollutants at global and regional scales during the 1980 – 2010 period. pp.163-190.

Gregory, D. and Rowntree, P. 1990. A mass flux convection scheme with representation of cloud ensemble characteristics and stabilitydependent closure. *Mon. Weather Rev.* **118**, pp.1483-1506.

Griffith, S.M., Huang, X.H.H., Louie, P.K.K. and Yu, J.Z. 2015. Characterizing the thermodynamic and chemical composition factors controlling PM2.5 nitrate: Insights gained from two years of online measurements in Hong Kong. *Atmospheric Environment.* **122**, pp.864-875.

Griffiths, P.T., Badger, C.L., Cox, R.A., Folkers, M., Henk, H.H. and Mentel, T.F. 2009. Reactive Uptake of N_2O_5 by Aerosols Containing Dicarboxylic Acids. Effect of Particle Phase, Composition, and Nitrate Content. *The Journal of Physical Chemistry A.* **113**(17), pp.5082-5090.

Guenther, A., Hewitt, C.N., Erickson, D., Fall, R., Geron, C., Graedel, T., Harley, P., Klinger, L., Lerdau, M., McKay, W.A., Pierce, T., Scholes, B., Steinbrecher, R., Tallamraju, R., Taylor, J. and Zimmerman, P. 1995. A global model of natural volatile organic compound emissions. *Journal of Geophysical Research.* **100**(D5), pp.8873-8873.

Guibert, S., Snider, S. and Brenguier, J.-S. 2003. Aerosol activation in marine stratocumulus clouds: 1. Measurement validation for a closure study. *Journal of Geophysical Research.* **108**(D15).

Guo, H., Otjes, R., Schlag, P., Kiendler-Scharr, A., Nenes, A. and Weber, R.J. 2018. Effectiveness of Ammonia Reduction on Control of Fine Particle Nitrate. *Atmospheric Chemistry and Physics Discussions.* pp.1-31.

Hallquist, M., Stewart, D.J., Stephenson, S.K. and Anthony Cox, R. 2003. Hydrolysis of N_2O_5 on sub-micron sulfate aerosols. *Phys. Chem. Chem. Phys.* **5**(16), pp.3453-3463.

Halmer, M.M., Schmincke, H.U. and Graf, H.F. 2002. The annual volcanic gas input into the atmosphere, in particular into the stratosphere: A global data set for the past 100 years. *Journal of Volcanology and Geothermal Research.* **115**(3-4), pp.511-528.

Hand, J.L., Schichtel, B.A., Pitchford, M., Malm, W.C. and Frank, N.H. 2012. Seasonal composition of remote and urban fine particulate matter in the United States. *Journal of Geophysical Research: Atmospheres.* **117**(D5).

Harrison, R.M., Jones, A.M., Beddows, D.C.S. and Derwent, R.G. 2013. The effect of varying primary emissions on the concentrations of inorganic aerosols predicted by the enhanced UK Photochemical Trajectory Model. *Atmospheric Environment.* **69**, pp.211-218.

Hauglustaine, D.A., Hourdin, F., Jourdain, L., Filiberti, M.A., Walters, S., Lamarque, J.F. and Holland, E.A. 2004. Interactive chemistry in the Laboratoire de Météorologie Dynamique general circulation model: Description and background tropospheric chemistry evaluation. *Journal of Geophysical Research: Atmospheres.* **109**(D4).

Hauglustaine, D.A., Balkanski, Y. and Schulz, M. 2014. A global model simulation of present and future nitrate aerosols and their direct radiative forcing of climate. *Atmospheric Chemistry and Physics.* **14**(20), pp.11031-11063.

Heald, C.L., Coe, H., Jimenez, J.L., Weber, R.J., Bahreini, R., Middlebrook, A.M., Russell, L.M., Jolleys, M., Fu, T.M., Allan, J.D., Bower, K.N., Capes, G., Crosier, J., Morgan, W.T., Robinson, N.H., Williams, P.I., Cubison, M.J., DeCarlo, P.F. and Dunlea, E.J. 2011. Exploring the vertical profile of atmospheric organic aerosol: comparing 17 aircraft field campaigns with a global model. *Atmospheric Chemistry and Physics.* **11**(24), pp.12673-12696.

Heald, C.L., J. L. Collett, J., Lee, T., Benedict, K.B., Schwandner, F.M., Li, Y., Clarisse, L., Hurtmans, D.R., Van Damme, M., Clerbaux, C., Coheur, P.F., Philip, S., Martin, R.V. and Pye, H.O.T. 2012. Atmospheric ammonia and particulate inorganic nitrogen over the United States. *Atmospheric Chemistry and Physics.* **12**(21), pp.10295-10312.

Henze, D.K., Hakami, A. and Seinfeld, J.H. 2007. Development of the adjoint of GEOS-Chem. *Atmospheric Chemistry and Physics.* **7**(9), pp.2413-2433.

Hering, S. and Cass, G. 1999. The Magnitude of Bias in the Measurement of PM25 Arising from Volatilization of Particulate Nitrate from Teflon Filters. *Journal of the Air & Waste Management Association.* **49**(6), pp.725-733.

Hewitt, H.T., Copsey, D., Culverwell, I.D., Harris, C.M., Hill, R.S.R., Keen, A.B., McLaren, A.J. and Hunke, E.C. 2011. Design and implementation of the infrastructure of HadGEM3: the next-generation Met Office climate modelling system. *Geoscientific Model Development.* **4**(2), pp.223-253.

Hoesly, R.M., Smith, S.J., Feng, L., Klimont, Z., Janssens-Maenhout, G., Pitkanen, T., Seibert, J.J., Vu, L., Andres, R.J., Bolt, R.M., Bond, T.C., Dawidowski, L., Kholod, N., Kurokawa, J.I., Li, M., Liu, L., Lu, Z., Moura, M.C.P., O'Rourke, P.R. and Zhang, Q. 2018. Historical (1750–2014) anthropogenic emissions of reactive gases and aerosols from the Community Emissions Data System (CEDS). *Geosci. Model Dev.* **11**(1), pp.369-408.

Holt, J., Selin, N.E. and Solomon, S. 2015. Changes in Inorganic Fine Particulate Matter Sensitivities to Precursors Due to Large-Scale US Emissions Reductions. *Environmental Science & Technology.* **49**(8), pp.4834-4841.

Hoppel, W.A., Frick, G.M., Fitzgerald, J.W. and Larson, R.E. 1994. Marine boundary layer measurements of new particle formation and the effects nonprecipitating clouds have on aerosol size distribution. *Journal of Geophysical Research.* **99**(D7), pp.14443-14443.

Huijnen, V., Williams, J. and Flemming, J. 2014. Modeling global impacts of heterogeneous loss of HO 2 on cloud droplets, ice particles and aerosols. *Atmospheric Chemistry and Physics Discussions.* **14**(6), pp.8575-8632.

Institute for Health Metrics and Evaluation, I. 2016. *Global Burden of Disease. Population Estimates 1950-2015.* Seattle, United States: Institute for Health Metrics and Evaluation (IHME).

Itahashi, S., Hayami, H., Uno, I., Pan, X. and Uematsu, M. 2016. Importance of coarse-mode nitrate produced via sea salt as atmospheric input to East Asian oceans. *Geophysical Research Letters.* **43**(10), pp.5483-5491.

IUPAC, S. *IUPAC Subcommittee for Gas Kinetic Data Evaluation for Atmospheric Chemistry. Evaluated Kinetic Data,*

Jacobson. 2001. Global direct radiative forcing due to multicomponent anthropogenic and natural aerosols. *Journal of Geophysical Research: Atmospheres.* **106**(D2), pp.1551-1568.

Jacobson, M.Z., Tabazadeh, A. and Turco, R.P. 1996. Simulating equilibrium within aerosols and nonequilibrium between gases and aerosols. *Journal of Geophysical Research: Atmospheres.* **101**(D4), pp.9079-9091.

Jacobson, M.Z. 1997. Numerical Techniques to Solve Condensational and Dissolutional Growth Equations When Growth is Coupled to Reversible Reactions. *Aerosol Science and Technology.* **27**(4), pp.491-498.

Jacobson, M.Z. 1999. Studying the effects of calcium and magnesium on size-distributed nitrate and ammonium with EQUISOLV II. *Atmospheric Environment.* **33**(22), pp.3635-3649.

Jaeglé, L., Steinberger, L., Martin, R.V. and Chance, K. 2005. Global partitioning of NOx sources using satellite observations: Relative roles of fossil fuel combustion, biomass burning and soil emissions. *Faraday Discussions.* **130**, p407.

Janssens-Maenhout, G., Crippa, M., Guizzardi, D., Dentener, F., Muntean, M., Pouliot, G., Keating, T., Zhang, Q., Kurokawa, J., Wankmüller, R., Denier van der Gon, H., Kuenen, J.J.P., Klimont, Z., Frost, G., Darras, S., Koffi, B. and Li, M. 2015. HTAP_v2.2: a mosaic of regional and global emission grid maps for 2008 and 2010 to study hemispheric transport of air pollution. *Atmospheric Chemistry and Physics.* **15**(19), pp.11411-11432.

Jöckel, P., Kerkweg, A., Pozzer, A., Sander, R., Tost, H., Riede, H., Baumgaertner, A., Gromov, S. and Kern, B. 2010. Development cycle 2 of the Modular Earth Submodel System (MESSy2). *Geoscientific Model Development.* **3**(2), pp.717-752.

Kapadia, Z. 2015. *Quantifying the climate and air quality impacts of nonCO2 species from the combustion of standard and alternative fuels in aviation*. PhD thesis, University of Leeds, U.K.

Kapadia, Z.Z., Spracklen, D.V., Arnold, S.R., Borman, D.J., Mann, G.W., Pringle, K.J., Monks, S.A., Reddington, C.L., Benduhn, F., Rap, A., Scott, C.E., Butt, E.W. and Yoshioka, M. 2016. Impacts of aviation fuel sulfur content on climate and human health. *Atmospheric Chemistry and Physics.* **16**(16), pp.10521-10541.

Karydis, V., Capps, S., H. Moore, R., G. Russell, A., K. Henze, D. and Nenes, A. 2012a. Using a global aerosol model adjoint to unravel the footprint of spatially-distributed emissions on cloud droplet number and cloud albedo. *Geophysical Research Letters.* **39**(L24804).

Karydis, V.A., Capps, S.L., Russell, A.G. and Nenes, A. 2012b. Adjoint sensitivity of global cloud droplet number to aerosol and dynamical parameters. *Atmospheric Chemistry and Physics.*

Karydis, V.A., Tsimpidi, A.P., Pozzer, A., Astitha, M. and Lelieveld, J. 2016. Effects of mineral dust on global atmospheric nitrate concentrations. *Atmospheric Chemistry and Physics.* **16**(3), pp.1491-1509.

Kelly, J.M., Doherty, R.M., O'Connor, F.M. and Mann, G.W. 2018. The impact of biogenic, anthropogenic, and biomass burning volatile organic compound emissions on regional and seasonal variations in secondary organic aerosol. *Atmos. Chem. Phys.* **18**(10), pp.7393-7422.

Kettle, A.J. and Andreae, M.O. 2000. Flux of dimethylsulfide from the oceans: A comparison of updated data sets and flux models. *Journal of Geophysical Research: Atmospheres.* **105**(D22), pp.26793-26808.

Kipling, Z., Stier, P., Schwarz, J.P., Perring, A.E., Spackman, J.R., Mann, G.W., Johnson, C.E. and Telford, P.J. 2013. Constraints on aerosol processes in climate models from vertically-resolved aircraft observations of black carbon. *Atmospheric Chemistry and Physics.* **13**(12), pp.5969-5986.

Kipling, Z., Stier, P., Johnson, C.E., Mann, G.W., Bellouin, N., Bauer, S.E., Bergman, T., Chin, M., Diehl, T., Ghan, S.J., Iversen, T., Kirkevåg, A., Kokkola, H., Liu, X., Luo, G., van Noije, T., Pringle, K.J., von Salzen, K., Schulz, M., Seland, Ø., Skeie, R.B., Takemura, T., Tsigaridis, K. and Zhang, K. 2016. What controls the vertical distribution of aerosol? Relationships between process sensitivity in HadGEM3–UKCA and inter-model variation from AeroCom Phase II. *Atmospheric Chemistry and Physics.* **16**(4), pp.2221-2241.

Klemm, R.J., Thomas, E.L. and Wyzga, R.E. 2011. The impact of frequency and duration of air quality monitoring: Atlanta, GA, data modeling of air pollution and mortality. *J Air Waste Manag Assoc.* **61**(11), pp.1281-1291.

Kodros, J.K., Wiedinmyer, C., Ford, B., Cucinotta, R., Gan, R., Magzamen, S. and Pierce, J.R. 2016. Global burden of mortalities due to chronic exposure to ambient PM2.5 from open combustion of domestic waste. *Environmental Research Letters.* **11**(12), p124022.

Kreidenweis, S.M., Walcek, C.J., Feingold, G., Gong, W., Jacobson, M.Z., Kim, C.H., Xiaohong, L., Penner, J.E., Nenes, A. and Seinfeld, J.H. 2003. Modification of aerosol mass and size distribution due to aqueous-phase SO 2 oxidation in clouds: Comparisons of several models. *Journal of Geophysical Research.* **108**(D7), pp.4213-4213.

Kulmala, M., Korhonen, P., Laaksonen, A. and Vesala, T. 1995. Changes in cloud properties due to NOx emissions. *Geophysical research letters.* **22**(3), pp.239-242.

Kulmala, M., Laaksonen, A. and Pirjola, L. 1998a. Parameterizations for sulfuric acid/water nucleation rates. *Journal of Geophysical Research: Atmospheres.* **103**(D7), pp.8301-8307.

Kulmala, M., Toivonen, A., Mattila, T. and Korhonen, P. 1998b. Variations of cloud droplet concentrations and the optical properties of clouds due to

changing hygroscopicity: A model study. *Journal of Geophysical Research: Atmospheres.* **103**(D13), pp.16183-16195.

Lamarque, J.F., Bond, T.C., Eyring, V., Granier, C., Heil, A., Klimont, Z., Lee, D., Liousse, C., Mieville, A., Owen, B., Schultz, M.G., Shindell, D., Smith, S.J., Stehfest, E., Van Aardenne, J., Cooper, O.R., Kainuma, M., Mahowald, N., McConnell, J.R., Naik, V., Riahi, K. and van Vuuren, D.P. 2010. Historical (1850–2000) gridded anthropogenic and biomass burning emissions of reactive gases and aerosols: methodology and application. *Atmospheric Chemistry and Physics.* **10**(15), pp.7017-7039.

Lamsal, L.N., Martin, R.V., Padmanabhan, A., van Donkelaar, A., Zhang, Q., Sioris, C.E., Chance, K., Kurosu, T.P. and Newchurch, M.J. 2011. Application of satellite observations for timely updates to global anthropogenic NOxemission inventories. *Geophysical Research Letters.* **38**(5), pp.n/a-n/a.

Lanzinger, S., Schneider, A., Breitner, S., Stafoggia, M., Erzen, I., Dostal, M., Pastorkova, A., Bastian, S., Cyrys, J., Zscheppang, A., Kolodnitska, T. and Peters, A. 2016. Ultrafine and Fine Particles and Hospital Admissions in Central Europe. Results from the UFIREG Study. *American Journal of Respiratory and Critical Care Medicine.* **194**(10), pp.1233-1241.

Lee, C.J., Martin, R.V., Henze, D.K., Brauer, M., Cohen, A. and Donkelaar, A.v. 2015. Response of Global Particulate-Matter-Related Mortality to Changes in Local Precursor Emissions. *Environmental Science & Technology.* **49**(7), pp.4335-4344.

Lee, H.-M., Henze, D.K., Alexander, B. and Murray, L.T. 2014. Investigating the sensitivity of surface-level nitrate seasonality in Antarctica to primary sources using a global model. *Atmospheric Environment.* **89**, pp.757-767.

Lee, L.A., Pringle, K.J., Reddington, C.L., Mann, G.W., Stier, P., Spracklen, D.V., Pierce, J.R. and Carslaw, K.S. 2013. The magnitude and causes of uncertainty in global model simulations of cloud condensation nuclei. *Atmospheric Chemistry and Physics.* **13**(17), pp.8879-8914.

Lee, T., Yu, X.-Y., Ayres, B., Kreidenweis, S.M., Malm, W.C. and Collett, J.L. 2008. Observations of fine and coarse particle nitrate at several rural locations in the United States. *Atmospheric Environment.* **42**(11), pp.2720-2732.

Leibensperger, E.M., Mickley, L.J., Jacob, D.J., Chen, W.T., Seinfeld, J.H., Nenes, A., Adams, P.J., Streets, D.G., Kumar, N. and Rind, D. 2012. Climatic effects of 1950-2050 changes in US anthropogenic aerosols ; Part 1: Aerosol trends and radiative forcing. *Atmos. Chem. Phys.* **12**(7), pp.3333-3348.

Lelieveld, J., Evans, J.S., Fnais, M., Giannadaki, D. and Pozzer, A. 2015. The contribution of outdoor air pollution sources to premature mortality on a global scale. *Nature.* **525**(7569), pp.367-371.

Li, C., Martin, R.V., Van Donkelaar, A., Boys, B.L., Hammer, M.S., Xu, J.W., Marais, E.A., Reff, A., Strum, M., Ridley, D.A., Crippa, M., Brauer, M. and Zhang, Q. 2017. Trends in Chemical Composition of Global and Regional Population-Weighted Fine Particulate Matter Estimated for 25 Years. *Environmental Science and Technology.*

Li, J., Wang, W.-C., Liao, H. and Chang, W. 2015. Past and future direct radiative forcing of nitrate aerosol in East Asia. *Theoretical and Applied Climatology.* **121**(3-4), pp.445-458.

Li, K., Jacob, D.J., Liao, H., Shen, L., Zhang, Q. and Bates, K.H. 2019. Anthropogenic drivers of 2013–2017 trends in summer surface ozone in China. *Proceedings of the National Academy of Sciences.* **116**(2), p422.

Li, S., Wang, T., Zhuang, B. and Han, Y. 2009. Indirect radiative forcing and climatic effect of the anthropogenic nitrate aerosol on regional climate of China. *Advances in Atmospheric Sciences.* **26**(3), pp.543-552.

Li, Y., Henze, D.K., Jack, D. and Kinney, P.L. 2016. The influence of air quality model resolution on health impact assessment for fine particulate matter and its components. *Air Quality, Atmosphere & Health.* **9**(1), pp.51-68.

Liao, H., Seinfeld, J.H., Adams, P.J. and Mickley, L.J. 2004. Global radiative forcing of coupled tropospheric ozone and aerosols in a unified general circulation model. *Journal of Geophysical Research: Atmospheres.* **109**(D16).

Liao, H. and Seinfeld, J.H. 2005. Global impacts of gas-phase chemistry-aerosol interactions on direct radiative forcing by anthropogenic aerosols and ozone. *Journal of Geophysical Research D: Atmospheres.* **110**(18), pp.1-22.

Lim, S.S. et al. 2012. A comparative risk assessment of burden of disease and injury attributable to 67 risk factors and risk factor clusters in 21 regions, 1990–2010: a systematic analysis for the Global Burden of Disease Study 2010. *The Lancet.* **380**(9859), pp.2224-2260.

Liss, P.S. and Merlivat, L. 1986. Air–Sea Gas Exchange Rates: Introduction and Synthesis. In: P., B.-M. ed. *The Role of Air-Sea Exchange in Geochemical Cycling. NATO ASI Series (Series C: Mathematical and Physical Sciences).* Dordrecht: Springer.

Liu, F., Zhang, Q., van der A, R.J., Zheng, B., Tong, D., Yan, L., Zheng, Y. and He, K. 2016. Recent reduction in NO x emissions over China: synthesis of satellite observations and emission inventories. *Environmental Research Letters.* **11**(11), p114002.

Liu, Y., Zhang, S., Fan, Q., Wu, D., Chan, P., Wang, X., Fan, S., Feng, Y. and Hong, Y. 2015. Accessing the Impact of Sea-Salt Emissions on Aerosol Chemical Formation and Deposition over Pearl River Delta, China. *Aerosol and Air Quality Research.* **15**(6), pp.2232-2245.

Lock, A., Brown, A., Bush, M., Martin, G. and Smith, R. 2000. A new boundary layer mixing scheme. Part I: Scheme description and single-column model tests. *Mon. Weather. Rev.* **128**, pp.3187-3199.

Lowe, D., Archer-Nicholls, S., Morgan, W., Allan, J., Utembe, S., Ouyang, B., Aruffo, E., Le Breton, M., Zaveri, R.A., Di Carlo, P., Percival, C., Coe, H., Jones, R. and McFiggans, G. 2015. WRF-Chem model predictions of the regional impacts of N2O5 heterogeneous processes on night-time chemistry over north-western Europe. *Atmospheric Chemistry and Physics.* **15**(3), pp.1385-1409.

Lu, Z., Zhang, Q. and Streets, D.G. 2011. Sulfur dioxide and primary carbonaceous aerosol emissions in China and India, 1996–2010. *Atmos. Chem. Phys.* **11**(18), pp.9839-9864.

Lund, M.T., Myhre, G., Haslerud, A.S., Skeie, R.B., Griesfeller, J., Platt, S.M., Kumar, R., Myhre, C.L. and Schulz, M. 2018. Concentrations and radiative forcing of anthropogenic aerosols from 1750 to 2014 simulated with the Oslo CTM3 and CEDS emission inventory. *Geosci. Model Dev.* **11**(12), pp.4909-4931.

Macintyre, H.L. and Evans, M.J. 2010. Sensitivity of a global model to the uptake of N_2O_5 by tropospheric aerosol. *Atmos. Chem. Phys.* **10**(15), pp.7409-7414.

Macintyre, H.L. and Evans, M.J. 2011. Parameterisation and impact of aerosol uptake of HO_2 on a global tropospheric model. *Atmospheric Chemistry and Physics.* **11**(21), pp.10965-10974.

Mahowald, N. 2011. Aerosol Indirect Effect on Biogeochemical Cycles and Climate. *Science.* **334**(6057), p794.

Makkonen, R., Romakkaniemi, S., Kokkola, H., Stier, P., Räisänen, P., Rast, S., Feichter, J., Kulmala, M. and Laaksonen, A. 2012. Brightening of the global cloud field by nitric acid and the associated radiative forcing. *Atmospheric Chemistry and Physics.* **12**(16), pp.7625-7633.

Malm, W.C., Schichtel, B.A., Pitchford, M.L., Ashbaugh, L.L. and Eldred, R.A. 2004. Spatial and monthly trends in speciated fine particle concentration in the United States. *Journal of Geophysical Research: Atmospheres.* **109**(D3).

Manktelow, P.T., Mann, G.W., Carslaw, K.S., Spracklen, D.V. and Chipperfield, M.P. 2007. Regional and global trends in sulfate aerosol since the 1980s. *Geophysical Research Letters.* **34**(14), pp.L14803-L14803.

Mann, G.W., Carslaw, K.S., Spracklen, D.V., Ridley, D.A., Manktelow, P.T. and Chipperfield, M.P. 2010. Description and evaluation of GLOMAP-mode : a modal global aerosol microphysics model for the UKCA composition-climate model. pp.519-551.

Mann, G.W., Carslaw, K.S., Ridley, D.A., Spracklen, D.V., Pringle, K.J., Merikanto, J., Korhonen, H., Schwarz, J.P., Lee, L.A., Manktelow, P.T., Woodhouse, M.T., Schmidt, A., Breider, T.J., Emmerson, K.M., Reddington, C.L., Chipperfield, M.P. and Pickering, S.J. 2012. Intercomparison of modal and sectional aerosol microphysics representations within the same 3-D global chemical transport model. *Atmospheric Chemistry and Physics.* **12**(10), pp.4449-4476.

Mann, G.W. et al. 2014. Intercomparison and evaluation of global aerosol microphysical properties among AeroCom models of a range of complexity. *Atmospheric Chemistry and Physics.* **14**(9), pp.4679-4713.

Mao, J., Jacob, D.J., Evans, M.J., Olson, J.R., Ren, X., Brune, W.H., Clair, J.M.S., Crounse, J.D., Spencer, K.M., Beaver, M.R., Wennberg, P.O., Cubison, M.J., Jimenez, J.L., Fried, A., Weibring, P., Walega, J.G., Hall, S.R., Weinheimer, A.J., Cohen, R.C., Chen, G., Crawford, J.H., McNaughton, C., Clarke, A.D., Jaeglé, L., Fisher, J.A., Yantosca, R.M., Le Sager, P. and Carouge, C. 2010. Chemistry of hydrogen oxide radicals (HOx) in the Arctic troposphere in spring. *Atmospheric Chemistry and Physics.* **10**(13), pp.5823-5838.

Marple, V.A., Rubow, K.L. and Behm, S.M. 1991. A Microorifice Uniform Deposit Impactor (MOUDI): Description, Calibration, and Use. *Aerosol Science and Technology.* **14**(4), pp.434-446.

Martin, G.M., Ringer, M.A., Pope, V.D., Jones, A., Dearden, C. and Hinton, T.J. 2006. The Physical Properties of the Atmosphere in the New Hadley Centre Global Environmental Model (HadGEM1). Part I: Model Description and Global Climatology. *J. Climate.* **19**, pp.1274-1130.

Masson-Delmotte, V., Zhai, P., Pörtner, H.O., Roberts, D., Skea, J., Shukla, P.R., Pirani, A., Moufouma-Okia, W., Péan, C., Pidcock, R., Connors, S., Matthews, J.B.R., Chen, Y., Zhou, X., Gomis, M.I., Lonnoy, E., Maycock, T.,

Tignor, M. and Waterfield, T. 2018. IPCC, 2018: Summary for Policymakers. *Global warming of 1.5°C. An IPCC Special Report on the impacts of global warming of 1.5°C above pre-industrial levels and related global greenhouse gas emission pathways, in the context of strengthening the global response to the threat of climate change, sustainable development, and efforts to eradicate poverty* Geneva, Switzerland: World Meteorological Organization, p.32.

Megaritis, A.G., Fountoukis, C., Charalampidis, P.E., Pilinis, C. and Pandis, S.N. 2013. Response of fine particulate matter concentrations to changes of emissions and temperature in Europe. *Atmospheric Chemistry and Physics.* **13**(6), pp.3423-3443.

Megaritis, a.G., Fountoukis, C., Charalampidis, P.E., Denier van der Gon, H.a.C., Pilinis, C. and Pandis, S.N. 2014. Linking climate and air quality over Europe: effects of meteorology on PM2.5 concentrations. *Atmos. Chem. Phys. Discuss.* **14**(7), pp.10345-10391.

Meng, Z. and Seinfeld, J.H. 1996. Time scales to achieve atmospheric gas-aerosol equilibrium for volatile species. *Atmospheric Environment.* **30**(16), pp.2889-2900.

Mensah, A.A., Holzinger, R., Otjes, R., Trimborn, A., Mentel, T.F., Ten Brink, H., Henzing, B. and Kiendler-Scharr, A. 2012. Aerosol chemical composition at Cabauw, the Netherlands as observed in two intensive periods in May 2008 and March 2009. *Atmospheric Chemistry and Physics.* **12**(10), pp.4723-4742.

Mentel, T.F., Sohn, M. and Wahner, A. 1999. Nitrate effect in the heterogeneous hydrolysis of dinitrogen pentoxide on aqueous aerosols. *Physical Chemistry Chemical Physics.* **1**(24), pp.5451-5457.

Mercado, L.M., Bellouin, N., Sitch, S., Boucher, O., Huntingford, C., Wild, M. and Cox, P.M. 2009. Impact of changes in diffuse radiation on the global land carbon sink. *Nature.* **458**(7241), pp.1014-1017.

Merikanto, J., Spracklen, D.V., Mann, G.W., Pickering, S.J. and Carslaw, K.S. 2009. Impact of nucleation on global CCN. *Atmospheric Chemistry and Physics.* **9**(21), pp.8601-8616.

Mezuman, K., Bauer, S.E. and Tsigaridis, K. 2016. Evaluating secondary inorganic aerosols in three dimensions. *Atmospheric Chemistry and Physics.* **16**(16), pp.10651-10669.

Morgan, W.T., Allan, J.D., Bower, K.N., Highwood, E.J., Liu, D., McMeeking, G.R., Northway, M.J., Williams, P.I., Krejci, R. and Coe, H. 2010a. Airborne measurements of the spatial distribution of aerosol chemical composition across Europe and evolution of the organic fraction. *Atmospheric Chemistry and Physics.* **10**(8), pp.4065-4083.

Morgan, W.T., Allan, J.D., Bower, K.N., Esselborn, M., Harris, B., Henzing, J.S., Highwood, E.J., Kiendler-Scharr, A., McMeeking, G.R., Mensah, a.a., Northway, M.J., Osborne, S., Williams, P.I., Krejci, R. and Coe, H. 2010b. Enhancement of the aerosol direct radiative effect by semi-volatile aerosol components: airborne measurements in North-Western Europe. *Atmospheric Chemistry and Physics.* **10**(17), pp.8151-8171.

Morgan, W.T., Ouyang, B., Allan, J.D., Aruffo, E., Di Carlo, P., Kennedy, O.J., Lowe, D., Flynn, M.J., Rosenberg, P.D., Williams, P.I., Jones, R., McFiggans, G.B. and Coe, H. 2015. Influence of aerosol chemical composition on N_2O_5

uptake: airborne regional measurements in northwestern Europe. *Atmospheric Chemistry and Physics.* **15**(2), pp.973-990.

Morgenstern, O., Braesicke, P., O'Connor, F.M., Bushell, A.C., Johnson, C.E., Osprey, S.M. and Pyle, J.A. 2009. Evaluation of the new UKCA climate-composition model – Part 1: The stratosphere. *Geoscientific Model Development.* **2**(1), pp.43-57.

Morino, Y., Kondo, Y., Takegawa, N., Miyazaki, Y., Kita, K., Komazaki, Y., Fukuda, M., Miyakawa, T., Moteki, N. and Worsnop, D.R. 2006. Partitioning of HNO_3 and particulate nitrate over Tokyo: Effect of vertical mixing. *Journal of Geophysical Research.* **111**(D15), pp.D15215-D15215.

Moya, M., Ansari, A.S. and Pandis, S.N. 2001. Partitioning of nitrate and ammonium between the gas and particulate phases during the 1997 IMADA-AVER study in Mexico City. *Atmospheric Environment.* **35**(10), pp.1791-1804.

Murphy, J.G., Gregoire, P.K., Tevlin, A.G., Wentworth, G.R., Ellis, R.A., Markovic, M.Z. and VandenBoer, T.C. 2017. Observational constraints on particle acidity using measurements and modelling of particles and gases. *Faraday Discussions.* **200**(0), pp.379-395.

Murray, G.L.D., Kimball, K.D., Hill, L.B., Hislop, J.E. and Weathers, K.C. 2013. Long-term trends in cloud and rain chemistry on Mount Washington, New Hampshire. *Water, Air, and Soil Pollution.*

Myhre, G., Grini, A. and Metzger, S. 2006. Modelling of nitrate and ammonium-containing aerosols in presence of sea salt. *Atmospheric Chemistry and Physics.* **6**(12), pp.4809-4821.

Myhre, G., Berglen, T.F., Johnsrud, M., Hoyle, C.R., Berntsen, T.K., Christopher, S.a., Fahey, D.W., Isaksen, I.S.a., Jones, T.a., Kahn, R.a., Loeb, N., Quinn, P., Remer, L., Schwarz, J.P. and Yttri, K.E. 2009. Modelled radiative forcing of the direct aerosol effect with multi-observation evaluation. *Atmospheric Chemistry and Physics.* **9**(4), pp.1365-1392.

Myhre, G. et al. 2013a. Radiative forcing of the direct aerosol effect from AeroCom Phase II simulations. *Atmospheric Chemistry and Physics.* **13**(4), pp.1853-1877.

Myhre, G., Shindell, D., Bréon, F., Collins, W., Fuglestvedt, J., Huang, J., Koch, D., Lamarque, J., Lee, D. and Mendoza, B. 2013b. Anthropogenic and Natural Radiative Forcing. In: Climate Change 2013: The Physical Science Basis. Contribution of Working Group 1 to the Fifth Assessment Report of the Intergovernmental Panel on Climate Change. *Table.* **8**, p714.

Myhre, G., Aas, W., Cherian, R., Collins, W., Faluvegi, G., Flanner, M., Forster, P., Hodnebrog, Ø., Klimont, Z., Lund, M.T., Mülmenstädt, J., Lund Myhre, C., Olivié, D., Prather, M., Quaas, J., Samset, B.H., Schnell, J.L., Schulz, M., Shindell, D., Skeie, R.B., Takemura, T. and Tsyro, S. 2017. Multi-model simulations of aerosol and ozone radiative forcing due to anthropogenic emission changes during the period 1990–2015. *Atmos. Chem. Phys.* **17**(4), pp.2709-2720.

Nenes, A., Pandis, S.N. and Pilinis, C. 1998. ISORROPIA: A new thermodynamic equilibrium model for multiphase multicomponent inorganic aerosols. *Aquatic Geochemistry.*

Nenes, A. and Seinfeld, J.H. 2003. Parameterization of cloud droplet formation in global climate models. *Journal of Geophysical Research.* **108**(D14), pp.4415-4415.

O'Connor, F.M., Johnson, C.E., Morgenstern, O., Abraham, N.L., Braesicke, P., Dalvi, M., Folberth, G.A., Sanderson, M.G., Telford, P.J., Voulgarakis, A., Young, P.J., Zeng, G., Collins, W.J. and Pyle, J.A. 2014. Evaluation of the new UKCA climate-composition model-Part 2: The troposphere. *Geoscientific Model Development.*

O'Sullivan, M., Rap, A., Reddington, C.L., Spracklen, D.V., Gloor, M. and Buermann, W. 2016. Small global effect on terrestrial net primary production due to increased fossil fuel aerosol emissions from East Asia since the turn of the century. *Geophysical Research Letters.* **43**(15), pp.8060-8067.

O'Sullivan, M., Spracklen, D.V., Batterman, S.A., Arnold, S.R., Gloor, M. and Buermann, W. 2019. Have Synergies Between Nitrogen Deposition and Atmospheric CO_2 Driven the Recent Enhancement of the Terrestrial Carbon Sink? *Global Biogeochemical Cycles.* **33**(2), pp.163-180.

Olivier, J.G.J., Bouwman, A.F., Van der Hoek, K.W. and Berdowski, J.J.M. 1998. Global air emission inventories for anthropogenic sources of NO_x, NH_3 and N_2O in 1990. In: Van der Hoek, K.W., et al. eds. *Nitrogen, the Confer-N-s.* Amsterdam: Elsevier, pp.135-148.

Osthoff, H.D., Roberts, J.M., Ravishankara, A.R., Williams, E.J., Lerner, B.M., Sommariva, R., Bates, T.S., Coffman, D., Quinn, P.K., Dibb, J.E., Stark, H., Burkholder, J.B., Talukdar, R.K., Meagher, J., Fehsenfeld, F.C. and Brown, S.S. 2008. High levels of nitryl chloride in the polluted subtropical marine boundary layer. *Nature Geoscience.*

Ostro, B., Feng, W.-Y., Broadwin, R., Green, S. and Lipsett, M. 2007. The Effects of Components of Fine Particulate Air Pollution on Mortality in California: Results from CALFINE. *Environmental Health Perspectives.* **115**(1), pp.13-19.

Ostro, B., Reynolds, P., Goldberg, D., Hertz, A., Burnett, R.T., Shin, H., Hughes, E., Garcia, C., Henderson, K.D., Bernstein, L. and Lipsett, M. 2011. Assessing Long-Term Exposure in the California Teachers Study. *Environmental Health Perspectives.* **119**(6), pp.A242-A243.

Pan, Y., Wang, Y., Zhang, J., Liu, Z., Wang, L., Tian, S., Tang, G., Gao, W., Ji, D., Song, T. and Wang, Y. 2016. Redefining the importance of nitrate during haze pollution to help optimize an emission control strategy. *Atmospheric Environment.* **141**, pp.197-202.

Pathak, R.K., Wu, W.S. and Wang, T. 2009. Summertime $PM_{2.5}$ ionic species in four major cities of China: nitrate formation in an ammonia-deficient atmosphere. *Atmos. Chem. Phys.* **9**(5), pp.1711-1722.

Paulot, F. and Jacob, D.J. 2014. Hidden Cost of U.S. Agricultural Exports: Particulate Matter from Ammonia Emissions. *Environmental Science & Technology.* **48**(2), pp.903-908.

Paulot, F., Ginoux, P., Cooke, W.F., Donner, L.J., Fan, S., Lin, M.Y., Mao, J., Naik, V. and Horowitz, L.W. 2016. Sensitivity of nitrate aerosols to ammonia emissions and to nitrate chemistry: implications for present and future nitrate optical depth. *Atmospheric Chemistry and Physics.* **16**(3), pp.1459-1477.

Peng, Y., Lohmann, U. and Leaitch, R. 2005. Importance of vertical velocity variations in the cloud droplet nucleation process of marine stratus clouds. *Journal of Geophysical Research.* **110**(D21).

Perrino, C., Catrambone, M., Dalla Torre, S., Rantica, E., Sargolini, T. and Canepari, S. 2014. Seasonal variations in the chemical composition of particulate matter: a case study in the Po Valley. Part I: macro-components and mass closure. *Environ Sci Pollut Res Int.* **21**(6), pp.3999-4009.

Petters, M.D. and Kreidenweis, S.M. 2007. A single parameter representation of hygroscopic growth and cloud condensation nucleus activity. *Atmos. Chem. Phys.* **7**(8), pp.1961-1971.

Pham, M., Müller, J.F., Brasseur, G.P., Granier, C. and Mégie, G. 1995. A three-dimensional study of the tropospheric sulfur cycle. *Journal of Geophysical Research.* **100**(D12), pp.26061-26061.

Pilinis, C., Capaldo, K.P., Nenes, A. and Pandis, S.N. 2000. MADM-A New Multicomponent Aerosol Dynamics Model. *Aerosol Science and Technology.* **32**(5), pp.482-502.

Pinault, L., Tjepkema, M., Crouse, D.L., Weichenthal, S., van Donkelaar, A., Martin, R.V., Brauer, M., Chen, H. and Burnett, R.T. 2016. Risk estimates of mortality attributed to low concentrations of ambient fine particulate matter in the Canadian community health survey cohort. *Environ Health.* **15**, p18.

Pinder, R.W., Gilliland, A.B. and Dennis, R.L. 2008. Environmental impact of atmospheric NH3 emissions under present and future conditions in the eastern United States. *Geophysical Research Letters.* **35**(12).

Plaza, J., Pujadas, M., Gómez-Moreno, F.J., Sánchez, M. and Artíñano, B. 2011. Mass size distributions of soluble sulfate, nitrate and ammonium in the Madrid urban aerosol. *Atmospheric Environment.* **45**(28), pp.4966-4976.

Pope, C.A., Dockery, D.W. and Schwartz, J. 1995. Review of Epidemiological Evidence of Health Effects of Particulate Air Pollution. *Inhalation Toxicology.* **7**(1), pp.1-18.

Pope, C.A., 3rd, Burnett, R.T., Krewski, D., Jerrett, M., Shi, Y., Calle, E.E. and Thun, M.J. 2009. Cardiovascular mortality and exposure to airborne fine particulate matter and cigarette smoke: shape of the exposure-response relationship. *Circulation.* **120**(11), pp.941-948.

Pope, C.A., 3rd, Burnett, R.T., Turner, M.C., Cohen, A., Krewski, D., Jerrett, M., Gapstur, S.M. and Thun, M.J. 2011. Lung cancer and cardiovascular disease mortality associated with ambient air pollution and cigarette smoke: shape of the exposure-response relationships. *Environ Health Perspect.* **119**(11), pp.1616-1621.

Pope, C.A., 3rd, Cohen, A.J. and Burnett, R.T. 2018. Cardiovascular Disease and Fine Particulate Matter: Lessons and Limitations of an Integrated Exposure-Response Approach. *Circ Res.* **122**(12), pp.1645-1647.

Pope III, C.A. and Dockery, D.W. 2006. Health Effects of Fine Particulate Air Pollution: Lines that Connect. *Journal of the Air & Waste Management AssociationOnline) Journal Journal of the Air & Waste Management Association.* **566**, pp.1096-2247.

Pope, R.J., Chipperfield, M.P., Savage, N.H., Ordóñez, C., Neal, L.S., Lee, L.A., Dhomse, S.S., Richards, N.A.D. and Keslake, T.D. 2015. Evaluation of a regional air quality model using satellite column NO2: treatment of observation errors and model boundary conditions and emissions. *Atmospheric Chemistry and Physics.* **15**(10), pp.5611-5626.

Pöschl, U., Kuhlmann, R.v., Poisson, N. and Crutzen, P.J. 2000. Development and Intercomparison of Condensed Isoprene Oxidation Mechanisms for Global Atmospheric Modeling. *Journal of Atmospheric Chemistry.* **37**(1), pp.29-52.

Pozzer, A., Tsimpidi, A.P., Karydis, V.A., de Meij, A. and Lelieveld, J. 2017. Impact of agricultural emission reductions on fine-particulate matter and public health. *Atmospheric Chemistry and Physics.* **17**(20), pp.12813-12826.

Price, C. and Rind, D. 1992. A simple lightning parameterization for calculating global lightning distributions. *Journal of Geophysical Research: Atmospheres.* **97**(D9), pp.9919-9933.

Price, C. and Rind, D. 1993. What determines the cloud-to-ground lightning fraction in thunderstorms? *Geophysical Research Letters.* **20**(6), pp.463-466.

Priestley, A. 1993. A Quasi-Conservative Version of the Semi-Lagrangian Advection Scheme. *Mon. Weather. Rev.* **121**, pp.621-629.

Pringle, K.J., Tost, H., Message, S., Steil, B., Giannadaki, D., Nenes, A., Fountoukis, C., Stier, P., Vignati, E. and Lelieveld, J. 2010. Description and evaluation of GMXe: a new aerosol submodel for global simulations (v1). *Geoscientific Model Development.* **3**(2), pp.391-412.

Pringle, K.J., Carslaw, K.S., Fan, T., Mann, G.W., Hill, A., Stier, P., Zhang, K. and Tost, H. 2012. A multi-model assessment of the impact of sea spray geoengineering on cloud droplet number. *Atmos. Chem. Phys.* **12**(23), pp.11647-11663.

Punger, E.M. and West, J.J. 2013. The effect of grid resolution on estimates of the burden of ozone and fine particulate matter on premature mortality in the USA. *Air Quality, Atmosphere & Health.* **6**(3), pp.563-573.

Pusede, S.E., Duffey, K.C., Shusterman, A.A., Saleh, A., Laughner, J.L., Wooldridge, P.J., Zhang, Q., Parworth, C.L., Kim, H., Capps, S.L., Valin, L.C., Cappa, C.D., Fried, A., Walega, J., Nowak, J.B., Weinheimer, A.J., Hoff, R.M., Berkoff, T.A., Beyersdorf, A.J., Olson, J., Crawford, J.H. and Cohen, R.C. 2016. On the effectiveness of nitrogen oxide reductions as a control over ammonium nitrate aerosol. *Atmospheric Chemistry and Physics.* **16**(4), pp.2575-2596.

Putaud, J.P. et al. 2010. A European aerosol phenomenology – 3: Physical and chemical characteristics of particulate matter from 60 rural, urban, and kerbside sites across Europe. *Atmospheric Environment.* **44**(10), pp.1308-1320.

Pye, H.O.T., Liao, H., Wu, S., Mickley, L.J., Jacob, D.J., Henze, D.J. and Seinfeld, J.H. 2009. Effect of changes in climate and emissions on future sulfate-nitrate-ammonium aerosol levels in the United States. *Journal of Geophysical Research Atmospheres.*

Rao, S., Klimont, Z., Smith, S.J., Van Dingenen, R., Dentener, F., Bouwman, L., Riahi, K., Amann, M., Bodirsky, B.L., van Vuuren, D.P., Aleluia Reis, L., Calvin, K., Drouet, L., Fricko, O., Fujimori, S., Gernaat, D., Havlik, P., Harmsen, M., Hasegawa, T., Heyes, C., Hilaire, J., Luderer, G., Masui, T., Stehfest, E., Strefler, J., van der Sluis, S. and Tavoni, M. 2017. Future air pollution in the Shared Socio-economic Pathways. *Global Environmental Change.* **42**, pp.346-358.

Rap, A., Scott, C.E., Spracklen, D.V., Bellouin, N., Forster, P.M., Carslaw, K.S., Schmidt, A. and Mann, G. 2013. Natural aerosol direct and indirect radiative effects. *Geophysical Research Letters.* **40**(12), pp.3297-3301.

Rap, A., Mercado, L., Reddington, C.L., Haywood , J.M., J., E.R., L., P.O., P., A., D., B., N., R.C. and N., B. 2015. Fires increase Amazon forest productivity through increases in diffuse radiation. *Geophysical Research Letters.* **42**(11), pp.4654-4662.

Reddington, C.L. et al. 2017. The global aerosol synthesis and science project (GASSP): Measurements and modeling to reduce uncertainty. *Bulletin of the American Meteorological Society.* **98**(9), pp.1857-1877.

Reddington, C.L.S. 2012. *Primary versus secondary contributions to particle number concentrations in the European boundary layer*. PhD thesis, University of Leeds, U.K.

Reiss, R., Anderson, E.L., Cross, C.E., Hidy, G., Hoel, D., McClellan, R. and Moolgavkar, S. 2007. Evidence of health impacts of sulfate-and nitrate-containing particles in ambient air. *Inhalation toxicology.* **19**(5), pp.419-449.

Riedel, T.P., Bertram, T.H., Ryder, O.S., Liu, S., Day, D.A., Russell, L.M., Gaston, C.J., Prather, K.A. and Thornton, J.A. 2012. Direct N₂O₅ reactivity measurements at a polluted coastal site. *Atmospheric Chemistry and Physics.* **12**(6), pp.2959-2968.

Riemer, N., Vogel, H., Vogel, B., Schell, B., Ackermann, I., Kessler, C. and Hass, H. 2003. Impact of the heterogeneous hydrolysis of N 2 O 5 on chemistry and nitrate aerosol formation in the lower troposphere under photosmog conditions. *Journal of Geophysical Research.* **108**(D4), pp.4144-4144.

Robinson, N.H., Hamilton, J.F., Allan, J.D., Langford, B., Oram, D.E., Chen, Q., Docherty, K., Farmer, D.K., Jimenez, J.L., Ward, M.W., Hewitt, C.N., Barley, M.H., Jenkin, M.E., Rickard, A.R., Martin, S.T., McFiggans, G. and Coe, H. 2011. Evidence for a significant proportion of Secondary Organic Aerosol from isoprene above a maritime tropical forest. *Atmospheric Chemistry and Physics.* **11**(3), pp.1039-1050.

Rodhe, H., Dentener, F. and Schulz, M. 2002. The Global Distribution of Acidifying Wet Deposition. *Environmental Science & Technology.* **36**(20), pp.4382-4388.

Rogers, R. and Yau, M. 1989. Cloud physics. *Butterworth–Heinemann.*

Rohr, A.C. and Wyzga, R.E. 2012. Attributing health effects to individual particulate matter constituents. *Atmospheric Environment.* **62**, pp.130-152.

Rossow, W.B. and Schiffer, R.A. 1999. Advances in Understanding Clouds from ISCCP. *Bulletin of the American Meteorological Society.* **80**(11), pp.2261-2288.

Russell, L.M., Hawkins, L.N., Frossard, A.A., Quinn, P.K. and Bates, T.S. 2010. Carbohydrate-like composition of submicron atmospheric particles and their production from ocean bubble bursting. *Proceedings of the National Academy of Sciences.* **107**(15), p6652.

Savoie, D. and Prospero, J. 1982. Particle size distribution of nitrate and sulfate in the marine atmosphere. *Geophysical Research Letters.* **9**(10), pp.1207-1210.

Schaap, M., van Loon, M., ten Brink, H.M., Dentener, F.J. and Builtjes, P.J.H. 2004. Secondary inorganic aerosol simulations for Europe with special attention to nitrate. *Atmospheric Chemistry and Physics.* **4**(3), pp.857-874.

Schaap, M., Otjes, R.P. and Weijers, E.P. 2011. Illustrating the benefit of using hourly monitoring data on secondary inorganic aerosol and its precursors for model evaluation. *Atmospheric Chemistry and Physics.* **11**(21), pp.11041-11053.

Schlesinger, R.B. and Cassee, F. 2003. Atmospheric Secondary Inorganic Particulate Matter: The Toxicological Perspective as a Basis for Health Effects Risk Assessment. *Inhalation Toxicology.* **15**(3), pp.197-235.

Schmidt, G.A. et al. 2014. Configuration and assessment of the GISS ModelE2 contributions to the CMIP5 archive. *Journal of Advances in Modeling Earth Systems.* **6**(1), pp.141-184.

Scott, C.E., Rap, A., Spracklen, D.V., Forster, P.M., Carslaw, K.S., Mann, G.W., Pringle, K.J., Kivekäs, N., Kulmala, M., Lihavainen, H. and Tunved, P. 2014. The direct and indirect radiative effects of biogenic secondary organic aerosol. *Atmospheric Chemistry and Physics.* **14**(1), pp.447-470.

Scott, C.E., Spracklen, D.V., Pierce, J.R., Riipinen, I., amp, apos, Andrea, S.D., Rap, A., Carslaw, K.S., Forster, P.M., Artaxo, P., Kulmala, M., Rizzo, L.V., Swietlicki, E., Mann, G.W. and Pringle, K.J. 2015. Impact of gas-to-particle partitioning approaches on the simulated radiative effects of biogenic secondary organic aerosol. *Atmospheric Chemistry and Physics.* **15**(22), pp.12989-13001.

Scott, C.E., Monks, S.A., Spracklen, D.V., Arnold, S.R., Forster, P.M., Rap, A., Äijälä, M., Artaxo, P., Carslaw, K.S., Chipperfield, M.P., Ehn, M., Gilardoni, S., Heikkinen, L., Kulmala, M., Petäjä, T., Reddington, C.L.S., Rizzo, L.V., Swietlicki, E., Vignati, E. and Wilson, C. 2018. Impact on short-lived climate forcers increases projected warming due to deforestation. *Nature Communications.* **9**(1), pp.157-157.

Seinfeld, J.H. and Pandis, S.N. 1998. Atmospheric Chemistry and Physics John Wiley & Sons. *New York.*

Seinfeld, J.H. and Pandis, S.N. 2006. *Atmospheric Chemistry and Physics: From Air Pollution to Climate Change. 2nd Edition.* New York: John Wiley and Sons.

Sekhon, H. and Srivastava, R. 1971. Doppler observations of drop size distributions in a thunderstorm. *J. Atmos. Sci.* **28**, pp.983-994.

Shin, H.H., Cohen, A.J., Pope, C.A., 3rd, Ezzati, M., Lim, S.S., Hubbell, B.J. and Burnett, R.T. 2016. Meta-Analysis Methods to Estimate the Shape and Uncertainty in the Association Between Long-Term Exposure to Ambient Fine Particulate Matter and Cause-Specific Mortality Over the Global Concentration Range. *Risk Anal.* **36**(9), pp.1813-1825.

Shindell, D.T., Faluvegi, G. and Bell, N. 2003. Preindustrial-to-present-day radiative forcing by tropospheric ozone from improved simulations with the GISS chemistry-climate GCM. *Atmospheric Chemistry and Physics.* **3**(5), pp.1675-1702.

Shindell, D.T. et al. 2013. Radiative forcing in the ACCMIP historical and future climate simulations. *Atmospheric Chemistry and Physics.* **13**(6), pp.2939-2974.

Silva, P.J., Vawdrey, E.L., Corbett, M. and Erupe, M. 2007. Fine particle concentrations and composition during wintertime inversions in Logan, Utah, USA. *Atmospheric Environment.* **41**(26), pp.5410-5422.

Silva, R.A., Adelman, Z., Fry, M.M. and West, J.J. 2016. The impact of individual anthropogenic emissions sectors on the global burden of human mortality due to ambient air pollution. *Environmental Health Perspectives.* **124**(11).

Silver, B., Reddington, C.L., Arnold, S.R. and Spracklen, D.V. 2018. Substantial changes in air pollution across China during 2015–2017. *Environmental Research Letters.* **13**(11), p114012.

Simpson, D., Benedictow, A., Berge, H., Bergström, R., Emberson, L.D., Fagerli, H., Flechard, C.R., Hayman, G.D., Gauss, M., Jonson, J.E., Jenkin, M.E., Nyíri, A., Richter, C., Semeena, V.S., Tsyro, S., Tuovinen, J.P., Valdebenito, Á. and Wind, P. 2012. The EMEP MSC-W chemical transport model - technical description. *Atmospheric Chemistry and Physics.* **12**(16), pp.7825-7865.

Skeie, R., Berntsen, T., Myhre, G., Tanaka, K., Kvalevåg, M. and Hoyle, C. 2011. Anthropogenic radiative forcing time series from pre-industrial times until 2010. *Atmospheric Chemistry and Physics.* **11**(22), pp.11827-11857.

Slanina, J., Ten Brink, H.M., Otjes, R.P., Even, A., Jongejan, P., Khlystov, A., Waijers-Ijpelaan, A., Hu, M. and Lu, Y. 2001. The continuous analysis of nitrate and ammonium in aerosols by the steam jet aerosol collector (SJAC): extension and validation of the methodology. *Atmospheric Environment.* **35**(13), pp.2319-2330.

Slinn, W. 1984. Precipitation Scavenging. In: Randerson, D. ed. Springfield, VA, USA: US Department of Energy, pp.466-532.

Slinn, W.G.N. 1982. Predictions for particle deposition to vegetative canopies. *Atmospheric Environment (1967).* **16**(7), pp.1785-1794.

Smith, R.I., Fowler, D., Sutton, M.A., Flechard, C. and Coyle, M. 2000. Regional estimation of pollutant gas dry deposition in the UK: model description, sensitivity analyses and outputs. *Atmospheric Environment.* **34**(22), pp.3757-3777.

Snider, G. et al. 2016. Variation in global chemical composition of PM2.5: emerging results from SPARTAN. *Atmospheric Chemistry and Physics.*

Søvde, O.A., Prather, M.J., Isaksen, I.S.A., Berntsen, T.K., Stordal, F., Zhu, X., Holmes, C.D. and Hsu, J. 2012. The chemical transport model Oslo CTM3. *Geosci. Model Dev.* **5**(6), pp.1441-1469.

Spracklen, D.V., Pringle, K.J., Carslaw, K.S., Chipperfield, M.P. and Mann, G.W. 2005. A global off-line model of size-resolved aerosol microphysics: I. Model development and prediction of aerosol properties. *Atmospheric Chemistry and Physics.* **5**(8), pp.2227-2252.

Spracklen, D.V., Carslaw, K.S., Kulmala, M., Kerminen, V.M., Mann, G.W. and Sihto, S.L. 2006. The contribution of boundary layer nucleation events to total particle concentrations on regional and global scales. *Atmospheric Chemistry and Physics.* **6**(12), pp.5631-5648.

Spracklen, D.V., Carslaw, K.S., Pöschl, U., Rap, A. and Forster, P.M. 2011a. Global cloud condensation nuclei influenced by carbonaceous combustion aerosol. *Atmospheric Chemistry and Physics.* **11**(17), pp.9067-9087.

Spracklen, D.V., Jimenez, J.L., Carslaw, K.S., Worsnop, D.R., Evans, M.J., Mann, G.W., Zhang, Q., Canagaratna, M.R., Allan, J., Coe, H., McFiggans, G., Rap, A. and Forster, P. 2011b. Aerosol mass spectrometer constraint on the

global secondary organic aerosol budget. *Atmospheric Chemistry and Physics.*

Squire, O.J., Archibald, A.T., Abraham, N.L., Beerling, D.J., Hewitt, C.N., Lathière, J., Pike, R.C., Telford, P.J. and Pyle, J.A. 2014. Influence of future climate and cropland expansion on isoprene emissions and tropospheric ozone. *Atmos. Chem. Phys.* **14**(2), pp.1011-1024.

Squizzato, S., Masiol, M., Brunelli, A., Pistollato, S., Tarabotti, E., Rampazzo, G. and Pavoni, B. 2013. Factors determining the formation of secondary inorganic aerosol: A case study in the Po Valley (Italy). *Atmospheric Chemistry and Physics.*

Stier, P., Feichter, J., Kinne, S., Kloster, S., Vignati, E., Wilson, J., Ganzeveld, L., Tegen, I., Werner, M., Balkanski, Y., Schulz, M., Boucher, O., Minikin, A. and Petzold, A. 2005. The aerosol-climate model ECHAM5-HAM. *Atmospheric Chemistry and Physics.* **5**(4), pp.1125-1156.

Stone, D., Evans, M.J., Walker, H., Ingham, T., Vaughan, S., Ouyang, B., Kennedy, O.J., McLeod, M.W., Jones, R.L., Hopkins, J., Punjabi, S., Lidster, R., Hamilton, J.F., Lee, J.D., Lewis, A.C., Carpenter, L.J., Forster, G., Oram, D.E., Reeves, C.E., Bauguitte, S., Morgan, W., Coe, H., Aruffo, E., Dari-Salisburgo, C., Giammaria, F., Di Carlo, P. and Heard, D.E. 2014. Radical chemistry at night: comparisons between observed and modelled HO_x, NO_3 and N_2O_5 during the RONOCO project. *Atmospheric Chemistry and Physics.* **14**(3), pp.1299-1321.

Strahan, S.E., Duncan, B.N. and Hoor, P. 2007. Observationally derived transport diagnostics for the lowermost stratosphere and their application to the GMI chemistry and transport model. *Atmospheric Chemistry and Physics.* **7**(9), pp.2435-2445.

Sudo, K., Takahashi, M., Kurokawa, J.-i. and Akimoto, H. 2002. CHASER: A global chemical model of the troposphere 1. Model description. *Journal of Geophysical Research: Atmospheres.* **107**(D17), pp.ACH 7-1-ACH 7-20.

Sutton, M.A., Dragosits, U., Tang, Y.S. and Fowler, D. 2000. Ammonia emissions from non-agricultural sources in the UK. **34**(August 1999).

Tang, M., Huang, X., Lu, K., Ge, M., Li, Y., Cheng, P., Zhu, T., Ding, A., Zhang, Y., Gligorovski, S., Song, W., Ding, X., Bi, X. and Wang, X. 2017. Heterogeneous reactions of mineral dust aerosol: implications for tropospheric oxidation capacity. *Atmospheric Chemistry and Physics.* **17**(19), pp.11727-11777.

Telford, P.J., Braesicke, P., Morgenstern, O. and Pyle, J.A. 2008. Technical Note: Description and assessment of a nudged version of the new dynamics Unified Model. *Atmospheric Chemistry and Physics.* **8**(6), pp.1701-1712.

ten Brink, H., Otjes, R., Jongejan, P. and Slanina, S. 2007. An instrument for semi-continuous monitoring of the size-distribution of nitrate, ammonium, sulphate and chloride in aerosol. *Atmospheric Environment.* **41**(13), pp.2768-2779.

Tie, X., Brasseur, G., Emmons, L., Horowitz, L. and Kinnison, D. 2001. Effects of aerosols on tropospheric oxidants: A global model study. *Journal of Geophysical Research: Atmospheres.* **106**(D19), pp.22931-22964.

Tørseth, K., Aas, W., Breivik, K., Fjæraa, A.M., Fiebig, M., Hjellbrekke, A.G., Lund Myhre, C., Solberg, S. and Yttri, K.E. 2012. Introduction to the European Monitoring and Evaluation Programme (EMEP) and observed

atmospheric composition change during 1972–2009. *Atmospheric Chemistry and Physics.* **12**(12), pp.5447-5481.
Tost, H. 2017. Chemistry&ndashclimate interactions of aerosol nitrate from lightning. *Atmospheric Chemistry and Physics.* **17**(2), pp.1125-1142.
Trail, M., Tsimpidi, A.P., Liu, P., Tsigaridis., K., Rudokas, J., Miller, P., Nenes, A., Hu, Y., Russel, A.G. 2014. Sensitivity of air quality to potential future climate change and emissions in the United States and major cities. *Atmospheric Environment.* **94**, pp.552-563.
Trump, E.R., Fountoukis, C., Donahue, N.M. and Pandis, S.N. 2015. Improvement of simulation of fine inorganic PM levels through better descriptions of coarse particle chemistry. *Atmospheric Environment.* **102**, pp.274-281.
Tsimpidi, A.P., Karydis, V.A. and Pandis, S.N. 2008. Response of Fine Particulate Matter to Emission Changes of Oxides of Nitrogen and Anthropogenic Volatile Organic Compounds in the Eastern United States. *Journal of the Air & Waste Management Association.* **58**(11), pp.1463-1473.
Tuomisto, J.T., Wilson, A., Evans, J.S. and Tainio, M. 2008. Uncertainty in mortality response to airborne fine particulate matter: Combining European air pollution experts. *Reliability Engineering & System Safety.* **93**(5), pp.732-744.
Turnock, S. 2016. *The impact of changing anthropogenic emissions on European atmospheric aerosols over the second half of the 20th Century*. PhD thesis, University of Leeds.
Turnock, S.T., Spracklen, D.V., Carslaw, K.S., Mann, G.W., Woodhouse, M.T., Forster, P.M., Haywood, J., Johnson, C.E., Dalvi, M., Bellouin, N. and Sanchez-Lorenzo, A. 2015. Modelled and observed changes in aerosols and surface solar radiation over Europe between 1960 and 2009. *Atmospheric Chemistry and Physics.* **15**(16), pp.9477-9500.
Turnock, S.T., Butt, E.W., Richardson, T.B., Mann, G.W., Reddington, C.L., Forster, P.M., Haywood, J., Crippa, M., Janssens-Maenhout, G., Johnson, C.E., Bellouin, N., Carslaw, K.S. and Spracklen, D.V. 2016. The impact of European legislative and technology measures to reduce air pollutants on air quality, human health and climate. *Environmental Research Letters.* **11**(2), pp.024010-024010.
Twomey, S. 1977. The influence of pollution on the shortwave albedo of clouds. *Journal of the atmospheric sciences.* **34**(7), pp.1149-1152.
van der Werf, G.R., Randerson, J.T., Giglio, L., Collatz, G.J., Mu, M., Kasibhatla, P.S., Morton, D.C., DeFries, R.S., Jin, Y. and van Leeuwen, T.T. 2010. Global fire emissions and the contribution of deforestation, savanna, forest, agricultural, and peat fires (1997–2009). *Atmospheric Chemistry and Physics.* **10**(23), pp.11707-11735.
van Donkelaar, A., Martin, R.V., Brauer, M. and Boys, B.L. 2015. *Use of Satellite Observations for Long-Term Exposure Assessment of Global Concentrations of Fine Particulate Matter*. 123. pp.135-143.
van Donkelaar, A., Martin, R.V., Brauer, M., Hsu, N.C., Kahn, R.A., Levy, R.C., Lyapustin, A., Sayer, A.M. and Winker, D.M. 2016. Global Estimates of Fine Particulate Matter using a Combined Geophysical-Statistical Method with Information from Satellites, Models, and Monitors. *Environmental Science & Technology.* **50**(7), pp.3762-3772.
van Vuuren, D.P., Edmonds, J., Kainuma, M., Riahi, K., Thomson, A., Hibbard, K., Hurtt, G.C., Kram, T., Krey, V., Lamarque, J.-F., Masui, T., Meinshausen, M.,

Nakicenovic, N., Smith, S.J. and Rose, S.K. 2011. The representative concentration pathways: an overview. *Climatic Change.* **109**(1-2), pp.5-31.

Vasilakos, P., Russell, A., Weber, R. and Nenes, A. 2018. Understanding nitrate formation in a world with less sulfate. *Atmospheric Chemistry and Physics Discussions.* pp.1-27.

Vecchi, R., Valli, G., Fermo, P., D'Alessandro, A., Piazzalunga, A. and Bernardoni, V. 2009. Organic and inorganic sampling artefacts assessment. *Atmospheric Environment - ATMOS ENVIRON.* **43**, pp.1713-1720.

Vestreng, V., Myre, G., Fagerli, H., Reis, S. and Tarrason, L. 2007. Twenty-five years of continuous sulphur dioxide emission reduction in Europe. pp.3663-3681.

Vieno, M., Heal, M.R., Twigg, M.M., MacKenzie, I.A., Braban, C.F., Lingard, J.J.N., Ritchie, S., Beck, R.C., Móring, A., Ots, R., Di Marco, C.F., Nemitz, E., Sutton, M.A. and Reis, S. 2016. The UK particulate matter air pollution episode of March–April 2014: more than Saharan dust. *Environmental Research Letters.* **11**(4), pp.044004-044004.

Wagner, N.L., Riedel, T.P., Young, C.J., Bahreini, R., Brock, C.A., Dubé, W.P., Kim, S., Middlebrook, A.M., Öztürk, F., Roberts, J.M., Russo, R., Sive, B., Swarthout, R., Thornton, J.A., VandenBoer, T.C., Zhou, Y. and Brown, S.S. 2013. N_2O_5 uptake coefficients and nocturnal NO_2 removal rates determined from ambient wintertime measurements. *Journal of Geophysical Research Atmospheres.* **118**(16), pp.9331-9350.

Wahner, A., Mentel, T.F., Sohn, M. and Stier, J. 1998. Heterogeneous reaction of N_2O_5 on sodium nitrate aerosol. *Journal of Geophysical Research: Atmospheres.* **103**(D23), pp.31103-31112.

Walters, D.N., Best, M.J., Bushell, A.C., Copsey, D., Edwards, J.M., Falloon, P.D., Harris, C.M., Lock, A.P., Manners, J.C., Morcrette, C.J., Roberts, M.J., Stratton, R.A., Webster, S., Wilkinson, J.M., Willett, M.R., Boutle, I.A., Earnshaw, P.D., Hill, P.G., MacLachlan, C., Martin, G.M., Moufouma-Okia, W., Palmer, M.D., Petch, J.C., Rooney, G.G., Scaife, A.A. and Williams, K.D. 2011. The Met Office Unified Model Global Atmosphere 3.0/3.1 and JULES Global Land 3.0/3.1 configurations. *Geoscientific Model Development.* **4**(4), pp.919-941.

Walton, J.J., MacCracken, M.C. and Ghan, S.J. 1988. A global-scale Lagrangian trace species model of transport, transformation, and removal processes. *Journal of Geophysical Research.* **93**(D7), pp.8339-8339.

Wang, J., Xing, J., Mathur, R., Pleim, J.E., Wang, S., Hogrefe, C., Gan, C.-M., Wong, D.C. and Hao, J. 2017. Historical Trends in PM(2.5)-Related Premature Mortality during 1990–2010 across the Northern Hemisphere. *Environmental Health Perspectives.* **125**(3), pp.400-408.

Wang, T., Li, S., Shen, Y., Deng, J. and Xie, M. 2010. Investigations on direct and indirect effect of nitrate on temperature and precipitation in China using a regional climate chemistry modeling system. *Journal of Geophysical Research.* **115**.

Wang, Y., Zhang, Q.Q., He, K., Zhang, Q. and Chai, L. 2013. Sulfate-nitrate-ammonium aerosols over China: Response to 2000-2015 emission changes of sulfur dioxide, nitrogen oxides, and ammonia. *Atmospheric Chemistry and Physics.* **13**(5).

Warneck, P. 2000. *Chemistry of the natural atmosphere.*

Watanabe, S., Hajima, T., Sudo, K., Nagashima, T., Takemura, T., Okajima, H., Nozawa, T., Kawase, H., Abe, M., Yokohata, T., Ise, T., Sato, H., Kato, E., Takata, K., Emori, S. and Kawamiya, M. 2011. MIROC-ESM 2010: Model description and basic results of CMIP5-20c3m experiments. *Geoscientific Model Development.*

Weber, R., Guo, H., Russell, A. and Nenes, A. 2016. *High aerosol acidity despite declining atmospheric sulfate concentrations over the past 15 years.*

Wesely, M.L. 1989. Parameterization of surface resistances to gaseous dry deposition in regional-scale numerical models. *Atmospheric Environment (1967).* **23**(6), pp.1293-1304.

Wexler, A.S. and Seinfeld, J.H. 1992. Analysis of aerosol ammonium nitrate: departures from equilibrium during SCAQS. *Atmospheric Environment. Part A. General Topics.* **26**(4), pp.579-591.

WHO. 2013. *World Health Organization Regional Office for Europe. Review of evidence on health aspects of air pollution – REVIHAAP Project: Technical Report [Internet].* Copenhagen: WHO Regional Office for Europe.

Wild, O., Zhu, X. and Prather, M.J. 2000. Fast-J: Accurate Simulation of In- and Below-Cloud Photolysis in Tropospheric Chemical Models. *Journal of Atmospheric Chemistry.* **37**(3), pp.245-282.

Wilhelm, M., Ghosh, J.K., Su, J., Cockburn, M., Jerrett, M. and Ritz, B. 2011. Traffic-related air toxics and preterm birth: a population-based case-control study in Los Angeles county, California. *Environmental Health.* **10**(1), p89.

Wittmaack, K. 2007. In search of the most relevant parameter for quantifying lung inflammatory response to nanoparticle exposure: particle number, surface area, or what? *Environmental health perspectives.* **115**(2), pp.187-194.

Woodward, S. 2001. Modeling the atmospheric life cycle and radiative impact of mineral dust in the Hadley Centre climate model. *Journal of Geophysical Research: Atmospheres.* **106**(D16), pp.18155-18166.

Woodward, S. 2011. *Mineral Dust in HadGEM2. Hadley Centre Technical Note 87.*

Wyzga, R.E. and Rohr, A.C. 2015. Long-term particulate matter exposure: Attributing health effects to individual PM components. *Journal of the Air and Waste Management Association.*

Xing, J., Mathur, R., Pleim, J., Hogrefe, C., Gan, C.M., Wong, D.C., Wei, C., Gilliam, R. and Pouliot, G. 2015. Observations and modeling of air quality trends over 1990–2010 across the Northern Hemisphere: China, the United States and Europe. *Atmos. Chem. Phys.* **15**(5), pp.2723-2747.

Xing, J., Wang, J., Mathur, R., Wang, S., Sarwar, G., Pleim, J., Hogrefe, C., Zhang, Y., Jiang, J., Wong, D.C. and Hao, J. 2017. Impacts of aerosol direct effects on tropospheric ozone through changes in atmospheric dynamics and photolysis rates. *Atmos. Chem. Phys.* **17**(16), pp.9869-9883.

Xu, L. and Penner, J.E. 2012. Global simulations of nitrate and ammonium aerosols and their radiative effects. *Atmospheric Chemistry and Physics.* **12**(20), pp.9479-9504.

Yang, T., Sun, Y., Zhang, W., Wang, Z., Liu, X., Fu, P. and Wang, X. 2017. Evolutionary processes and sources of high-nitrate haze episodes over Beijing, Spring. *Journal of Environmental Sciences.* **54**, pp.142-151.

Yin, G., Liu, C., Hao, L., Chen, Y., Wang, W., Huo, J., Zhao, Q., Zhang, Y., Duan, Y., Fu, Q., Chen, R. and Kan, H. 2019. Associations between size-fractionated

particle number concentrations and COPD mortality in Shanghai, China. *Atmospheric Environment.* **214**, p116875.

Yin, J. and Harrison, R.M. 2008. Pragmatic mass closure study for PM1.0, PM2.5 and PM10 at roadside, urban background and rural sites. *Atmospheric Environment.* **42**(5), pp.980-988.

Yin, P., Brauer, M., Cohen, A., Burnett, R.T., Liu, J., Liu, Y., Liang, R., Wang, W., Qi, J., Wang, L. and Zhou, M. 2017. Long-term fine particulate matter exposure and nonaccidental and cause-specific mortality in a large national cohort of Chinese men. *Environmental Health Perspectives.* **125**(11), p117002.

Ying, Q., Wu, L. and Zhang, H. 2014. Local and inter-regional contributions to PM2.5 nitrate and sulfate in China. *Atmospheric Environment.* **94**, pp.582-592.

Yoshioka, M.R., L. A.; Pringle, K. J.; Johnson, J. S.; Mann, G. W.; Partridge, D. G.; D. M. Sexton; G. M. S. Lister; N. Schutgens; P. Stier; Z. Kipling; N. Bellouin; J. Browse; B. Booth; C. E. Johnson; J. D. P. Mollard; K. S. Carslaw. 2019 in prep. Ensembles of Global Climate Model Variants Designed for the Quantification and Constraint of Uncertainty in Aerosols and their Radiative Forcing. *Journal of Advances in Modeling Earth Systems.*

Zaveri, R.A., Easter, R.C., Fast, J.D. and Peters, L.K. 2008. Model for Simulating Aerosol Interactions and Chemistry (MOSAIC). *Journal of Geophysical Research.* **113**(D13), pp.D13204-D13204.

Zhang, B., Wang, Y. and Hao, J. 2015. Simulating aerosol–radiation–cloud feedbacks on meteorology and air quality over eastern China under severe haze conditionsin winter. *Atmospheric Chemistry and Physics.* **15**(5), pp.2387-2404.

Zhang, K.M. and Wexler, A.S. 2006. An asynchronous time-stepping (ATS) integrator for atmospheric applications: Aerosol dynamics. *Atmospheric Environment.* **40**(24), pp.4574-4588.

Zhang, L., Gong, S., Padro, J. and Barrie, L. 2001. A size-segregated particle dry deposition scheme for an atmospheric aerosol module. *Atmospheric Environment.*

Zhang, Y., Seigneur, C., Seinfeld, J.H., Jacobson, M., Clegg, S.L. and Binkowski, F.S. 2000. A comparative review of inorganic aerosol thermodynamic equilibrium modules: similarities, differences, and their likely causes. *Atmospheric Environment.* **34**(1), pp.117-137.

Appendix A
Chapter 4 Supplementary Information

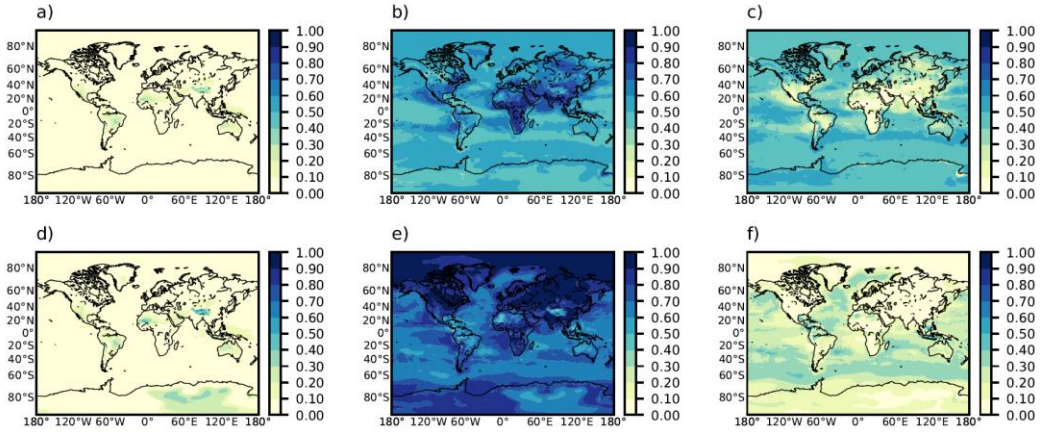

Fig. A1. Annual-mean simulated surface nitrate mass fraction in the (a + d) Aitken, (b + e) accumulation and (c + f) coarse mode, simulated using an (a-c, top row) equilibrium and (d-e, bottom row) hybrid dissolution solver. Nucleation mode is not shown as it accounts for less than 5% of nitrate mass in any given grid square and is relatively unaffected by the choice of solver complexity.

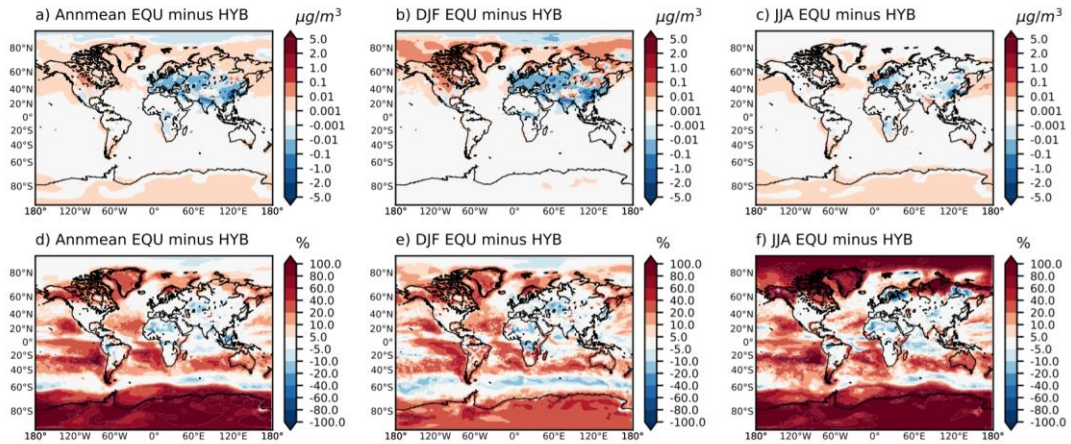

Figure A2. Absolute (top row) and percentage (bottom row) changes in annual (left), DJF (centre) and JJA (right) mean surface nitrate concentrations when switching from a hybrid (HYB) to an equilibrium (EQU) assumption for gas-particle partitioning ie. EQU minus HYB.

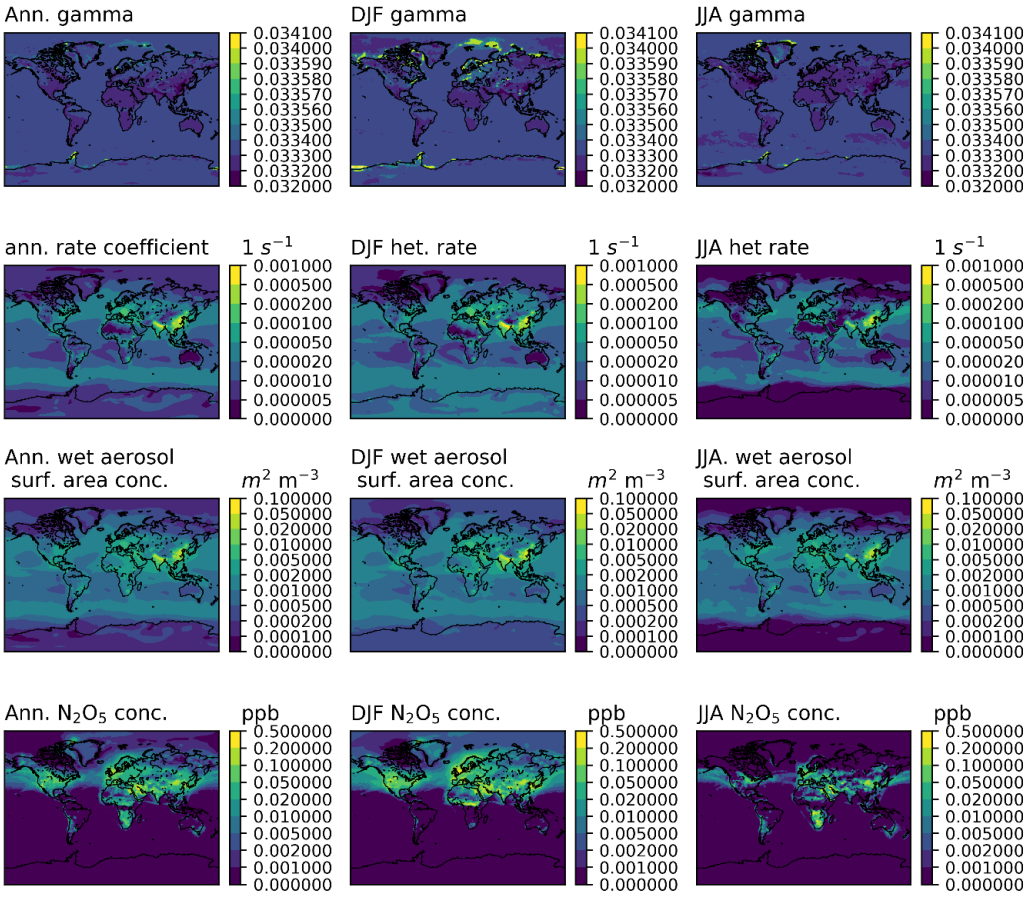

Figure A3. Annual, DJF and JJA seasonal mean surface values for N_2O_5 reaction probability (gamma) on aerosol, heterogeneous N_2O_5 hydrolysis rate coefficient, wet aerosol surface area concentration and ambient N_2O_5 concentration.

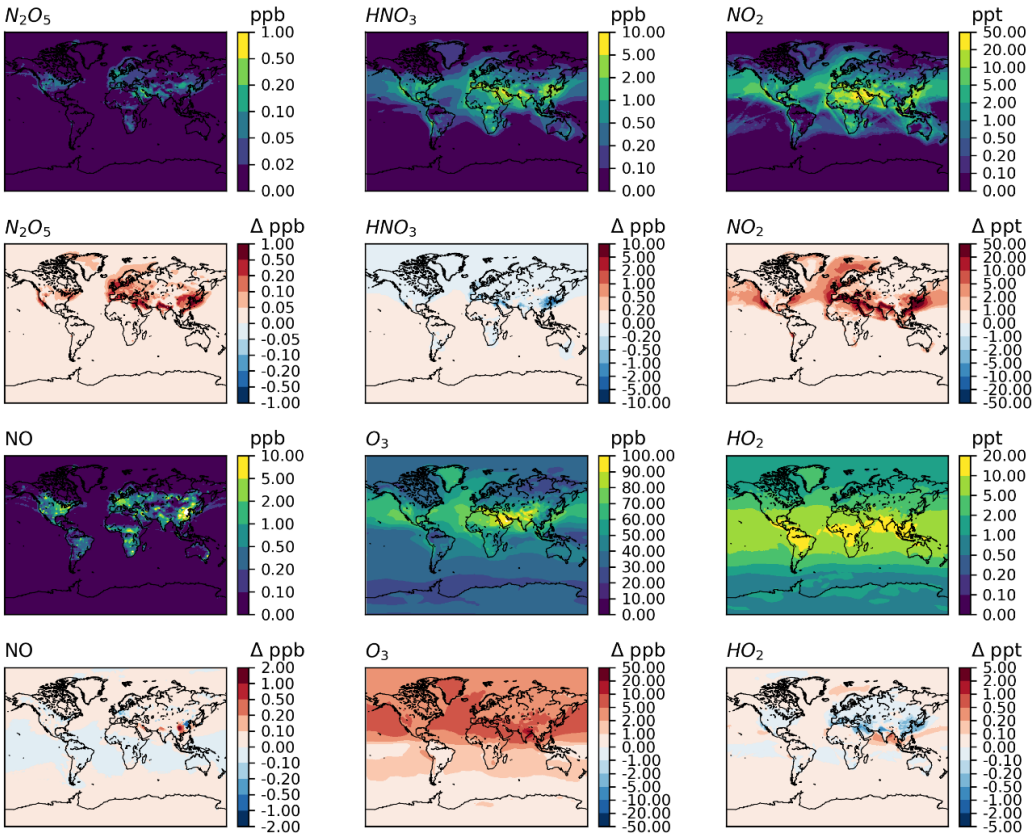

Figure A4: Surface mass mixing ratios of N_2O_5, HNO_3 and NO_2 (top row) and NO, O_3 and HO_2 (third row) from HYB, and their absolute differences in concentrations (second and bottom row) when switching off heterogeneous N_2O_5 hydrolysis (i.e. Hyb-NoHet minus HYB). Units are ppb or ppt.

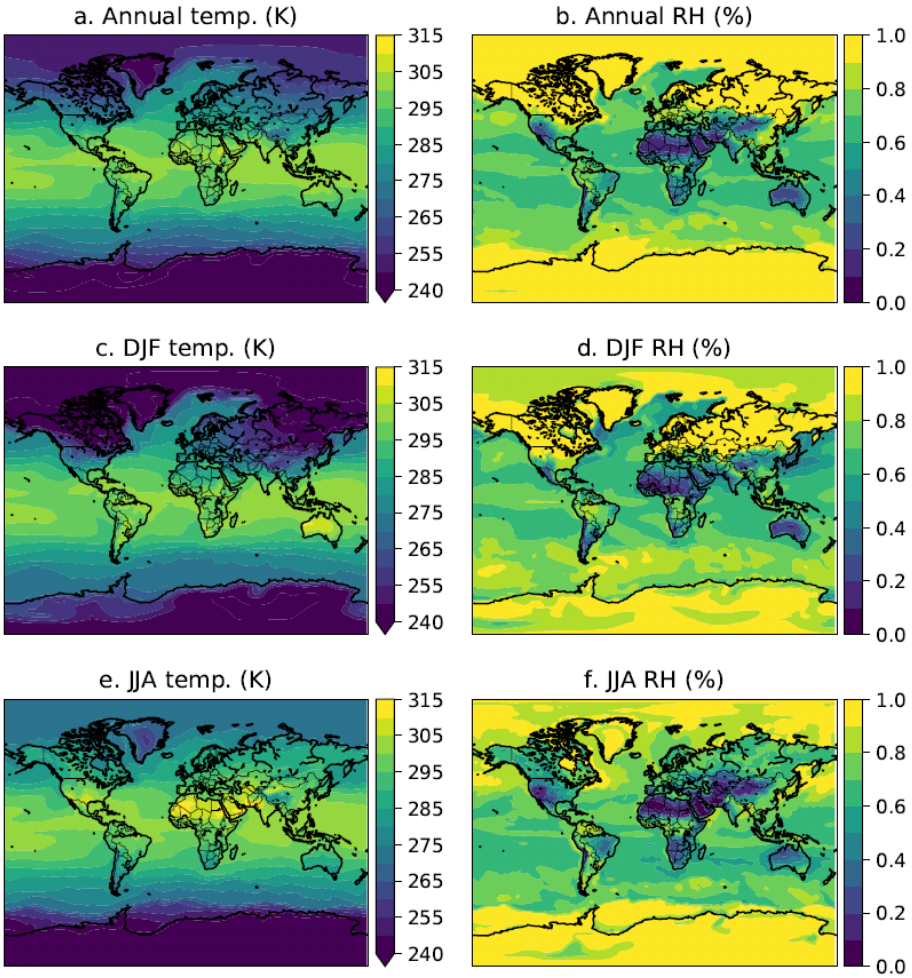

Figure A5. Annual (top), DJF (middle) and JJA (bottom) mean surface temperature (left) and surface relative humidity (right) for the year 2008 sensitivity simulations in chapter 4.

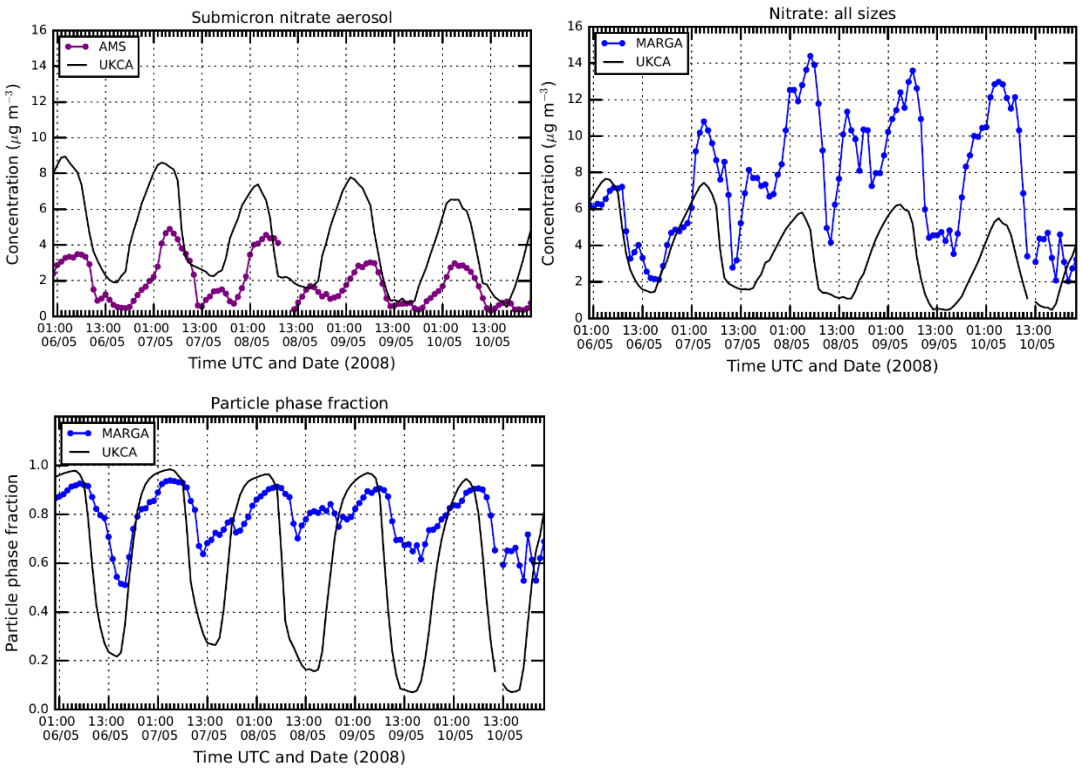

Figure A6. Nitrate near-surface diurnal variability from 6 – 11th May 2008. a) UM-UKCA-simulated and AMS-observed submicron nitrate aerosol concentrations at 60m height. b) UM-UKCA-simulated and MARGA-observed nitrate aerosol concentrations at 4m height c) UM-UKCA-simulated and MARGA-observed particulate phase fraction ie. particulate nitrate / (gaseous nitric acid + particulate nitrate).

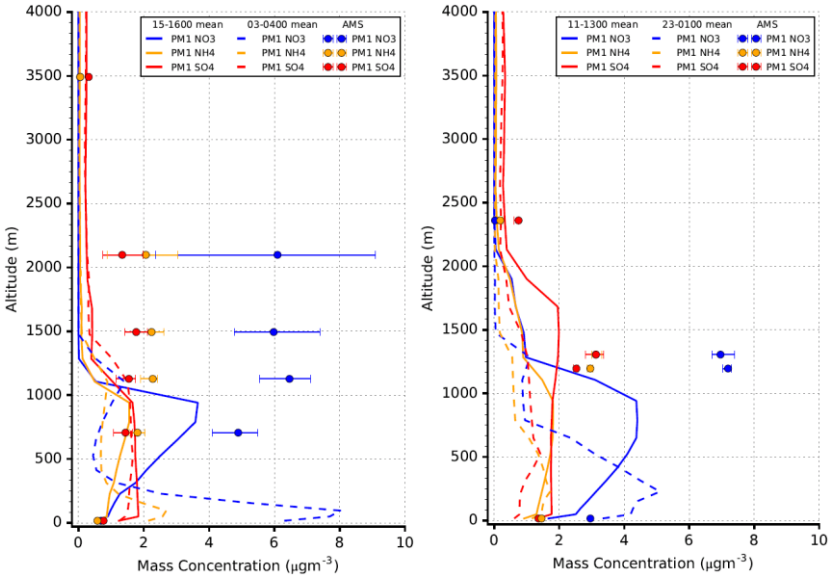

Figure A7. AMS-observed [circles] and UM-UKCA-simulated [solid lines] vertical distribution of nitrate, ammonium and sulphate aerosol in the vicinity of Cabauw (4°-6°E, 51°-53°N) at the times indicated on a) 6th May flight B366 and b) 21st May flight B379 2008. Simulated night-time concentrations are also presented [dashed lines] to indicate diurnal variability.

Appendix B
Chapter 5 Supplementary Information

Table B.1. Statistical summary of seasonal model-observation comparison with nitrate aerosol included and excluded from UM-UKCA.

Region	Observational method		DJF		JJA	
			With NO_3^-	Without NO_3^-	With NO_3^-	Without NO_3^-
Europe	Ground-based (2008)	R	0.11	-0.01	0.28	0.23
		NMB	-0.53	-0.61	0.05	-0.09
USA	Ground-based (2008)	R	0.32	0.23	0.41	0.41
		NMB	-0.62	-0.30	-0.70	-0.31
India	Ground-based (2016)	R	0.86	0.84	-0.35	-0.38
		NMB	-0.65	-0.70	-0.32	-0.38
China	Ground-based (2014)	R	0.67	0.66	0.59	0.56
		NMB	-0.77	-0.79	-0.85	-0.87

Table B.2. Normalised mean bias (NMB) in satellite-derived $PM_{2.5}$ datasets compared to ground-based $PM_{2.5}$ observations.

Region	Observational method	NMB	NMB	NMB
		Year 2008 satellite	Year 2014 satellite	Year 2016 satellite
Europe	Ground-based (2008)	0.16	-	-
USA	Ground-based (2008)	0.18	-	-
India	Ground-based (2016)	-0.27	-	-0.20
China	Ground-based (2014)	-0.21	-0.25	-

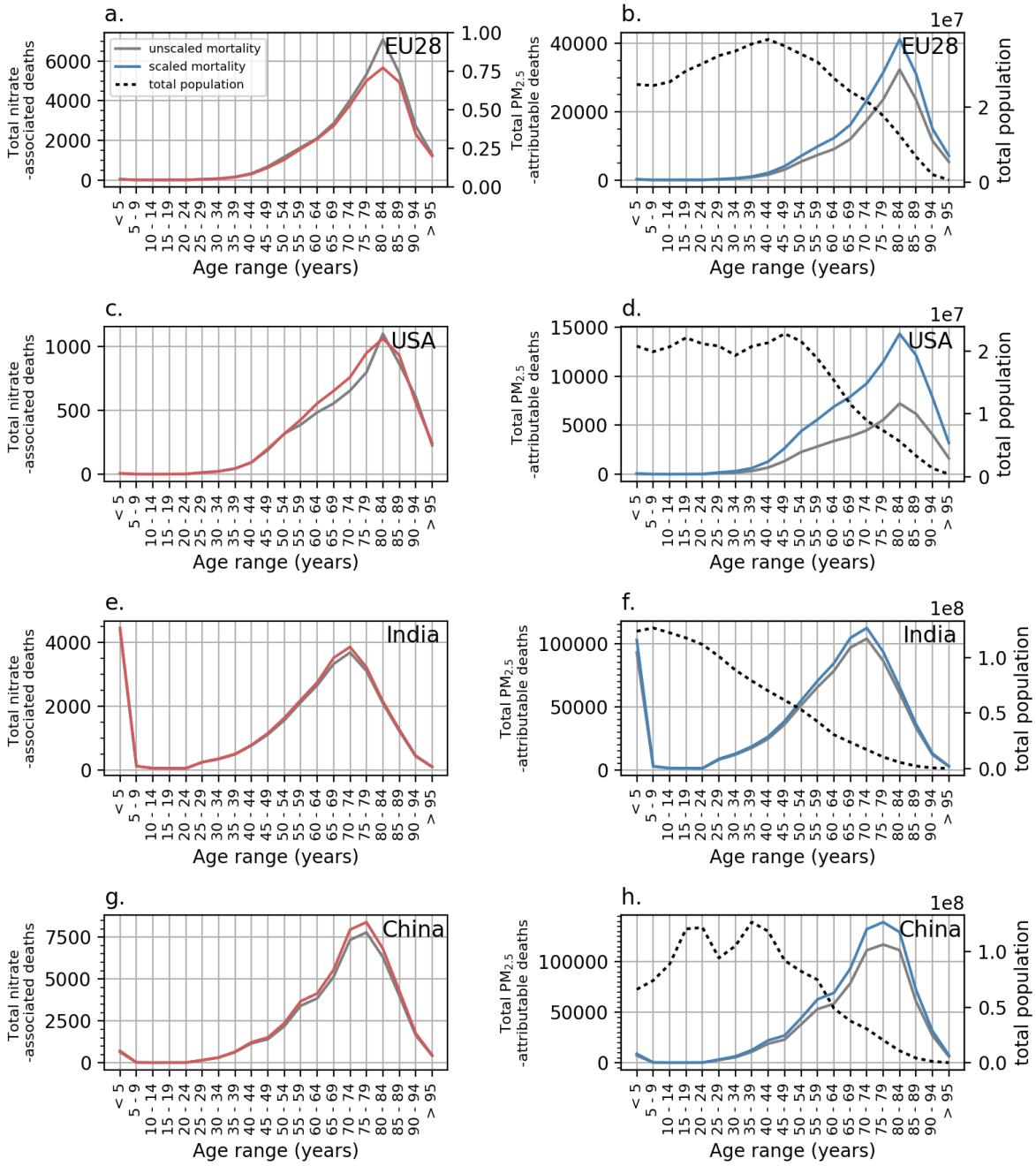

Figure B1 Age distribution of (left column) total nitrate-associated and (right column) total $PM_{2.5}$-attributable premature mortality over the EU28, USA, India and China. The second axis on subplots (b, d, f and h) shows the total population per age group. Results are shown as calculated from bias-corrected fields (coloured lines) and unscaled fields (grey line).

Table A5.1. Mass concentration (μg m^{-3}) and fractional contribution (in parentheses) of each $PM_{2.5}$ component, calculated from UM-UKCA with 1980 emissions. Total and speciated $PM_{2.5}$ are shown as calculated using the speciation method, in addition to the nitrate aerosol contribution to $PM_{2.5}$ calculated using the subtraction method.

Component	EU28	USA	India	China
	Speciation method			
Nitrate	0.82	0.24	0.45	0.43
	(9.1%)	(6.7%)	(1.5%)	(2.3%)
Ammonium	0.88	0.31	0.43	0.42
	(9.7%)	(8.7%)	(1.4%)	(2.21%)
Sulphate	2.6	1.067	0.85	1.08
	(28.4%)	(29.5%)	(2.8%)	(5.7%)
Sea salt	0.34	0.113	0.22	0.04
	(3.7%)	(3.1%)	(0.7%)	(0.2%)
Black carbon	0.45	0.15	0.86	0.63
	(5.0%)	(4.1%)	(2.9%)	(3.36%)
Organic carbon	1.60	0.50	5.8	2.98
	(17.8%)	(13.9%)	(19.4%)	(15.8%)
Dust	2.37	1.24	21.3	13.3
	(26.3%)	(34.2%)	(71.1%)	(70.4%)
Total $PM_{2.5}$	9.0	3.6	30.0	18.9
	Subtraction method			
Nitrate	0.99	0.29	0.56	0.51
	(11.0%)	(7.9%)	(1.86%)	(2.7%)